Optimizing the Performance of Asphalt Mixes with High Reclaimed Asphalt Pavement Content Using Rejuvenators

by

Hui Liao

A thesis

presented to the University of Waterloo

in fulfillment of the

thesis requirement for the degree of

Doctor of Philosophy

in

Civil Engineering

Waterloo, Ontario, Canada, 2022

Examining Committee Membership

The following served on the Examining Committee for this thesis. The decision of the Examining Committee is by majority vote.

External Examiner	**Dr. Silvia Caro** Civil and Environmental Engineering, Universidad de los Andes
Supervisor	**Dr. Hassan Baaj** Civil and Environmental Engineering, University of Waterloo
Supervisor	**Dr. Pejoohan Tavassoti** Civil and Environmental Engineering, University of Waterloo
Internal Member	**Dr. Susan Tighe** Civil and Environmental Engineering, University of Waterloo
Internal Member	**Dr. Christine Moresoli** Chemical Engineering, University of Waterloo
Internal Member	**Dr. Anh Pham** Civil and Environmental Engineering, University of Waterloo

Author's Declaration

I hereby declare that I am the sole author of this thesis. This is a true copy of the thesis, including any required final revisions, as accepted by my examiners.

I understand that my thesis may be made electronically available to the public.

Abstract

Reusing reclaimed asphalt pavement (a.k.a., RAP) has become a routine in the production of asphalt paving materials. Theoretically, RAP is a hundred percent recyclable material since its main components are high-quality, graded aggregates coated with durable asphalt binder. Unfortunately, due to the presence of the aged asphalt binder, most agencies only approve a limited percentage of RAP, either less than 20% to 30% of RAP (by weight of the total mix) or less than 25% of RAP binder replacement (by weight of the total binder content), to be incorporated in new asphalt mixes. For decades, pavement researchers have shown great enthusiasm for promoting the RAP rate in asphalt mixes. One of the most promising approaches is to use rejuvenators to restore the aged asphalt binder to a comparable or even better performance than the virgin asphalt binder. However, there is still a lack of knowledge and practice in using rejuvenators in producing sustainable and durable recycled asphalt mixes. The gap is not only limited to the type of rejuvenators to be used, but also to the optimal dosage, compatibility with virgin and RAP binder, stability under the elevated temperature atmosphere, mix design and manufacturing process, and uncertainties about the long-term performance of the revitalized high RAP mixes. As a result, this research was initiated to investigate the use of rejuvenators for optimizing the performance of asphalt mixes with higher RAP content.

This study used seven commercial rejuvenators provided by various suppliers, as well as materials collected at local asphalt plants and refineries for the experimental work, which included six bio-based oils, one petroleum-based oil, one processed RAP, graded virgin aggregates, and two virgin asphalt binders. A sequential screening methodology was applied to evaluate the rejuvenating efficacy of these rejuvenators and a soft binder using various binder and mix tests and data analysis tools. In the first part of this research, rejuvenated binder blends with different RAP binder ratios (25%, 50%, and 75%) and rejuvenator dosages (0%, 5%, and 10%) were prepared to select candidate rejuvenators with better restoration capacities in terms of reducing the viscosities at mixing and compaction temperatures as well as recovering the continuous performance grade (PG) temperatures, non-recoverable compliance, and crossover temperature measured binder testing using the Dynamic Shear Rheometer (DSR) and the Bending Beam Rheometer (BBR). Four bio-based rejuvenators were selected in the first stage and used for dosage optimization through the blending chart method and the response surface modelling (RSM) method. The blending chart method assumes a linear relationship between the rheological index and two variables, rejuvenator dosage and RAP binder ratio. Therefore, the optimal rejuvenator dosage can

be determined when the rejuvenated binder blend resembles the same rheological index as a target virgin binder. Meanwhile, the response surface model was built based on a two-level factorial design, which involved the different rheological indices as the responses and the rejuvenator dosage and RAP binder ratio as the two factors. This method can verify the linear relationship and then the model can be used to calculate the optimal dosages. From the results, the blending chart method was proved to be reliable because most of the rheological indices were expected to have a linear relationship with the rejuvenator dosage and the RAP binder ratio. Furthermore, the recommended indices, the low PG temperature based on m-value (PGL_m) and the crossover temperature (T_{cross}), exhibited the potential to ensure that the rejuvenated binder blends have adequate cacking resistance without compromising the permeant deformation resistance at high temperatures.

In the mix testing phase, the Hamburg Wheel-Tracking (HWT) test results revealed concerns about increased permanent deformation and moisture susceptibility due to the additions of rejuvenators in high RAP mixes at both test temperatures, 44°C and 50°C. However, the rejuvenated high RAP mixes outperformed the control mix (with 20% RAP), particularly at the higher test temperature. The cracking test results obtained from the Indirect Tensile Asphalt Cracking Test (IDEAL-CT) indicated that the addition of rejuvenators or replacing the base binder with a softer virgin binder was beneficial in improving the cracking resistance; however, more testing results, preferably from plant trial mixes, are needed for statistical analyses. Nonetheless, the rejuvenated high RAP mixes achieved decent high-temperature stability and acceptable cracking resistance, especially after an extended oven conditioning period. The dynamic modulus test was used to investigate the effect of increased RAP content with the use of a rejuvenator (or a soft binder) on mix rheology at a variety of temperature and loading frequency combinations. The measured modulus and phase angle data were analyzed using two master curve models and several time-temperature-dependent shifting equations. Additionally, the long-term performance of the asphalt mixes was assessed by comparing test results obtained from samples before and after the long-term oven aging (LTOA) protocol. The high RAP asphalt mix with the addition of a rejuvenator showed the most stiffness increase after long-term aging; however, it retained relatively better flexibility and temperature sensitivity compared to other mixes.

According to the findings of this study, using rejuvenators in asphalt mixes with a high RAP content can produce a recycled HMA with balanced rutting and cracking performance and long-term sustainability. Whereas in the high pavement in-serve temperature range, extra care should be taken for moisture susceptibility.

Acknowledgements

I wish to express my sincere thanks to my supervisors Professor Hassan Baaj and Professor Pejoohan Tavassoti for their support, guidance, and encouragement during my PhD study. I would also like to express my sincere appreciation to my PhD defence committee members Prof. Susan Tighe, Prof. Christine , Prof. Anh Pham from University of Waterloo, and Prof. Silvia Caro from Universidad de los Andes.

This study was funded by the Natural Sciences and Engineering Research Council of Canada (NSERC), [funding reference number: CRDPJ 543959-19] and Imperial Oil Ltd. I would like to thank Dr. Payman Pirzadeh and Dr. John A. Noël from Imperial Oil for their useful feedback during the meetings we had in the past years. I would also like to thank the CPATT partner Steed and Evans Ltd., especially Mr. Richard Marco and Mr. Jim Karageorgos for their help with the collection of RAP and virgin aggregates that were utilized in this research project.

My gratitude is also extended to the outstanding technical staff members at the Department of Civil and Environmental Engineering, Mr. Richard Morrison, Mr. Peter Volcic, Mr. Rob Kaptein, and Mr. Douglas Hirst, for their assistance and help with many of the laboratory tests detailed in this thesis.

I would also like to thank all my dearest friends and colleagues in the Centre for Pavement and Transportation Technology (CPATT) at the University of Waterloo for their help and the wonderful times and enjoyable moments we share in both the lab and the office.

Last but not least, I am so grateful to my family for their love and support that helped me to get to where I am today.

Table of Contents

List of Figures

List of Tables

List of Abbreviations

AASHTO	American Association of State Highway and Transportation Officials
ASTM	American Society for Testing and Material
BBR	Bending Beam Rheometer
CRI	Cracking Resistance Index
CS	Creep Slope
CT_{index}	Cracking Tolerance Index
DOA	Degree of binder Activation
DOAv	Degree of binder Availability
DOB	Degree of Blending
DOT	Department of Transportation
DSR	Dynamic Shear Rheometer
DTG	Derivative Thermogravimetric
FTIR	Fourier Transform Infrared
HMA	Hot Mix Asphalt
HWT	Hamburg Wheel-Tracking
IDEAL-CT	Indirect Tensile Asphalt Cracking Test
IDT	Initial Decomposition Temperature
LMLC	Lab-Mixed and Lab-Compacted
LTOA	Long-Term Oven Aging
LVE	Linear Viscoelasticity
MDT	Maximum Decomposition Temperature
MEPDG	Mechanistic-Empirical Pavement Design Guide
MR	Moisture Ratio
MSCR	Multiple Stress Creep Recovery
MTO	Ministry of Transportation Ontario
MTS	Material Testing Systems
NAPA	National Asphalt Pavement Association
NCAT	National Center for Asphalt Technology
NCHRP	National Cooperative Highway Research Program
NMAS	Nominal Maximum Aggregate Size

OAPC	Ontario Asphalt Pavement Council
OPSS	Ontario Provincial Standard Specification
PAV	Pressure Ageing Vessel
PG	Performance Grading
PGAC	Performance Graded Asphalt Cement
RAP	Reclaimed Asphalt Pavement
RB	RAP Binder
RBR	RAP Binder Replacement
RD	Rut Depth
RDCI	Rate Dependent Cracking Index
RRI	Rutting Resistance Index
RSM	Response Surface Modeling
RTFO	Rolling Thin Film Oven
SARA	Saturates, Aromatics, Resins, Asphaltenes
SB	Soft Binder
SGC	Superpave Gyratory Compactor
SHRP	Strategic Highway Research Program
SIP	Stripping Inflection Point
SN	Stripping Number
SS	Stripping Slope
STOA	Short-Term Oven Aging
TGA	Thermogravimetric Analysis
TTSP	Time-Temperature Superposition Principle
V_a	Air Voids
VFA	Voids Filled with Asphalt
VMA	Voids in Mineral Aggregate
VR	Visco-plastic Ratio
WLF	William-Landel-Ferry
WMA	Warm Mix Asphalt

Chapter 1
Introduction

1.1 Background

Construction of new asphalt pavements and maintenance of deteriorated asphalt pavements demand massive amounts of natural resources such as mineral aggregates, asphalt binders, and fossil fuels. It is, therefore, of utmost importance to reuse the milled and reprocessed asphalt mixes (Reclaimed Asphalt Pavement, a.k.a. RAP) after pavement repair and rehabilitation activities, which is a rich source of asphalt binder and aggregates. RAP application brings both environmental and economic benefits by preserving non-renewable natural resources and cutting down material production and transportation costs. The material cost constitutes about 70 percent of the total cost to produce Hot Mix Asphalt (HMA), which is a combination of aggregates, such as gravel and sands, mixed and coated with asphalt binder under an elevated temperature environment. In addition, the fluctuating price of crude oil directly influences that of virgin asphalt binder. Therefore, reusing the aged binder and mineral aggregates in RAP can lower the need for virgin materials and help with the economy of construction projects [1,2].

Previous projects conducted by the Centre for Pavement and Transportation Technology (CPATT) have shown that using RAP in asphalt mix has a minimal negative impact on the performance of rutting and fatigue when compared to conventional asphalt mixtures fabricated with virgin bitumen and aggregates [3–6]. The previous collaboration between the CPATT and Imperial Oil, investigated the effect of extended silo storage in improving the quality and durability of asphalt mixes containing RAP [7]. The findings have shown significant improvement in the performance of recycled asphalt mixes due to enhanced blending between virgin and aged asphalt binders. However, due to the uncertainties of highly oxidized asphalt binders in RAP, transportation agencies and municipalities impose restrictions on the amount of RAP that can be used in HMA. Currently, RAP content is limited to 20 to 30 percent by weight of the total recycled asphalt mix by most agencies. Nevertheless, there is a growing interest in maximizing RAP usage in the asphalt industry. On the other hand, using higher contents of RAP in the mixes will require feasible rejuvenation methods, such as incorporating rejuvenators or using softer virgin binders. Rejuvenators, also called recycling agents or rejuvenating agents, are products designed to restore the properties of an aged binder to a condition that resembles that of virgin binders. As more stiff and brittle aged asphalt binders are included in the high RAP asphalt mix, using rejuvenators is a promising approach to offset the side effects

of increased RAP content, but it indeed requires more in-depth research on the rejuvenators. So far, there is still a significant gap in the knowledge and the practice of using rejuvenators in the paving industry. This gap is not only limited to the type of the rejuvenating product to be used, but also to the rejuvenator dosage, compatibility with virgin and RAP binder, the impact of diffusion and blending between rejuvenators and asphalt binders, mix design and manufacturing process, and finally uncertainties regarding the long-term performance of the high RAP mixes recycled through the use of rejuvenators. As a result, it requires further investigations to ensure that rejuvenated RAP-incorporated mixes perform better than, or at least the same as, the conventional asphalt mixes. To this end, this research set out to conduct a thorough investigation into optimizing the performance of asphalt mixes containing high RAP content using rejuvenators.

The work presented in this thesis was carried out under the supervision of Professor Hassan Baaj and Professor Pejoohan Tavassoti who provided tremendous help and support during my Ph.D. study. This project was funded by the Natural Sciences and Engineering Research Council of Canada (NSERC), [funding reference number: CRDPJ 543959-19] and Imperial Oil Ltd. All materials used in the creation of the original articles included in the thesis are the sole work of the primary investigator, who is listed as the first author in journal publications (or paper manuscripts). The research presented in this thesis is a result of collaboration with materials suppliers, Imperial Oil Ltd and Steed & Evans Ltd.

1.2 Problem statement and research objectives

As a popular topic in the asphalt industry, rejuvenation has yet to be fully explored. For example, there are no standardized specifications or guidelines on how to properly use the rejuvenators in asphalt mixes with excessive RAP content. There are no standardized specifications or guidelines, for example, on how to properly use rejuvenators in asphalt mixes with high RAP content. Even if a rejuvenator has been used successfully in trail sections or field projects in other research, it is not convincing to use the same product in local constructions due to the variety of material sources and qualities, as well as the different climate conditions. Furthermore, hundreds of commercialized rejuvenators are available in the market; it is critical to select the appropriate rejuvenator type and optimal rejuvenator dosage before incorporating them into plant production. Moreover, there has been little research into a rejuvenator's long-term effectiveness, which is essential for predicting the field performance of rejuvenated high RAP mixes and building sustainable flexible pavements.

The overall goal of this research is to provide a systematic rejuvenator application guide in optimizing the performance of recycled HMA with high RAP content. To achieve this goal, the main objectives are summarized as follows:

- To evaluate the impact of the different rejuvenators on the rheology of binder blends with a high RAP binder ratio through rheological tests as screening tools.
- To compare and evaluate different rheological indices as the criteria for optimizing the rejuvenator dosage in the binder blends with a high RAP binder ratio.
- To investigate the behavior and performance of asphalt mixes with high RAP rates and different rejuvenators with a focus on both the short- and long-term performance through laboratory performance testing and rheological characterization.

As an outcome of this study, the answers to the following questions would be provided:

- Do all rejuvenators improve the performance of the asphalt binder or mix?
- Does the selected rejuvenator (with optimized dosage) lead to any insufficient rutting, moisture, or cracking resistance compared to the traditional asphalt mixes?
- Will the selected rejuvenator retain its efficiency after the long-term lab aging protocol?

Finally, the findings and conclusions will be used to guide plant mixing trials for producing recycled HMA with up to 50% RAP and rejuvenators. Meanwhile, the testing framework and data analysis methods can be applied on evaluating similar materials, and the test results can be used as input for mechanistic-empirical pavement design.

1.3 Thesis organization

This manuscript-based thesis consists of nine chapters, Chapter 4 to Chapter 8 were modified from conference proceedings or published journal papers and drafted manuscripts.

- Chapter 1: General scope and overall objectives of the research are explained in this chapter.
- Chapter 2: A comprehensive literature review is presented in this chapter covering various topics related to this research.
- Chapter 3: A description of the materials used in this research is provided as well as the research methodology used to achieve the goals of this research.

- Chapter 4: Preliminary evaluation of the rejuvenating effectiveness of commercial rejuvenator products through binder testing.
- Chapter 5: Rejuvenator dosage optimization and characterization of optimized binder blends.
- Chapter 6: Evaluation of rutting resistance and moisture susceptibility of recycled hot mix asphalt containing bio-based rejuvenators.
- Chapter 7: Effect of extended oven conditioning on the cracking and rutting performance of rejuvenated high RAP content asphalt mixes
- Chapter 8: Rheological characterization of rejuvenated high RAP mixes under both short- and long-term aging conditions.
- Chapter 9: Summary of findings in previous chapters, the overall conclusion, and recommended future research directions.

1.4 Thesis contribution

The main contribution of this thesis is to propose an optimization procedure regarding the rejuvenator type selection and dosage optimization to increase the RAP content over the limitation, which is promising in producing the high RAP asphalt mix with acceptable cracking resistance without compromising the high-temperature stability. Also, the rejuvenated high RAP mixes exhibited satisfactory long-term performance in terms of better flexibility and less temperature sensitivity compared to the control mix with an allowable RAP amount. To be more specific, the following contributions can be generated based on the experimental work, data analysis, and findings in each chapter:

- Chapter 4: The major contribution of this chapter was providing insightful information on which rheological parameters are critical for approving the selection of a certain rejuvenator.
- Chapter 5: The first contribution was that the traditional blending chart method was validated by a more robust DOE method to be used for rejuvenator dosage optimization. The second contribution is the two recommended optimization criteria, crossover temperature (T_{cross}) and low continuous performance grade based on m-value (PGL_m), were able to determine a proper rejuvenator dosage which restored the binder flexibility and relaxation capacity as well as maintained sufficient high-temperature stability.

- Chapter 6: The findings in this chapter provided abundant information in choosing the proper performance indicators to evaluate the rutting and moisture resistance of rejuvenated high RAP mixes. Also, the rutting test temperature was recommended to be based on the performance grade of the blended binder in recycled mixes according to the rutting results obtained from two test temperatures. An excel spreadsheet was used for computing the novel performance indicator which was preferred in differentiating the mixes by separating the plastic deformation from moisture damage. A MATLAB code will be developed as a more user-friendly HWT data analysis tool which applies to results obtained from different devices and data acquisition systems.
- Chapter 7: The effect of extended conditioning suggested a feasible way to improve the blending and diffusion between the virgin binder, rejuvenator, and aged binder in actual plant scale mixing; thus, acquiring optimized high RAP mixes with balanced cracking and rutting performances.
- Chapter 8: The findings in this chapter offered insightful information on the long-term performance of rejuvenated high RAP mixes using the rheological characterization results. The application of different master curve models and shift factor equations provided various rheological parameters which can be used as indicators for evaluating the aging resistance of mixes. Additionally, the measured data can be used for future research as input in mechanistic-empirical pavement design software to predict the in-service performance of rejuvenated high RAP mixes.

Although the work was limited to the laboratory scale, the outcomes from this research will offer the Ontario asphalt industry a better insight into selecting the appropriate rejuvenator for producing high RAP mixes. The results of this research will be shared with the Canadian technical asphalt and paving community through the publication and presentation of the findings of this research in journal papers and conferences.

Chapter 2
Literature review

The overall goal of this chapter is to provide a synthesis of the current studies and practices on the use of rejuvenators in high RAP-content asphalt mixtures, which has been recognized as a promising method to mitigate the negative impacts of increasing the RAP content. It covers the major benefits and side effects of high-content RAP mixtures, aging and rejuvenation mechanisms, degree of blending (DOB) scenarios, application of different rejuvenators and their effects on recycled asphalt mixes, and the pertinent details of plant production of high-content RAP mixture.

2.1 Advantages and disadvantages of high-content RAP mixes

Reclaimed Asphalt Pavement (RAP) refers to the removed or reprocessed asphalt mixes milled from existing asphalt pavements when the roads need rehabilitation or reconstruction. The major fractions in RAP are aged asphalt binder and RAP aggregates. Instead of disposing of these materials, it is more common to produce recycled asphalt mixture with RAP, which brings both environmental and economic benefits. Less demand for raw materials results in reduced energy consumption in terms of fuel usage for manufacturing and transporting these materials, which also mitigates greenhouse gas emissions. In addition, replacing part of the virgin materials with RAP preserves non-renewable resources and saves landfill space for RAP disposal. As demonstrated by Figure 2.1, the unit cost can be potentially reduced by about 50% to 70% by using 100% recycled asphalt mixtures. Such reduction mostly resulted from cutting down the cost of virgin asphalt binder and mineral aggregates [1].

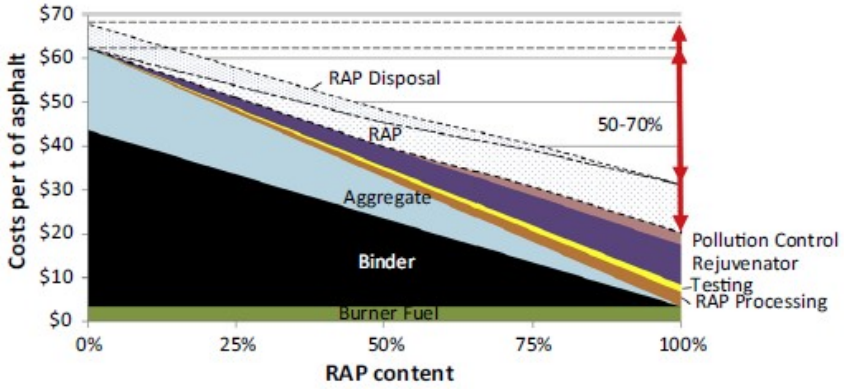

Figure 2.1 Cost estimation in recycled asphalt mixture [1]

RAP is theoretically 100% reusable as the major components in it are aged asphalt binder and well-graded RAP aggregates. However, the content of RAP in recycled asphalt mixture is usually restricted by agencies due to the poor workability of RAP during mixing and compaction, and the potential premature distresses (e.g. thermal cracking, fatigue cracking, and ravelling) caused by the stiff binder in RAP [8]. Therefore, the RAP content in actual practices is usually limited to less than 20% to 30% by the mass of the total asphalt mixture. According to the annual survey report published by the National Asphalt Pavement Association (NAPA) in 2021, RAP is utilized at an average rate of 21.1% in new asphalt mixtures across the United States [9], which was close to the allowable RAP percentage. The U.S. Federal Highway Administration defines the high-content RAP (HRAP) as mixes with RAP proportions larger than 25% [8]. In Ontario, RAP content is restricted to 15% and 30% when it is used in the surface course and binder course, respectively. The former can be increased to 20% contingent on the terms of the municipal contract. An additional approval by the contract administrator is required in mix design if 31% to 50% of RAP is used in the binder course. Nevertheless, RAP content beyond 50% is not allowed in any cases [10].

The proportion of RAP in HMA affects the selection of virgin asphalt binder since a softer binder is required to balance the increased stiffness due to high RAP content. The binder property can be characterized by the Superpave performance grading (PG) system, which includes two numbers representing the average seven-day maximum pavement temperature and the minimum pavement design temperature, respectively. The determination of recommended virgin binder performance grade selection was based on the percentage of RAP in the total asphalt mixture [11]. However, NCHRP Report 752 proposed the virgin binder selection to be based on the RAP binder replacement (RBR) ratio, which describes how much of the RAP binder content contributes to the total binder content in the mix [12]. The report concluded that no changes in binder selection are required when the RBR is less than 25% by weight of the total binder content which includes the virgin asphalt binder and RAP binder (both activated and non-activated), otherwise, a blending chart that elucidates the relationship between the PG of virgin asphalt binder and RAP binder proportion is required to select the proper virgin asphalt binder. Ontario Asphalt Pavement Council (OAPC) does not recommend any adjustments in the Performance Graded Asphalt Cement (PGAC) of the virgin binder when the RBR is less than 15%. When RBR is greater than 15%, the OAPC recommendation in Table 2.1 can be used as a guide to PGAC selection. For RBR ratios from 26% to 50% engineers should use a blending chart to determine the required grade of virgin binder to achieve a target PGAC value. This value should be calculated using the given PG of the aged binder in RAP and the RBR (or percentage of RAP) to be used in the final mix.

Table 2.1 PGAC selection in Ontario [13]

Binder replacement ratio	Performance Graded Asphalt Cement		
	Zone 1	Zone 2	Zone 3
0-15%	PG 52-34	PG 58-34	PG 58-28
16%-25%	PG 52-40	PG 52-40	PG 52-34
26%-50%	Confirmed by blending chart		

Figure 2.2 Ontario PGAC zones [14]

Agencies restrict the RAP fraction in a new mix primarily due to the following major concerns with high-content RAP mixes such as (1) the stiffness and brittleness of aged binders; (2) the blending efficiency between RAP and virgin materials; and (3) the gradation of RAP, especially the fine aggregates. Using a softer virgin binder, increasing the asphalt binder content, and introducing warm mix additives can be mentioned as some possible approaches to alleviate these concerns [15]. However, it should be noted that making adjustments to the PG of the virgin binder or the amount of virgin asphalt binder works well at lower RAP contents but is less effective for cases with high RAP contents. As the RAP content increases, the virgin binder contribution to the total binder content decreases. It is difficult to activate the RAP binder through purely mechanical mixing with virgin asphalt binder and aggregates. Furthermore, the required preheating and mixing temperatures rise as the RAP content increases [16], which leads to more fuel consumption, air pollution (e.g. blue smoke), and oxidative aging of materials due to overheating. In this

case, Warm Mix Asphalt (WMA) techniques can be used to reduce the mixing and compaction temperatures by lowering the viscosity of the asphalt binder. The addition of WMA additives can either increase the adhesion between asphalt binder and aggregates (e.g., surfactants) or reduce the asphalt binder viscosity to make it more flowable. Nonetheless, most of these additives are unable to restore the rheological properties of the aged binder. To this end, the idea of asphalt binder rejuvenation has been developed for RAP recycling, which is achieved by adding a product called rejuvenator to restore the properties of RAP binder to a condition that resembles that of virgin asphalt binder, thus the recycled asphalt mixes can perform equally or even better than the asphalt mixes with limited or no RAP. To better understand the mechanism of rejuvenators, it is important to recognize the effect of aging and rejuvenation on the asphalt binder at a micro-scale level.

2.2 Aging and rejuvenation of asphalt binder

2.2.1 Asphalt binder chemistry

The colloidal system is widely used for describing the internal structure of asphalt binder, in which the asphaltenes are covered with resins and disperse in a medium formed by saturates and aromatics which are forming the oily phase called maltenes [17,18]. In the colloidal system, asphaltenes are the heaviest component in the asphalt binder and are responsible for providing the necessary stiffness to resist the load. They are insoluble in the dispersing medium and tend to associate or agglomerate if not probably stabilized. Resins constitute the intermediate fraction between asphaltenes and the dispersing medium, they are attracted to the asphaltenes through polar groups, preventing them from organizing clusters. Aromatics consist of lightweight mono- and polycyclic aromatic hydrocarbons that are associated with the flexibility and flowability of the binder, together with the saturated hydrocarbons which are chemically inert, aromatics and saturates constitute the dispersing medium.

As shown in Figure 2.3, colloidal systems can be classified as sol and gel structures. Colloids with sol structures behave like a Newtonian fluid, in which the asphaltenes are highly stabilized by the resins. Since resins are soluble in the oily phase, the asphaltene-resin micelles are highly organized in the dispersive medium. Whereas those with gel structures are highly non-Newtonian because the asphaltenes formulate a continuous network with a large area and increase the stiffness and brittleness of the asphalt binder. The concept of sol- and gel-type colloids distinguish the asphalt binders with a low (5% to 10%) and high (20% to 35%) asphaltene content, respectively [19,20]. While most asphalt binders behave in between these extremes; therefore, their colloidal structure can be referred to “sol-gel” type. The changes in the rheological

property of asphalt binder that happened before and after aging (or rejuvenation) can be attributed to the concentration changes of these chemical components [21].

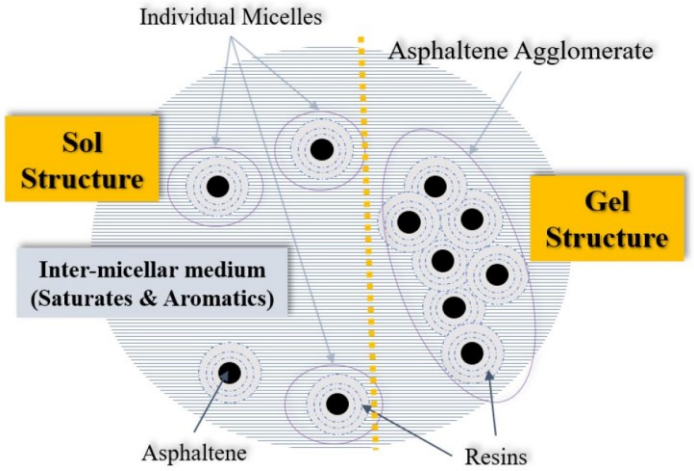

Figure 2.3 Colloidal structure of asphalt binder [22]

2.2.2 Aging mechanism

Aging of asphalt binder is dominated by multiple factors, including oxygen, moisture, temperature variations, and sunlight, which results in both physical and chemical changes in asphalt binder (see Figure 2.4). In general, aging process stiffens and embrittles asphalt binders, thus reducing the workability of RAP incorporated mixes, impairing the thermal stress relaxation capability of materials, and reducing fatigue resistance. These physical changes are reflected in the pavement performance in terms of distresses, such as striping, ravelling, transverse cracking, and block cracking in asphalt pavements.

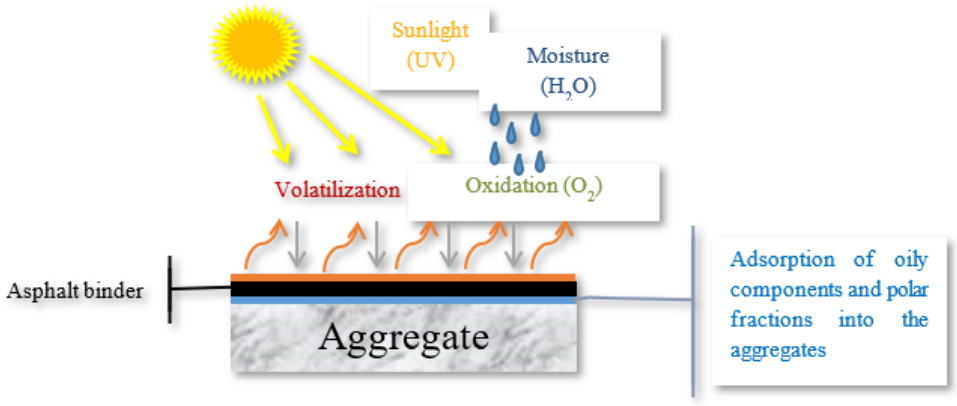

Figure 2.4 Asphalt binder aging phenomena [2]

For unaged asphalt, the colloidal system is in a stable balance. With aging, the chemical composition of the asphalt binder is changed by losing the softer and stabilizing fractions: aromatics and resins, with the stiffer fraction (i.e., asphaltenes) increasing. Due to the reduced volume of the dispersing medium, asphaltenes start to agglomerate and form a stiff and brittle structure that is not easily separated [23]. Several researchers have used Fourier Transformed Infrared Spectroscopy (FTIR) to detect asphalt aging at the functional group level. The increase in carbonyl (C=O) and sulfoxide (S=O) functional groups was observed in the virgin bitumen (Pen 70/100) after aging [24]. Chen et al. performed both FTIR and SARA analyses and found that all three aged binders (Pen 60/80, Pen 40/60, and SBS modified binder) had increased intensities of C=O and S=O peaks, which was consistent with the increase in asphaltene proportions [25]. In addition to these two techniques, Atomic Force Microscope (AFM) can also reveal the surface microstructures of asphalt binders, and the variation in these structures can be used to validate the aging effects. In general, aging causes an increase in the number and decrease in the size of dispersed domains, as well as an increase in modulus at the micro-scale [26,27]. Menapace et al. discovered a third phase between the dispersed domains and the matrix after PAV aging, which is considered an indicator of the increasing association of molecules, resulting in reduced molecular mobility [28].

The variation in the rheological properties of asphalt binders caused by aging can be associated with the formation or disappearance of different chemical components and the changes in molecular composition. However, even two asphalt binders which exhibit similar physical properties may have different chemical compositions and/or show different morphologies in microscopic images. Therefore, it is essential to investigate the aging effect at micro-scale levels to better understand the rejuvenation mechanism by introducing different chemical products (i.e., rejuvenators), rather than solely studying the restoration of rheological properties.

2.2.3 Rejuvenation mechanism

The definition of rejuvenation is to bring someone or something back to its younger or even fresh state. Chemically, it means reversing the oxidation process. Therefore, it is inaccurate to use “rejuvenation” in this context, as the rejuvenators do not reverse the oxidative aging of asphalt binders, it only reverses the impact of aging on asphalt materials. This term, however, is given a technological concept when used in the asphalt industry, which is to restore the rheology and physical performance of aged bitumen to the level of virgin asphalt binder. In other research publications, rejuvenators are also referred to interchangeable terms like rejuvenating agents or recycling agents [23,29]. However, these terms need to be distinguished

from the term “softening agent”, which is occasionally misused to describe the concept of rejuvenators, as softening agent only aims to reduce the viscosity or the stiffness of the aged asphalt binder. Rejuvenator, however, in addition to potentially reducing the viscosity, has the potential to restore the balance of component fractions, restore phase/colloidal stability, reduce brittleness, restore healing ability, achieve equal (or better) aging behavior than the original binder [30–32]. A good candidate rejuvenator is capable of balancing the fractions of asphaltenes and maltenes by introducing the light components such as aromatics and resins and even restoring the colloidal structure by breaking the clusters of asphaltene molecules and enchanting the dispersion ability of the maltene phase [33]. Figure 2.5 shows the fractions of the four components in two asphalt binders, PG 58-10 and PG 58-22. Both the aged asphalt binders showed a significant increase in the asphaltene fractions and a decrease in the proportions of aromatics, compared to their virgin counterparts. The addition of aromatic extract partially restores the ratio of asphaltenes and maltenes (saturates, aromatics, and resins), but it fails to duplicate the same ratio between these four components. This result indicates that rejuvenation is not a reversed process to reproduce the original asphalt binder.

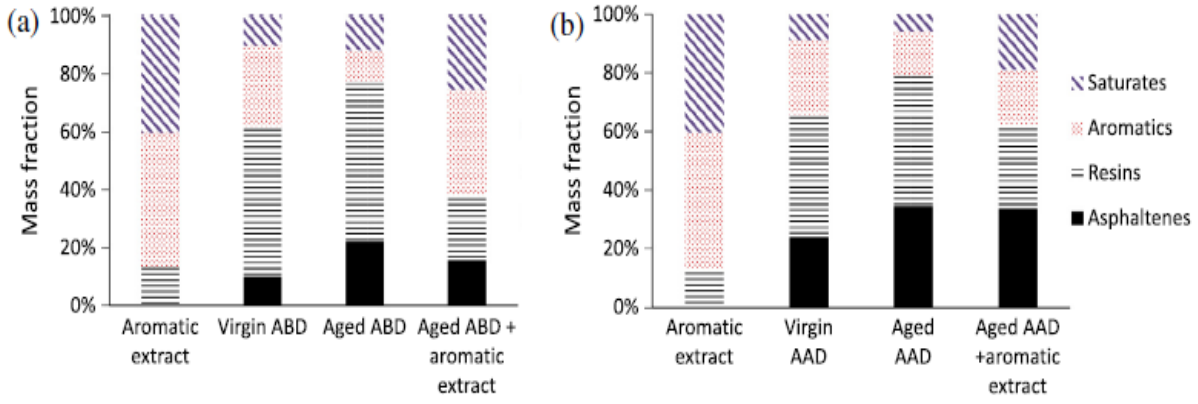

Figure 2.5 SARA fractions of the virgin, aged and rejuvenated asphalt [27]

The goal of rejuvenation is to restore the aged asphalt binder that has been heavily oxidized and coats the RAP aggregates as a thin layer of binder film. Hence, the rejuvenator should come into full contact with the aged asphalt binder, diffusing from the outer binder film to the inner layer of the RAP binder. Therefore, the rejuvenation happens through the contact between the rejuvenator and the RAP binder and the diffusion of the rejuvenator into the binder film, and hence the rejuvenation occurs. Carpenter and Wolosick discovered the rejuvenation process first, but the term "modifier" was used to describe the diffusion process [34]. According to their findings, rejuvenator diffusion can be divided into the following steps (seen Figure 2.6):

(1) Under the first stage, the outer layer of the RAP binder contacts with the rejuvenator when the RAP particles are surrounded by the low viscosity layer of the rejuvenator.

(2) The outer layer becomes softer with higher mobility, which allows the rejuvenator to penetrate from the outside to the inner layer.

(3) The diffusion of the rejuvenator continues, thus softening the inside aged asphalt binder and decreasing the amount of rejuvenator around the outer layer, therefore the viscosity of the outer recycled blend (aged asphalt binder and rejuvenator) will increase.

(4) Finally, diffusion completes when the equilibrium is achieved, which means the whole aged binder film exhibits a constant viscosity.

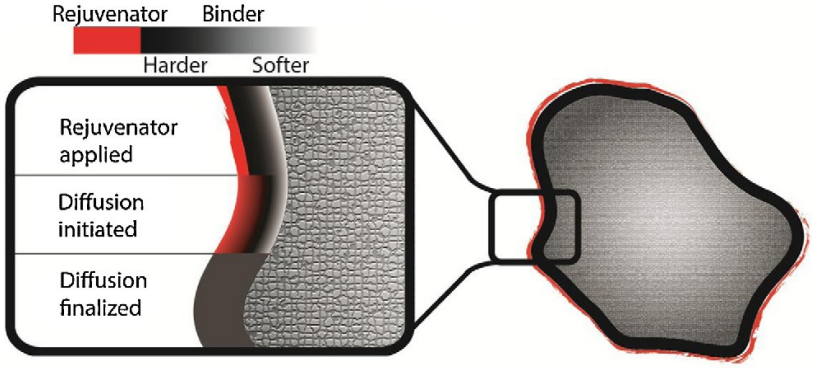

Figure 2.6 Rejuvenator diffused into aged binder film [1]

The rejuvenator diffusion process can be investigated by modelling simulation as well. Zaumanis and Mallick [35] developed finite element (FE) models to investigate the diffusion process by using different rejuvenators. Figure 2.7 illustrates the viscosity variation of the innermost point of the aged asphalt binder with the increasing time at 145°C. This figure indicates that it takes about 205 to 210 seconds to complete the diffusion process when the discrepancy of the viscosity is less than 1%. This simulation result confirms the diffusion mechanism proposed by Carpenter and Wolosick.

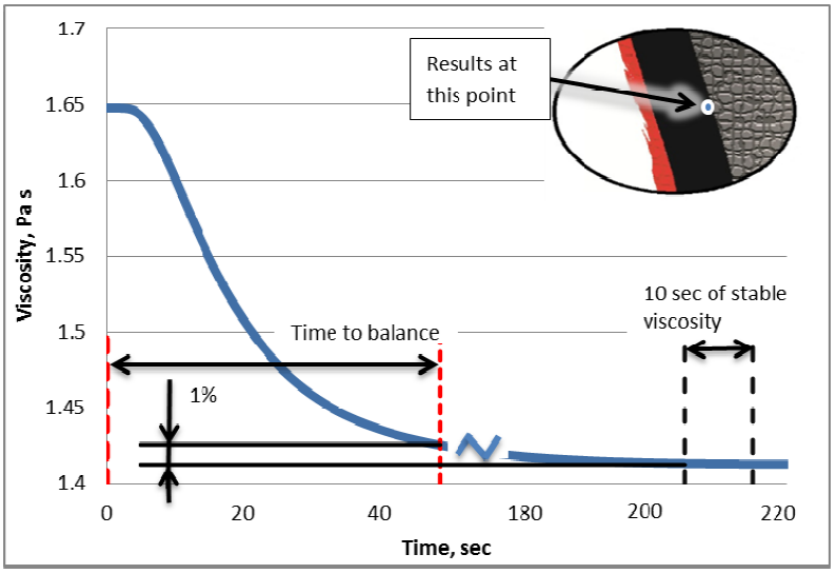

Figure 2.7 The viscosity of inner aged binder film at different times, 145°C [35]

Xu et al. [36] applied molecular dynamics to simulate the rejuvenator diffusion at the molecular scale. As can be seen in Figure 2.8, the interface remains stable when the rejuvenator contacts the RAP binder at the beginning of the process. Once the rejuvenator molecules start to diffuse in the RAP binder, a portion of RAP binder molecules penetrates the rejuvenator as well. Although the penetration occurs mutually, the rejuvenator molecules diffuse more deeply than the RAP binder. This is mainly because the rejuvenator has a relatively lower viscosity and higher mobility (due to its smaller molecule size).

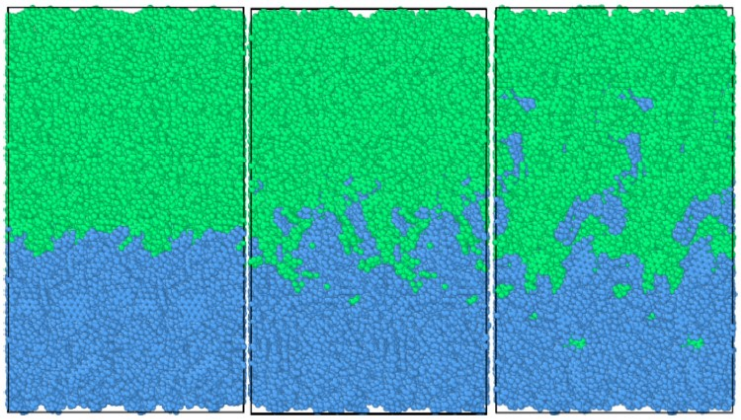

Figure 2.8 The evolution of molecules in a rejuvenator (green) - RAP binder (blue) system, 433K [36]

Rejuvenation of aged asphalt binder does not reverse the oxidative aging process. The rejuvenated asphalt binder has different constitutions of chemical components and can perform equally or even better than the

virgin asphalt binder. The essential step of the rejuvenation mechanism is diffusion, which needs sufficient time to reach an equilibrium state, in which the aged biner is fully activated and mobilized and ready to blend with rejuvenators and virgin asphalt binders.

2.3 Degree of blending (DOB)

2.3.1 Diffusion, binder activation, and blending

As mentioned in the previous section, diffusion is the homogenization process between binders and rejuvenators, which is affected by time, temperature, and the intrinsic property of the material (i.e., viscosity) [37,38]. The completion of binder diffusion does not need external mechanical force, and it continues during silo storage, transport, and placement, even in the pavement during the service period. Whereas blending refers to the binder interaction during mixing, which needs an external force to facilitate the process. Blending can happen between virgin aggregates and RAP by pure mechanical mixing, which is called dry mixing [39]. It is practical when pre-blend the superheated virgin aggregates with RAP to enhance the mobilization of the aged binder. It can also refer to the blending between the virgin and aged binder during wet mixing when the liquid virgin binder and rejuvenators (if applied) are incorporated. The blended binder, consisting of virgin asphalt binder, rejuvenator, and RAP binder, coats the virgin and RAP aggregates in the mixing process. As a result, the diffusion of rejuvenator or virgin asphalt binder helps activate and mobilize the RAP binder to be ready for blending, while the blending between RAP and virgin materials offers more contact opportunities for rejuvenators and virgin binder to complete diffusion. In short, blending between RAP binder and virgin asphalt binder occurs regardless of the presence of the rejuvenator; however, it can be enhanced by the addition of rejuvenators.

DOB is an important index that affects the performance of the final recycled asphalt mixture. Presti and Orekovic defined DOB by contrasting it with the concepts of the degree of binder activity (DOA) and degree of binder availability (DOAv) [40,41]. DOA is the amount of activated RAP binder that is available for use as a lubricant in mixing and compaction. It is calculated as the ratio of the minimum amount of aged binder that is considered active in the production of recycled asphalt mixes to the total amount of RAP binder. DOA is an inherent property of RAP that is only affected by the RAP binder composition and processing conditions such as mixing time and temperature. Menegusso et al. applied the artificial lab mixed 100% RAP mixture (recovered RAP binder and RAP aggregates) as a control mix to compare with 100% RAP mixtures prepared at different mixing temperatures and times [42]. It was discovered that increasing the mixing temperatures reduced the air voids and increased the indirect tensile strength of the 100% RAP

mix samples, indicating an increase in the effective binder content (activated RAP binder). DOAv refers to the contribution from the active RAP binder, including the activated RAP binder by rejuvenation and the residual rejuvenator. All these components are available for blending with virgin materials during mixing. Figure 2.9 depicts the distinction between DOA and DOAv. Because only RAP is considered in the first scenario, the available RAP binder equals the active RAP binder. The RAP binder is divided into two parts: active (or available) RAP binder and inactive (or unavailable) RAP binder. When a rejuvenator is used, the amount of inactivated RAP binder is reduced in both short and long-term rejuvenation. Also, the residual rejuvenator content should be considered as part of the activated binder content as a lubricating component during mixing and compaction, as well as part of the effective binder film, which contributes to the final asphalt mixture's performance.

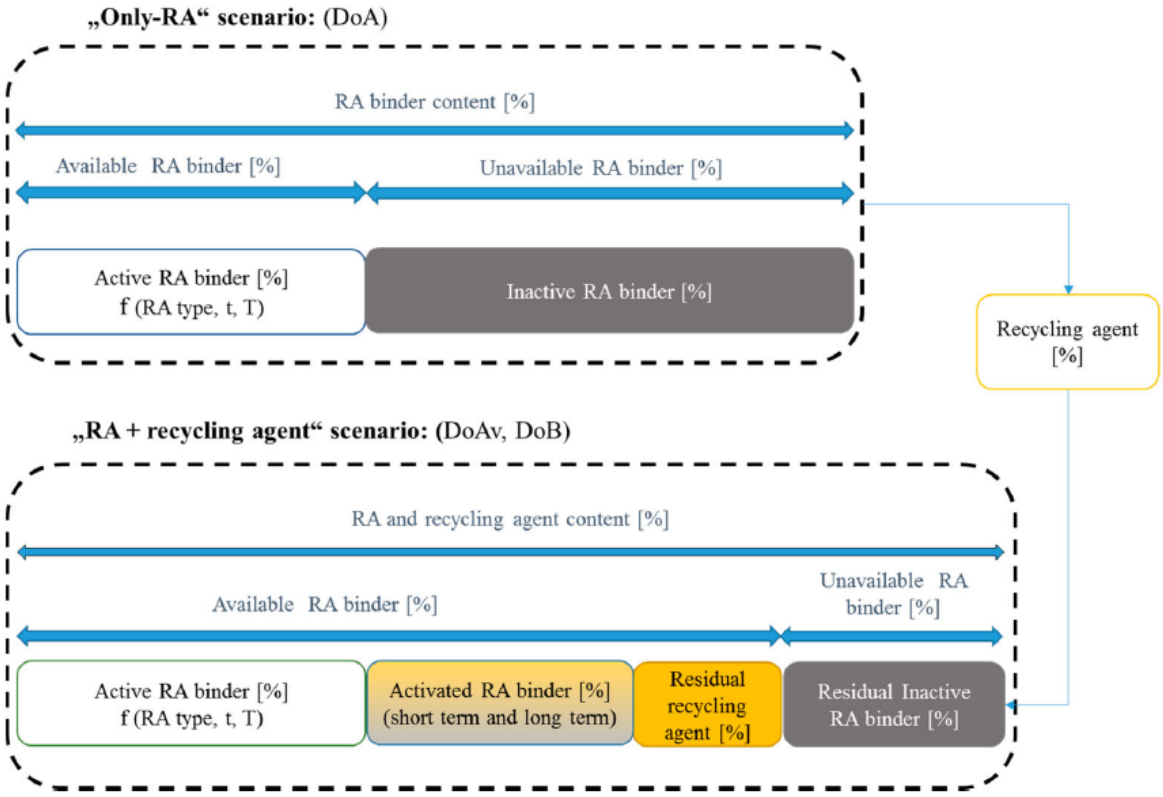

Figure 2.9 DOA, DOAv, and DOB in “only-RAP and “RAP + rejuvenator” scenarios [40]

The main difference between DOB and these two parameters is that DOB is a parameter that defines the properties of the final mixtures, with a focus on the contribution of RAP binder to the effective binder blend in the asphalt mixture, rather than being solely related to RAP binder properties. This concept is only

applicable when other lubricating materials, such as virgin binders and rejuvenators, are present. DOB enables blending efficiency to be focused on the properties of the final blend rather than the amount of binder.

2.3.2 Different blending scenarios

In general, there are three blending scenarios (see Figure 2.10): (1) No blending, the RAP particle acts as "black rock" that the RAP binder is not activated and still adheres to the aggregates and does not blend with the virgin binder and/or rejuvenators. (2) Partial blending, part of the RAP binder is flowable and can mix with the virgin materials, but the inner binder layer is not removed from the aggregate surface. (3) Full blending, all the RAP binder is activated and able to blend with the virgin asphalt binder, then coat the virgin aggregates and RAP aggregates again.

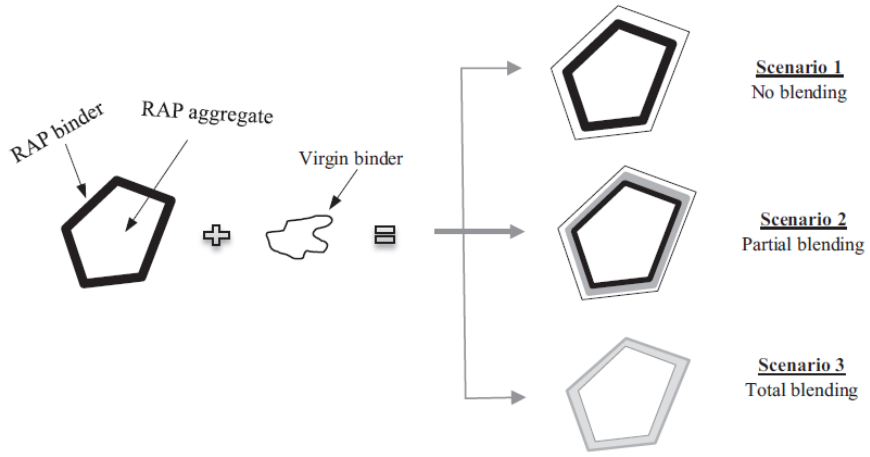

Figure 2.10 Scenarios of different degrees of blending [2]

In NCHRP report 452, blending was considered in the recycled asphalt mixture design by using blending charts at high, intermediate, and low temperatures [11]. This method is recommended to select the virgin asphalt binder with appropriate PG or estimate the percentage of RAP to achieve the required PG for the final blended asphalt binder. Although this method assumes that full blending occurs between RAP binder and virgin asphalt binder, several other studies suggest that partial blending does exist between the RAP and virgin materials during the production process [43–46]. This scenario results in two major issues: (1) Partial blending will cause non-uniform distribution of soft additives, like rejuvenator and softer virgin asphalt binder, which forms a low viscosity outer layer with high concertation of soft binder (or rejuvenator) when diffusion is not completed. It is detrimental to the rutting resistance of recycled asphalt mixture during the earlier stage after construction [29]. (2) If full blending was considered in the RAP mix design process,

all the aged asphalt binder is assumed to contribute to the total bitumen content. This will lead to insufficient virgin binder content, which can affect the cracking resistance, fatigue performance, and moisture susceptibility of the recycled asphalt mixture [47].

It is difficult to quantify the RAP binder contribution to the total blended binder, which is not only influenced by the properties of the mix components, such as the stiffness and extent of aging of RAP binder (DOA and DOAv), the virgin binder quality (DOAv), and the addition of rejuvenators (DOAv), but also the mixing conditions, primarily the mixing temperature and mixing time. Kaseer et al. proposed the RAP binder availability factor (BAF) as a function of mixing temperature and the high PG of the RAP binder [48]. They claimed that about 50% to 95% RAP binder was available for blending with the virgin materials at a mixing temperature between 140℃ and 150℃. They also found that the addition of rejuvenators was more effective in the lower mixing temperature scenarios and adding the rejuvenator to the RAP directly, as opposed to mixing it with the virgin binder, did not show any significant effect on RAP binder availability. However, the possible reason could be the insufficient time for diffusion to complete at room temperature. Zhao et al. suggested that increasing the RAP content would reduce the RAP binder mobilization, as the RAP binder contribution measured in the blended binder reduced from 73% to 24% as the RAP content increased from 30% to 80% [49]. However, Abed et al. reported a plausible full blending case (DOB = 96%) occurred in the 50% RAP mixes prepared with a softer binder (Pen 160/220) when mixing at 135℃ with an extended mixing time to 5 minutes [50].

2.3.3 DOB measuring methods

The methods for measuring DOA and DOAv are usually based on mechanical blending with binder testing methods. Whereas DOB is more complicated to quantify than the other two parameters since it needs to evaluate the properties of recycled asphalt mixes or the recovered binder to examine the RAP binder contribution in the effective binder blend. Given the crucial role of blending assumption in the design of new asphalt mixes with high RAP contents, it is essential to determine the actual contribution of the RAP binder and the virgin asphalt binder needed in the mix design. Different DOB quantification methods were developed in previous research, including staged binder extraction, studying the difference between predicted and measured performance parameters, and micro-scale characterization techniques.

Staged extraction divides the soaking process into several periods, each period takes less time so the binder films can be recovered layer by layer. Huang et al. adopted this approach, a four-stage extraction method with a 3-minute washing duration per extraction, to estimate the amount of RAP binder blended

with virgin asphalt binder under a normal mixing process [43]. The binder testing results of different extracted samples showed that the inner binder layers had similar viscosity and complex shear modulus to the pure RAP binder, denoting that these binders remained stiff and adhered to the RAP aggregates, and only part of the outside layers of RAP binder (about 40%) were effectively blended with virgin asphalt binder. On the other hand, molecule size separation techniques such as Gel permeation chromatography (GPC), which can provide information about the molecular weight distribution in asphalt binder, have been implemented to investigate the blending efficiency between virgin and RAP binders at a micro-scale [51,52]. In this technique, an index (i.e., LMS) is defined as the proportion of large molecules (greater than 3000 Dalton) in all molecules. This index increases with aging since the aged asphalt binder contains more large molecules than virgin asphalt binder. Therefore, this index can be used to distinguish virgin asphalt binder, RAP binder, and their blends. If blending between virgin asphalt binder and RAP binder does exist, the LMS (%) of their blend should be between those of the virgin and RAP binders [53]. In addition, Zhao and Huang et al. proved that the amount of RAP/RAS binder in the recycled blend has a linear relationship with LMS (%) [49]. They also found out the LMS (%) is highly correlated with the rheological property of asphalt binder (i.e. complex shear modulus) [51]. Therefore, staged extraction can be applied to evaluate the blending efficiency of RAP binder, and even provides quantitative measurements of binder blending with the implementation of rheological property parameters and GPC. Based on this DOB measuring method, the partial blending scenario can be interpreted as given in Figure 2.11, blending between RAP binder and virgin binder leads to a composite binder film, coating the virgin aggregates and recoating the RAP aggregates, with part of inactivated RAP binder remained on the RAP aggregates.

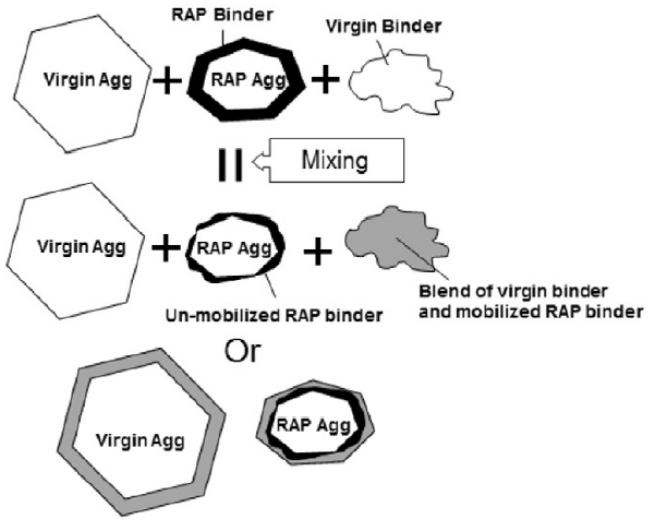

Figure 2.11 Partial blending scenario [54]

Yu et al. [47] applied the gap-graded blending method, mixing fine RAP particles and coarse virgin aggregates, to separate "Virgin Agg." and "RAP Agg." mentioned in Figure 9. Therefore, the blending efficiency in this partial blending scenario can be determined by comparing the binders extracted from coarse mixtures and fine mixtures (i.e., CM binder and FM binder), since the properties of CM binder and FM binder should be the same if full blending occurs. Moreover, they developed the index of blending ratio (BR) by comparing those two binders with RAP binder, virgin binder, and proportion binder which represented the full blending situation at the same RAP binder content. This index was defined as the following equation:

$$BR = \frac{\ln R_c' - \ln R_v}{\ln R_p - \ln R_v} \times 100\% \tag{2-1}$$

Where R_c' is the binder property parameter (e.g., G*/sinδ) of CM binder, which should be corrected as the fine mixtures might remain on coarse mixtures; R_v is the binder property parameter of FM binder; and R_p is the binder property parameter of the proportion binder. If no blending happens, BR should equal zero, as the property of CM binder should be the same as the virgin binder and the virgin coarse aggregates are coated by only the virgin binder. If full blending happens, BR should equal one. The result suggested that the predicted binder property by using BR showed a similar value to that of the measured property, and it was not sensitive to which parameter, either rutting or fatigue, was used in that equation as the BR of RAP

mixtures reached the highest (81.6% to 84.8%) at same RAP content (40%) by inputting different binder property parameters.

Mogawer et al. [55,56] adopted the method developed by Christensen et al. [57] to investigate the DOB between RAP (40%) and asphalt binders that were modified with different rejuvenators. The blending efficiency is determined by comparing a predicted dynamic modulus (|E*|), calculated by the Hirsch model (see Equation (2-2) and (2-3)) with the inputs of complex shear modulus (G*), voids filled with asphalt (VFA), and voids in the mineral aggregates (VMA).

$$|E^*|_{mix} = P_c\left[4{,}200{,}000\left(\frac{1-VMA}{100}\right) + 3|G^*|_{binder}\left(\frac{VFA \times VMA}{10{,}000}\right)\right] + \frac{1-P_c}{\left[\left(\left(1-\left(\frac{VMA}{100}\right)\right)/4{,}200{,}000\right) + \left(\frac{VMA}{3VFA|G^*|_{binder}}\right)\right]} \quad (2\text{-}2)$$

$$P_c = \frac{(20 + ((VFA \times 3|G^*|_{binder})/VMA))^{0.58}}{650 + ((VFA \times 3|G^*|_{binder})/VMA)^{0.58}} \quad (2\text{-}3)$$

where $|E^*|_{mix}$ is the predicted mixture dynamic modulus, psi; $|G^*|_{binder}$ is complex shear modulus derived from the master curve (the reference temperature is 25℃), VMA represents the voids in mineral aggregates, %, and VFA represents the voids filled with asphalt, %. As the control virgin bitumen (PG 52-28) and the bio-modified asphalt binder were assumed to be completely blended with the extracted RAP binder, the $|E^*|_{mix}$ of different mixture samples represent the full blending scenarios. Therefore, a good degree of blending can be concluded if the confidence intervals (α=0.05) of the $|E^*|_{mix}$ and the measured dynamic modulus overlap. This method requires fewer mixture tests to evaluate the blending efficiency of RAP binder and virgin asphalt binder, however, it fails to provide a quantitative measurement of the DOB.

Nahar et al. [58] reported the observation of the blending zone at the interface between virgin bitumen and RAP binder by AFM. The morphologic characteristics (like the size, aspect ratio, and fraction of the domain phase) of the blending zone were between those of the virgin and RAP binder samples. In addition, new microstructures were founded, and no original microstructures existed after blending, indicating that the blending mechanism of virgin bitumen and RAP binder tends to be scenario B as shown in Figure 2.12.

Although this method provided intuitive observation of the blending zone, it was conducted on extracted RAP binder which may not represent the actual blending situation between binder and aggregates. Abd et al. [46] investigated the blending efficiency by using the nanoindentation test, which can measure the nanomechanical properties at the interfacial transition zone (ITZ) and asphalt mastics in RAP mixtures. If the ITZ between RAP binder and RAP aggregates exhibited a relatively higher stiffness compared to other areas, it means that the RAP aggregates are still coated with RAP binder. However, it can only be used to test whether a complete blending is achieved by studying the variation of nanomechanical properties over different regions in one RAP mixture.

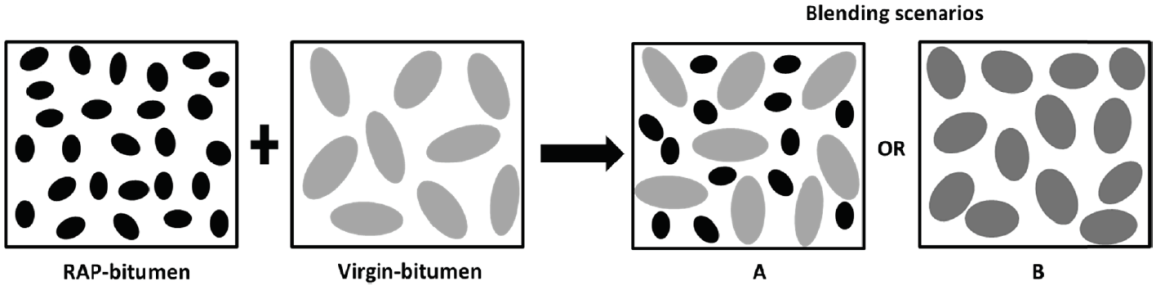

Figure 2.12 Possible blending scenarios of microstructures between virgin and RAP asphalt cerement [58]

The ideal full blending is difficult to achieve, and partial blending is a more realistic scenario, especially in high RAP content mixtures. Partial blending influences the RAP mix design process, the RAP production conditions, and the performance of the final RAP mixture. Increasing mixing temperature and mixing time can improve the degree of blending, however, it is impractical and inefficient in asphalt mixing plants, considering that higher RAP content requires longer mixing time and higher mixing temperature [16]. Instead of changing the external factors and internal factors of virgin materials, the inclusion of a rejuvenator is feasible to enhance the blending efficiency, as the rejuvenated RAP binder is easier to be removed from RAP aggregates and is flowable enough to blend with virgin materials.

2.4 Application of rejuvenators

As mentioned in previous sections, one viable solution to dealing with potential barriers to increasing RAP content is to use rejuvenators. A good rejuvenator should satisfy both short- and long-term requirements: (1) rapidly diffuse into the RAP binder and promote binder mobilization (or activation), thereby improving the workability of recycled mixes; (2) recover the rheological properties of the recycled binder blend to prevent fatigue and cracking potential at low temperatures without causing extra softening and rutting issues; and (3) maintain the rejuvenating effectiveness over a long period. A substantial amount of research

has been conducted to investigate the potential of various products as rejuvenators, to determine the optimum doses of these products, and to evaluate the rejuvenation effectiveness by the different binder and mixture tests, chemical analysis, and micro characterization methods.

2.4.1 Different types of rejuvenators

The traditional rejuvenators are the refinery base oils, such as paraffinic oils, aromatic extracts, and naphthenic oils, which were originally used for pavement maintenance and have been developed as petroleum-based products for asphalt recycling uses [59–62]. These refined petroleum oils are from the same source as the asphalt binder but have rich saturated alkanes, cycloalkanes, and unsaturated polar aromatic ring structures; therefore, they can replenish the light components in the aged binder [63]. Recently, using rejuvenators derived from sources like plant oils, animal fat, and waste has gained great popularity in the asphalt industry. There have been tremendous bio-based products and waste-derived oils emerged in publications about asphalt rejuvenation:

- Plant oils: corn oil [32], cashew shell oil [32], cotton seed oil [64], tall oil (distilled or crude) [28,60,65], soybean fatty acids [66,67], date seed oil [68], castor oil [69,70], pongamia oil [70,71].
- Animal fats or wastes: refined tallow [59], swine manure (pre-blend with asphalt binder) [55].
- Waste-derived oils: waste vegetable oils (WVO) [60,64], WV grease[59,60,64], waste engineering oil (WEO) [32,72], waste engine oil bottoms/residues (WEOB) [72].

Due to the various sources of the rejuvenators, the categorization of rejuvenators is usually based on the origins of the competent consist of the rejuvenator. Zaumanis investigated six rejuvenators, waste vegetable oil, waste vegetable grease, Hydrogreen S^{TM}, distilled tall oil, aromatic extracts, and waste engine oil, and classify the first four as organic-based rejuvenators and the last two as petroleum-based rejuvenators [60]. Apostolidis et al. also classified the rejuvenators as organic and petroleum types of rejuvenators [73]. The organic-type rejuvenators are usually referred to as vegetable-based oils and the molecular structures of these rejuvenators are mainly triglyceride, which is an ester formed from glycerol and three fatty acid groups. Except for product origins, Al-Saffar et al. defined the rejuvenators based on both their processing methods or original applications, including waste-derived rejuvenators, refined base oils, and commercially applied products; a softer binder that has lower high and low-performance grades was also treated as a type of rejuvenator, while it can be recognized as a petroleum-based rejuvenator as well [20]. Table 2.2 shows the classification of rejuvenators from a report published by the National Center for Asphalt Technology (NCAT) and Nebraska DOT (NDOT). They divided the commonly used rejuvenators into five categories

according to their components, application, and resources. The Belgian Road Research Centre (BRRC) proposed a categorization into six groups which were based on the nature and origin of the examples of commercially available products (see Table 2.3). There are other categorization methods of rejuvenators. Bajaj et al. classified the rejuvenators into three categories: (a) Softeners, (b) Replenishers, and (c) Emulsifiers based on their rejuvenator mechanisms [74]. The current ASTM standard divides the rejuvenators into seven grades (RA 0, RA 1, RA 5, RA 25, RA 75, RA 250, and RA 500) primarily based on the viscosity of the rejuvenator [75].

Table 2.2 Classification of rejuvenators [76,77]

Category	Representative products	Description
Paraffinic oils	Waste engine oils (WEO) Waste engine oil bottoms (WEOB) Valero VP 165® Storbit®	Refined used lubricating oils
Aromatic Extracts	Hydrolene® Reclamite® Cyclogen L® ValAro 130A®	Refined crude oil products with polar aromatic oil components
Naphthenic oils	SonneWarmix RJ® Ergon HyPrene®	Engineered hydrocarbons for asphalt modification
Triglycerides and fatty acids	Waste vegetable oil Waste vegetable grease Brown grease Oleic acid	Derived primarily from vegetable oils
On-purpose bio-based products	Sylvaroad™ RP1000 Hydrogreen® Cargill Anova®	Derived from vegetable oils or tall oils, a paper industry by-product

Table 2.3 Categorization of rejuvenators into six groups [78]

Origin	Originally manufactured or derived	Recycling of waste
From petrochemical industry/petroleum	(1) aromatic extracts and naphthenic oils derived from crude oil	(2) recycling of machine oils
Vegetal/biological	(4) vegetal oils from agro-industry (5) engineered bio-based oils (e.g., tall oil derivatives))	(3) recycling of food oils (oils and fats of vegetable or animal origin)
Residual category	(6) various specifically engineered additives (e.g., biomass, biogeneric mixtures, flux oil)	

Some publications preferred to refer to non-petroleum products as bio-based rejuvenators rather than organic-based rejuvenators [67,79]. Bio-based products are made with substances derived from living organisms on purpose. They have, however, undergone extensive processing, as opposed to unprocessed raw materials. The definition of bio-based products is similar to that of organic-based products when it comes to substances derived from living organisms; however, the manufacturing process of bio-based products is not always organic. Most organic-based products are included in bio-based products, but not all bio-based products are organic. As a result, bio-based and petroleum-based rejuvenators are the most straightforward rejuvenator classifications; however, more detailed information can be obtained by investigating component fractions and processing methods.

In summary, most commercial rejuvenators can be divided into two types: petroleum-based rejuvenators and bio-based rejuvenators. However, waste-derived products can be classified as petroleum-based or bio-based based on their major components after purification. Petroleum-based products include softer asphalt binder and other refined oils. Bio-based rejuvenators are favored by pavement researchers due to the fewer expenses and lower required dosages compared to petroleum-based products [60]. Furthermore, most bio-based rejuvenators are bio-degradable and do not harm the environment or humans during construction or operation. Because of the presence of polar aromatic constituents, petroleum-based rejuvenators are potentially carcinogenic [63]. However, the challenges of using bio-based products are the compatibility with the asphalt binder and the instability of the triglycerides due to the chemical reaction with moisture,

UV, and acidic medium, resulting in the dissolution of fatty acids and glycerol [20]. It is difficult to categorize rejuvenators because there have been numerous commercial products that contain various types of chemical substances or biomaterials, and the majority of them are mixtures of different ingredients. Even if the same RAP binder and rejuvenator content is used, the difference in rejuvenator components will result in different rejuvenating effects because it changes the properties of rejuvenated asphalt binder at a chemical level by rearranging the SARA fractions. As a result, it is critical to choose the appropriate rejuvenator type in terms of compatibility with asphalt binder, rejuvenating effect, and cost-effectiveness.

2.4.2 Optimum rejuvenator dosage

The amount of rejuvenator should be carefully determined as inadequate rejuvenator dosage will lead to insufficient activation of aged asphalt binder and the excessive rejuvenator amount will have detrimental effects on the rutting resistance. In general, the rejuvenator supplier will recommend the optimum rejuvenator dosage. However, the rejuvenator content is affected by the aging level of the recycled materials [56], the quality of virgin asphalt binder [23], and the criteria used for selecting rejuvenator dosage. Instead, it is essential to determine the optimum rejuvenator dosage before applying it to a specific project to account for the uncertainties.

The most prevalent method is to establish a softening curve or blending chart based on the properties of the recycled blend (extracted RAP binder and rejuvenator) and the rejuvenator proportions. Those properties can be based on either the penetration system or the PG system. Ongel et al. [24] determined the optimum rejuvenator content according to the linear regression result of different rejuvenator dosages and penetration values, the optimum rejuvenator dosage was identified to achieve the penetration of the target virgin asphalt binder. Chen et al. [25] conducted a study in which the optimum rejuvenator dosage was calculated by four regression equations based on the relationships of four physical property indexes (penetration, softening point, ductility, and viscosity) with rejuvenator percentages. The final optimum dosage should be able to recover those indexes of the aged asphalt binder to the level of the virgin asphalt binder or meet the specification requirements.

Zaumanis et al. [60] developed a process to select the optimum rejuvenator dosage according to PG temperatures. The results indicated the high PG and low PG of RAP binder linearly decreased with the increasing rejuvenator content, and the dosage range varies as different types of rejuvenators were used. Moreover, as can be seen in Figure 2.13, the rejuvenator dosage should be between the maximum value, defined to ensure enough rutting resistance (high PG), and the minimum value that meets the requirement

of either low-temperature cracking resistance (low PG) or fatigue resistance (intermediate PG). The continuous high and low temperatures (i.e., continuous high PG and low PG) which exactly pass the rheological property criteria can also be adopted to determine the rejuvenator dosage. Arámbula-Mercado et al. [80] investigated another rejuvenator dosage selection method by restoring ΔT_c of the rejuvenated binder. ΔT_c is the difference between two continuous low temperatures determined by stiffness and m-value from the BBR binder test. The value of ΔT_c decreases after aging (more negative), a minimum value of -5°C is recommended to ensure adequate thermal cracking resistance after long-term aging, thus the optimum rejuvenator content should restore the ΔT_c of the RAP binder to -5°C. On the other hand, Im et al. developed an initial rejuvenator dosage selection method using the low PG temperature and the Glover-Rowe (G-R) parameter measured after long-term binder aging [81]. This initial rejuvenator dosage considered both the low-temperature performance and durability of the binder. A recently published NCHRP report recommended the use of high PG as the rejuvenator dosage optimization criterion and determine the "slope rate" as the capacity of reducing the high PG of the recycled binder blend to a target value [82]. Some researchers only construct the blending charts of rejuvenator dosages and high PG temperatures of the recovered RAP binder to choose the optimum rejuvenator dosage [62,83]. This approach may result in an excessive rejuvenator content, which can make the mix prone to rutting distress.

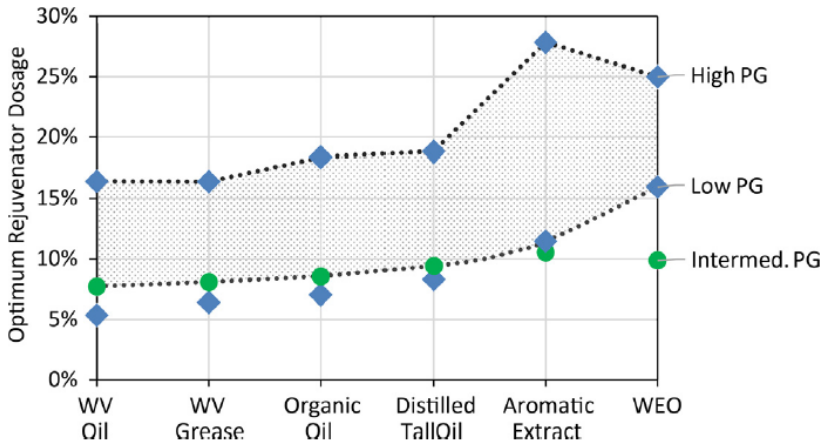

Figure 2.13 Optimum rejuvenator dosage to achieve the PG of virgin asphalt binder (PG 64-22) [84]

In conclusion, it is recommended to ascertain the proper rejuvenator dosage before applying it in actual practice. Although the optimum rejuvenator dosage can be determined by blending chart, the addition of a rejuvenator requires extra attention when a softer virgin asphalt binder or severely aged asphalt materials (e.g., RAS) is used, which may require less or more rejuvenator content. Proper amount of rejuvenator is the premise for desirable short- and long-term rejuvenating effects.

2.5 Rejuvenating effects in previous studies

2.5.1 Rejuvenating effects on binder properties and mixture performances

Zaumanis et al. [60] compared the rejuvenating effects of six different rejuvenators to produce a 100% recycled asphalt mixture. These six rejuvenators were aromatic extract, waste engineered oil (WEO) waste vegetable oil (WVO), waste vegetable (WV) grease, distilled tall oil, and an organic oil called Hydrogreen S™. In general, all those rejuvenators can restore the rheological properties of the RAP binder and present a greater sum of PG than virgin bitumen (PG 64-22). The organic-based rejuvenators outperformed the petroleum-based rejuvenators in terms of workability and fatigue resistance, and WEO showed the least rejuvenating effect among all these products, which may be caused by incompatibility with the asphalt binder.

Chen et al. [25] used waste edible vegetable oil (WEVO) as a rejuvenator to evaluate their rejuvenating effects on different asphalt binders. This rejuvenator can restore the physical and rheological properties of different binders to the level of the virgin asphalt binder at different optimum dosages. However, the rejuvenating effect on aged SBS-modified asphalt binder, which showed greater ductility at the virgin state compared to the other two virgin asphalt binders, needs more investigation on the low-temperature properties. Moreover, Chen et al. [64] compared the waste cooking oil, cotton seed oil, and a commercial rejuvenator by evaluating the impact of rejuvenators on the high-temperature properties of asphalt binder. The results indicated that waste cooking oil and cotton seed oil achieved a more significant softening effect than those commercial products, and easily reduced the high PG of age asphalt binder (94℃ or 100℃) to the target value (64℃). Hereafter, Cao and Chen ta al. [32] investigated the rejuvenating effect on SBS-modified asphalt binder by using four different rejuvenators, cashew shell oil, vacuum stream oil, corn oil, and waste engine oil. These four rejuvenators could soften the aged SBS-modified binder in terms of reducing the viscosity, fatigue factor ($G^*\sin\delta$), and rutting factor ($G^*/\sin\delta$). However, the rejuvenated binder with the addition of cashew shell oil showed the least temperature sensitivity changes and increase of crossover temperature (crossover point of loss modulus and storage modulus) after long-term aging, compared to other rejuvenators and the aged SBS modified binder, denoting that the binder rejuvenated by cashew shell oil has the best anti-aging performance.

Mogawer et al. conducted a series of research to investigate the rejuvenating potential of different products, including commercial products, light oils, and bio-binder, to offset the reduced workability and fatigue performance caused by high RAP and/or recycled asphalt shingles (RAS) content. In 2013, they

evaluated three commercial rejuvenators (BituTech RAP, SonneWarmix RJT, and SonneWarmix RJ) from different suppliers by introducing them into the virgin bitumen first and then blending them with virgin aggregates and recycled materials. All these commercial rejuvenators mitigated the increased stiffness and cracking susceptibility attributed to the high content of RAP and/or RAS, however, they might increase the sensitivity to rutting and moisture damage [56]. Therefore, a more reasonable procedure should be developed to determine the optimal dosage of rejuvenator, instead of following the manufacturers' recommendation. Nazzal and Mogawer et al. [85] tried three different light oils (paraffinic oil, and two organic oils) as rejuvenators in high RAP content mixtures. The addition of those oils softened the recycled blend (RAP binder and virgin binder) and changed the PG of this blend from PG 70-22 to PG 64-28. Although the incorporation of rejuvenators notably increased the fatigue life of recycled mixtures containing 50% RAP, it had a negative impact on rutting performance and moisture resistance. In 2016, Mogawer et al. [55] selected a bio-binder which is derived from swine manure to manufacture the bio-modified asphalt binder and produce the high RAP content mixture (40%). The mixture test results proved that the addition of this bio-modified binder can decrease the stiffness of the RAP mixture with neat bitumen, as well as the susceptibility to fatigue cracking, and increased the workability of the RAP mixture. In addition, the RAP mixture with bio-modified binder showed similar rutting resistance and moisture susceptibility to the control asphalt mixture without RAP, and no stripping inflection point (SIP) was observed in the wheel tracking test.

Elkashef et al. [86,87] investigated the rejuvenating effect of the rejuvenator derived from soybean oil by adding this rejuvenator into virgin bitumen to produce a modified binder, then blended with RAP binder and RAP, which provided a complete evaluation of the low-temperature cracking resistance and fatigue performance in both rejuvenated binder and mixtures. The result suggested that the addition of bio-modified bitumen showed significant improvement in thermal cracking resistance and fatigue cracking resistance, and the aging rate of the rejuvenated binder sample was lower than that of the RAP binder.

Cavalli and Zaumanis et al. [88] tested three commercial bio-based rejuvenators which were made of natural seed oil, cashew nutshell oil, and tall oil respectively, to investigate both the rejuvenating effect and the impact of aging on rejuvenated RAP binder. They reported that all these rejuvenators performed well in restoring the mechanical properties of RAP binder at both high- and low-temperature ranges. Some rejuvenated binders, however, were more susceptible to the impact of aging, as the cracking temperatures significantly increased compared to those of the virgin and RAP binders. Therefore, it is critical to consider

the impact of aging when rejuvenators are applied, which can affect the long-term performance of rejuvenated asphalt binder and mixture.

Zhang and Jiang et al. [89,90] manufactured a self-developed rejuvenator, composed of rubber oil, plasticizer and surface-active agent (antiaging agent) at a ratio of 100:10:2 (or 100:9:1), and compared the rejuvenating effect with two commercial rejuvenators. These three components were mixed by high shear mixing method to reach a target viscosity (60°C) of those two commercial rejuvenators. The results showed that the developed rejuvenator restored the properties, like penetration, softening point, ductility, and viscosity, to the level of the virgin bitumen, and exhibited similar values of the rheological parameters, including complex modulus (G*) and rutting parameter (G*sinδ), to those of the virgin bitumen, which indicated a similar rejuvenating effect to those two commercial rejuvenators. Moreover, the rejuvenated binder by adding the developed rejuvenator showed enhanced elastic recovery than those were rejuvenated by commercial rejuvenators, and all three rejuvenated binder samples showed improved low-temperature cracking resistance compared to the virgin bitumen [90]. As for recycled asphalt mixtures, the addition of RAP (35% and 50%) increased the stability at a higher temperature and reduced the low-temperature cracking resistance and fatigue performance. Those performances can be restored by adding two different rejuvenators but not to the level of the conventional asphalt mixture, and the self-developed rejuvenator exhibited a slightly better rejuvenating effect than the commercial rejuvenator [89].

2.5.2 Rejuvenating effects characterized by chemical analysis and micro morphology

Despite the bulk properties characterized by binder rheological tests and mix performance tests, chemical analysis and micromorphology characterization methods are also adopted by pavement engineers to investigate the rejuvenating effect and mechanism. Since the changes in micro-scale properties, including the functional group intensity, the chemical components, the surface morphology, the bonding and adhesive strength, and the molecule size etc., are related to the macro properties that are evaluated to meet specific requirements [28,62]. Therefore, there is an increasing interest in evaluating the rejuvenating effects by various micro characterization methods because less material, personnel, and cost are needed for these tests. Table 2.4 summarized the most used micro-scale characterization methods in evaluating the rejuvenating effects.

Table 2.4 Rejuvenating effects investigated by chemical analysis and micro characterization methods

Methods	Purposes	Characterizations of rejuvenated binder blends	References
FTIR	To detect the intensities of different functional groups	The intensities of carbonyl (C=O) and sulfoxide (S=O) groups increase with aging and decrease with rejuvenation. $I_{C=O} = \frac{\text{Peak area (C=O)}}{\text{Peak area } (CH_3 \text{ and } CH_2)}$ $I_{S=O} = \frac{\text{Peak area (S=O)}}{\text{Peak area } (CH_3 \text{ and } CH_2)}$	Chen et al., 2014. Ongel & Hugener, 2015.
SARA analysis	To determine the factions of four chemical components	The ratio of asphaltenes and maltenes increases with aging due to the volatilization of light components. Colloidal stability index $= \frac{\%\text{asphaltenes} + \%\text{saturates}}{\%\text{reins} + \%\text{aromatics}}$	Zhang et al., 2019. Menapace et al., 2018.
AFM	To investigate the surface morphology and micro mechanical properties	Aging and addition of rejuvenators will change the morphologies and mechanical properties of the domain structures (i.e., bee-structure) and the matrix.	Cavalli et al., 2018. Menapace et al., 2018. X. Yu et al., 2014.
GPC	To capture the molecule weight distribution	Aging and addition of rejuvenators will affect the LMS (%) due to the change of the ratio between large and small molecule components. LMS (%) $= \frac{\text{area of molecule size} > 3000 \text{ dalton}}{\text{total area of distribution curve}}$	Cavalli et al., 2018.

Note: FTIR (Fourier-transform infrared spectroscopy), SARA (saturates, aromatics, resins and asphaltenes), AFM (Atomic Force Microscope), and GPC (Gel permeation chromatography)

Among these methods, the parameters derived from FTIR and GPC were reported to have a linear relationship with the bulk property parameters of asphalt binder [49,51,62], which can be used to identify the rejuvenating effect. With respect to SARA analysis results, the fractions of four components are more sensitive if the major components in the rejuvenator are aromatics and resins. It, nevertheless, can be used for evaluating the aging resistance of rejuvenated asphalt binders by determining the volatilization of light components. As for AFM results, the changes in surface morphology are complex due to the different types of virgin asphalt binders and rejuvenators. A third phase which is different from the domain structures (bee structure) and matrix was detected after rejuvenation by previous research [27,91]. Furthermore, the micromechanical properties derived from AFM (e.g. stiffness and adhesive strength) are not always

consistent with the macro bitumen properties (e.g. dynamic modulus), as it only measures the surface of asphalt binder samples [28].

2.6 Factors affecting rejuvenation effectiveness

The rejuvenating effect depends on the RAP and rejuvenator properties, including the types of rejuvenators, the dosages of the rejuvenators, the performance grades of the virgin asphalt binder, the source of RAP or aging history of RAP, and the incorporation method of rejuvenators. All these factors should be considered when using rejuvenators in the high-content RAP mix.

2.6.1 Rejuvenator composition

The addition of rejuvenators will change the fractions of chemical components in the aged asphalt binder, the chemical alterations lead to bulk physical property restorations. Zaumanis et al. [60] reported the use of organic-based rejuvenators, in which the major components are fatty acids, generally had better rejuvenating effectiveness than petroleum-based rejuvenators like aromatic extracts and WEO with more polar molecules. Cao et al. also found that cashew nutshell oil, containing aromatic derivatives with weak polarity, had the best softening effect on aged SBS-modified binder compared to two other rejuvenators, WEO and vacuum stream oil [32]. The major components of WEO are unsaturated hydrocarbons and resins with a higher polarity, while the dominant fraction in vacuum stream oil is non-polar straight-chain hydrocarbons. The result is contrary to previous conclusions that the less viscous rejuvenator was considered to have a better softening effect [24], as the vacuum stream oil showed lower viscosity than cashew nut shell oil. Therefore, in addition to the physical properties (e.g., viscosity) of the rejuvenator, the polarity and the molecular structures also affect the rejuvenating effects. Therefore, the difference in rejuvenator composition results in various diffusion capacities and compatibilities with asphalt binder [23]. Cong et al. [92] compared two types of rejuvenators in terms of the diffusion rate in the aged asphalt binder. They claimed that the agent with higher aromatic content showed a higher diffusion rate at the same temperatures. Due to the colloidal structure of asphalt binder, in which the highly polar asphaltene phase is dispersed in the maltene phase; compatibility refers to the balance between soluble and insoluble fractions in the colloid, which controls the flow properties. Incompatible (insoluble) components in rejuvenators can reduce the rejuvenating efficiency, increase the diffusion time, and result in oils migrating toward the pavement surface [29]. The poor compatibility of WEO and the aged asphalt binder was indicated in the previous research which resulted in an increased mass loss after aging [60].

2.6.2 Recycled material properties

The properties of RAP materials, including the degree of aging (stiffness of the aged asphalt binder) and the gradation of the RAP material, especially amount of the fine particles affect the optimum rejuvenator content and the mixture's workability. As discussed in section 2.4.2, the optimum dosage of the rejuvenator is related to the PG of the aged asphalt binder. Stiffer asphalt binder would require a higher amount of rejuvenator to lower the viscosity and restore the rheological properties. Mogawer et al. [56] indicated that the same dosage of rejuvenator had better rejuvenating effects in recycled asphalt mixture containing RAP compared to RAS, as the asphalt binder in RAS is more aged and stiffer than the RAP binder and needs a higher amount of rejuvenator to activate the aged asphalt binder. Furthermore, the fine RAP contains more aged asphalt binder than the coarse RAP because of the larger surface area. It is good mentioning that, an excessive amount of fines affects the binder ratio, air voids and other volumetric properties in the recycled asphalt mixtures during the mix design process [29,67].

2.6.3 Rejuvenator incorporation methods

According to the literature, there are two main rejuvenator incorporation methods: (1) mixing the rejuvenator with the virgin asphalt binder and manufacturing a modified binder, and (2) mixing the rejuvenator with RAP before blending with other raw materials (e.g., virgin asphalt binder and aggregates). The first method was widely used for bio-based products to produce a bio-modified binder function as a “softer binder” [55,86]. Yu et al. [16] recommended spraying the rejuvenator to the preheated RAP, and then mix with aggregates and virgin asphalt binder, which was expected to lead to a better rejuvenating effect by providing direct contact between the rejuvenator and the RAP, subsequently increasing the diffusion. However, adding rejuvenators directly to RAP might not show significant improvements if the rejuvenators are only added to RAP at room temperature and just prior to mixing, because diffusion and RAP binder activation is not likely to accomplish within limited time and ambient temperature conditions [93]. Rathore and Zaumanis compared three rejuvenation incorporation methods, spraying on RAP with 2 hours rest period, spraying on RAP with 24 hours rest period, and pre-blended with the virgin binder, but none of these methods showed a statistical difference between each other or a significant impact on the mix and binder testing results [94]. In addition, increasing the mixing time and temperatures will enhance the diffusion rate of rejuvenators into aged asphalt binder, which in turn makes the RAP binder more flowable to blend with virgin asphalt binder and coat the aggregates [23].

2.7 Rejuvenation incorporation in asphalt plants

The current practice is lack of experience in incorporating rejuvenators in asphalt plant as the conventional plant design does not consider the rejuvenator application. There are different potential and applicable methods of incorporating rejuvenators in the plant mixing process [78,95,96]:

- Pre-blend into the virgin asphalt binder in the separate asphalt tank.
- In-line into the virgin asphalt binder using an additive pump.
- Spray on RAP during RAP processing, on the RAP conveyor belt (see Figure 2.14), or at the RAP drum inlet.
- Inject into the pugmill or mixing drum.

Figure 2.14 Rejuvenator spraying nozzles on the RAP conveyor belt [78]

In traditional drum mix plants, the rejuvenator is usually fed with the virgin asphalt binder (see Figure 2.15 (a)). The drawbacks of this method are that the rejuvenator cannot have full contact with RAP and that the virgin asphalt binder may not fully blend with RAP and virgin aggregates. Shao et al. [97] developed a double drum mixing method to rearrange the material feeding sequence. As shown in Figure 2.15 (b), this method divides the virgin asphalt binder into two parts and the rejuvenator and RAP will be mixed first before blending with the aggregates and half virgin asphalt binder. The mixture testing results suggested that the hot recycled asphalt mixture showed improved performance and reduced air voids compared to their counterparts produced by the traditional mixing method. The new mixing process, however, requires one more mixing drum and two independent devices for feeding virgin asphalt binder, which will increase the cost and complicate the mixing process.

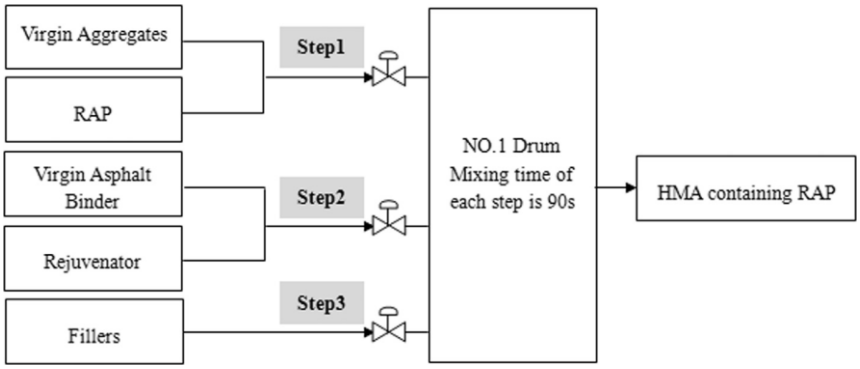

(a) Single drum mixing

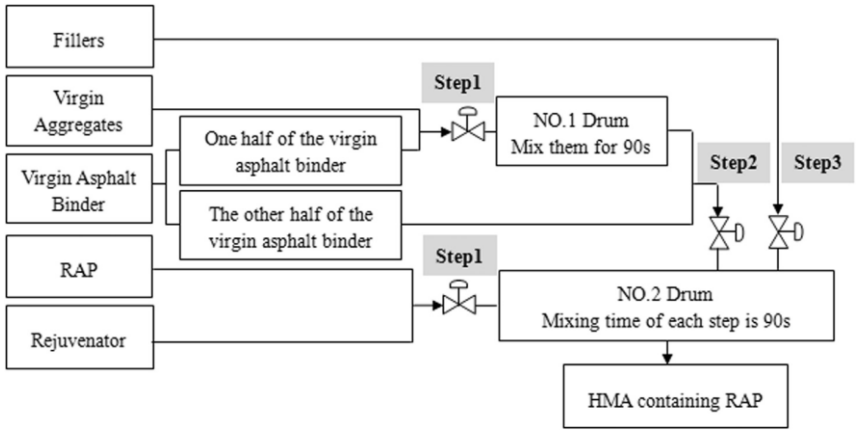

(b) Double drum mixing

Figure 2.15 The schematic setup of the two mixing processes [97]

Zaumanis et al. [95] compared different rejuvenator addition locations in batch asphalt plant and their impact on plant exhaust gas emissions, the performance of recycled asphalt mixtures, and rejuvenating effectiveness (e.g. degree of blending, rejuvenator homogeneity, and rejuvenator loss). Figure 2.16 depicts the potential rejuvenator addition locations in a batch asphalt plant, which can be categorized as adding the rejuvenator to RAP before drying/preheating the RAP, adding the rejuvenator to RAP after drying/preheating the RAP, and adding the rejuvenator with virgin bitumen. The author recommended two promising locations for further study, the conveyor belt and dryer outlet chute (or plant mixer). And the gas emissions of RAP mix production on these two rejuvenator addition locations are equal, while the RAP mix with rejuvenator addition on the conveyor belt exhibited higher fatigue resistance. Meanwhile, based on the test results of the rejuvenated binder recovered from mixes collected at different plant locations, applying the rejuvenators before or after the heating drum shows no influence on the mechanical performance and chemical compositions of the recovered binder [96]. Therefore, it indicated that there is

no negative effect of an early rejuvenator addition on RAP if the rejuvenator dosage is precisely controlled. The work is conducted in a certain batch asphalt plant, the optimum adding location might be different for other plant types although the rationale behind it can be prevalent for any plant mixing process. Therefore, a lab rejuvenator addition procedure which can simulate the asphalt plant scenario should be established to provide instructions on rejuvenator incorporation methods on specific projects.

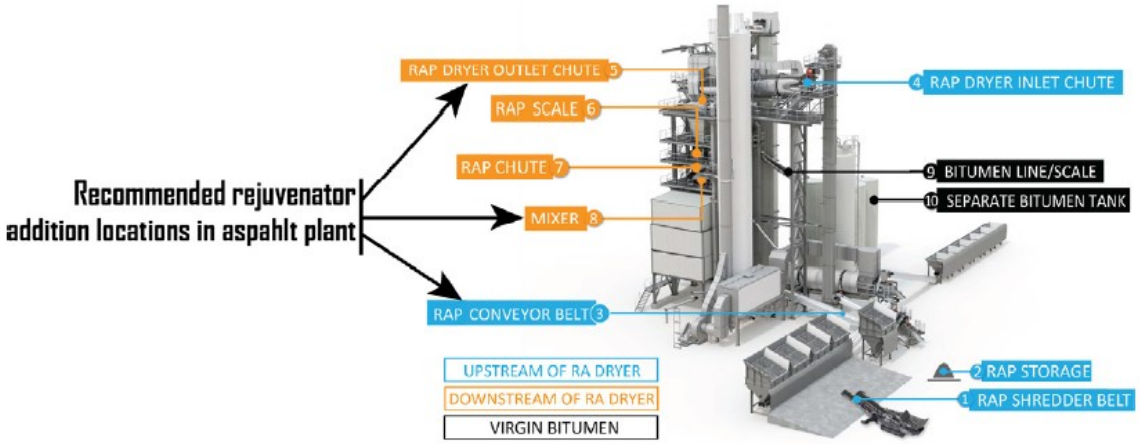

Figure 2.16 Rejuvenator addition locations [95]

There are limited investigations on plant-produced high-content RAP by using rejuvenators, which may discourage agencies from using rejuvenators. The way adding a rejuvenator to RAP during mixing in the asphalt plant impacts the rejuvenator distribution, the activation of RAP binder, and the virgin asphalt binder content, thus affecting the performance of RAP mixtures. To fulfil the use of a rejuvenator and produce sustainable high-content RAP mixtures, a thorough investigation of the rejuvenator incorporation method should be conducted before plant-scale production.

2.8 Summary of literature review

This chapter reviews the current practices and research which aimed to produce recycled asphalt mixtures containing high-rate RAP. Increasing the existing cap of the maximum rate of RAP incorporation in new asphalt concrete mixes, even up to 100%, can offer great advantages by saving non-renewable resources (e.g., petroleum-derived asphalt binder and mineral aggregates), reducing fuel consumption, and minimizing greenhouse gas emissions. However, increasing the RAP content historically arises some concerns regarding workability and cracking resistance due to the stiff RAP binder and insufficient blending. The application of rejuvenators is reported as a feasible solution to produce sustainable recycled asphalt mixtures, which aims to restore the RAP binder properties to resemble those of the virgin asphalt

binder. The concept of rejuvenation in asphalt binder does not refer to the restoration of the aging process but to producing a rejuvenated asphalt binder to meet the mix design specification. The consummation of the rejuvenation process is when the rejuvenator diffusion completes and the whole RAP binder film reaches an equilibrium state. The rejuvenated asphalt binder, therefore, can be separated from RAP aggregates and blended with virgin materials. The degree of blending is a critical index for recycled asphalt mixture, which is considerably affected by both internal and external factors, like the diffusion rate, the mixing temperature, and the mixing time. Generally, a partial blending scenario exists in RAP mixtures, in which only part of the RAP binder is activated, and the rest is still coating on RAP aggregates. Determining the degree of blending is essential to guarantee the rejuvenating effectiveness and the selection of proper bitumen content in recycled asphalt mixture.

Currently, many potential products have been investigated as rejuvenators, which are of different sources, consist of different components, and exhibit varying rejuvenating effects. Selecting the proper rejuvenator type and optimum dosage is important to ensure the rejuvenating effectiveness, as incompatible products and excessive rejuvenator content can lead to loss of adhesion between bitumen and aggregates, while the inadequate dosage will result in the "black rock" problem. Rejuvenators have been proven to improve the workability, thermal cracking resistance, and fatigue performance of high-content RAP mixtures, while extra attention should be paid to verifying the rutting and moisture susceptibility of mixes. Furthermore, the application of micro characterization methods provides a better understanding of the rejuvenation mechanism and effectiveness at a micro-scale. These methods require smaller sample sizes and provide more precise results. By establishing relationships between the micro properties and the bulk properties measured by the conventional binder and mixture tests it is prospected to be able to predict the rejuvenating effect by limited materials and tests. In addition to the rejuvenator composition and dosage, the material incorporation approach and the mixing conditions also impacts the performance of the final mixtures, the influence of those factors is more significant during the plant mixing stage.

Nevertheless, there are still more challenges in the application of rejuvenators that should be addressed. The following gaps are elucidated for further investigations:

- The rejuvenation mechanism is still not fully investigated, as the diffusion rate is more related to the viscosity and molecule size of the rejuvenator. However, a less viscous rejuvenator may not show better rejuvenating effects. Further investigation on the rejuvenator composition is needed for the selection of the right rejuvenators.

- The current optimum dosage selection method is based on the blending chart which provides the relationship between the rheological properties of recycled blend and the rejuvenator content. Therefore, different optimum dosages will be captured due to different rheological parameters used. There is a lack of a standard method to determine the optimum rejuvenator dosage. Moreover, the aging resistance of rejuvenated asphalt binders should be considered as a criterion to ensure long-term performance.
- There are limited models for a three-phase blend of rejuvenated materials (i.e., rejuvenator, RAP binder, virgin asphalt binder), whereas most of the studies use a two-phase interaction for the sake of simplicity. Further investigation to understand the actual interaction between these three different phases and their associated inter-transient zones is needed.
- The use of rejuvenators is proved to compensate for the loss in mixture workability and cracking resistance, while limited research has been conducted on the impact of rejuvenators on the long-term performance of recycled asphalt mixtures. Since cracking damage tends to occur after a long period in the field, the durability of recycled asphalt mixture is a premise to manufacture a sustainable high-content RAP mix.
- There are limited studies on rejuvenator addition in plant-scale hot recycled asphalt mixtures. The rejuvenator incorporation method in asphalt mixing plants concerning addition timing, addition location, consideration of rejuvenator loss, and homogeneity needs to be determined in specific plant types, RAP fractions, and the mix design.
- Most of the studies published to date have investigated the properties of rejuvenator-binder blends and rejuvenated mixes immediately or shortly after rejuvenation. However, it is of utmost importance to characterize the sensitivity of rejuvenated blends and mixes to short- and long-term aging as well. Research on this area has been very limited and needs further investigation. To this end, studying the high-content RAP mixes through innovative mixture aging processes in the lab is also deemed necessary.

Chapter 3
Materials and methodology

This chapter illustrates the details of the materials, including the commercial rejuvenators, virgin asphalt binders, RAP, and virgin aggregates. The mix design of both the control mix with 20% RAP and the high RAP mix with 50% RAP is displayed in this chapter as well. The methodology depicts the sequential screening framework for evaluating the effectiveness of different commercial rejuvenators and optimizing the performance of rejuvenated high RAP content mixes within the lab testing scale.

3.1 Materials description

3.1.1 Virgin asphalt binders

Two virgin binders that are graded as PG 58-28 and PG 46-34 based on Superpave specifications were selected for this project. PG 58-28 asphalt is commonly used for producing asphalt paving materials in southern Ontario. Whereas the PG 46-34 is not separately used on its own and is chosen in this project as a very soft binder that could potentially act as a rejuvenator, counteracting the effect of increased RAP content in a new highly recycled HMA mix. Both binders were provided by the Imperial Oil Ltd. refinery located in Sarnia, Ontario. Table 3.1 lists the basic physical properties of these two virgin binders following the specifications in AASHTO M320 [98]. The continuous PG is the temperature when the asphalt binder achieves the same value as the grading criteria. For example, the continuous high PG temperature of the unaged asphalt binder is the temperature at which the measured $G^*/\sin\delta$ (G^* is the complex shear modulus and δ is the phase angle) equals 1.0 kPa.

Table 3.1 Performance grading results of virgin asphalt binders

Parameter	PG 58-28			PG 46-34			AASHTO M320 Specification
	Temperature [°C]	Test result	Continuous PG [°C]	Temperature [°C]	Test result	Continuous PG [°C]	
Continuous PG	60.8-31.8 (19.0)			49.7-36.9 (10.1)			-
Viscosity [Pa·s] (original)	135	0.267	-	135	0.147	-	< 3 Pa·s
	165	0.083		165	0.051		-
G*/sinδ [kPa] (original)	58	1.434	60.8	46	1.670	49.7	≥ 1.0 kPa
	64	0.662		52	0.725		
G*/sinδ [kPa] (RTFO aged)	58	3.459	61.4	46	3.877	49.9	≥ 2.2 kPa
	64	1.542		52	1.629		
G*sinδ [kPa] (PAV aged)	16	7323.294	19.0	10	5058.873	10.1	≤ 5000 kPa
	19	4960.940		13	3422.580		
Stiffness [MPa] (PAV aged)	-18	230.0	-31.8	-24	193.0	-36.9	≤ 300 MPa
	-24	476.5		-30	477.0		
m-value (PAV aged)	-18	0.320	-31.9	-24	0.362	-38.8	≥ 0.3
	-24	0.266		-30	0.286		

3.1.2 Rejuvenators

Figure 3.1 displays the seven commercially available products used in this project. They are derived from different sources or produced by different techniques. Due to confidentiality reasons, the names of the products cannot be shared with the public. Instead, these rejuvenators were labelled from A to G to simplify the nomenclature of the rejuvenated binder blends.

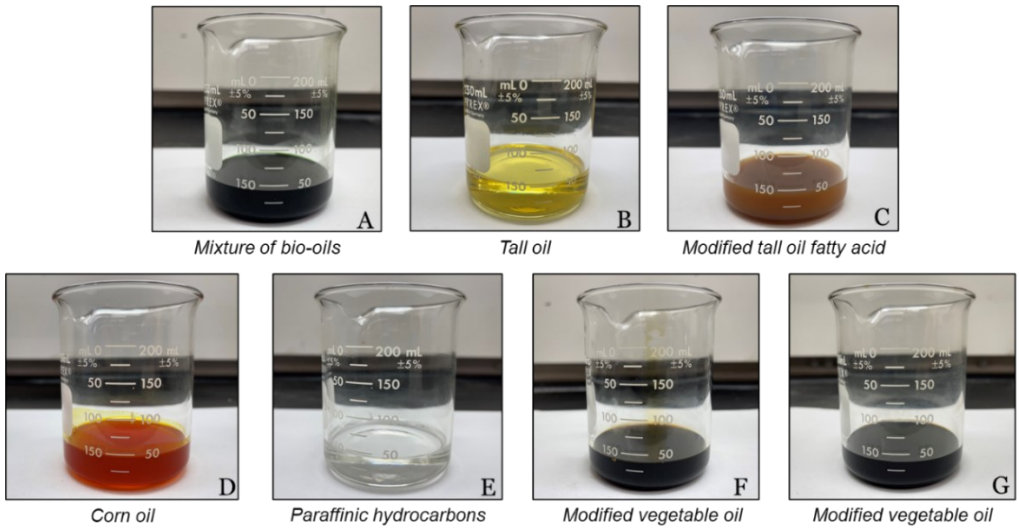

Figure 3.1 View of rejuvenators used in this study

Except for rejuvenator E, the other six products are all bio-based, in which the main components are vegetable oils or tall oils. Rejuvenator A is a mixture of bio-oils without any animal fats or greases. It is a dark green fluid that can be easily blended with asphalt binders or sprayed on RAP directly. Rejuvenator B and C are both derived from crude tall oil, a renewable raw material that is a by-product of the paper industry. B is a transparent yellow liquid, while C is a turbid amber liquid. Both the two rejuvenators are claimed to be manufactured by green technologies, non-hazardous, safe to handle, and sustainable. Rejuvenator D is made from 100% homegrown American corn, which is a light reddish to transparent orange oil. As stated in the product booklet, rejuvenator D has an RTFO mass loss of 3.8%, which will need attention regarding its thermal stability. Rejuvenator E is the only petroleum-based product in this project since several studies have claimed that petroleum-based rejuvenators perform worse than their bio-based counterparts with respect to softening efficiency, safety, and sustainability [20]. The reason to use this rejuvenator is to compare it with bio-based counterparts. Rejuvenator E and F were provided by the same supplier; both are dark and greasy liquids made from 100% modified vegetable oil. Table 3.2 shows the fundamental physical properties of each rejuvenator summarized from their safety data sheets or product brochures. In addition, other details of the rejuvenators, in terms of their composition, compatibility, and toxicity, were also summarized as illustrated in Table 3.3.

Table 3.2 Physical properties of rejuvenators

Basic Properties	A	B	C	D	E	F	G
Odor	Slight	Mild	Almost odorless	N/A	Petroleum	N/A	Slight sulfur
Boiling Point [°C]	N/A	> 300	> 200	N/A	> 230	N/A	N/A
Melting point [°C]	-14	N/A	0-10	N/A	N/A	N/A	N/A
Specific Gravity	0.918	0.927	0.95	0.98	< 1	< 1	< 1
Water Solubility	Insoluble	0.6 mg/L at 20°C	Insoluble	Immiscible	Insoluble	Insoluble	Insoluble
Flash Point* [°C]	> 204.4	279.4	> 190	> 250	> 93.4	> 250	> 200
Dynamic viscosity [Pa·s]	0.062 (75°F)	0.093 (20°C)	0.062 (20°C)	0.015 (60°C)	>0.018 (40°C)	0.09-0.11 (25°C)	N/A

* Except B (Cleveland Open Cup), the flash point of rejuvenators is determined via closed cup.

Table 3.3 Description of rejuvenators

Product	Composition	Stability and reactivity	Toxicity and carcinogen status
A	Bio-oils, amine (< 1%), surfactant (< 1%)	Oxidizing agents	Slightly hazardous Not a carcinogen
B	Polyol ester	Strong oxidizing agents	Not a carcinogen
C	Modified tall oil, fatty acids (≤ 5%), alkyl acid phosphates (≤ 2.9%)	Oxidizing and reducing materials	N/A
D	Modified corn oil, fatty acids	Strong oxidizing agents	Not classified
E	Paraffinic hydrocarbons	N/A	N/A
F	Modified vegetable oil	Strong oxidizing agents, strong acid	Low to no toxicity
G	Modified vegetable oil	Stable under prescribed the storage conditions	Not a carcinogen

3.1.3 Virgin aggregates and RAP

The virgin aggregates used in this study were supplied by a local asphalt plant, they were limestones obtained from the same quarry as the coarse and fine aggregate fractions, which were labelled as HL3 and AS. The nominal maximum aggregate size (NMAS) for the coarse aggregate and the fine aggregate were

12.5mm and 4.75mm, respectively. The single source RAP was collected from the same asphalt plant as the virgin aggregates, which had a NMAS of 12.5mm and a binder content of 4.3% (by weight of the RAP). The RAP binder was extracted and recovered in accordance with the Ontario lab testing manuals, LS 282 – Rev. No.33 [99] and LS 284 – Rev. No.34 [100], and was used for preparing the recycled and rejuvenated binder blends. The grading of the recovered RAP binder is different from that of the virgin binder. According to AASHTO M323 [101], the intermediate PG temperature and low PG temperature are determined using the RTFO residue of the recovered RAP binder since RAP has already been long-term aged. However, it is rational to treat the recovered RAP binder as a virgin component since the purpose of rejuvenation is to reuse RAP for HMA production; therefore, the RAP binder also undergoes both short- and long-term aging during the production and service life. Table 3.4 shows the grading results of the recovered RAP binder. The recovered RAP binder can be graded as a PG 88-16 asphalt with a continuous grading of 88.6℃-16.8℃ (33.1℃). Although the RAP binder had been aged in the field during its service life, the laboratory's long-term aging process still increased its continuous intermediate PG and low PG by about 2℃.

Table 3.4 Performance grading results of recovered RAP binder

Parameter	Sample condition	Test results
Viscosity @135℃ [Pa·s]	Original	1.125
Viscosity @165℃ [Pa·s]		0.314
Continuous PGH [℃]	Original	89.8
	RTFO aged	88.6
Continuous PGI [℃]	RTFO aged	30.3
	PAV aged	33.1
Continuous PGL (Stiffness) [℃]	RTFO aged	-21.8
	PAV aged	-20.7
Continuous PGL (m-value) [℃]	RTFO aged	-19.5
	PAV aged	-16.8

3.1.4 Rejuvenated binder blend preparation

The preparation of the rejuvenated binder blend followed the recommended procedure, including the material adding sequence, the blending temperature, and the stabilizing time, in a drafted AASHTO standard in NCHRP Report No.927 [82]. As illustrated in Figure 3.2, the binder blend preparation is conducted in the following steps:

(1) The base binder was preheated at 155°C in the oven until it was fluid enough, then a proper amount of the base binder was poured into a beaker.

(2) The required dosage of the rejuvenator was added to the liquid base binder at room temperature and hand-stirred using a spatula for 30 seconds.

(3) The binder blend was placed back in the oven at 135°C for one minute, then the preheated RAP binder was added to the blend and hand-stirred using a spatula for another 30 seconds.

(4) The beaker was placed on a hot plate at 135°C and the binder blend was mixed for 10 minutes using a blender at a rotational speed of 500rpm.

(5) After the blending, the binder blend was moved back into the oven setting for one minute.

In the blending procedure, the heating temperature of the base binder was selected as per the mixing temperature determined by the measured viscosities at 135°C and 165°C. According to the Ontario lab testing manual, the mixing temperature was calculated using interpolation when the base binder achieves the viscosity of 0.17 ± 0.02 Pa·s [102]. Since the rejuvenators are in liquid form at room temperature, so they can be added to a heated binder without extra preparation. The amount of rejuvenator was added as a 100% replacement of the base binder; therefore, the base binder content was reduced by the same amount of the added rejuvenator. It was recommended to perform the short-term binder aging and binder testing on the unaged binder blends immediately after the blending was accomplished to avoid additional re-heating, which could result in further aging.

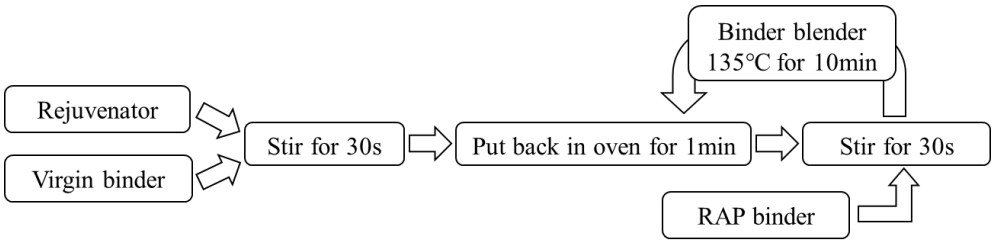

Figure 3.2 Blending protocol of rejuvenated binder blend

3.1.5 Mix design

The aggregate and mix passing percentages for each sieve size are shown in Table 3.5. The control mix was a Superpave 12.5mm mix with 20% RAP (i.e., R20), which has 35% coarse aggregates and 45% fine aggregates by weight of the total blended aggregates. The proportion of 20% was recognized as an allowable RAP amount that can be used in surface asphalt layers without changing the mix design procedure in Ontario. The job mix formula of the control mix was provided by the local asphalt plant and has already been used in pavement construction. This control mix is designed for the traffic category D in Ontario (OPSS 1151), which is applicable for major arterial roads and transit roads with a 20-year design ESALs between 10 and 30 million. As for the high RAP mix (i.e., R50), the RAP proportion was increased to 50% and the fractions of the coarse and fine aggregates were adjusted to maintain a similar gradation to the control mixture. Based on the results listed in Table 3.5 and the gradation curves are shown in Figure 3.3, the blended gradations of the two mixes are nearly identical, despite that the R50 mix has slightly higher fine content due to the increase of RAP fraction. However, they both meet the specification of SP12.5 according to the OPSS 1151 guide [10].

Table 3.5 Percent passing (%) of virgin aggregates and mix gradation

Sieve Size (mm)	Aggregate Fractions				Blended Gradation of Mixes		SP12.5 Specification
	HL3	AS	RAP Aggregate		SP12.5-R20	SP12.5-R50	
19	100.0	100.0	100.0		100.0	100.0	
12.5	95.8	100.0	97.8		98.1	97.9	90.0-100.0
9.5	65.4	100.0	87.0		85.4	85.4	28.0-90.0
4.75	4.1	98.1	65.7		59.0	59.9	
2.36	2.5	84.2	53.6		49.9	49.8	28.0-58.0
1.18	1.8	68.8	42.2		40.5	39.8	
0.6	1.4	52.0	31.6		30.7	29.9	
0.3	1.3	29.1	20.3		18.2	18.2	
0.15	1.2	10.1	13.0		8.3	9.5	
0.75	1.0	2.8	8.4		4.0	5.2	2.0-10.0
Specific gravity			Coarse	Fine			
G_{sb}	2.688	2.685	2.685	2.699	2.688	2.690	
G_{sa}	2.795	2.767	2.746	2.785	2.778	2.776	

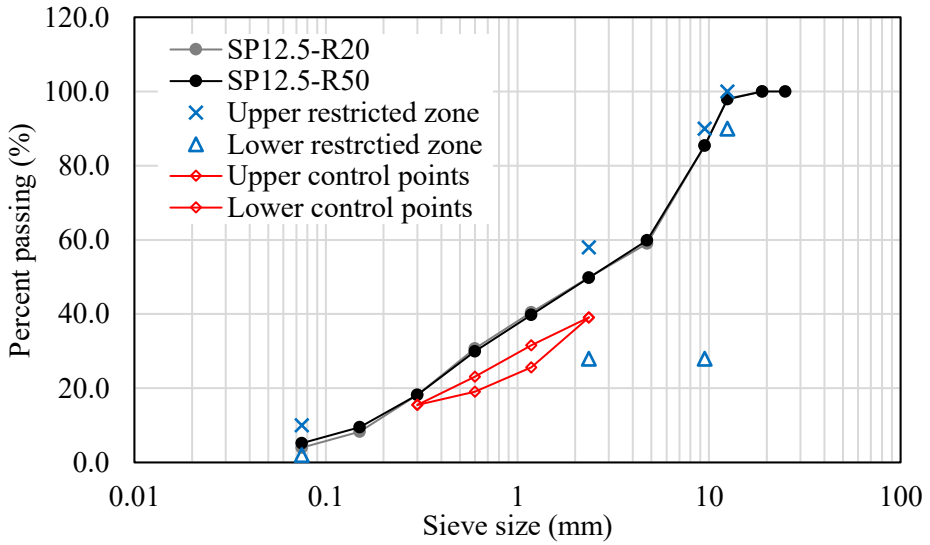

Figure 3.3 Mix gradation curves

3.2 Laboratory Testing

This section briefly illustrates the information on binder tests applied to the rejuvenated binder blends, including test devices, test conditions, sample conditioning, and measured parameters.

3.2.1 Asphalt binder extraction and recovery

The RAP collected from the asphalt plant was extracted and recovered using the centrifuge extraction method as per ASTM D2172 and the rotavapor recovery procedure as per ASTM D5404. Figure 3.4 shows the test setup for centrifuge extraction and rotavapor recovery. Dichloromethane was used as the solvent to extract the RAP binder from the RAP. Figure 3.5 displays the RAP before and after centrifuge extraction. Then the RAP binder was recovered from the excluded solution containing RAP binder and dichloromethane using the rotavapor recovery procedure. The procedure was performed under a vacuum condition using the oil bath at 140℃. A steady nitrogen flow with a speed of 500ml/min was applied to assure no oxidative aging occurs during the recovery.

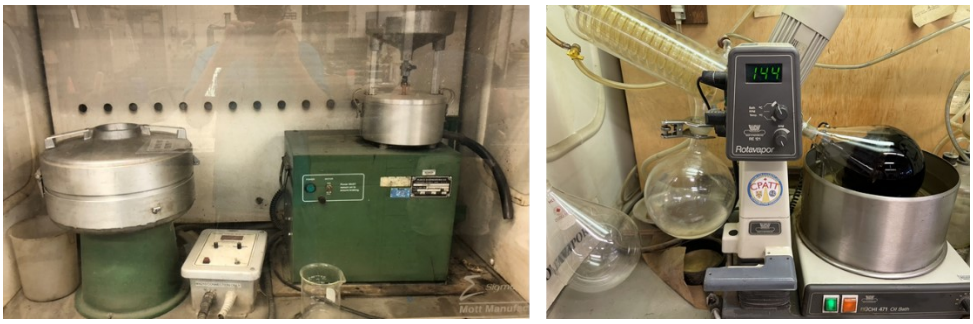

Figure 3.4 Centrifuge extraction and rotavapor recovery setup

(a) (b) (c)

Figure 3.5 (a) Oven-dried RAP, (b) Solvent soaking, (c) RAP aggregates after extraction

3.2.2 Asphalt binder conditioning

There are two asphalt binder conditioning methods which have been widely used for aging the asphalt samples before conducting different tests on them. The first conditioning applies the Rolling Thin Film Oven (RTFO) which uses hot air blowing to simulate the short-term aging of asphalt binder that occurs during mixing, storing, and transporting as per ASTM D2872 [103]. The conditioning procedure is conducted at 163℃ for 85 minutes, with an air flow of 4000 ± 200 ml/min blowing into the glass bottle which has a thin layer of asphalt binder (35 ± 0.5 g) attached to the inside wall. The second conditioning procedure uses a Pressure Aging Vessel (PAV) which applies a pressure of 2.1 MPa on the asphalt binder (50 ± 0.5 g) distributed in a metal pan for 20 hours. The test temperature was selected as 100℃ for a PG 58-28 climate region according to ASTM D6521 [104]. The procedure should be performed on samples that have been RTFO aged. Figure 3.6 shows the sample preparation for the PAV procedure and the standard conditioning time is 20 hours.

(a) (b) (c)

Figure 3.6 (a) Metal pan with RTFO aged binder, (b) Sample rack, (3) Pressure vessel

3.2.3 Asphalt binder testing

Table 3.6 depicts the binder testing used in this study to evaluate the rejuvenating effectiveness of rejuvenated binder blends. From the information listed in the table, viscosity measured at 135°C and 165°C were used as an indication of the fluidity of the binder blends, which is important for the workability of the binder blends during mixing and compaction. The complex shear modulus (G*) and phase angle (δ) measured from the were used for determining the continuous high PG temperature (PGH) and the continuous intermediate PG temperature (PGI). While the continuous low PG temperature (PGL) was selected from the higher value (less negative) between the PGL determined by the creep stiffness (PGL_S) and the PGL determined by the m-value (PGL_m) which is the slope of the creep stiffness against time curve. Both creep stiffness and m-value were obtained at 60 seconds.

Table 3.6 Binder testing information

Test device	Binder condition	Measure parameters	Standard
Rotational viscometer (RV)	Unaged	Viscosity	AASHTO T316
Dynamic Shear Rheometer (DSR)	Unaged RTFO aged PAV aged	Complex shear modulus (G*), Phase angle (δ)	AASHTO T315
Bending Beam Rheometer (BBR)	PAV aged	Creep stiffness, m-value	AASHTO T313

The crossover temperature of the asphalt binder was determined when the phase angle of the asphalt binder equals 45° at the intermediate temperature range. The test procedure follows the Ontario lab testing manual LS-319 [105], which measures the phase angle of the PAV aged asphalt binder at four test

temperatures and different train levels (see Table 3.7). Then, the crossover temperature is calculated by the linear interpolation of those phase angles tested at different temperatures when the phase angle equals 45°.

Table 3.7 Test conditions for determining the crossover temperature

Temperature (°C)	Strain (%)	Agular frequency (rad/s)
PGI	1.0	10
PGI - 3	0.5	10
PGI - 6	0.2	10
PGI - 9	0.1	10

3.2.4 Asphalt mix testing

The preliminary mix tests conducted in this study were the Hamburg Wheel-Tracking (HWT) test and the Indirect Tensile Asphalt Cracking Test (IDEAL-CT). HWT was used for evaluating the rutting and moisture resistance of the asphalt mixes according to AASTHO T324 [106]. The test setup is shown in Figure 3.7. two pairs of cylinder samples (63 mm in height and 150 mm in diameter) were assembled in the moulds, which are put under two wheel-tracking sides. The samples were saturated in the heated water tank, which also controls the test temperature. An LVDT device was used to measure the depth of the impression along the wheel-tracking path (rut depth). The rut depth from each side was monitored and measured at least every 400 passes using a data acquisition system.

Figure 3.7 HWT test setup

As for the IDEAL-CT setup shown in Figure 3.8, the cylinder sample (62 mm in height and 150 mm in diameter) was loaded with a monotonic loading using the Material Testing System (MTS) loading frame placed in an environmental chamber. The test temperature is 25°C and the loading speed is 50 mm/min according to ASTM D8225 [107]. The test completes when the sample was fractured along the loading line and the load versus load-line displacement (LLD) data were recorded for determining the peak force, failure work, and post-peak slope for data analysis.

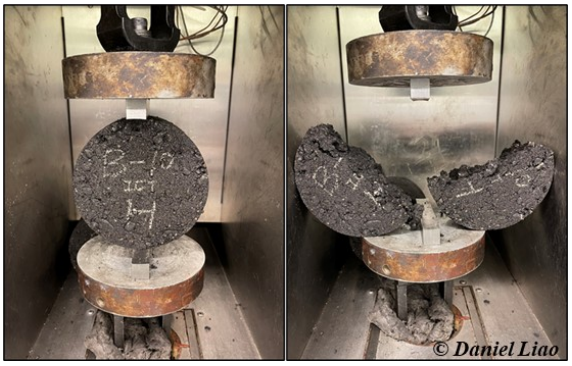

Figure 3.8 Indirect Tensile Asphalt Cracking Test (IDEAL-CT) setup

Dynamic modulus test was performed on cored cylindrical samples (150 mm in height and 100 mm in diameter) using frequency sweep mode under stress control mode, following AASHTO T342 [108]. These tests were carried out using the MTS loading frame and environmental chamber under a sinusoidal cyclic compressive loading. Sample response, when subjected to cyclic compressive loading was measured using three extensometers attached at 120º intervals at mid-height of the samples (see Figure 3.9).

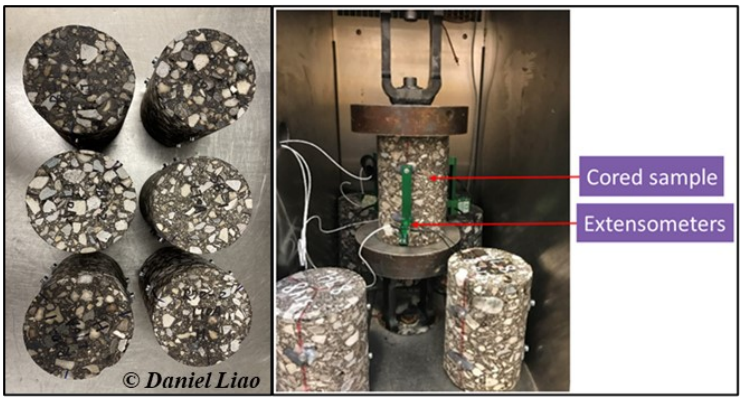

Figure 3.9 Dynamic modulus test setup

The details of sample preparation, test conditions, and data analysis methods will be clarified in the corresponding methodology section in each chapter.

3.3 Methodology

The global objective of this research is to provide a proper optimization procedure for applying rejuvenators in maximizing the allowable RAP content in hot mix asphalt (HMA). To reach this goal, two subtasks were defined as follows.

- To evaluate the impact of commercial rejuvenator products and one soft binder through Superpave binder testing specifications and then selecting proper rheological indices to optimize the rejuvenator dosage via blending chart method and factorial experimental design method.
- To apply practical and quick asphalt mix performance tests and non-destructive tests to examine the rutting and cracking resistance and the rheological behavior of high RAP mixes prepared with rejuvenators and soft binder at both short- and long-term conditioning protocols.

This section will elaborate on the details of the sequential screening framework and the selected experimental and data analysis methods to accomplish the task targets. Figure 3.10 illustrates the research methodology in a flow chart. The literature review study and material collection task have been elucidated in Chapter 2 and Chapter 3. The review of previous work has shown the limitations on the applications of rejuvenators in asphalt mixes containing high RAP contents:

(1) Lack of standardized and/or systematic procedures to evaluate the rejuvenator's effectiveness.

(2) No agreement on the selection of optimization criteria and methods for determining the proper rejuvenator dosage.

(3) Lack of performance testing specifications and performance indicators to assess and balance the performance of high RAP asphalt mixes, especially when the partial blending scenario exists in the discarded mixes.

(4) Limited research on the long-term performance of the high RAP mixes prepared with optimized rejuvenator contents.

Together with the experimental materials presented in Chapter 3, the rest chapters will target pursuing the optimized use of commercial rejuvenators in producing outperformed and sustainable high RAP mixes

on a laboratory scale. There are four major tasks established in this thesis which are elucidated in the flow chart as shown in Figure 3.10:

- Task 1 (Chapter 4): To propose a systematic approach to select the proper rejuvenator using different rheological parameters over a full temperature range from mixing and compaction to the in-service pavement stage. The outcome of this task will screen out the products showing worse regeneration capacities in resorting to the rheological properties of binder blends containing high RAP binder replacement.
- Task 2 (Chapter 5): To determine the optimal rejuvenator dosage through blending chat method and factorial DOE process and recommend the proper rheological indices as optimization criteria. The outcome of this task is for calculating the optimal rejuvenator dosage which enables the rejuvenated binder blends to have adequate cacking resistance without compromising the resistance to permeant deformation at high temperatures.
- Task 3 (Chapter 6 and 7): To evaluate the rutting resistance, moisture susceptibility, and cracking resistance of high RAP mixes containing optimized rejuvenator dosages determined from Task 2. Also, this task aims to consider the effect of extended conditioning time on the mix performance by considering continued blending and diffusion occurring at an elevated temperature atmosphere. The findings derived from this task will continue to screen out the rejuvenated high RAP mixes with poor rutting resistance and moisture susceptibility. At the same time, the use of various performance indicators is promising to assure the mixes with balanced performance in terms of restored cracking tolerance and adequate resistance to permanent deformation.
- Task 4 (Chapter 8): To characterize the rheological behavior of the selected rejuvenated asphalt mixes using a dynamic modulus test which is conducted at different temperature and frequency combinations. Also, this task covers the investigation of the long-term aging effect on the properties of asphalt mixes. The conclusion from this task will benefit in predicting the field performance from a long-term perspective.

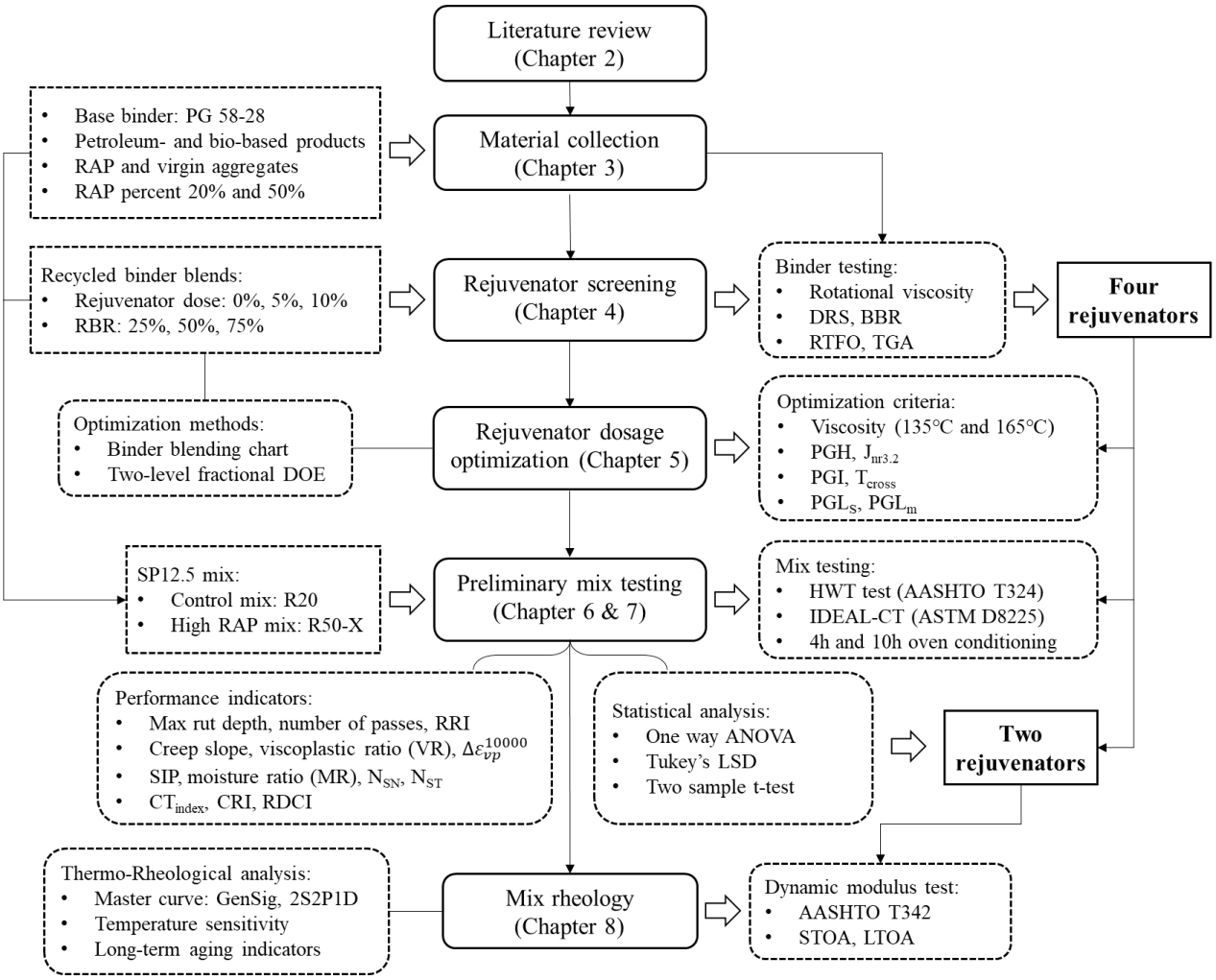

Figure 3.10 Flow chart illustration of research methodology

Chapter 4

Preliminary evaluation of rejuvenators for high RAP binder ratio blend

This chapter is modified based on an extended abstract that was accepted for presentation in the 76th RILEM Annual Week and International Conference on Regeneration and Conservation of Structures (ICRCS 2022), Kyoto, Japan. The conference presentation is entitled "A Systematic Approach to Evaluate the Efficacy of Different Rejuvenators for Regenerating Reclaimed Asphalt Cement". The purpose of this chapter is to screen the candidate rejuvenators by their restoration capacities using binder testing methods, comparing them to the target virgin binder and the binder blends with soft binder replacement.

4.1 Introduction

Rejuvenators have become popular to boost the use of Reclaimed Asphalt Pavement (RAP) in hot mix asphalt (HMA) production. A rejuvenator is a chemical product, usually containing low-viscosity oil fractions, which can rebalance the chemical fractions in reclaimed asphalt binder. Rejuvenators have the potential to restore the performance of the aged binder to be comparable with the virgin asphalt binder [2] and facilitate the diffusion between virgin and aged asphalt binder [109]. Typically, the rejuvenators are evaluated in terms of their ability to restore the high-temperature properties of the aged binder. However, a proper understanding of the impact of different rejuvenator types and dosages requires investigating both high- and low-temperature properties. Due to the lack of experience and limited standardized instructions on these additives in the Canadian asphalt industry, there has not been an established guideline or specification for rejuvenator applications. Therefore, this study aims to establish a systematic approach to selecting the proper rejuvenator using different rheological parameters over a full temperature range from mixing and compaction to the in-service pavement stage.

4.2 Research objectives and experimental methods

To fulfill the aim of this study, the seven rejuvenators and one soft binder were blended into a high RAP binder ratio blend using the blending procedure mentioned in Figure 3.2. Then their rejuvenating effectiveness was evaluated by testing the rejuvenated binder blends using the Superpave PG system. The thermal stability of the binder blends and the rejuvenators themselves were examined by the Rolling Thin Film Oven (RTFO) conditioning and the Thermogravimetric Analysis (TGA), respectively. The RBR of 50% in the binder blend was selected as a starting point to represent a high RAP content scenario. As shown

in Figure 4.1, the recycled or rejuvenated binder blends were prepared using 50% recovered RAP binder and 50% base binder, with the addition of various rejuvenator contents ranging from 0% (control blend) to 10% by weight of the total binder blend. The softer binder (SB) blend was also prepared by completely replacing the base binder with the PG 46-34 asphalt. First, the rotational viscosity of the binder blend was measured to assess its workability at a very high-temperature range. Then, the rejuvenating effectiveness of different rejuvenators was evaluated by comparing the rheological parameters of their rejuvenated binder blends to the control binder blend or a target virgin asphalt. Different rheological parameters, including the continuous PG temperatures, crossover temperature (T_{cross}), and ΔT_c were determined by performing Dynamic Shear Rheometer (DSR) and Bending Beam Rheometer (BBR) tests on the binder blend specimens, per AASHTO T315 [110] and AASHTO T313 [111], respectively. Additionally, the Multiple Strain Creep Recovery (MSCR) test [112] was performed to obtain the non-recoverable creep compliance (J_{nr}) to evaluate the high-temperature performance of rejuvenated binder blends. The binder blends were treated with two different aging protocols, Rolling Thin Film Oven (RTFO) aging and Pressure Aging Vessel (PAV) aging, as required by different testing methods as per AASHTO M320 [98]. The PG temperatures and ΔT_c were calculated according to AASHTO M320 and the crossover temperature of the PAV-aged binder blend was obtained following the test manual of LS – 319 Rev. No.33 [105]. Additionally, the rotational viscosity test was also performed on both original and PAV-aged samples to provide insight into the aging resistance of the binder blends.

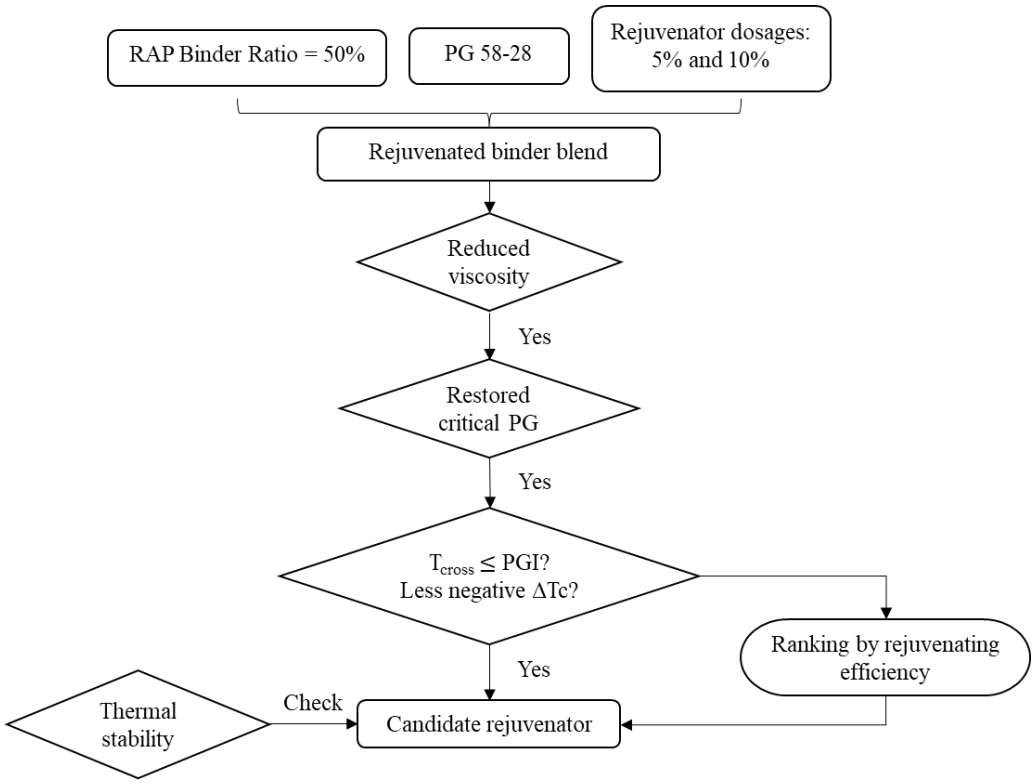

Figure 4.1 Experimental scheme of rejuvenator screening

As Figure 3.2 shows, blending duration, blender speed, and temperature during sample preparation were carefully controlled and kept at the required time and temperature to ensure the rejuvenator binder blend is homogeneously mixed. At this stage, it is assumed that during the binder testing phase, the complete blending happens between the RAP binder and virgin binder, and the activation of the RAP binder is accomplished due to the complete contact between the RAP binder and rejuvenator. Therefore, the only variables that affect the properties of the binder blends were rejuvenator type and rejuvenator dosage.

4.3 Results and discussion

4.3.1 RTFO mass change

Table 4.1 shows the RTFO mass change results of two virgin binders and the recycled binder blends without a rejuvenator. 50RB and 50RB_SB stand for the 50% recovered RAP binder blended with 50% PG 58-28 and 50% PG 46-34, respectively. Except for PG 58-28, the other three samples exhibited mass loss after RTFO aging. The percent of mass change in virgin binders was acceptable (<1%), while the two binder

blends showed a significant mass loss above one percent, which can be attributed to the possible existence of residual extraction solvent (dichloromethane) in the recovered RAP binder.

Table 4.1 RTFO mass change (%) of virgin binder and recycled binder blends

	PG 58-28	PG 46-34	50RB	50RB_SB
RTFO mass change	0.053	-0.245	-1.033	-1.217
Standard Deviation	0.002	0.004	0.103	0.017

Figure 4.2 compared the mass loss results between binder blends with different types of rejuvenators, the error bars are the standard deviations between the replicates. The binder blend with rejuvenator A (i.e., 50RB_A) showed the most prominent mass loss (above 1.1%) with the rejuvenator dosage at 5% and 10%; however, the difference between the 5% sample and 10% sample was not significant. 50RB_B was the only sample that experienced reduced mass loss with the increase in rejuvenator dosage. For both rejuvenators C and D, there was a notable increase in mass loss when the dosage increased from 5% to 10%. As for the other three samples, 50RB_E, 50RB_F, and 50RB_G, they showed relatively smaller mass changes at both dosages and a marginally increased mass loss with the increase of rejuvenator dosage. In addition, the mass change of 10% rejuvenated binder blends were likely to have higher variations compared to those with 5% rejuvenator dosage, as the standard deviation is shown in Figure 4.2 RTFO mass loss (%) of rejuvenated binder blends. Compared to the results of the 50RB sample, which already showed 1% mass loss, the addition of rejuvenators resulted in similar or even less mass loss as the 50RB blend; therefore, it indicated that the rejuvenator remained stable during the RTFO process, and no noticeable volatilization was observed. However, the recovered RAP binder and virgin binder will also affect the results in rejuvenated binder blends, especially when a significant residual solvent amount was expected in the recovered RAP binder. To further investigate the existence of residual solvent, X-ray fluorescence (XRF) was performed on the 50RB and 50RB_A binder blends at different aging conditions to track the presence of chlorine. From the results listed in Table 4.2, the unaged binder blends showed a significant amount of chlorine compared to those after RTFO and PAV conditioning. The main source of chlorine in the binder blend was the extraction solvent dichloromethane, which demonstrated that there is residual solvent in the recovered RAP binder. Nevertheless, the RTFO and PAV conditioned blends were merely affected by the solvent, given that the aging procedure facilitated the elimination of any significant remainder of the solvent component. It should also be noted that the boiling point of dichloromethane used in extraction and recovery

is below 40℃, so the residual solvent might evaporate during the blending process or repeated high-temperature conditioning of the RAP binder.

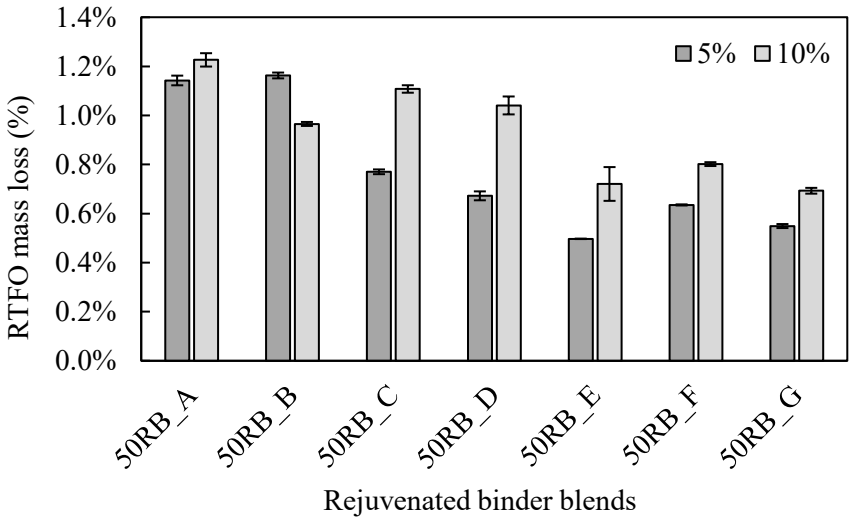

Figure 4.2 RTFO mass loss (%) of rejuvenated binder blends

Table 4.2 Weight of Chlorine (%) detected by X-ray fluorescence (XRF) analysis

Sample Description	Dosage of Rejuvenator A		
	0%	5%	10%
Unaged	0.43	0.39	0.28
RTFO	0.01	0.01	0.01
PAV	0.01	0.01	TRACE

4.3.2 Rotational viscosity

Figure 4.3 and Figure 4.4 summarize the rotational viscosity values of different binder blends measured at 135°C and 165°C, both error bars are the standard deviations. As expected, the addition of the rejuvenators significantly reduced the viscosity of the binder blend compared to the blend without a rejuvenator or softer binder. However, none of the rejuvenated binder blends could achieve a similar viscosity value to that of PG 58-28 when the rejuvenator dosage is 5% at both 135°C and 165°C. Increasing the rejuvenator dosage to 10% could lead to lower or similar viscosity of the binder blend compared to PG 58-28, except for rejuvenator C and G. Binder blends containing rejuvenator A, B, and D outperformed other counterparts in terms of reducing the viscosity. The addition of rejuvenator A resulted in the lowest viscosity at 5% dosage, while rejuvenator D achieved the most significant viscosity decrease when the dosage was increased from

5% to 10%. In addition, replacing the virgin binder with a softer graded binder (i.e., PG 46-34) could reduce the viscosity comparable to rejuvenated binder blends with a 5% dosage.

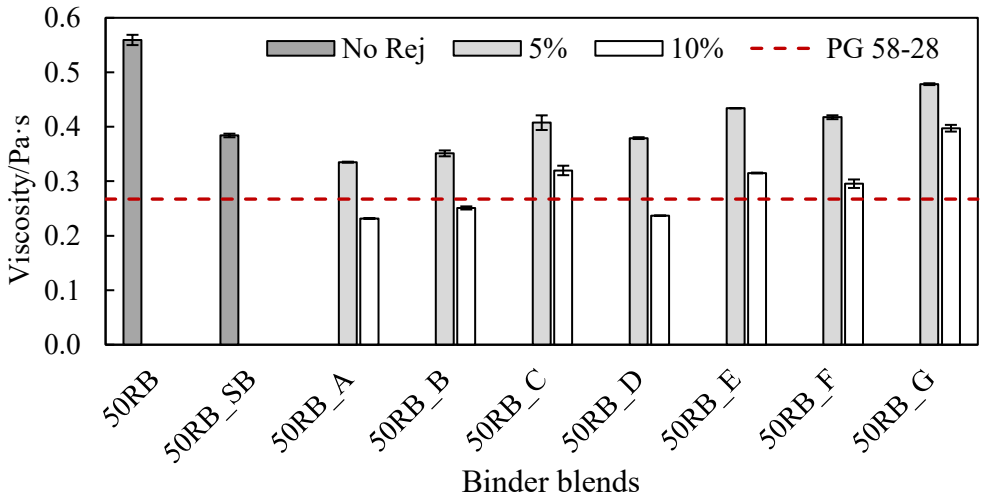

Figure 4.3 Rotational viscosity (Pa·s) of different binder blends at 135°C

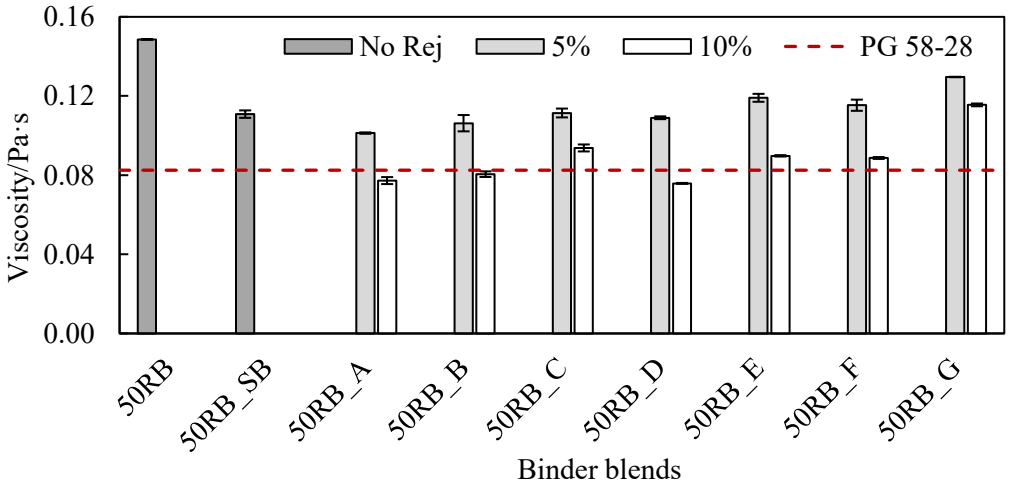

Figure 4.4 Rotational viscosity (Pa·s) of different binder blends at 165°C

Additionally, the temperature sensitivity of the binder blends was compared in terms of the activation energy (E_a) calculated from the Arrhenius equation below [32].

$$\eta = A \exp\left(\frac{E_a}{RT}\right) \tag{4-1}$$

Equation (4-1) can be transformed into a logarithmic form expressed by Equation (4-2):

$$ln\,\eta = ln\,A + \frac{E_a}{R} \times \frac{1}{T} \tag{4-2}$$

where:

$A =$ pre-exponential factor.

$R =$ the universal gas constant, 8.314 J/(mol·K).

$T =$ test temperature in Kelvin (K).

Viscosity is a measure of the resistance of a liquid to shear flow, which is highly affected by temperature. E_a presents the barrier for resisting the viscous flow, the smaller E_a indicates the fluid is easier to flow at a specific temperature. Based on the equation, a temperature-sensitive sample will have a higher E_a and the temperature change will result in a more noticeable change in the property (e.g., viscosity). The temperature sensitivity of binder blends was evaluated based on the regression results of viscosity data at 120°C, 135°C, 150°C, and 165°C. Table 4.3 shows the E_a for each binder blend sample. The E_a for PG 58-28 is 61.37 kJ/mol; therefore, the inclusion of 50% RAP binder significantly increased the temperature sensitivity (indicated by a value of 69.64 in Table 4.3) and only applying 10% rejuvenator A, B, D, and F could reduce E_a to a value that is smaller than that of PG 58-28. Using a softer binder showed a better capacity to reduce the temperature sensitivity compared to some binder blends with a 5% rejuvenator dosage.

Table 4.3 Calculated activation energy (E_a) results of different binder blends

Rejuvenator	E_a (kJ/mol)	
	5%	10%
50% PG 58-28	69.64	
50% PG 46-34	65.20	
A	62.74	57.71
B	63.26	59.30
C	68.21	63.66
D	65.65	59.43
E	68.73	64.60
F	66.89	60.89
G	68.25	64.49

As mentioned above, the residual solvent in the recovered RAP binder could potentially affect the test results obtained from unaged samples. Therefore, the rotational viscosity test was also performed on PAV-aged binder blends to get more precise results. Moreover, it is essential to evaluate the durability of the rejuvenator in the binder blends after lab-simulated long-term aging. Figure 4.5 and Figure 4.6 display the viscosity of four PAV-aged binder blends with 10% rejuvenator compared to their original counterparts, in which the error bars are the standard deviations. All the samples experienced a considerable increase in viscosity after PAV aging. Binder blends with 10% A and 10% B showed slightly higher viscosity than binder blends with the same amount of D and F.

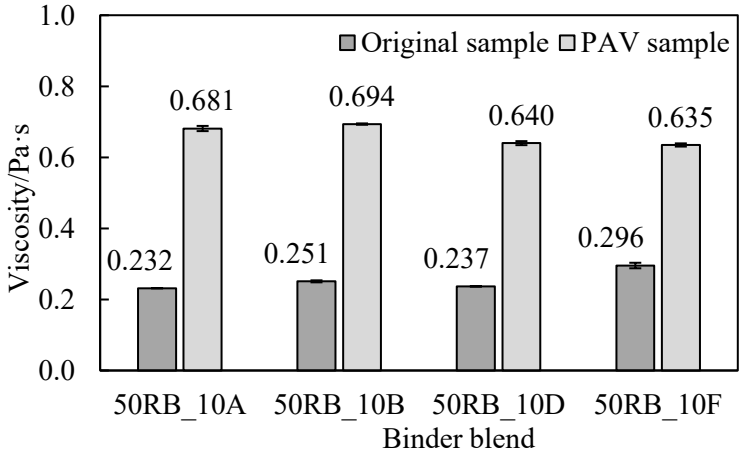

Figure 4.5 Comparison of viscosity results of original and PAV aged sample (135°C)

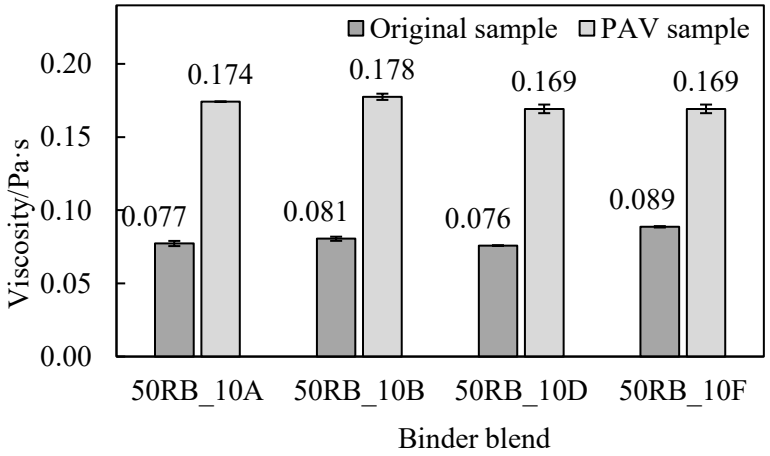

Figure 4.6 Comparison of viscosity results of original and PAV aged sample (165°C)

Table 4.4 summarizes the ratio between the viscosity results of the original and PAV-aged binder blends with a 10% rejuvenator dosage. At 135°C, the binder blend with rejuvenator A exhibited the most significant increase in viscosity after PAV aging, with the value almost tripled. The viscosity ratio of binder blends with B and D were similar at both 135°C and 165°C. Rejuvenator F has the lowest viscosity ratio, which may indicate a better aging resistance in terms of maintaining the softening effectiveness. As for the E_a, the results showed (see Table 4.5) that a similar trend was captured from the viscosity ratio results, with rejuvenator A achieving the greatest E_a ratio. Rejuvenators D and F had the smallest increase of E_a after PAV aging, however, the viscosity and activation energy of 50RB_10F was higher than the other three samples, suggesting the binder blend is less workable during mixing and compaction when the binder is still at unaged or short-term aged states. Therefore, despite that rejuvenator F showed a promising better aging resistance compared to the other three rejuvenators, its fresh binder blend will need a higher dosage to achieve identical workability during mixing production.

Table 4.4 Viscosity ratio (PAV/original) between original and PAV aged binder blends (Pa·s)

Sample	135℃	165℃
50RB_10A	2.94	2.25
50RB_10B	2.76	2.20
50RB_10D	2.70	2.23
50RB_10F	2.15	1.91

Table 4.5 E_a of original and PAV aged binder blends (kJ/mol)

Sample	Original	PAV residue	Ratio (PAV/Original)
50RB_10A	57.7	72.4	1.25
50RB_10B	59.3	71.0	1.20
50RB_10D	59.4	70.3	1.18
50RB_10F	60.9	70.8	1.16

4.3.3 Superpave performance grading (PG) and crossover temperature (T_{cross})

Performance grading (PG) was commonly used for evaluating the rejuvenation effectiveness of rejuvenators on aged binders and for determining the optimal dosage of a rejuvenator. Figure 4.7 and Figure 4.8 display the continuous grading results of the binder blends at high, intermediate, and low temperatures. The grading results obtained from RTFO-aged samples were selected as the high PG temperature since the original grading results could be unreliable due to the existence of residual solvent. Most rejuvenated binder blends achieved a larger Useful Temperature Interval (UTI) than that of the virgin binder (86°C). For rejuvenators A, B, D, and F, a 5% dosage could obtain a binder blend with a PG of PG 64-28 or even PG 64-34; and a 10% dosage could reach PG 52-34 or PG 52-40. In terms of the continuous high PG (PGH) temperature, rejuvenator D has the best softening effect by reducing the value from 74.9°C to 64.9°C and 56.2°C at 5% and 10% dosages, respectively; however, none of the rejuvenated binder blends could reach the same continuous high PG (61.2°C) as the base binder PG 58-28 when the dosage is 5%. When increasing the dosage to 10%, four rejuvenators, A, B, D, and F, resulted in an extra soft binder blend with a high PG of 52°C. Therefore, the appropriate dosage to restore the continuous high PG is between 5% and 10%. Replacing the base binder with PG 46-34 could not reduce the high PG temperature to the target value, and the restoration capacity was worse than the addition of a 5% rejuvenator.

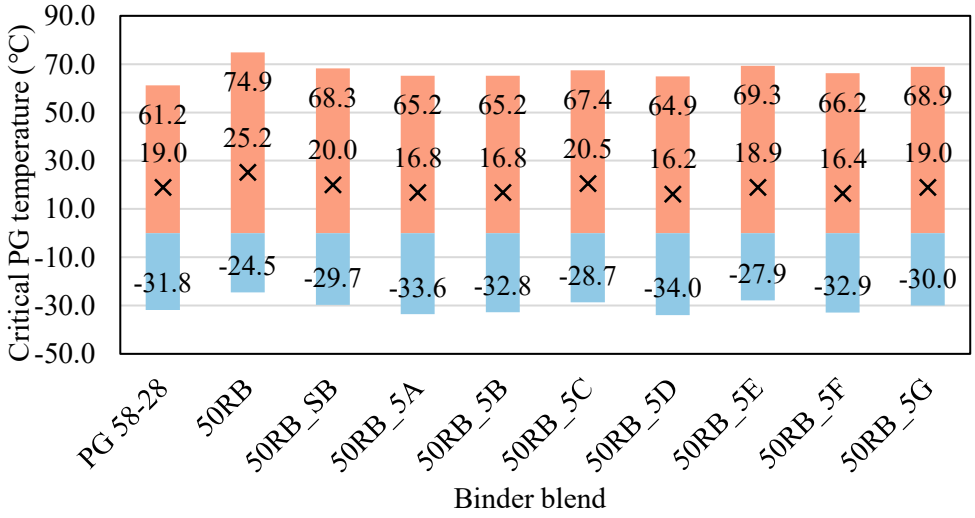

Figure 4.7 Continuous grading results of virgin binder and rejuvenated binder blends (5% dosage)

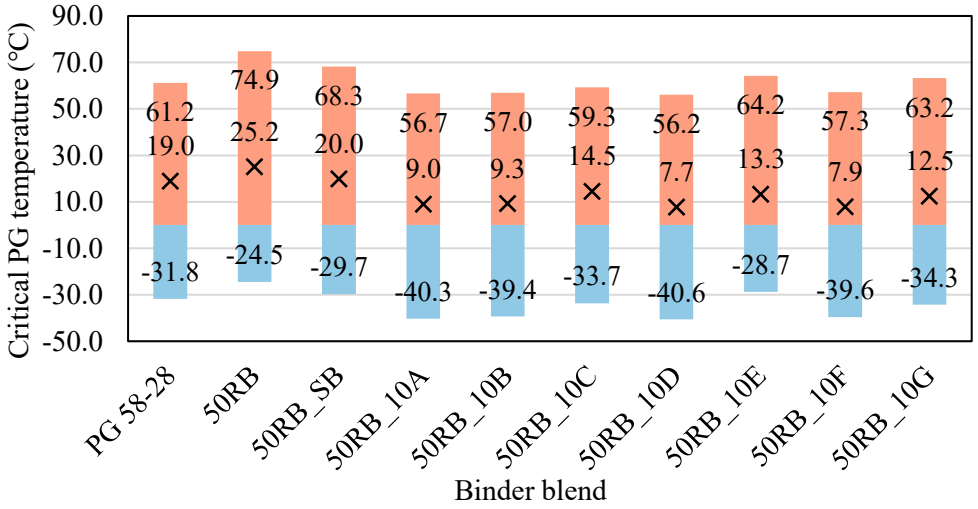

Figure 4.8 Continuous grading results of virgin binder and rejuvenated binder blends (10% dosage)

Unlike the PGH criterion, a 5% rejuvenator dosage could already decrease the continuous intermediate (PGI) temperature to be similar to or less than those of the base binder (19.0°C), except for the rejuvenator type C. Apart from PGI, the crossover temperature (T_{cross}) was also determined on the PAV-aged sample. The sample was tested on DSR using an 8mm plate at an angular frequency of 10 rad/s under four different temperatures, generally at PGI, PGI - 3°C, PGI - 6°C, and PGI - 9°C with a shear strain of 1%, 0.5%, 0.2%, and 0.1%, respectively. Crossover temperature was then calculated based on the linear regression fitted equation when the phase angle is equal to 45°, which represents the balance between the elastic portion and the viscous portion of the asphalt binder. This parameter offers more insightful information to characterize the viscoelastic behavior of the binder blends at the intermediate service temperatures. Table 4.6 provides the comparison between PGI and T_{cross} of the binder blends. Most rejuvenators resulted in slightly higher T_{cross} values than the PGI temperatures, except binder blends containing rejuvenator C, E, and G. The PGI parameter is determined based on both the complex modulus and phase angle ($G^*\sin\delta \leq 5000$ kPa) and T_{cross} is solely based on the measurements of phase angle, the lower PGI values indicated that some rejuvenators might be able to offset the increased stiffness due to aged binder, but the same amount of rejuvenator could not restore the viscous property related to the decreased phase angle. Especially for rejuvenator E, which could successfully restore the continuous intermediate PG, but it failed to restore the T_{cross} and the value even increased with increasing the dosage.

Table 4.6 Comparison between PGI and T_{cross} of rejuvenated binder blends (°C)

Rejuvenator	PGI		T_{cross}		Diff	
	5%	10%	5%	10%	5%	10%
50% PG 58-28	25.2		26.2		1.0	
50% PG 46-34	20.0		20.4		0.4	
A	16.8	9.0	17.3	9.5	0.5	0.5
B	16.8	9.3	17.1	8.3	0.3	-1.0
C	20.5	14.5	18.4	10.4	-2.1	-4.1
D	16.2	7.7	17.3	8.3	1.1	0.5
E	18.9	13.3	24.6	26.9	5.7	13.6
F	16.4	7.9	17.1	8.7	0.7	0.8
G	19.0	12.5	18.6	10.6	-0.4	-1.9

In terms of the low PG temperature, 5% rejuvenator A, B, D, and F was already too much to achieve the target value of the PG 58-28; and a 10% dosage could even result in a -40°C low PG temperature. Furthermore, low temperature behavior of the blends was evaluated using ΔT_c parameter, which is the difference between the PGL based on creep stiffness (PGL_S) and the PGL based on m-value (PGL_m). ΔT_c was suggested as an indicator of the aging level of an asphalt binder, a more positive value of ΔT_c indicates a less aged binder. For most rejuvenators, increasing the dosage to 10% could lead to a positive ΔT_c except rejuvenator E. Rejuvenator E failed to restore the m-value as ΔT_c became even more negative with the increasing dosage. In this study, however, ΔT_c might not be a preferable parameter for screening rejuvenators. For instance, adding 10% of rejuvenator type C resulted in the most positive ΔT_c value, but the PGL of this binder blend is much higher (less desirable) compared to the other blends with rejuvenators A, B, D, and F.

Table 4.7 Continuous low temperature of rejuvenated binder blends (°C)

Rejuvenator	PGL_S		PGL_m		ΔT_c	
	5%	10%	5%	10%	5%	10%
50% PG 58-28	-26.7		-24.5		-2.2	
50% PG 46-34	-30.4		-29.7		-0.7	
A	-33.8	-40.3	-33.6	-40.6	-0.2	0.3
B	-32.8	-39.4	-34.0	-40.7	1.2	1.3
C	-28.8	-33.7	-28.7	-35.5	-0.1	1.8
D	-34.1	-40.6	-34.0	-41.0	-0.1	0.4
E	-32.3	-38	-27.9	-28.7	-4.4	-9.3
F	-33.3	-39.6	-32.9	-40.8	-0.4	1.2
G	-30.4	-34.3	-30.0	-35.0	-0.4	0.7

4.3.4 Multiple Strain Creep Recovery (MSCR)

The MSCR test characterizes the resistance to permanent deformation of asphalt binders and is used for the performance grading of asphalt binders according to AASHTO M332 [112]. J_{nr} is the non-recoverable creep compliance, which measures the amount of residual strain left in the sample after repeated creep and recovery. The lower J_{nr} value indicates a better rutting resistance of the binder. The MSCR test is conducted at the high PG temperature of the virgin binder (PG 58-28) for all the recycled binder blends. As shown in Figure 4.9, most binder blends at 5% dosage are categorized for "heavy traffic" ($J_{nr3.2} \leq 2.0$ kPa^{-1}) at the test temperature 58℃, except E and G, which were graded as "very heavy" ($J_{nr3.2} \leq 1.0$ kPa^{-1}). In addition, when the dosage increased to 10%, most of the rejuvenated binder blends at 10% dosage did not meet the requirement ($J_{nr3.2} \leq 4.5$ kPa^{-1}) for "standard traffic", while the binder blend with 10% E satisfied the "heavy traffic" category and binder blends with C and G satisfied the "standard traffic" category. The results are consistent with the high continuous temperatures of the binder blends, and 10% rejuvenator content will compromise the high-temperature stability of the recycled binder blend.

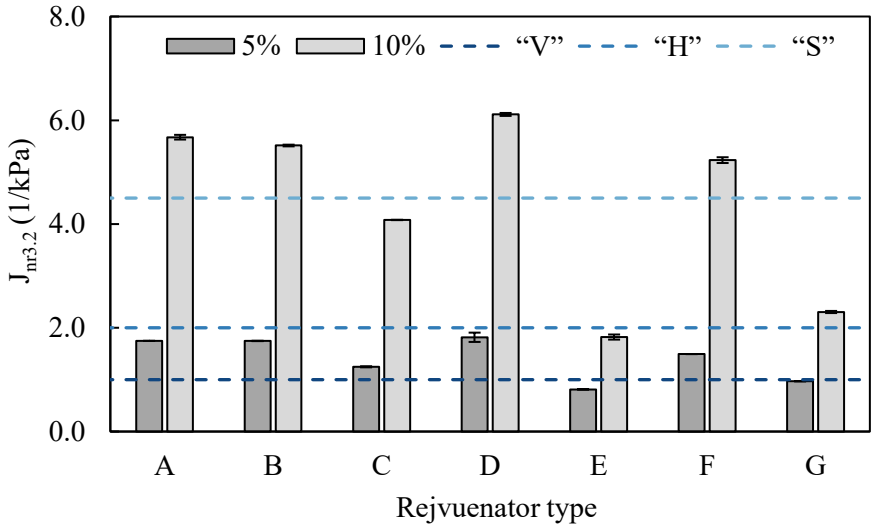

Figure 4.9 Non-recoverable creep compliance ($J_{nr3.2}$) of rejuvenated binder blends

4.3.5 Thermal stability

The thermal stability of the rejuvenators was investigated using Thermogravimetric Analysis (TGA). The TGA test was performed using a TA Instruments TGA Q500. The test procedure starts by ramping the temperature of the furnace from room temperature to 800°C at a constant heating rate of 20°C/min with a nitrogen flow rate of 60ml/min. The initial weight of the sample was between 10 and 20mg, and the change in sample weight versus time and temperature was recorded during the test. Figure 4.10 shows the thermogravimetric (TG) curves of different rejuvenators. It plots the percent of remaining weight against the increasing temperature. For rejuvenators C and E, they showed a steep decreasing trend around 280°C and 330°C, respectively; and most of the components decomposed before 400°C, with less than 10% residue. Rejuvenators F and G were from the same supplier and presented very close TG curves, showing the sharpest mass change around 380°C. The largest first derivative of the curve is defined as the maximum decomposition temperature (MDT), which signifies the highest rate of mass change during the thermal ramping. As shown in Figure 4.11 and Figure 4.12, rejuvenators C and E showed the highest decomposition rate around 280°C and 330°C, which are corresponding to their TG curves, indicating most of the components have already decomposed at these temperatures. F and G were collected from the same supplier, whose chemical components are similar, showing similar peaks in the DTG curves, while both showed high MDT values larger tan 380°C. Unlike the aforesaid rejuvenators, A, B, and D exhibited multiple steps of mass change instead of a dominant steep curve slope and they also show multiple peaks in the DTG curves,

indicating a more complex chemical composition of these three rejuvenators. However, rejuvenator B showed the MDT at the highest temperature among these rejuvenators. The initial decomposition temperature (IDT), obtained from the beginning of the mass change, is usually used for evaluating thermal stability [113–115]. It is determined as the temperature when the sample shows a certain amount of mass loss (e.g., 1% or 2%).

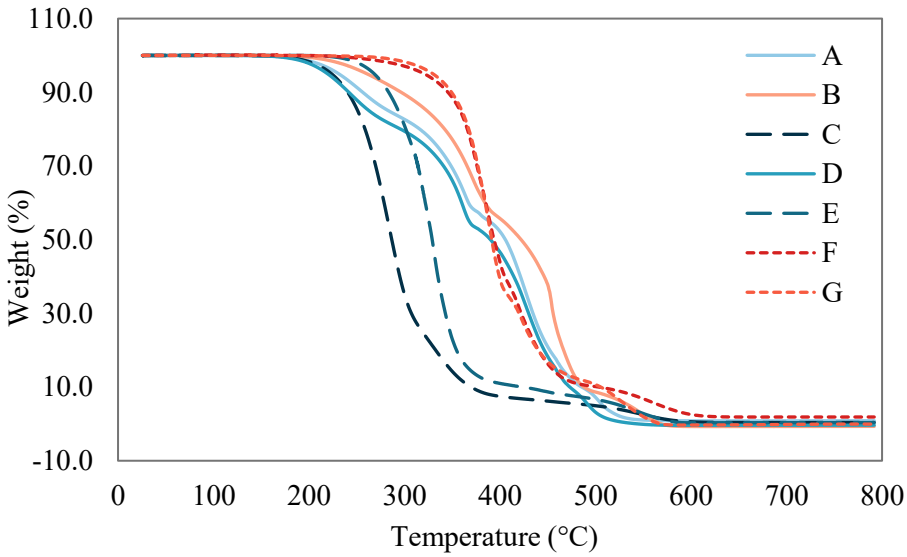

Figure 4.10 Thermogravimetric (TG) curve of rejuvenators

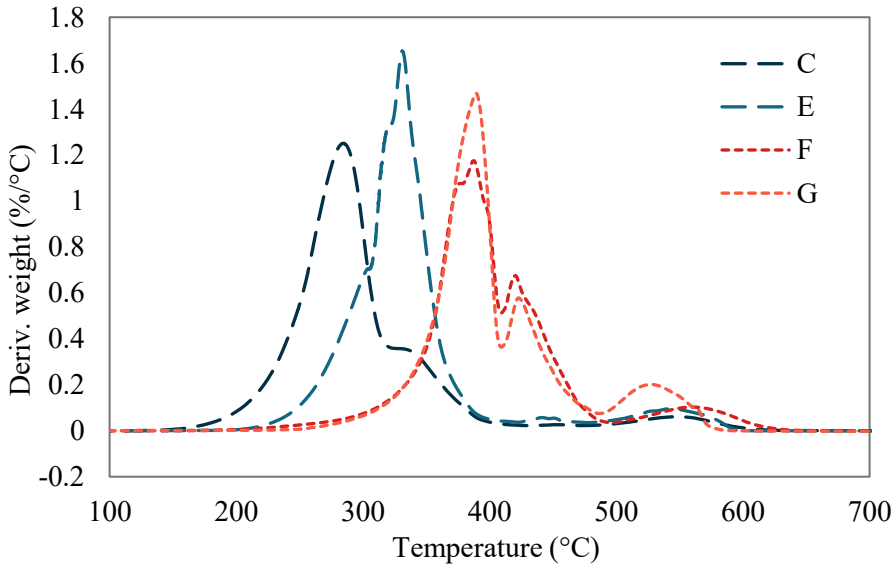

Figure 4.11 Derivative thermogravimetric (DTG) curve of rejuvenators (C, E, F, and G)

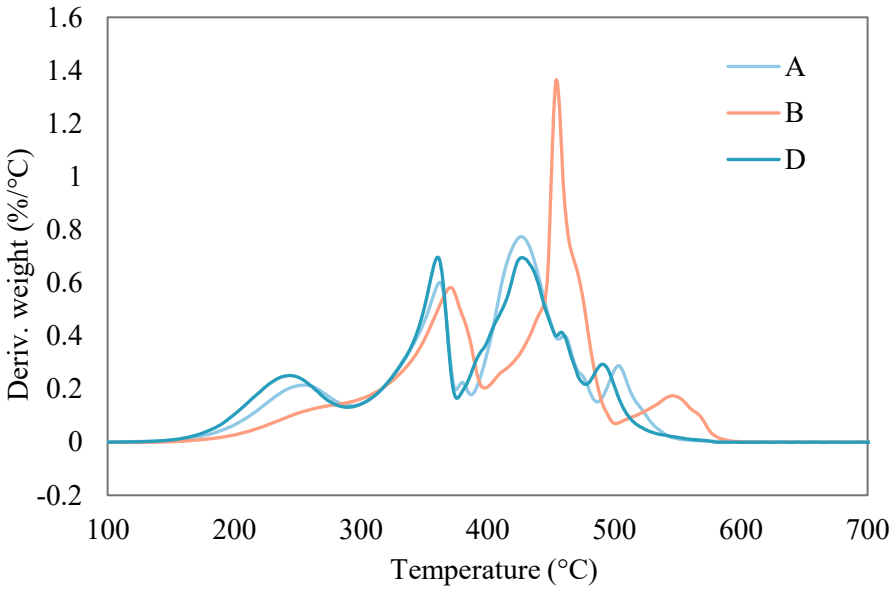

Figure 4.12 Derivative thermogravimetric (DTG) curve of rejuvenators (A, B, and D)

Table 4.8 summarizes the TGA results of different rejuvenators. According to the IDT results of the samples, rejuvenators F and G were the most stable due to the higher temperatures when 1% and 2% weight loss happened. Rejuvenators A, C, and D showed a relatively lower IDT that is below 200℃ for a 1% weight loss. Although rejuvenators A and B showed relatively higher MDT values, there were several obvious curve steps before the MDT in these two rejuvenators as well, which indicated some extent of instability of the material. Therefore, IDT is a better indicator for thermal stability than MDT, and the thermal stability ranking of these rejuvenators is G ≈ F > E > B > A ≈ D ≈ C. Nonetheless, the IDTs of these rejuvenators were all above 180℃, which is higher than the typical mixing temperatures of asphalt binders and asphalt mixes.

Table 4.8 Summary of rejuvenator TGA results

Rejuvenator	IDT (1% weight loss)	IDT (2% weight loss)	MDT (°C)	Rate (%/°C)	Residue
A	190.95	206.79	426.83	0.774	0.855%
B	213.62	230.82	454.23	1.365	0%
C	189.53	203.34	284.58	1.251	0.385%
D	184.67	198.26	360.35	0.696	0%
E	239.09	250.78	330.85	1.653	0.344%
F	260.25	285.18	387.72	1.175	1.873%
G	285.77	303.76	388.71	1.465	0%

4.4 Conclusions

This chapter focused on a systematic screening procedure for rejuvenators in terms of their softening effect on reducing the stiffness and ability to restore the relaxation capacity of the binder blends with a high RAP binder ratio. The thermal stability of rejuvenators and rejuvenated binder blends was also examined using TGA. The following conclusions can be summarized based on the test results:

- The RTFO mass change results indicated a noticeable amount of residual solvent in the recovered RAP binder which was later demonstrated that the lab conditioning processes can remove the residual solvent. Hence, it was recommended to use the test results from the RTFO and PAV aged binder blends to avoid the impact of residual solvent.
- The addition of a 10% rejuvenator could achieve a lower or similar viscosity of the binder blend compared to PG 58-28, except for rejuvenators C and G. Replacing the virgin binder with a softer binder (PG 46-34) could reduce the viscosity comparable to rejuvenated binder blends with a 5% dosage. Also, the temperature sensitivity was reduced with the increasing dosage of the rejuvenator.
- The restoration ability on continuous temperatures varies by rejuvenator types and the selected criteria. The petroleum-based rejuvenator (rejuvenator E) only reduced the stiffness but failed to restore the relaxation capacity of the binder blends. And a more positive ΔT_c did not necessarily imply a better restoring effectiveness, when looking at the continuous low PG.

- A 5% dosage could obtain a binder blend with a PG of PG 64-28 or even PG 64-34; a 10% dosage could reach PG 52-34 or PG 52-40. Also, the non-recoverable creep compliance results of the binder blends are consistent with the high-temperature grading results, evidencing the inadequate rutting resistance of the binder blends with a 10% rejuvenator. Therefore, a 5% rejuvenator dosage is favored to maintain both the high and low-temperature performances, while 10% can cause over-softening based on the results of high-temperature rheological parameters
- The decomposition temperature of the rejuvenator varies depending on the rejuvenator type. Nevertheless, all rejuvenators only show a 1% mass loss when the temperature is above 180℃ and had a maximum decomposition temperature ranging from 250℃ to 450℃, which guarantees sufficient stability during the mixing process.

Based on the summary of the rejuvenator screening results, four rejuvenators A, B, D, and F, were selected for dosage optimization and future binder and mix testing. The similarity of the composition of many of the available rejuvenators inherently leads to similar preliminary screening results. Nevertheless, as a recommended step to screen the selected rejuvenators, the rejuvenated binder blends containing optimized rejuvenator dosages will be prepared for both chemical and rheological characterizations. Different aging residues of the binder blends will then be assessed through FTIR spectroscopy and SARA analysis to capture chemical changes in the sample, and additional rheological tests, including frequency and temperature sweep, linear amplitude sweep, will be conducted as well. Part of the chemical characterization results (i.e., FTIR and SARA results) are presented in Appendix D and Appendix E. Because the results do not affect the final selection of the rejuvenators, the content was not included in this chapter. Furthermore, if multiple rejuvenators meet the expectations for the high RAP content recycling of mixes, other factors such as availability and rejuvenator-associated costs should be taken into the account for making the final decision.

Chapter 5
Rejuvenator dosage optimization

This chapter is based on a journal paper published on 19th October 2022 (online). The detailed information can be found in the citation: Liao, H., Tavassoti, P., & Baaj, H. (2022). Comparing Rheological Indexes to Optimize Rejuvenator Dosage for Asphalt Binders Containing High Ratios of Recycled Asphalt. *Journal of Testing and Evaluation*, *51*(4). https://doi.org/10.1520/JTE20220274

5.1 Rejuvenator dosage optimization

Using rejuvenators is known as one of the most promising solutions to maximize Reclaimed Asphalt Pavement (RAP) incorporation in pavement construction. Rejuvenators have the potential to reverse the impact of aging on binder performance. They balance the proportions of the light and heavy hydrocarbon components in asphalt binder by introducing the light fractions, such as resins, aromatics, and naphthenic hydrocarbons, that may have considerably volatilized during aging. Therefore, the rejuvenated aged binder becomes more workable and compatible during mixing and compaction and can contribute to improved mechanical properties and durability of recycled asphalt mixtures. Various studies have proven the positive effects of rejuvenators in terms of increasing the workability, reducing the stiffness, decreasing the critical cracking temperature, and prolonging the fatigue life of both aged binder and RAP incorporated mixtures by using different rejuvenators [2,55,72,87].

According to the composition of rejuvenators, they are usually divided into two major categories: petroleum-based rejuvenators and bio-based rejuvenators. Petroleum-based rejuvenators are derived from the same source as the asphalt binders like aromatic extracts and naphthenic oil that are distilled from crude petroleum [76]. On the other hand, researchers have been also exploring the feasibility of utilizing bio-based oils as rejuvenators due to their sustainability and availability. Different types of bio-based rejuvenators, such as tall oil, soybean oil, cashew nutshell oil, waste vegetable oil etc., have been used in laboratory scale research and showed promising results in terms of restoring the microstructures of aged binder and the cracking performance of highly recycled asphalt mixes [28,86,88]. Bio-based rejuvenators are favored by the asphalt industry due to their relatively lower required dosage as compared to their petroleum counterparts since the bio-oils exhibit relatively lower viscosity than that of petroleum products [20]. However, the rejuvenator content should be carefully determined since an inadequate rejuvenator

dosage will lead to insufficient activation of aged asphalt binder, whereas excessive amounts of rejuvenator will have detrimental effects such as impaired rutting resistance [116,117].

Rejuvenator suppliers typically provide a recommended range for the optimum rejuvenator dosage, but the rejuvenator content is affected by the aging level of the recycled materials [56], the characteristics of the virgin asphalt binder [23], and the criteria used for selecting rejuvenator dosage. Therefore, it is essential to determine the optimum rejuvenator dosage before applying it to a specific project, rather than solely relying on the manufacturer's recommended dosage. To this end, the most prevalent method is to establish a softening curve or blending chart based on the properties of recycled blends (i.e., blend of extracted RAP binder and rejuvenator) and rejuvenator proportions. Those properties can be based on either the penetration system or the Superpave Performance Grading (PG) system [60,64]. Several methods of rejuvenator dosage optimization can be found in the literature. For example, Ongel and Hugener selected the optimum rejuvenator dosage by the linear regression of rejuvenator content and penetration value of the rejuvenated binder blend [24]. They identified the optimum rejuvenator dosage when the rejuvenated binder blend achieved the same penetration value as the virgin binder. In another study, Chen et al. used four physical property parameters, namely penetration, softening point, ductility, and viscosity, of the asphalt binder as rejuvenation criteria to determine the rejuvenator dosage [25]. The final optimum dosage reported in their study was able to restore those properties of the aged binder to the level of virgin asphalt binder or such that it could meet the specification requirements. Zaumanis et al. also showed that the range of the rejuvenator dosage could be selected based on the linear relationship between rejuvenator content and reduction in the PG temperatures [84]. This method was also found to be the common practice across the U.S. DOTs according to a recently conducted survey under the NCHRP 586 project [77]. On the other hand, Im et al. developed an initial rejuvenator dosage selection method using the low PG temperature and the Glover-Rowe (G-R) parameter measured after the long-term binder aging [81]. This initial rejuvenator dosage considered both the low-temperature performance and durability of the binder. Some researchers only construct the blending charts of rejuvenator dosages and high PG temperatures of the recovered RAP binder to choose the optimum rejuvenator dosage [62,83]. This approach may result in an excessive rejuvenator content, which can make the mix prone to rutting distress.

Therefore, using the proper binder rheological indices to select the optimum rejuvenator dosage based on binder testing results and being cautious about the dosage differences caused by the rejuvenator type will be crucial to achieve performance-engineered high RAP mixtures. The optimization criteria should also reflect the dominant distress type for the specific region where the recycled mixes are to be

incorporated. In other words, while low-temperature cracking might not be the governing mode of failure for a dry-no-freeze climatic zone, it may be a major consideration for a wet-freeze climatic condition.

5.2 Problem statement and research objectives

Review of the literature on RAP incorporated binders/mixtures reveals that using different rejuvenator dosage optimization methods (based on different indices) can considerably affect the calculated optimum dosage and ultimately result in different properties of the subsequent rejuvenated aged binders and high RAP mixtures. However, there is currently no consensus about which index (or indices) should be used to determine the optimum rejuvenator dosage. The main goal of this paper is to compare and evaluate different rheological indices as the criteria for optimizing the rejuvenator dosage in binder blends with a high RAP binder ratio. In addition to studying the effect of different indices, two optimization methods including the commonly used blending chart method and the response surface modelling (RSM) were used in this study to develop predictive models for rejuvenator dosage optimization. In this study, the applicable rheological indices were selected as the optimization criteria based on the test results of the rejuvenated binder blends. The difference between rejuvenator dosages determined by the blending chart and RSM provides further insight into the linear relationship assumption between the rejuvenator dosages and the rheological properties of the asphalt binder. To this end, the following main objectives were defined and pursued in this research:

- To evaluate the ability of the conventional blending chart method as compared to the more robust response surface modelling (RSM) for the purpose of rejuvenator dosage optimization;
- To compare the optimum rejuvenator dosages determined using nine different rheological indices measured at very high, high, intermediate, and low temperature ranges;
- To study the ability of the bio-based rejuvenator types to restore the properties of high RAP binder ratio blends; and
- To identify the proper index (or indices) that could be used as the rejuvenator dosage optimization objective(s).

5.3 Material description and properties

The materials description and rejuvenated binder blend preparation methods were the same as the information described in Chapter 3. Based on the conclusion of Chapter 4, rejuvenator A, B, D, and F

showed similar effects on the high RAP binder ratio blend and better rejuvenating effectiveness than other products. Therefore, they were selected as the candidate rejuvenators to continue the rest of the study.

5.4 Optimization methodology

The rejuvenator dosage (by weight of the total binder blend) is optimized when the binder blend (with 50% RAP binder) achieves a similar rheological property to that of the target PG 58-28 base binder used in this study. For this purpose, the following rheological indices are selected as the criteria to determine the optimum rejuvenator dosage: (1) rotational viscosity (η) at 135°C and 165°C measured as per AASHTO T316 [118]. (2) high, intermediate, and low continuous PG temperatures. (3) non-recoverable compliance ($J_{nr3.2}$) at a stress level of 3.2 kPa, which was measured using the Multiple Strain Creep Recovery (MSCR) test conducted at 58°C according to AASHTO T350 [112]. (4) crossover temperature (T_{cross}) determined by the linear regression of phase angles at four different testing temperatures according to the Ontario lab testing manual, LS 319 - Rev. No.33. Consequently, a total of nine rheological indices, including η at 135°C, η at 165°C, PGH, PGI, PGL_S, PGL_m, $J_{nr3.2}$, and T_{cross}, were selected for determining the optimal rejuvenator dosage in this study. The optimization process followed in this study ensures that the rejuvenated binder blends prepared at the determined optimum dosage will meet or even exceed the rheological requirements, especially at both the high and low of PG temperatures. The proposed process also identifies the dominant responses based on which the minimum and maximum dosages can be determined for a given rejuvenator and RAP materials.

The blending chart and the response surface modelling (RSM) methods, discussed below, were used to optimize the combination of RAP content and rejuvenator dosage, with the rheological indices mentioned above as the response criteria.

5.4.1 Blending chart

The blending chart is one of the most well-established methods to estimate the performance of a blended binder sample. Many researchers have utilized this method to determine the required virgin binder grade or the allowable RAP percentage in the recycled hot mix asphalt (HMA) [11]. As shown in Equation (5-1), the required virgin binder grade can be computed by the percent of RAP, the continuous PG of the RAP binder, and the continuous PG of the blended binder by linear regression.

$$T_{virgin} = \frac{T_{blend} - (\%RAP \times T_{RAP})}{(1 - \%RAP)} \quad (5\text{-}1)$$

where:

T_{virgin} = Continuous PG temperature of the virgin binder (high, intermediate, or low).

T_{blend} = Continuous PG temperature of the blended asphalt binder (high, intermediate, or low).

$\%RAP$ = Percentage of RAP.

T_{RAP} = Continuous PG temperature of recovered RAP binder (high, intermediate, or low).

In the case of including a rejuvenator in the recycled binder blend, the dosage of the rejuvenator can be estimated using the method stated in NCHRP Report No.927 [82]. However, it should be noted that the percentage of RAP in Equation (5-1) is adapted by using the RAP binder ratio (RBR) for a full blending scenario, and the continuous temperature of the binder blend will be estimated using Equation (5-2):

$$T_{blend} = \left(\%virgin\ binder \times T_{virgin}\right) + (\%RBR \times T_{RAP}) \quad (5\text{-}2)$$

The required rejuvenator dosage can be determined using the parameter "slope rate", which was obtained from the linear regression results based on the measured parameters of rejuvenated binder blends with 0%, 5%, and 10% rejuvenator dosages. Thus, the slope rate is an indicator of the effectiveness of the rejuvenator with increasing dosage. As shown in Equation (5-3), the desired rejuvenator dosage is estimated when the continuous PG of the blended binder reaches the target continuous PG temperature.

$$\%Rejuvenator = (T_{blend} - T_{target})/Slope\ Rate \quad (5\text{-}3)$$

5.4.2 Response surface modelling

A two-level factorial Central Composite Design (CCD) was utilized in this method. Figure 5.1 exhibits two types of CCDs. The Central Composite Circumscribed (CCC) design (Figure 5.1 (*A*)) includes an embedded factorial design (i.e., four factorial points) with the center point, and a group of "star points" which allows estimation of curvature. If the distance from the center of the design space to a factorial point is ±1 unit for

each factor, the distance from the center to a star point is $|\alpha| > 1$. The star points in this design present new extremes for the high and low levels of the factors. However, for those situations in which the factorial points have already reached the limits of the factor levels, the start points should be set within the limits, meaning that $|\alpha| < 1$ (Figure 5.1 (*B*)).

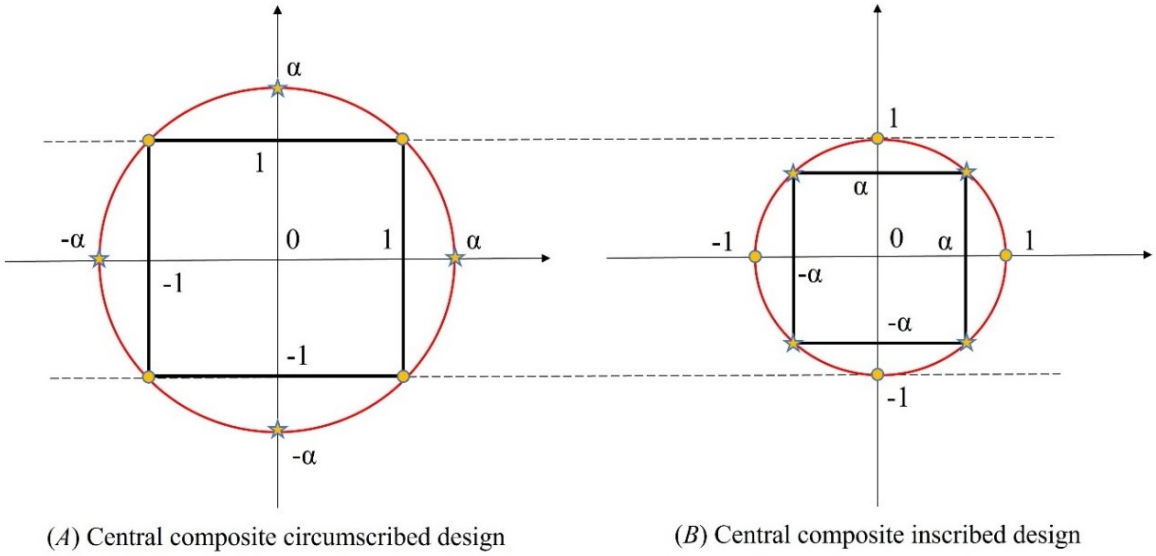

Figure 5.1 Central composite design types: (*A*) CCC, (*B*) CCI

As Table 5.1 Levels of continuous variables shows. the considered factors in rejuvenator dosage optimization were:

- Continuous variable X1: Rejuvenator dosage.
- Continuous variable X2: RAP binder ratio (RBR).

Table 5.1 Levels of continuous variables

Variables		Coded	Uncoded
X1	Rejuvenator dosage	-1	0%
		0	5%
		1	10%
X2	RBR	-1	25%
		0	50%
		1	75%

For each combination, two replicates of the test responses will be measured from different binder tests (except the BBR test results). In the initial experimental design, the relationship between the response and the two variables was assumed to be a first-degree polynomial model without quadratic terms. Therefore, a full 2^2 Central Composite Circumscribed (CCC) design without curvature was used for the optimization procedure, the combinations of the coded factor levels can be found in Table 5.2. A full 2^2 Central Composite Inscribed (CCI) design with a smaller design space will be applied for data analysis and model optimization if curvature was identified, since the previous factorial levels, 0% rejuvenator dosage, had already reached the factor level limit. The combinations of the factor levels of the CCI design with curvature are displayed in Table 5.3. Combinations 5 and 6 indicate that two test runs were conducted at the center point in the experimental design.

Table 5.2 Full 2^2 CCC design without curvature

Combination	X1	X2	X1X2	Uncoded X1	Uncoded X2
1	-1	-1	1	0.00%	25.00%
2	1	-1	-1	10.00%	25.00%
3	-1	1	-1	0.00%	75.00%
4	1	1	1	10.00%	75.00%
5	0	0	0	5.00%	50.00%
6	0	0	0	5.00%	50.00%

Table 5.3 Full 2^2 CCI design with curvature

Combination	X1	X2	X1X2	Uncoded X1	Uncoded X2
1	-1	0	0	0.00%	50.00%
2	1	0	0	10.00%	50.00%
3	0	-1	0	5.00%	75.00%
4	0	1	0	5.00%	75.00%
5	0	0	0	5.00%	50.00%
6	0	0	0	5.00%	50.00%
7	0.707	0.707	0.5	8.54%	67.68%
8	-0.707	0.707	0.5	1.47%	67.68%
9	0.707	-0.707	0.5	8.54%	32.33%
10	-0.707	-0.707	0.5	1.47%	32.33%

The entire experimental design and data analysis process is depicted as per the following steps:

(1) Obtain a first-degree polynomial model $\hat{y} = \beta_0 + \beta_1 x_1 + \beta_2 x_2 + \beta_{12} x_1 x_2$ based on the 2^2 CCC design without curvature.

(2) Use F-test to check the significance of the interaction term $x_1 x_2$. If it is not significant at a 95% confidence level, remove it into the error term, and the model becomes $\hat{y} = \beta_0 + \beta_1 x_1 + \beta_2 x_2$.

(3) Check if curvature exists by using the lack of fit (LOF) test or examining the difference between the average response of the factorial points ($\bar{y}_f$) and the observed response at the center point (y_c).

(4) If the curvature is not detected, use the first-degree polynomial model in (2) to find the factor levels that achieve the required response.

(5) If the curvature is detected, then quadratic terms (e.g., x_1^2 and x_2^2) will be added to the polynomial model using the 2^2 CCI design with curvature.

5.5 Results and discussion

5.5.1 Optimum rejuvenator dosage (blending chart)

Table 5.4 to Table 5.7 show the measured rheological properties of the binder blends containing different types of rejuvenators at three dosages, 0%, 5%, and 10%. For each rejuvenator dosage and each rheological parameter, at least two measured values were obtained to establish the blending chart and determine the slope rate based on Equation (5-1) and Equation (5-2). Then, Equation (5-3) was used to calculate the optimum rejuvenator dosage by choosing the rheological parameters of the virgin binder as the target values. The measured rheological properties were mostly repeatable according to the relatively small standard errors (S.E.). Hence, the rheological parameters at three dosage levels were considered to be reliable to establish the blending chart using the first-degree linear regression.

Figure 5.2 Optimum rejuvenator dosage determined by blending chart shows the optimum dosages for each rejuvenator determined by the blending chart method. It demonstrates that even for a specific rejuvenator type, the optimum dosages are determined by using different rheological indices as the responses can vary in a significantly wide range (e.g., from 3.5% to 12% for rejuvenator F). From Figure 5.2, it can also be noted that the indices measured at higher temperatures resulted in relatively higher rejuvenator dosages, such as the logarithm of η at 135°C and 165°C, as compared to the other indices measured at a lower temperature range such as the PGI, PGL_s, and PGL_m. The required dosage for rejuvenator F to restore the viscosity of the recycled binder blend was over three times the dosage to restore the PGI. Therefore, choosing the rejuvenator dosage using the higher temperature rheological indices had the potential to over soften the recycled binder blend. Additionally, the difference in the optimum dosages between the different rejuvenators became negligible when using the lower temperature rheological indices.

As for the continuous temperatures, the results in this paper were consistent with the findings in previous publications [84], in which the minimum required rejuvenator dosage was controlled by the low and intermediate PG grades, whereas the high PG grade determined the maximum required rejuvenator dosage. Furthermore, two distinct groups of indices measured at intermediate- and low-temperature ranges can be recognized based on the results of this study: (1) PGL based on stiffness (PGL_S) and PGI; and (2) PGL based on m-value (PGL_m) and T_{cross}. Except for rejuvenator B, the optimized dosages obtained by the restoration of PGL_m and T_{cross} were consistently 0.5% to 1.0% higher than those determined by PGL_S and PGI for all the rejuvenators evaluated in this study. Increasing the rejuvenator content by 1% was enough to induce noticeable changes in the rheological properties of the blended binder. Although those two groups

of indices were measured at the same low and intermediate temperature ranges, PGL_S and PGI were computed using parameters like the complex shear modulus (G^*), which is related to the binder stiffness. In contrast, PGL_m is the slope of the creep stiffness curve at the 60-second loading time, which is an indication of the stress relaxation capacity of the sample. And T_{cross} was determined when the phase angle equals 45°, which represented the balance between the elastic portion (i.e., storage modulus, G') and the viscous portion (i.e., loss modulus, G''). In other words, when the temperature is above the T_{cross}, the behavior of the asphalt binder is dominated by the loss modulus and becomes more fluidlike; therefore, the binder is less likely to crack [119]. According to the fact that PGL_S and PGI resulted in lower rejuvenator dosages than PGL_m and T_{cross}, the adequate rejuvenator amount to reduce the binder stiffness in low- and intermediate-temperature regions was probably not enough for restoring the flexibility or relaxation ability of the binder.

The results of this study confirm that in addition to the rejuvenator type, the optimization indices/criteria have a considerable impact on the optimum rejuvenator content even for a given rejuvenator.

Table 5.4 Measured rheological properties of binder blends with 50% RAP binder and rejuvenator A

Rheological indices	0%		5%		10%	
	Mean	S.E.	Mean	S.E.	Mean	S.E.
log(η) @135℃ (mPa·s)	2.748	0.007	2.525	0.001	2.365	0.001
log(η) @165℃ (mPa·s)	2.172	0.000	2.005	0.002	1.888	0.010
Original PGH (℃)	71.4	0.354	61.7	0.283	53.4	0.071
RTFO PGH (℃)	74.9	0.000	65.2	0.000	56.7	0.000
PGI (℃)	25.2	0.354	16.8	0.212	9.0	0.354
PGL_S (℃)	-26.7	-	-33.8	-	-40.3	-
PGL_m (℃)	-24.5	-	-33.6	-	-40.6	-
T_{cross} (℃)	26.2	0.035	17.3	1.365	9.5	0.120
$J_{nr3.2}$ (1/kPa)	0.318	0.000	1.747	0.000	5.674	0.045

Table 5.5 Measured rheological properties of binder blends with 50% RAP binder and rejuvenator B

Rheological indices	0%		5%		10%	
	Mean	S.E.	Mean	S.E.	Mean	S.E.
log(η) @135℃ (mPa·s)	2.748	0.007	2.545	0.007	2.400	0.005
log(η) @165℃ (mPa·s)	2.172	0.000	2.026	0.017	1.906	0.008
Original PGH (℃)	71.4	0.354	62.5	0.283	55.7	0.071
RTFO PGH (℃)	74.9	0.000	65.2	0.000	57.0	0.000
PGI (℃)	25.2	0.354	16.8	0.212	9.3	0.071
PGL_S (℃)	-26.7	-	-32.8	-	-39.4	-
PGL_m (℃)	-24.5	-	-33.6	-	-40.6	-
T_{cross} (℃)	26.2	0.035	17.1	0.028	8.3	0.283
$J_{nr3.2}$ (1/kPa)	0.318	0.000	1.747	0.004	5.513	0.016

Table 5.6 Measured rheological properties of binder blends with 50% RAP binder and rejuvenator D

Rheological indices	0%		5%		10%	
	Mean	S.E.	Mean	S.E.	Mean	S.E.
log(η) @135℃ (mPa·s)	2.748	0.007	2.579	0.002	2.374	0.000
log(η) @165℃ (mPa·s)	2.172	0.000	2.037	0.003	1.880	0.001
Original PGH (℃)	71.4	0.354	64.6	0.000	54.9	0.424
RTFO PGH (℃)	74.9	0.000	64.9	0.283	56.2	0.071
PGI (℃)	25.2	0.354	16.2	0.071	7.7	0.071
PGLS (℃)	-26.7	-	-34.1	-	-40.6	-
PGLm (℃)	-24.5	-	-34.0	-	-41.0	-
Tcross (℃)	26.2	0.035	17.3	0.007	8.3	0.424
Jnr3.2 (1/kPa)	0.318	0.000	1.817	0.090	6.112	0.028

Table 5.7 Measured rheological properties of binder blends with 50% RAP binder and rejuvenator F

Rheological indices	0%		5%		10%	
	Mean	S.E.	Mean	S.E.	Mean	S.E.
log(η) @135℃ (mPa·s)	2.748	0.007	2.621	0.004	2.470	0.011
log(η) @165℃ (mPa·s)	2.172	0.000	2.062	0.011	1.948	0.002
Original PGH (℃)	71.4	0.354	65.5	0.283	57.3	0.071
RTFO PGH (℃)	74.9	0.000	66.2	0.000	57.3	0.071
PGI (℃)	25.2	0.354	16.4	0.000	7.9	0.212
PGL_S (℃)	-26.7	-	-33.3	-	-39.6	-
PGL_m (℃)	-24.5	-	-32.9	-	-40.8	-
T_{cross} (℃)	26.2	0.035	17.1	0.099	8.7	0.163
$J_{nr3.2}$ (1/kPa)	0.318	0.000	1.494	0.001	5.232	0.056

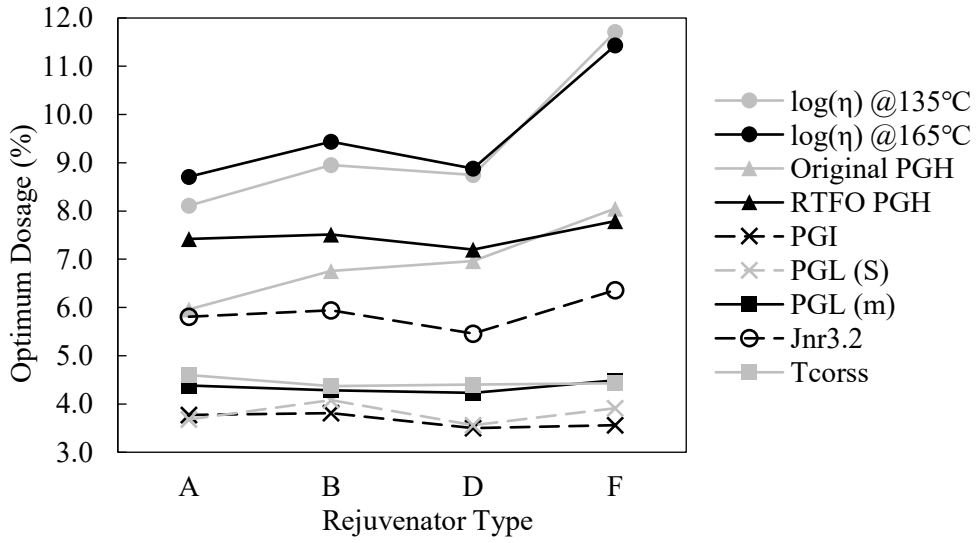

Figure 5.2 Optimum rejuvenator dosage determined by blending chart

5.5.2 Optimum rejuvenator dosage (RSM)

Interaction and curvature

The RSM method was applied for determining the optimum dosage of rejuvenators D and F and comparing with the results obtained from the blending hart method to verify the linear relationship. The significance of the interaction between the two variables, rejuvenator dosage and RBR, was first examined using the p-

value of the interaction term (x_1x_2). As shown in Table 5.8, except for using $J_{nr3.2}$ as the model response, the p-values were all larger than 0.05, which proved that the impact of the interaction between rejuvenator dosage and RBR was insignificant. Table 10 presents two indicators for checking the curvature of the response surface. The level of deviation in percent was calculated as the ratio of the absolute difference between $\bar{y}_f$ and y_c and the absolute value of y_c. A smaller deviation was expected if the response surface was without curvature. The p-value of the LOF error describes the significance of the error caused by the model fitting compared to the pure error estimated by the center points and the replicates at the fractional points. The p-value may not be available either if there were no replicates, or if the observed responses were identical among replicates. From the results in table 10, the deviation values for all the rheological indices were below 7%, which was relatively small. As for the available p-values of LOF, they were greater than 0.05, except for rejuvenator D with the model response of the original PGH and T_{cross}. Hence, it was reasonable to exclude the quadratic terms.

Table 5.8 P-values of the interaction between rejuvenator dosage and RBR

Model response	Rejuvenators	
	D	F
Original PGH	0.059	0.843
RTFO PGH	0.791	0.202
PGI	0.272	0.289
PGL_S	0.622	0.484
PGL_m	0.705	0.690
$J_{nr3.2}$	0.001	0.002
T_{cross}	0.577	0.825

Table 5.9 Parameters for checking RSM curvature

Model response	Deviation (%)		p-value (LOF)	
	D	F	D	F
Original PGH	1.70	1.91	0.002	0.583
RTFO PGH	0.65	0.28	0.638	0.088
PGI	4.18	4.65	0.089	0.088
PGL_S	3.15	2.55	-	-
PGL_m	6.25	4.18	-	-
T_{cross}	5.46	5.63	0.040	0.283

Therefore, except for $J_{nr3.2}$, a first-degree polynomial model without interaction terms and quadratic terms could be developed for all the other rheological indices. The rejuvenator dosage and RBR were two independent factors, showing linear relationships with the rheological properties of the blended binder. The results indicated that using linear regression in the blending chart could achieve authentic results for rejuvenator dosage optimization. However, Zhou et al. (2015) recommended using the regional linear blending chart in which the linear relationship only existed when the range of rejuvenator content was no more than 20% [120]. In this paper, the highest and lowest levels of the rejuvenator dosage were 10% and 0%, respectively; therefore, a linear relationship could be assumed between the rejuvenator dosages and rheological indices.

Comparison between blending chart and RSM methods

Table 5.10 shows the optimum rejuvenator dosages of rejuvenators D and F determined by the two optimization methods. The RSM method achieved slightly higher dosages than the blending chart method. Additionally, a similar trend in the rejuvenator dosages was observed when using rheological indices measured at different temperatures.

Table 5.10 Optimum rejuvenator dosage (%) determined by blending chart and RSM methods

Optimization method	Rejuvenator	Rheological indices					
		Original PGH	RTFO PGH	PGI	T_{cross}	PGL_S	PGL_m
Blending chart	D	6.96	7.20	3.50	4.40	3.56	4.23
	F	8.05	7.79	3.56	4.43	3.91	4.49
RSM	D	7.55	7.33	3.61	4.79	4.03	4.77
	F	8.42	8.04	3.75	4.68	4.40	5.06

Overall, the results suggest that the difference between the rejuvenator dosages determined by the blending chart and response surface modelling methods was marginal. For most of the rheological indices, the dosage difference between the two methods was less than 0.5%. As discussed previously, both optimization methods showed that the selection of optimization criteria has a significant impact on the rejuvenator dosage regardless of the rejuvenator type. As Table 5.10 shows, the rejuvenator dosage required to achieve the target PGH was considerably higher than that to restore low- and intermediate-temperature rheological indices.

Based on the discussions, it is recommended to choose PGL_m or T_{cross} which not only account for the stiffness reduction but also consider the restoration of flexibility and relaxation capacity. To this end, PGL_m was the final selection in this paper since it resulted in a sufficient rejuvenator dosage to restore the flexibility of the binder without over softening effects.

Validation of optimum rejuvenator dosage

In order to validate the optimum rejuvenator dosages determined in this study, optimized binder blends were prepared by adding the corresponding optimum rejuvenator content into the binder blend with 43% RAP binder which was equivalent to 50% RAP content in the mix. For rejuvenators A and B, the optimum dosages were 4.03% and 4.01% which was determined by the blending chart method. The optimum dosages for D and F were 4.27% and 4.52% which were estimated using the models developed from RSM methods. Table 5.11 shows the continuous temperatures of four rejuvenated binder blends. The predicted PGL_m values were all controlled to be an identical value of -31.9℃, which was the PGL_m of the base binder. Comparing the continuous temperatures of the base binder and the rejuvenated binder blends, all the rejuvenated binder blends achieved similar low continuous temperatures and showed higher PGH results at

the same time. Except for rejuvenator B, the rejuvenated binder blends showed similar T_{cross} values compared to the PG 58-28 binder, since the optimal dosages determined using T_{cross} and PGL_m were close. In addition, the rejuvenated binder blends achieved significantly lower $J_{nr3.2}$ values than that of the virgin binder. This parameter has been proved to have good correlations with field rutting resistance, the lower the non-recoverable compliance, the less susceptible to rutting [121]. Therefore, this estimated rejuvenator dosage was promising in balancing the rutting and cracking resistance of the recycled binder blend.

Finally, in addition to the nine rheological indices discussed so far, the ΔT_c parameter was also examined to verify the effectiveness of the optimum rejuvenator dosage determined through the aforementioned processes. A less negative ΔT_c indicates better stress relaxation capacity [122]. Table 5.11 shows that only rejuvenator F achieved a similar ΔT_c value of the base binder, the other three rejuvenated binder blends showed negative ΔT_c but still higher (i.e., less negative) than that of the RAP binder (ΔT_c = -3.9).

Table 5.11 Continuous PG temperature (℃) of optimized binder blends (43% RAP binder)

	Parameters	PG 58-28	43RB-A	43RB-B	43RB-D	43RB-F
Measured value	Original PGH	60.4	65.2	65.3	63.4	64.9
	RTFO PGH	61.2	65.1	64.9	64.8	65.0
	PGI	19.0	17.4	17.8	17.00	16.9
	PGL_S	-31.8	-32.6	-32.3	-33.1	-32.8
	PGL_m	-31.9	-32.0	-31.9	-32.7	-33.1
	ΔT_c	0.1	-0.6	-0.4	-0.4	0.3
	T_{cross}	18.4	18.5	19.0	18.4	18.3
	$J_{nr3.2}$	3.014	1.666	1.649	1.648	1.593
Optimization criterion	PGL_m	-	-31.9	-31.9	-31.9	-31.9

The optimized binder blend represents a full blending case between the virgin binder and the aged binder. However, the full degree of blending or complete activation of the RAP binder is unlikely to happen using conventional mixing and conditioning processes, especially for highly recycled asphalt mixes. Therefore, The impact of the degree of aged binder mobilization and partial blending should be considered when using the results of rejuvenator optimization from the binder study stage to produce high RAP mixes, since a

longer conditioning time is required to allow for complete mobilization of the aged binder, and a higher degree of diffusion between the rejuvenator and the binder phases [109,123].

5.6 Conclusion

This study evaluates the rejuvenator dosage optimization through the commonly used blending chart method and the more statistically rigorous response surface modelling (RSM) approach. To this end, four different bio-based rejuvenators were investigated using mainly nine different rheological indices as the restoration criteria. For the materials investigated in this study, it was concluded that among the different indices that were measured at very high, high, intermediate, and low temperature ranges, the indices measured at the intermediate and low temperatures are more suitable to be used as the optimization criteria to avoid over softening of the aged binder. It should be, therefore, emphasized that a proper optimization methodology should account for the satisfactory material's response over the full temperature range while identifying the dominant criterion (or criteria) for determining the ideal dosage for a given rejuvenator. The results of this study indicate that some rheological indices, such as the low continuous temperature based on creep stiffness (PGL_S) and the intermediate continuous temperature (PGI), may only account for the required rejuvenator dosage solely based on its ability to reduce the binder stiffness, rather restoring the binder flexibility. The optimal rejuvenator dosage determined in this paper has the potential to ensure that the rejuvenated binder blends have adequate cacking resistance without compromising the resistance to permeant deformation at high temperatures. Lastly, for the range of rejuvenator dosages investigate in this study it can be concluded that the blending chart method can be a reliable approach for determining the optimum rejuvenator dosage at the binder evaluation phase since most of the rheological indices are expected to have a linear relationship with the rejuvenator dosage and RAP binder ratio.

It is noteworthy that the rejuvenator dosage optimization at the binder testing stage assumes a full blending scenario, which barely happens in the actual plant production of high RAP mixes. It is also recommended to verify the optimum rejuvenator dosage in the mix testing phase as the incomplete degree of blending or diffusion might lead to excessive free rejuvenator, which increases the ease of compaction and moisture susceptibly of the recycled mixes. Furthermore, the traditional lab aging protocols used in this study may not be harsh enough to account for the long-term aging of the rejuvenated binders and mixes in the field. The long-term effectiveness of the determined rejuvenator dosage should be evaluated in future studies.

Chapter 6

Evaluation of rutting resistance and moisture susceptibility of recycled hot mix asphalt containing bio-based rejuvenators

This chapter is based on a journal paper manuscript entitled "Evaluation of Rutting Resistance and Moisture Susceptibility of Recycled Hot Mix Asphalt Containing Bio-based Rejuvenators", which will be submitted to the Journal of Construction and Building Materials. This work applies different analysis methods to evaluate the rutting and moisture resistance of high RAP content asphalt mixes containing bio-based rejuvenators and the soft virgin binder using the Hamburg Wheel-Tracking (HWT) test. It also focused on establishing a proper HWT testing protocol, including the test temperature, failure criteria, and rutting and moisture resistance indices, for mixtures containing highly recycled materials and rejuvenators.

6.1 Introduction

Rutting is one of the major distress modes in asphalt pavements that manifests in permanent deformation accumulation over the service life of pavements. Different mechanisms such as aggregate re-structuring, viscous flow of the asphalt binder, and mix densification can contribute to rutting [124,125]. The relatively higher temperature leads to higher compressive and shear stresses in the upper portion of asphalt concrete layers, therefore the surface layer is more prone to wheel-path depression accompanied by shearing along the sides of wheel-path [126], While mix densification can occur either due to inadequate compaction during construction or due to the post-compaction at the early stage of pavement opening [127].

Including Reclaimed Asphalt Pavement (RAP) in Hot Mix Asphalt (HMA) production has become a common practice for decades. The addition of RAP is expected to generally improve the rutting resistance of asphalt mixes due to the increased stiffness from the aged binder. Review of the literature indicates that asphalt mixtures with RAP contents as high as 40% have exhibited better rutting resistance compared to mixes with virgin materials or less RAP content [45,55,123]. Previous studies have also shown that the addition of RAP improved the moisture resistance compared to the virgin asphalt mixes because of the stronger bonding between the aged binder and RAP aggregates [128]. However, RAP has a relatively higher content of fine particles, which can disrupt the aggregate skeleton and diminish interlocking between particles, hence reducing the shear resistance of the mixture. In addition, the insufficient blending zone between virgin and aged binder is a potential weak point for both shear resistance and moisture

susceptibility. The tensile strength ratio (TSR) results Zhao et al. [129] revealed that the addition of more than 30% RAP adversely affected the moisture resistance of the asphalt mix.

There is a growing interest in using rejuvenators to maximize the RAP incorporation in HMA production. The use of rejuvenators facilitates the activation of the RAP binder and improves the blending between virgin and RAP binder, thereby allowing the inclusion of higher RAP contents without sacrificing the mix performance [2,23,130]. However, if not properly accounted for, impaired rutting resistance can be a potential concern for rejuvenated RAP mixes due to the softening effect of rejuvenators. Some researchers claimed that although the use of rejuvenators negatively affected the rutting resistance of the high RAP mixes, the rejuvenated mixes still performed better than the virgin asphalt mixes [56,131]. Nevertheless, even at an optimized rejuvenator content, there is a possibility of the presence of free/excess rejuvenator content since diffusion of the rejuvenator into the RAP binder is unlikely to be completed during the short mixing period [132]. The additional amount of rejuvenator will promote lubrication during mixing and compaction but weaken the adhesion of the binder to the aggregate particles.

Hamburg Wheel-Tracking (HWT) test, performed on under water submerged specimens, is one of the most commonly used tools for rutting performance evaluation in North America. The test has been adopted by many agencies as a standardized method to evaluate rutting resistance as well as moisture susceptibility of asphalt mixes [133]. The interpretation of the HWT test results is based on the evolution of rut depth with the number of wheel passes. Figure 6.1 shows a typical plot of HWT data and the interpretation of some key parameters. Normally, there are three stages of deformation during the test: the post-compaction stage, creep stage and stripping stage [106]. In the post-compaction stage, the sample will continue to consolidate for the first few numbers of passes even after compaction. It symbolizes the densification of the asphalt mix caused by vehicle loading when the compacted pavement is open to traffic. The rut depth measured before 1,000 passes can be attributed to the post-compaction densification [125]. The rut depth curve in the creep stage is much flatter and has a much lower slope compared to the post-compaction stage. The creep stage captures the deformation that is mainly attributed to the visco-plastic flow of the material. Finally, when moisture damage begins to become the dominant mechanism, the rate of deformation abruptly accelerates, marking the stripping inflection point (SIP). SIP is the number of passes at the intersection of the two straight lines that fit the creep stage and the stripping stage. The stripping slope is the inverse of the rate of deformation in the stripping stage. It reflects the moisture sensitivity of the sample given that the deformation is primarily caused by moisture damage.

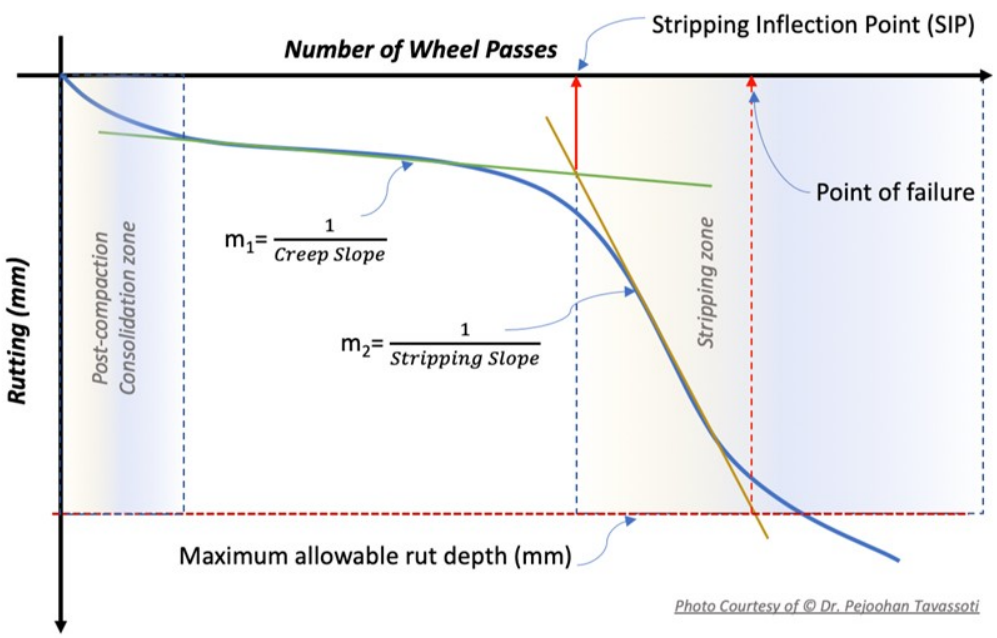

Figure 6.1 Typical failure pattern of HWT test

6.2 HWT test temperature and criteria

Different Departments of Transportation (DOT) have set different criteria in terms of testing temperature, passing/failing thresholds, and number of wheel passes, for a given mix or binder grade under HWT testing. Table 6.1 summarizes the recommended HWT test temperatures and criteria by different specifications. Some DOTs require varying the testing temperature (i.e., in a range of 40 to 56°C) as a function of the high-temperature PG of the binder, while others use a constant temperature (e.g., 50°C) for all mixes [126,134]. Regarding the failure criteria, the majority of DOT specifications require either a maximum permitted rut depth at a given number of passes or a minimum number of passes at a certain rut depth. However, only a small number of agencies set a limit on the number of passes at the SIP to control the moisture susceptibility of mixes.

Table 6.1 HWT test temperature and criteria in different DOT specifications

DOT	Test temperature (°C)	Binder high PG (°C)	Rut depth threshold (mm)	Minimum wheel passes
California	45	58	12.5	10000
	50	64		15000
	55	70 and 76		20000
Colorado	45	58	4.0	10000
	50	64		
	55	70 and 76		
Illinois	50	≤ 58	12.5	5000
		64		7500
		70		15000
		≥ 76		20000
Iowa	40	52 and 58	8.0	8000 (no SIP before 10000 or 14000)
	50	≥ 64		
Montana	44	58	12.5	15000
	50	64		
	56	70		
Oklahoma and Texas	50	64	12.5	10000
		70		15000
		76		20000
Ontario	44	52 and 58	12.5	20000
	50	64	12.5	20000
	50	70	6.0	20000
Utah	46	58	10.0	20000
	50	64		
	54	70		
Washington	50	All	10.0	15000 (no SIP)
Wisconsin	50	≤ 58	12.5	5000
		64		10000
		70		15000
		≥ 76		20000

The AASHTO T324 standard specification requires five parameters derived from the rut depth curve to evaluate the rutting resistance and moisture susceptibility of an asphalt mix [106]. These parameters include: 1) the maximum rut depth if the measured impression did not reach the maximum allowable limit, 2) the

number of wheel passes at the maximum rut depth if the test ended before 20,000 wheel passes, 3) Creep slope, 4) Stripping slope (if applicable), and 5) Stripping inflection point (SIP), which can be calculated based on the slopes and intercepts from the creep and stripping stages using Equation (6-1).

$$SIP = \frac{intercept\ (strip\ stage) - intercept\ (creep\ stage)}{slope\ (creep\ stage) - slope\ (strip\ stage)} \quad (6\text{-}1)$$

The AASHTO T324 standard, however, does not provide details on how to determine the creep and stripping slopes from the rut depth curve. The determination of the creep and stripping stages is based on a subjective judgement when the slope of the curve is steady. As a result, fitting two tangent straight lines on the creep and stripping stages will potentially introduce biases into the interpolation of SIP [135]. Furthermore, the rut depth in the HWT test under wet conditions is a result of the confounding effects of post-compaction, creep, and moisture. It may be misleading to rely solely on the maximum rut depth or the maximum number of passes as failure criteria to regulate the rutting performance of mixes [136,137]. The HWT test criteria provide insight into an overall evaluation of the mix performance in terms of the high-temperature rutting resistance and moisture susceptibility. To this end, different HWT data analysis methods have been developed to identify the creep and stripping stages and distinguish the resistance to shear flow at high temperatures from the confounding rut depth caused by moisture damage.

Sixth-degree polynomial approach

Iowa DOT characterizes the HWT data using a sixth-degree polynomial equation by least squares regression [138]. As Figure 6.2 shows, the stripping pass is first calculated as the number of wheel passes at which the first derivative of the fitted curve is the maximum (i.e., the second derivative is zero) near the end of the test. The stripping slope is the slope of the tangent line at the stripping pass. The point at which the first derivative is the smallest before the striping pass is then used to determine the creep pass. The SIP can be still calculated using Equation (6-1). The SIP is invalid if the ratio of the creep slope to the stripping slope is less than 2.0, which means no obvious stripping should be reported.

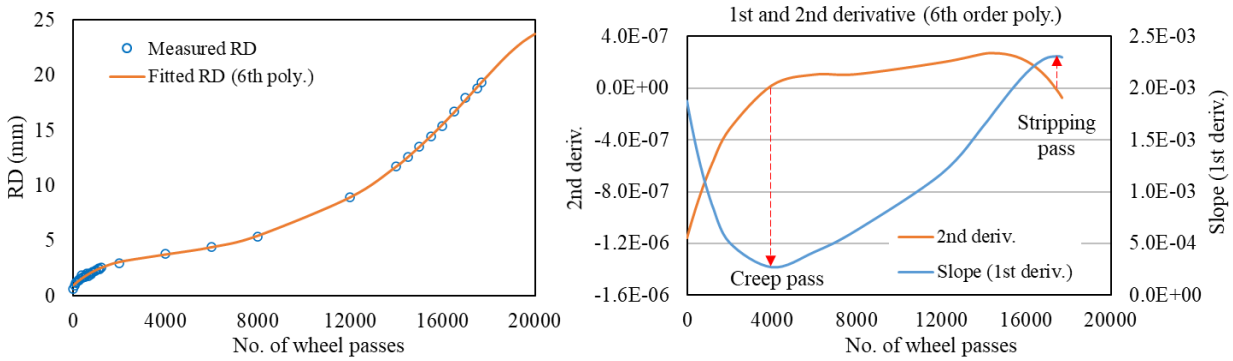

Figure 6.2 HWT data analysis (Iowa DOT)

Tseng-Lytton model and stripping number approach

The Texas DOT specification adopts the novel analysis method proposed by Yin et al. [135]. This method fits the HWT test data using Equation (6-2), which consists of one part of negative curvature and another part of positive curvature (see Figure 6.3). The stripping number (SN), at which the second derivative of the fitted curve equals zero, is the point at which the fitted curve transits from the negative curve to the positive curve. Therefore, the number of passes at SN can be determined using Equation (6-3).

$$RD(N) = \rho \times \left[ln(\frac{N_{ult}}{N})\right]^{-1/\beta} \tag{6-2}$$

$$N_{SN} = N_{ult} \times exp(-\frac{\beta + 1}{\beta}) \tag{6-3}$$

where:

$RD(N)$ – rut depth at a certain number of wheel passes (mm).

N – number of wheel passes.

N_{ult}, ρ, and β – model coefficients.

N_{SN} – the number of passes to SN, which is an indicator of the onset of stripping.

Before N_{SN}, the rut depth or the permanent strain is triggered by the post-compaction and the visco-plastic deformation. The Tseng-Lytton model (see Equation (6-4)) is used to fit the strain curve before N_{SN}

and then projected to the entire test period. The slope of the projected curve at 10,000 passes is used as a parameter to quantify the rutting resistance of the mix. This parameter reflects the increment of the visco-plastic strain which is not affected by the post-compaction and moisture-induced strain.

$$\varepsilon_{vp} = \varepsilon_{vp}^{\infty} \times exp\left[-\left(\frac{\alpha}{N}\right)^{\lambda}\right] \tag{6-4}$$

$$\Delta\varepsilon_{vp}^{10000} = \alpha^{\lambda}\lambda\varepsilon_{vp}^{\infty} exp\left[-\left(\frac{\alpha}{10000}\right)^{\lambda}\right] 10000^{-(\lambda+1)} \tag{6-5}$$

where:

ε_{vp} – visco-plastic strain.

$\varepsilon_{vp}^{\infty}$ – saturated visco-lactic strain.

α and λ – model coefficients.

$\Delta\varepsilon_{vp}^{10000}$ – visco-plastic strain increment at 10,000 passes.

In addition to the N_{SN}, the stripping life (N_{ST}) parameter is used to assess the moisture susceptibility of the mix. As Figure 6.3 shows, N_{ST} is determined as the additional wheel passes when the stripping strain, calculated as the difference between the total strain and ε_{vp}, reaches the level corresponding to the 12.5mm rut depth.

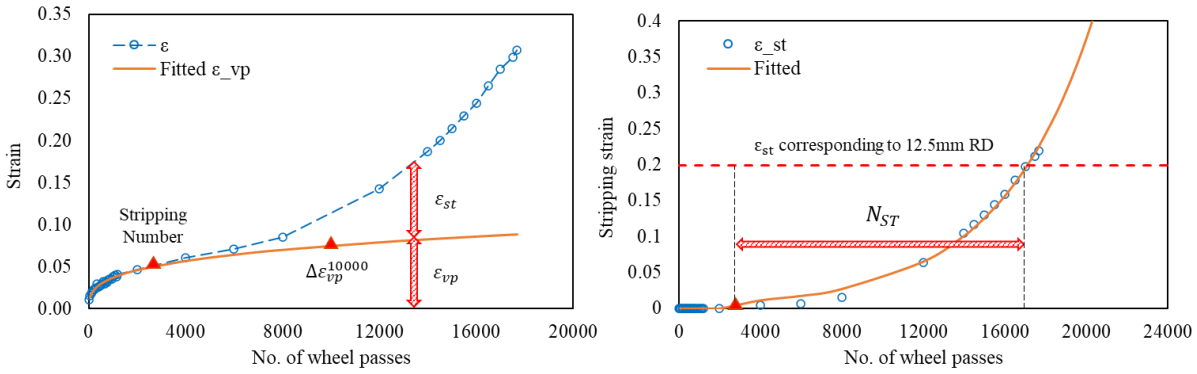

Figure 6.3 HWT data analysis (Texas DOT)

Visco-plastic power-law and moisture ratio approach

Lv and Bahia [136] proposed an analysis method based on the normalized rut depth (see Figure 6.4). First, the test data is fitted with a sixth-degree polynomial function, and the inflection point, similar to SN, is defined as the number of passes when the second derivate of the fitted curve first reached zero after 1000 passes. The normalized rut depth is then produced by subtracting the fitted rut depth at 1000 passes from the fitted curve. The rut depth measured at 1000 passes is usually contributed to the effects of post-compaction. After data normalization, the normalized rut depth data before the inflection number is fitted using a power-law model (see Equation (6-6)) and projected to the entire test period. This part of rut depth is only related to the visco-plastic deformation (RD_{vp}).

$$RD_{vp}(N) = a \times N^{VR} \tag{6-6}$$

where:

RD_{vp} – normalized rut depth attributed to the visco-plastic deformation (mm).

N – normalized number of wheel passes.

a – model coefficient.

VR – visco-plastic ratio.

As can be seen in Figure 6.4, the difference between the total normalized rut depth and the normalized RD_{vp} is the rut depth induced by moisture damage (RD_m). A new parameter moisture ratio (MR) is defined as the ratio between the RD_m and the total normalized rut depth at the NPF or the end of the test if the rut depth does not reach 12.5 mm after 20,000 passes. It identifies the contribution of the moisture damage to the failure of the sample in the stripping stage, reflecting the moisture susceptibility of the mix.

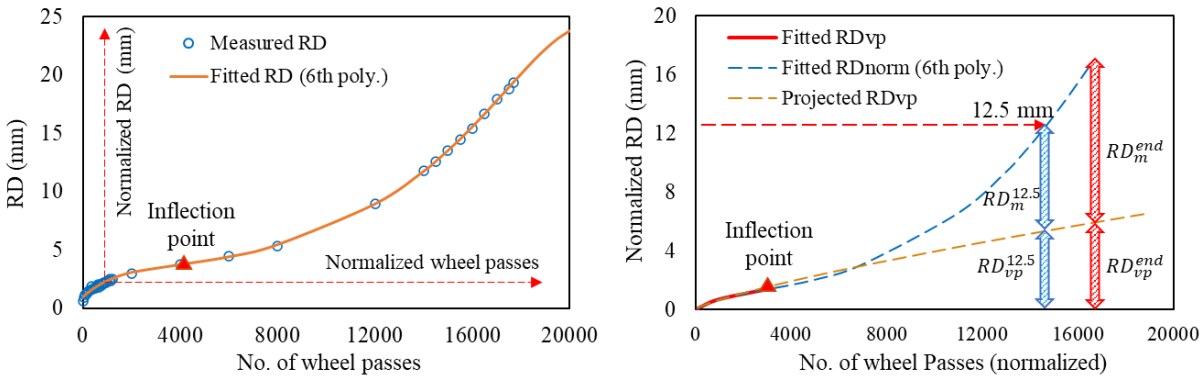

Figure 6.4 HWT data analysis (Lv and Bahia)

According to the analysis methods mentioned above, there are three major groups of parameters for evaluating the overall performance, rutting resistance, and moisture susceptibly, respectively. The maximum rut depth at the end of the test or the number of passes when the rut depth reaches the failure criteria can be used for evaluating the overall performance of the mix. Parameters obtained from the creep stage or isolated from the moisture-induced deformation, including the creep slope, VR, and $\Delta\varepsilon_{vp}^{10000}$, can be selected to quantify the rutting resistance of the mix. N_{SN} is an indicator of the onset of the stripping stage. A larger N_{SN} suggests that the asphalt mix can resist longer before the moisture damage starts to dominate the HWT test. N_{ST} and MR are determined after stripping occurs, they are invalid if the mix does not exhibit a stripping stage. These two parameters reveal the contribution of moisture damage to the final failure of the sample.

6.3 Research gaps and objectives

For many years, previous studies have used the HWT test to evaluate the asphalt mixtures' resistance to rutting and moisture damage. The AASHTO T324 standard is also adapted for regional balanced mix design (BMD) purposes by many agencies. However, even for the same mix design, using different test temperatures and criteria could result in controversial mix performance evaluation results. Additionally, there have been no established HWT test guidelines for high RAP mixes containing rejuvenators. Much uncertainty still exists for the rutting performance of recycled asphalt mixes, especially when the RAP fraction and rejuvenator content are both included. The rutting resistance of the asphalt mixture may be improved by adding more RAP, but the moisture susceptibility may suffer from insufficient blending between RAP and virgin materials. Furthermore, the use of a rejuvenator may result in concerns in terms of over softening the recycled binder, ease of compaction due to extra lubrication, and diminishing the

adhesion between asphalt and aggregate. This study, therefore, set out to evaluate the performance of rejuvenated high RAP mixes using the wet condition HWT test and innovative analysis approaches to better understand the rutting and moisture damage resistance of such mixes. The following specific objectives are defined in this study:

- To evaluate the effect of increased RAP content and the addition of different bio-based rejuvenators on rutting resistance and moisture susceptibility of asphalt mixes.
- To compare the influences of different HWT conditioning temperatures determined by the virgin binder grade and the blended binder grade.
- To differentiate the overall performance, rutting resistance, and moisture susceptibility of the asphalt mixes using conventional and novel parameters developed by different HWT data analysis methods.

6.4 Materials and experimental methods

6.4.1 Materials description and mix design

The materials description and mix design details were the same as the information described in Chapter 3. Based on the conclusions in Chapter 4 and Chapter 5, the four rejuvenators selected to continue the mix testing phase are A, B, D, and F. Therefore, the rejuvenated high RAP mixes prepared in this chapter are listed in Table 6.2. The rejuvenator dosage (%) is by weight of the total binder content, including the virgin binder and RAP binder. And the RAP binder replacement (%) is the ratio of RAP binder content to the total binder content. There are six rejuvenated high RAP mixes in total. Except for the mix R50-SB, which was prepared by replacing the base binder with the PG 46-34 asphalt, other rejuvenated high RAP mixes were produced by adding certain amounts of the four abovementioned rejuvenators. The rejuvenator dosage (by weight of the total binder content) of each rejuvenator was determined by the binder testing results when the rejuvenated binder blend achieved the same continuous low PG (based on m-value) of the target virgin binder (i.e., PG 58-28). R50-B* was prepared with a reduced rejuvenator content considering the assumption that the mobilization of the RAP binder will be less than 100% during the laboratory mixing and compaction process. In this case, the contribution of the RAP binder in R50-B* was assumed as 70% based on the review of previous studies. The reduced dosage of rejuvenator B was then calculated using the optimization method mentioned in Chapter 5, which is 3.22% in accordance with a 70% RAP binder contribution scenario.

Table 6.2 Rejuvenated high RAP mix information

Mix Code	Base binder	Rejuvenator dosage (%)	RAP binder replacement (%)	Original PGH (℃)	RTFO PGH (℃)
R20	PG 58-28	N/A	17.0	65.4	65.9
R50-SB	PG 46-34	N/A	43.0	66.9	66.5
R50-A	PG 58-28	4.03	43.0	63.2	65.7
R50-B	PG 58-28	4.01	43.0	64.1	65.9
R50-B*	PG 58-28	3.22	43.0	65.3	67.3
R50-D	PG 58-28	4.27	43.0	63.4	64.8
R50-F	PG 58-28	4.52	43.0	64.9	65.0
R50	PG 58-28	N/A	43.0	73.0	73.0

6.4.2 Sample preparation

The mixing and compaction temperatures were first determined based on the equivalent viscosities of the unaged asphalt binders to achieve 0.17 ± 0.02 Pa·s and 0.28 ± 0.02 Pa·s, respectively [102]. Table 6.3 For the control mix with 20% RAP, the mixing and compaction temperatures remained the same and the RAP did not require preheating before mixing. However, it should be noted that for high RAP contents, it will be challenging to maintain the targeted mixing temperature without adjusting the asphalt binder temperature and preheating the RAP. This is especially important when using an open mixing drum without a heating source, which is considered a limitation of most laboratory mixing equipment. Therefore, the mixing procedure of the 50% RAP mix was adjusted to compensate for the increased RAP content and heat loss during the mixing. To achieve the target mixing temperatures in Table 6.3, the preheating temperatures of the blended binders were increased to 160°C rather than using the temperatures listed in Table 6.3 and the RAP was preheated to 110°C for less than two hours before mixing.

Table 6.3 Mixing and compaction temperatures (℃) of different binders

	PG 58-28	PG 46-34	PG 58-28				
			A	B	B*	D	F
Mixing	146	132	130	132	135	129	133
Compaction	135	120	115	117	121	115	120

The sample preparation was completed by following steps:

(1) Preheat aggregates to 10℃ above the mixing temperature overnight (more than 16 hours).
(2) Preheat RAP to 110℃ (if RAP content is more than 20%) and maintain the temperature for less than 2 hours before mixing.
(3) Preheat the base binder to the mixing temperature and add the rejuvenator at its optimized dosage described in Table 6.2 into the base binder to achieve a homogenous binder blend using the regular binder blender. Then put back the blended binder in the oven at the mixing temperature for less than 1 hour before mixing.
(4) Premix the virgin aggregates with RAP for 45 seconds (30 seconds if %RAP is no more than 20%), and then add the binder to mix for another 90 seconds (60 seconds if %RAP is no more than 20%).
(5) Condition the loose mix for 4 hours at 135℃ to simulate short-term aging [139].
(6) Compact the loose mix using the Superpave Gyratory Compactor (SGC) to a target air void of 7.0 ± 0.5% by controlling the sample height to 63mm.

During the mixing, the temperature of the high RAP mixes was monitored using a thermal gun and a temperature range between 125℃ and 135℃ was successfully achieved before discharging the loose mix. Hence, the sample preparation proposed in this paper was able to attain the required mixing temperatures in Table 6.3.

6.4.3 HWT test protocol

For the lab-compacted specimens using the SGC, four disk-shaped specimens of 150mm diameter were grouped in pairs to run the test at the same time. The load on each of the steel wheels was 705 ± 4.5 N. The test was programmed to finish either after 20,000 wheel passes or when the rut depth reaches a maximum value of 20mm to allow for extracting the full range of mix performance data. Two test temperatures were selected in this study. All mix samples were first tested at 44℃ to verify whether the samples could pass the HWT criteria for the PG 58-XX asphalt binder as per the Ontario lab testing manual. Then, mixes which had fulfilled the requirement at 44℃ were tested again at 50℃. The test temperature of 50℃ was selected because most of the mixes had the equivalent binder high PG of 64℃ (see Table 6.3), which indicated that all the mixes could also pass the HWT criteria at 50℃ for a PG 64-XX binder grade. For each mix, the rut depth results obtained from the two wheel-tracking sides were averaged to get the final rut depth and to determine the variability of this test. Meanwhile, the rut depth against wheel passes curve from each side was analyzed using the three data analysis methods mentioned above to distinguish the rutting resistance parameters from moisture susceptibility parameters. So, four samples were prepared for each mix type to conduct the HWT test.

6.5 Results and discussions

6.5.1 Conventional performance evaluation

The HWT results of different mixes were first interpreted using conventional parameters like the maximum rut depth and maximum wheel passes. Due to the combined effects of visco-plastic deformation and moisture damage, these two parameters only fairly represented the overall performance of the mixes. As Figure 6.5 shows, except for mix R50-D and mix R50-F, the other six mixes did not reach the maximum allowable rut depth. According to the HWT test criteria in Ontario (see Table 6.1), the failure threshold is defined as 12.5mm at the test temperature of 44℃. Among these six mixes, R50-SB and R50-A showed that the rut depth could be statistically higher than 12.5mm. The control mix (R20) had a slightly lower average rut depth than the high RAP mixes manufactured with the soft binder, rejuvenator A, and rejuvenator B, but the difference in rut depth between these mixes was statistically insignificant. Furthermore, rut depth was significantly reduced in comparison to the other high RAP mixes, i.e. without rejuvenator (R50) and with reduced rejuvenator content (R50-B*).

All the mixes except for R50-D and R50-F (which already failed at 44℃) underwent HWT testing at 50℃. Figure 6.6 depicts the number of passes when the samples reached a rut depth of 12.5mm. The figure shows that the R50 mix successfully took up to 20,000 wheel passes without reaching the 12.5mm failure threshold at the end. This can be naturally attributed to the high stiffness of a 50% RAP mix without any rejuvenators. However, it should be noted that from the mix design perspective, the rutting criterion alone would not be enough, and the mixture should also meet the cracking requirements, which fall out of the scope of this research. Most DOT specifications regulate the minimum acceptable number of passes before failure to 7,500 or 10,000 for samples tested at 50℃ (see Table 6.1). From Figure 6.6, it can be therefore recognized that only R50-B and R50-B* meet the requirement to be considered to have a PG 64-XX binder grade. It is worth mentioning that although similar high PG results were obtained for the different binder blends used to prepare the mixes in this study, the control mix exhibited the lowest number of wheel passes when compared to the rejuvenated high RAP mixes at 50℃. This further underlines the fact that solely using binder testing results for rejuvenator optimization may not be reliable in terms of the mixture performance.

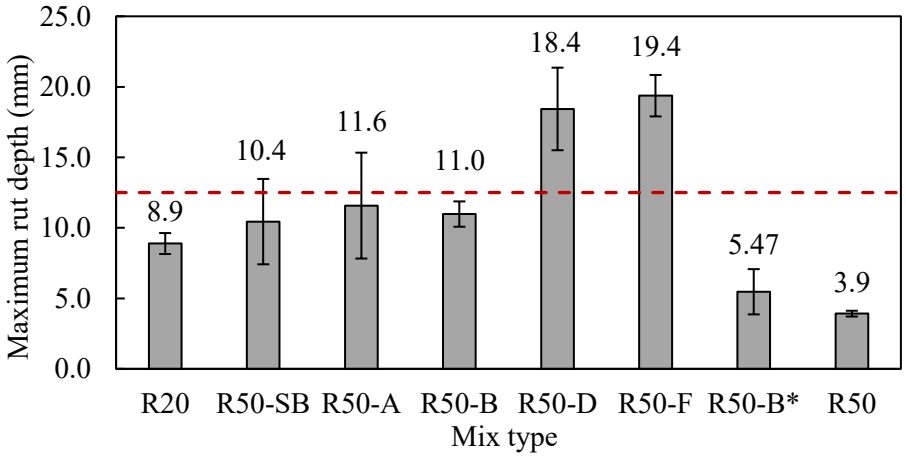

Figure 6.5 Maximum rut depth (44°C) of different mixes

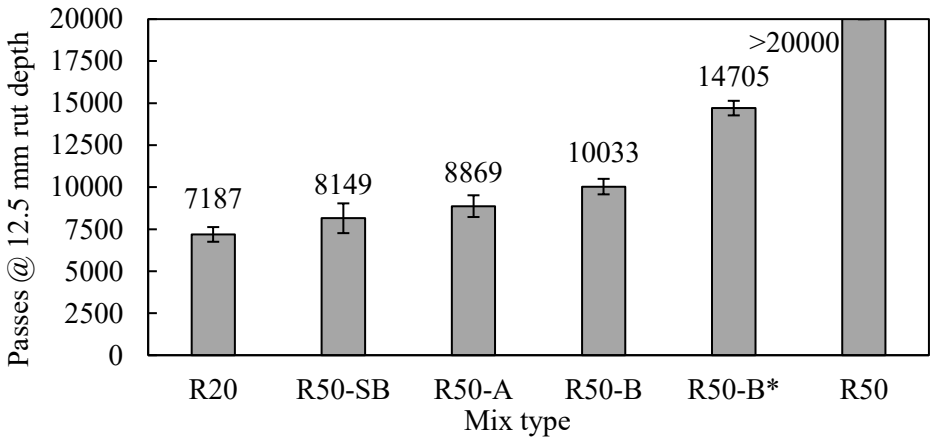

Figure 6.6 Number of passes to reach 12.5 mm rut depth (50°C) of different mixes

Equation (6-7) presents another parameter defined as the rutting resistance index (RRI) which was developed by Wen et al. [140]. RRI considers both the rut depth and the number of wheel passes. It allows the comparison between test results that were terminated at different thresholds, either the test was stopped at end of 20000 passes, or the test was stopped when the maximum allowable rut depth was reached. Previous research has proved a high correlation ($R^2 = 0.924$) between the field rut depth and RRI [134].

$$RRI = N_{max}(1 - RD) \quad (6\text{-}7)$$

where:

RRI – rutting resistance index (in).

N_{max} – the number of wheel passes when the test is completed.

RD – rut depth in inches when the test is completed.

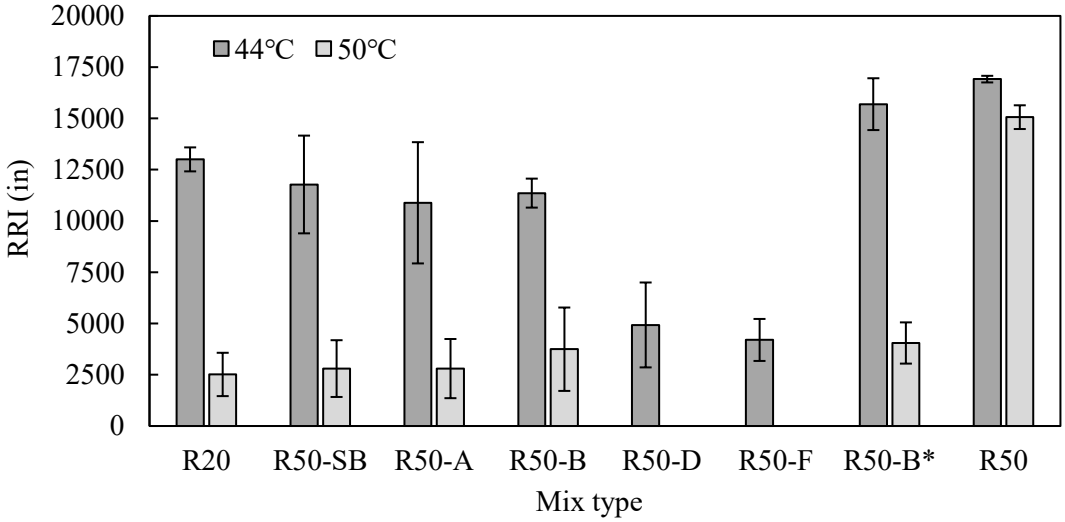

Figure 6.7 RRI of different mixes at 44°C and 50°C

Asphalt mixes with higher RRI values are expected to have a better overall performance during the HWT test. As shown in Figure 6.7, the RRI results obtained at 44°C were consistent with the rut depth results in Figure 6.5. All the mixes showed average RRI values higher than 10,000 except for the R50-D and R50-F mixes. With an increase in the testing temperature, the control mix as well as the rejuvenated high RAP mixes exhibited a drastic decrease in RRI values. Compared to other mixes, R50 demonstrated the highest RRI values at both test temperatures, and the difference between 44°C and 50°C was noticeably smaller.

Together, these results offered important insights into the overall performance of different mixes using the HWT test. The rut depth was significantly reduced by increasing the RAP content; however, either adding bio-based rejuvenators or replacing the base binder with a softer virgin binder counteracted the improvement in rutting resistance. As the test temperature increased, the rejuvenated high RAP mixes slightly surpassed the control mix by enduring a higher number of wheel passes, but they scarcely met the criteria for the PG 64-XX binder grade. The possible explanation for this observation could be that the blending was not completed between the virgin and RAP binders. Therefore, it is likely that some spare rejuvenator content existed in the mix due to inadequate diffusion which might have deteriorated the

bonding between binder and aggregates and facilitated the mastic to get washed out by water during the test. According to the results of the R50-B* mix, reducing rejuvenator dosage by about 0.8% was promising to alleviate the side effects of rejuvenators. It also indicates the possible reasons for the failure of R50-D and R50-F might be the slightly higher rejuvenator dosages (4.27% and 4.52%) compared to R50-A and R50-B (4.03% and 4.01%).

6.5.2 New rutting resistance parameters

Instead of using the overall performance parameters, the results of HWT tests can be interpreted through the novel parameters that can offer more perceptive information on the effects of rejuvenators. For instance, it is crucial to understand whether the rejuvenator just over softens the high RAP mix without increasing moisture susceptibility or the addition of rejuvenator made the mix more susceptible to moisture damage than to the deformation caused by traffic loading. The parameters discussed in this section are indicators for the resistance to visco-plastic deformation during the creep stage. They were obtained by subtracting the creep stage from the entire test period before moisture damage occurred. Chaturabong and Bahia [137] conducted the HWT test in both dry and wet conditions to evaluate the effect of moisture on the creep stage. They found that the difference in the fitted creep slope curve for both wet and dry conditions was within the experimental error. Hence, the accumulated deformation within the creep stage was marginally affected by moisture and it was primarily due to the cyclic loading. This finding supported the idea that the rutting resistance parameters without confounding effects of moisture can be estimated from the wet HWT test.

Table 6.4 and Table 6.5 summarize the mean value and the coefficient of variance (CV) of rutting resistance parameters for each mix at 44℃ and 50℃, respectively. Because the creep slope calculated on one wheel side was negative, indicating an unrealistic decreasing trend of the rut depth, the mean value and CV of the creep slope for R50 at 44°C were unavailable. Therefore, the fluctuation of the measured rut depth data resulted in multiple peaks in the slope of the sixth-order polynomial function. In general, the CV values of creep slope and the $\Delta\varepsilon_{vp}^{10000}$ were greater than those of the other parameter VR. Creep slope and $\Delta\varepsilon_{vp}^{10000}$ were generated from the models by fitting the rut depth including both the post-compaction stage and the creep stage. Consequently, the variability of rut depth during the post-compaction stage also contributed to the calculation of these two parameters. As can be seen from Table 6.5, the CV of all three parameters becomes relatively smaller when the test temperature increases to 50℃. This reduced variability might be attributed to the less amount of data available for fitting the creep stage as the mixes enter the stripping stage much earlier at 50℃.

R50-D resulted in the largest rutting parameters among the mixes based on the mean values of all three rutting parameters at 44°C, ranking it as the poorest in terms of rutting performance. Compared to the control mix and the non-rejuvenated high RAP mix, the rejuvenated high RAP mixes showed higher mean values (i.e., worse performance). Comparing the rutting parameters of R50-B and R50-B*, except for $\Delta\varepsilon_{vp}^{10000}$, it can be recognized that the rutting susceptibility was reduced when the Rejuvenator-B content was decreased in the R50-B* mix. Except for R50-D, the three parameters did not provide consistent rankings for the rejuvenated high RAP mixes. This indicates that either the addition of a rejuvenator with optimized dosage resulted in similar rutting performance of the 50% RAP mix or these parameters failed to distinguish the difference between different types of rejuvenated mixes. In terms of the rutting parameters at 50°C, creep slope and VR showed the same ranking of different mixes and they achieved relatively lower variability compared to $\Delta\varepsilon_{vp}^{10000}$. Nevertheless, R50 remained the least rutting susceptible among these mixes, followed by R50-B*. However, the mean values of creep slope and VR for the control mix became statistically higher than the rejuvenated high RAP mixes. Under both test temperatures, the parameter VR exhibited the least variability level among the rejuvenated mixes, with the VR value averaging around 0.80 at 44°C and rising to a range of 0.86 to 0.89 at 50°C. R20 and R50-B* both experienced increases in their corresponding VR values of 0.18 and 0.11, whereas R50 maintained a statistically constant VR value regardless of the test temperature.

Table 6.4 Rutting resistance parameters at 44℃

Mix type	Creep slope (10^{-4})			VR			$\Delta\varepsilon_{vp}^{10000}(10^{-6})$		
	Mean	Rank	CV (%)	Mean	Rank	CV (%)	Mean	Rank	CV (%)
R20	1.40	2	24.9	0.77	3	2.8	1.49	1	29.9
R50-SB	2.59	4	46.2	0.81	7	5.2	2.30	7	27.3
R50-A	2.72	6	39.9	0.80	6	4.7	2.18	5	25.7
R50-B	2.08	3	32.6	0.79	4	3.9	1.75	3	7.3
R50-D	4.55	7	32.7	0.85	8	4.8	2.59	8	5.7
R50-F	2.68	5	26.3	0.79	5	2.1	2.26	6	45.3
R50-B*	0.76	1	87.8	0.70	1	3.5	2.05	4	29.2
R50	N/A	N/A	N/A	0.73	2	3.3	1.51	2	2.3

Table 6.5 Rutting resistance parameters at 50℃

Mix type	Creep slope (10^{-4})			VR			$\Delta\varepsilon_{vp}^{10000}(10^{-6})$		
	Mean	Rank	CV (%)	Mean	Rank	CV (%)	Mean	Rank	CV (%)
R20	8.52	6	9.5	0.95	6	1.0	2.85	3	4.0
R50-SB	7.97	5	25.2	0.89	5	2.1	3.28	5	34.3
R50-A	6.85	4	0.7	0.89	4	0.2	3.05	4	34.7
R50-B	5.69	3	7.0	0.86	3	1.1	3.78	6	65.0
R50-B*	3.74	2	4.6	0.81	2	0.2	2.64	2	18.3
R50	0.83	1	0.3	0.72	1	3.7	2.24	1	7.0

As shown in Table 6.4 and Table 6.5, using different rutting parameters led to different rankings of the mix rutting resistance, but they were able to distinguish between the rejuvenated high RAP mixes and the control mix as well as the high RAP mixes without rejuvenators or with a lower rejuvenator content. Because the post-compaction stage was not accounted for during the curve fitting process, the parameter VR had the lowest coefficient of variation. Despite that the rejuvenator D showed the highest rutting susceptibility at 44℃, the other rejuvenated high RAP mixes exhibited similar VR values at both testing temperatures. Except for R50, increasing the test temperature significantly worsened the rutting performance of the mixes, with the control mix displaying the highest increase in these rutting resistance

parameters. This implies that the rejuvenated mixes can offer an advantage over the control mix in terms of their temperature sensitivities.

6.5.3 Moisture susceptibility parameters

Unlike the dry rutting tests, moisture-induced damage can trigger stripping under wet HWT testing conditions. In addition to the traditional parameters (e.g., SIP), three novel parameters (i.e., MR, N_{SN}, and N_{ST}) were computed in this study to evaluate the moisture susceptibility of the mixes. More specifically, MR and N_{ST} were determined from the rut depth data by excluding the contribution of loading-induced deformation during the stripping stage.

Figure 6.8 displays the SIP results of different asphalt mixes determined by the Iowa DOT analysis method. At 44℃, the SIP of the R50 should be considered invalid because the slope ratio between the stripping slope and the creep slope is less than two, which indicated no stripping occurred until the end of the test. R50-B* exhibited the best performance based on its largest SIP compared to the rejuvenated high RAP mixes and was followed by the control mix. The SIP of the high RAP mix prepared with the soft binder occurred slightly earlier than the rest of the rejuvenated high RAP mixes, while a substantial variation was observed between the two sample groups. In addition, no discernable differences were found between the four rejuvenated high RAP mixes since the SIP of those mixes was around 10,000 wheel passes. The SIP of the control mix experienced a significant drop from about 15,000 to below 6,000 when the temperature was increased to 50°C. Furthermore, the three rejuvenated high RAP mixes exhibited better moisture resistance than the control mix as they attained comparable SIP values that were higher than that of the control mix. Unlike at 44°C, the stripping stage was observed in the case of R50 mix at 50°C, with a SIP value of around 18,000 as shown in Figure 6.8; however, it was still the largest SIP among all asphalt mixes. Comparing R50-B and R50-B*, it can be recognized that lowering the rejuvenator content by 0.8% (by weight of the total binder content) tends to postpone the emergence of SIP.

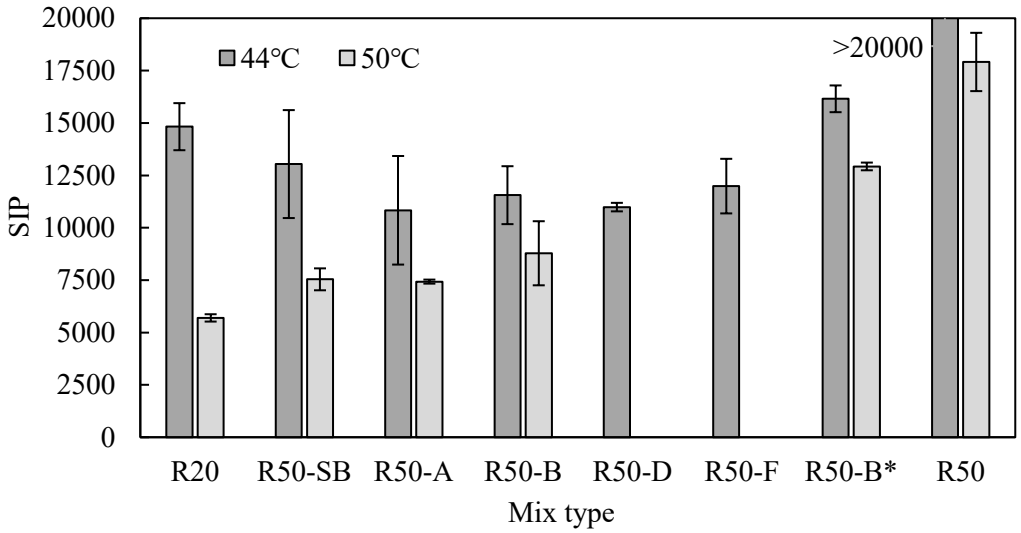

Figure 6.8 SIP of different mixes at 44℃ and 50℃

SIP has been used in several DOT specifications to control the moisture damage resistance of asphalt mixes. This parameter, however, is affected by both the creep slope and the stripping slope. As a result, even if there is actual moisture damage during the stripping stage, a stiffer mix with a very low creep slope may still pass the required SIP [141]. To this end, the novel moisture susceptibility parameters were introduced in this paper as listed in Table 6.6 and Table 6.7. Similar to the parameters for rutting resistance, the variability of these parameters, particularly the MR, was considerably smaller at 50°C. From Table 6.6, it can be recognized that the moisture susceptibility parameters did not apply to R50-B* and R50 mixes at 44°C, which indicates that the samples did not undergo the stripping stage throughout the completion of the testing. Obvious stripping damage was observed The high RAP mixes with rejuvenator D and rejuvenator F showed the most severe moisture-induced damage cases. Both mixes demonstrated stripping to affect the deformation evolution before reaching 4,000 wheel passes. Beyond this point, R50-D and R50-F undertook up to slightly less than 10,000 loading passes before reaching the commonly used maximum deformation of 12.5mm. The results indicated that moisture-induced damage played a significant role in the failure of R50-F and R50-D mixes by contributing to 65.6% and 47.4% of their corresponding final rut depths, respectively. Whereas R50-SB and R50-A showed the lowest moisture damage (about 24%) among the control mix and the rejuvenated high RAP mixes. In addition, based on the comparison of these three parameters, the mix with a larger N_{SN} does not guarantee better resistance to moisture damage in the

stripping stage. For instance, R50-A had the largest number of passes to SN, but the remaining wheel passes to failure (N_{ST}) of this mix was lower than the control mix.

Evaluating the results at 50℃ as presented in Table 6.7, more consistent rankings were captured using these moisture susceptibility parameters as compared to those at 44℃. It is worth mentioning that the control mix was found to be the most susceptible mix in terms of both the onset point of stripping and the ultimate failure caused by moisture. Whereas no obvious stripping was found in R50 since the calculated N_{SN} was larger than 20,000. In addition, the N_{SN} values of the rejuvenated high RAP mixes were all above 2,000, which is the recommended criterion proposed by Fan Yin et al. [134]. At the end of the test, moisture damage accounted for more than half of the rut depth for all the asphalt mixes. Additionally, R50-B demonstrated slightly lower MR and larger N_{ST} values as compared to asphalt mixes containing rejuvenator A or soft binder, indicating that the addition of rejuvenator B was less detrimental with respect to the mix's moisture damage resistance. However, the reason behind R50-B* exhibiting a higher moisture damage proportion than R50-B might be that the period between the stripping onset point (N_{SN}) and the failure point (N_{ST}) of R50-B* was longer than that of the R50-B. Therefore, the former was subjected to stripping for a longer time.

Table 6.6 Novel moisture susceptibility parameters (44℃)

Mix type	MR (%)			N_{SN}			N_{ST}		
	Mean	Rank	CV (%)	Mean	Rank	CV (%)	Mean	Rank	CV (%)
R20	37.8	4	21.8	5072	4	4.7	15025	1	0.8
R50-SB	23.8	1	21.8	5891	2	3.7	14308	2	13.9
R50-A	23.9	2	68.7	6259	1	32.7	13480	3	16.8
R50-B	36.6	3	32.1	5289	3	1.3	13354	4	1.4
R50-D	47.4	5	6.0	3743	5	14.7	9588	6	9.8
R50-F	65.6	6	7.2	3414	6	8.8	9705	5	0.3
R50-B*	N/A	N/A	N/A	>20000	N/A	N/A	N/A	N/A	N/A
R50	N/A	N/A	N/A	>20000	N/A	N/A	N/A	N/A	N/A

Table 6.7 Novel moisture susceptibility parameters (50°C)

Mix type	MR (%)			N_{SN}			N_{ST}		
	Mean	Rank	CV (%)	Mean	Rank	CV (%)	Mean	Rank	CV (%)
R20	61.8	5	0.1	1563	5	1.3	4944	5	7.8
R50-SB	56.8	3	0.3	2154	4	15.0	5630	4	6.5
R50-A	59.4	4	13.2	2303	3	8.0	6422	3	14.8
R50-B	51.8	1	1.6	2505	2	20.2	7366	2	3.8
R50-B*	54.4	2	0.3	3799	1	9.7	10083	1	0.4
R50	N/A	N/A	N/A	>20000	N/A	N/A	N/A	N/A	N/A

Overall, the results indicated that the high RAP mix without any rejuvenators had a robust resistance to moisture damage. Furthermore, depending on the rejuvenator type and rejuvenator dosage, the addition of a rejuvenator or switching to a softer virgin binder led to different extents of an increase in the mixture's moisture susceptibility. At a lower water conditioning temperature, the control mix showed acceptable moisture resistance, while drastic moisture damage appeared in the very early stage when the test temperature increased to 50°C. Even though reducing the rejuvenator content made the mix less vulnerable to moisture damage, stripping still existed and contributed significantly to the failure at the end of the HWT test. This, however, needs to be further confirmed through field performance results which are currently lacking to properly establish a correlation between the laboratory HWT testing results and the actual performance for such high RAP mixes.

6.6 Conclusions

This study aimed to better evaluate the rutting and moisture-induced damages of highly recycled asphalt mixes produced using bio-based rejuvenators and very soft binders through both conventional and novel metrics. To this end, the Hamburg Wheel Track (HWT) tests were performed at the recommended testing temperature for these mixes in Ontario (i.e., 44°C) and an elevated temperature of 50°C. Novel analysis methods were successfully used to uncover the confounding effects of the visco-plastic flow and moisture damage in the wet HWT test. The following conclusions can be drawn:

- For the mixes in this study, increasing the RAP content from 20 to 50% significantly improved the rutting resistance of the asphalt mix as expected, without worsening the moisture susceptibility of mixes. In contrast, the high RAP mix showed robust moisture damage resistance at both test temperatures.
- Although, the control mix and the rejuvenated high RAP mixes were designed to yield a similar high PG (64°C) of their corresponding 100% blended binder; only one mix (R50-B) met the criteria for a PG 64-XX mix based on several HWT DOT specifications. Two rejuvenated mixes (R50-D and R50-F) even failed at the lower test temperature (44°C). Therefore, extra caution should be taken when adding bio-based rejuvenators or replacing the virgin binder with a softer binder in high RAP mixes to avoid severe rutting and moisture damage.
- The confounding effects of the visco-plastic flow and moisture damage could result in misleading interpretations based on the conventional HWT criteria. Whereas the novel methods applied in this paper isolated the moisture-induced deformation from the total permanent deformation. The novel rutting resistance parameters exhibited less variability compared to other parameters that did consider the post-compaction stage in model fitting.
- The results of rutting parameters indicated that the rutting resistance of rejuvenated high RAP mixes varied depending on the rejuvenator type and rejuvenator dosage. However, except for rejuvenator D, the difference between the other rejuvenated high RAP mixes was marginal.
- The temperature sensitivity of mixes can significantly affect the interpretation of the HWT test results. While the control mix showed an acceptable moisture resistance at 44°C, but an early sign of stripping was observed after increasing the temperature to 50°C.
- R50 and R50-B* did not exhibit any sign of stripping at 44°C, while the addition of a rejuvenator at the optimized dosage based on the conventional binder blending or using a softer virgin binder resulted in noticeable stripping during the test. Particularly, the moisture damage accounted for over half of the failure at the end of the test when conducting the wet HWT test at 50°C.
- Reducing the rejuvenator dosage was an efficient way to alleviate the decrease in the rutting resistance and moisture damage resistance. Despite that the remaining stripping life was extended, the moisture-induced deformation was still the major concern that contributed to more than half of the rut depth failure as the test temperature increased.

The initiative of this study was to use the HWT test to differentiate between rejuvenated high RAP mixes prepared with different types of rejuvenators at their optimized dosages. The authors also looked into other parameters, like the test temperature and rejuvenator dosage, to gain a deeper understanding of the performance of rejuvenated high RAP mixes. The use of the novel analysis methods provided more subjective and insightful information in terms of rutting resistance and moisture susceptibility. The main limitations of this study were the unavoidable variation derived from the measuring system and the paucity of HWT data for model fitting if the test terminated early. Notwithstanding these limitations, the study suggests that testing the mixes at a higher water bath temperature allows us to better distinguish the asphalt mixes, especially when they have similarly graded binders. It is also recommended to use the novel parameters which separate the creep stage and the stripping stage to avoid the subjective interpretation of the HWT results. Admitting that reducing rejuvenator dosage in the high RAP asphalt mix showed better rutting resistance and moisture susceptibility than that with optimized rejuvenator dosage, further investigation is needed to determine if the cracking resistance was affected. It is also possible to conduct additional research using plant-produced mixes with prolonged silo storage times to facilitate the diffusion between rejuvenators and binders, which is anticipated to improve the mix performance to resist permanent deformation and moisture damage.

Chapter 7

Effect of extended oven conditioning on the cracking and rutting performance of rejuvenated high RAP content asphalt mixes

This chapter focused on the cracking and rutting performance of the rejuvenated high RAP mixes under different oven conditioning periods and the results were analyzed using different cracking and rutting indices together with a balanced mix design (BMD) idea. It is modified from another paper manuscript entitled "Effect of extended oven conditioning on the cracking and rutting performance of rejuvenated high RAP content asphalt mixes".

7.1 Introduction

The use of recycled asphalt materials, such as reclaimed asphalt pavement (RAP), to replace more expensive virgin asphalt binders and aggregates in paving materials has become a routine in the asphalt industry, bringing both economic and environmental benefits [142]. As the desire to promote a higher RAP recycling rate in new asphalt mixes grows, so do the concerns about the performance of recycled asphalt mixtures. Due to the high stiffness and brittleness of the aged binder, the increased inclusion of RAP makes the mixes more susceptible to cracking [45,55,143]. Although the inclusion of RAP is expected to improve the rutting performance due to the increased overall stiffness. The impact of the RAP binder becomes more significant when mixes containing high RAP content, which is defined as RAP proportion exceeding 25 percent of the total dry aggregate weight. To allow more RAP to be incorporated into asphalt mixes, numerous studies have been working on feasible solutions to offset the negative effect of aged binder on the cracking performance of recycled asphalt mixes, including the use of rejuvenators and softer asphalt binder [2,20].

There are several asphalt mixture cracking tests have been developed, including the semi-circular bending Illinois flexibility index test (SCB-IFIT) test and the Indirect Tensile Asphalt Cracking Test (IDEAL-CT) conducted at an intermediate temperature range, and the disk-shaped compact tension (DCT) conducted at low-temperature range. The idea of these tests is to interpret the fracture energy derived from the crack initiation and the crack propagation stages until the fracture failure of the asphalt mix samples as performance indicators to discriminate mixtures with distinct characteristics. IDEAL-CT was developed by Texas A&M Transportation Institute for practical and routine use in asphalt mix design, quality control (QC), and quality assurance (QA) testing [144,145]. This test has grown in popularity among agencies and

contractors due to its simplicity, practicability, and repeatability, as the sample does not require any cutting, gluing, drilling, or notching; and the test requires minimal training to operate and takes less than one minute to complete one sample. Furthermore, when compared to repeated loading cracking tests, the IDEAL-CT results showed less variation (25%) and a good correlation with field cracking. Recent studies also revealed that the IDEAL-CT results correlated well with the fatigue parameters derived from binder tests performed at high strain (e.g., 15%) or stress (e.g., 3.2kPa) levels [146,147].

The high sensitivity of the IDEAL-CT to mix design properties, including the gradation, air voids, binder grade, and additives, allows this test to be a good candidate used for balanced mix design (BMD) purposes. BMD is defined as "asphalt mix design using performance tests on conditioned asphalt mixture specimens that address multiple modes of distress taking into account consideration mix aging, traffic, climate, and location within the pavement structure." In short, BMD combines two or more performance-based tests, typically the rutting test and the cracking test, to assess how well the mixture resists the distresses and achieve a balance between different performance criteria instead of solely relying on the volumetric requirements [126,148,149]. Since the traditional volumetric mix design method is not sufficient for evaluating the contributions from the more and more complex components in the asphalt mixture, such as RAP or RAS, rejuvenators, and warm mix additives [150]. Therefore, it is essential to select proper performance testing protocols that are well-correlated to the field performance and practical for use in the mix design stage with established pass or fail criteria [151]. In the BMD framework proposed by the NCHRP Report 20-07/Task 406, the semi-circular bending Illinois flexibility index test (SCB-IFIT) procedure was favored by most state DOTs for having the greatest potential to evaluate the reflection, bottom-up, and top-down cracking [126]. Yan et al. compared the SCB-IFIT and the IDEAL-CT results for measuring the racking resistance of asphalt mixtures, the flexibility index (FI) from SCB-IFIT, and the cracking tolerance index (CT_{index}) from IDEAL-CT were highly correlated, but SCB-IFIT results showed relatively higher variation due to the notched surface [150,152]. Thus, IDEAL-CT could be an ideal alternative cracking performance test for BMD if a proper threshold can be established for CT_{index}. Moreover, the test was reported to be sensitive to the inclusion of RAP or RAS and the mix aging condition, allowing the test to evaluate the long-term performance of the mix. In terms of the rutting tests, the Hamburg Wheel-Tracking (HWT) is the most used rutting performance test in North America. It is widely used to assess the rutting resistance as well as the moisture susceptibility of asphalt mixtures. Currently, many state DOTs have applied HWT test specifications to develop performance criteria for BMD pilot projects [126,148].

Recent research has shown that storing the plant-produced recycled asphalt mix in a silo for an extra couple of hours can improve the thermal cracking resistance in terms of a lower fracture temperature, and the fatigue life of the mixes was also improved based on the four-point bending fatigue test results [7,123,153]. When there are trucking and paving breakdowns during pavement construction, silo storage is critical to keeping the mix hot. It has been proved to show a more significant impact on mixtures containing RAP as blending continues at an elevated temperature after mixing [109]. Although prolonged silo storage can promote blending, it can also cause some extent of hardening of the mix even in an inert atmosphere, which benefits the rutting resistance. Elkashef et al. claimed that the extended silo storage time resulted in additional aging and possible blending between RAP and virgin binders [154]. The additional blending of RAP and virgin binders with the effect of rejuvenators contributes to higher effective binder content, which benefits cracking resistance; however, the effective binder blend also becomes more brittle as more RAP binder is activated and the virgin binder and rejuvenator ages [154,155]. Ultimately, the role of the rejuvenator in the performance of high RAP asphalt mixes has not been thoroughly investigated yet. Several studies have attempted to optimize the rejuvenator content using the BMD concept [81,156]. However, incomplete blending may result in a false "rejuvenation" or "softening" occurrence, with less RAP binder contributing to the final effective binder blend during mixing and compaction. With the interest of promoting the mobilization of RAP binder and enhancing the blending and diffusion at an elevated temperature atmosphere, it is important to reveal the effect of rejuvenator on the cracking and rutting resistance of high RAP content asphalt mixes under different conditioning periods when using performance-based tests to implement the lab mix design and quick QC and QA testing on plant produced mixes.

7.2 Research motivation and objectives

The study was motivated by findings of the previous work on improving binder blending and diffusion through by extended silo storage time. However, what is less clear is the effect of the rejuvenator on the ongoing conditioning process, particularly at higher RAP rates. Because the more RAP binder replacement, the longer the conditioning time required to complete a full blending scenario. The overall stiffness of the effective binder blend increases as the RAP binder contribution increases. At the same time, rejuvenators and virgin binders are more prone to aging in a higher-temperature environment. Furthermore, the authors are interested in preliminarily examining the performance of the rejuvenated high RAP mixes prepared with the optimized rejuvenator content determined from binder testing results using quick performance-based

test methods. As a result, the rutting and cracking performance tests, HWT and IDEAL-CT, were chosen to assess the lab-mixed and compacted asphalt mix samples.

The objective of this study is to investigate the effect of the rejuvenator and the softer binder on balancing the performance of high RAP asphalt mixes, with different oven conditioning times applied on the loose mix. Also, different cracking and rutting performance indicators were calculated from the test data to examine their abilities in differentiating mixes with different RAP proportions, binder grades, rejuvenator types, and conditioning periods. The study's limitation is the difficulty in creating a completely inert atmosphere for loose asphalt mixes using the oven conditioning procedure. To reduce the impact of oxidative aging, the loose mix was sealed with aluminum foils without being stirred during the conditioning period.

7.3 Materials description and mix design

The materials description and mix design details were the same as the information described in Chapter 3. Based on the conclusions in Chapter 4 and Chapter 5, the four rejuvenators selected to continue the mix testing phase are A, B, D, and F. Chapter 6 discriminated the rejuvenators by evaluating the rutting and moisture resistance of the associated high RAP mixes, with mixes with rejuvenator A and B (R50-B was slightly better than R50-A) showed better performance compared to those with rejuvenator D and F. Therefore, rejuvenator B was selected as the best candidate rejuvenator in this study, while rejuvenator F was chosen as a comparison to rejuvenator B and to examine whether the unsatisfied rutting performance can be improved by extended condition time. Table 7.1 shows the different mix types prepared in this study. R20 and R50 are recycled asphalt mixes prepared with the same base binder, PG 58-28, containing 20 and 50 percent of RAP, respectively. For the rejuvenated high RAP mix design, rejuvenators B and F were incorporated in the mixes with their optimized dosages, 4.01% and 4.52%, respectively. R50-SB was prepared by replacing the base binder with the PG 46-34 asphalt. R50-B* was prepared with a reduced rejuvenator content considering the assumption that the mobilization of the RAP binder will be less than 100% during the laboratory mixing and compaction process. In this case, the contribution of the RAP binder in R50-B* was assumed as 70% based on the review of previous studies.

Table 7.1 Mix type information

Mix Code	Base Binder	Rejuvenator Type	Rejuvenator Dosage (%)
R20	PG 58-28	N/A	N/A
R50	PG 58-28	N/A	N/A
R50-SB	PG 46-34	N/A	N/A
R50-B	PG 58-28	B	4.01
R50-B*	PG 58-28	B	3.22
R50-F	PG 58-28	F	4.52

7.4 Experimental methods

7.4.1 Sample preparation and conditioning

For the control mix with 20% RAP, the mixing and compaction temperatures remained the same (146℃ and 135℃ for the base binder, PG 58-28) and the RAP did not require preheating before mixing. However, it is challenging to maintain the mixing temperature using an open mixing drum without a heating source due to the limitations of the laboratory mixing equipment. The mixing procedure of the 50% RAP mix should be adjusted to compensate for the increased RAP content and heat loss during the mixing. To achieve this, the preheating temperatures of the blended binders were increased to 160°C and the RAP was preheated to 110°C for less than two hours before mixing.

The sample preparation was completed by following steps:

(1) Preheat aggregates to 10℃ above the mixing temperature overnight (more than 16 hours).

(2) Preheat RAP to 110℃ (if RAP content is more than 20%) and maintain the temperature for less than 2 hours before mixing.

(3) Preheat the base binder to the mixing temperature and add the rejuvenator at its optimized dosage described in Table 6.2 into the base binder to achieve a homogenous binder blend using the regular binder blender. Then put back the blended binder in the oven at the mixing temperature for less than 1 hour before mixing.

(4) Premix the virgin aggregates with RAP for 45 seconds (30 seconds if %RAP is no more than 20%), and then add the binder to mix for another 90 seconds (60 seconds if %RAP is no more than 20%).

(5) The loose mix will be conditioned in the oven in two scenarios:

   a. 4 hours of conditioning at 135℃ to simulate the short-term aging that occurred in asphalt plant production and transportation as per AASHTO R30 [139].

   b. 10 hours of conditioning at 135℃ to facilitate the diffusion and blending between the aged binder and the softer virgin binder or the commonly used virgin binder pre-blended with rejuvenators. This idea is proposed to simulate the extended silo-storage time which was proved to be an effective solution to enhance the blending within the plant-produced mixes asphalt mix with a presence of less than 30 percent RAP content [7]. The optimal storage time was reported between 8 and 10 hours.

(6) Compact the loose mix using the Superpave Gyratory Compactor (SGC) by controlling the sample height.

After compaction, the extruded samples were cooled overnight and then the volumetric properties of each sample were measured since the cracking performance indicators have been reported to be sensitive to the sample's air voids [144]. Samples should be checked with air voids if out of the tolerance (i.e., 7 ± 1%). Then, the saturated samples were dried overnight again using the cooling fan before testing.

7.4.2 IDEAL-CT procedure and cracking resistance indicators

The cracking resistance of the mix was assessed using the IDEAL-CT procedure described in ASTM D8225-19 [107]. The asphalt mix sample was extruded from the Superpave gyratory compactor (SGC) with a diameter of 150mm and a thickness of 62mm. The test sample does not require any cutting, drilling, notching, or gluing before the test, the only instrumentations used in this study are a conditioning chamber and a servo-hydraulic loading cell with the capacity of applying a monotonic load at a rate of 50 mm/min. The dried samples were conditioned in the chamber at a temperature of 25 ± 1°C for 2 ± 0.5 hours before testing as per ASTM D8225-19.

Load and load line displacement (LLD) data were recorded at a frequency of 40 sampling data per second during the test period. The termination point of the test is determined when the load magnitude reaches 10% of the peak load. Figure 7.1 shows the typically obtained load-displacement curve. Similar to the flexibility

index (FI) developed from the SCB-IFIT, Zhou et al. [144] proposed the cracking tolerance index (CT_{index}) for evaluating the cracking potentials of asphalt mixes using IDEAL-CT. Instead of using the slope at the inflection point as the post-peak slope, this index defines the post-peak slope calculated at the point where the load equals 75 percent of the peak load to normalize the fracture energy. Since determining the inflection point needs a mathematical function to fit the curve, for one set of load-displacement data, different pre-smooth functions will generate different inflection points, which increases the variability [150]. In some cases, As shown in Equation (7-1), CT_{index} is a function of the parameters, including the fracture energy (G_f), the post-peak slope (m_{75}), and the corresponding post-peak displacement (l_{75}), obtained from the load-displacement curve. G_f is calculated by dividing the work of failure (the area under the load-displacement curve until the complete fracture of the sample) by the cross-sectional area of the specimen, which is the product of the sample's diameter and thickness. As for m_{75}, the value was computed by linear regression of all data points between the point corresponding to 65% of the peak load (PPP_{65}) and the point at 85% of the peak load (PPP_{85}), respectively.

$$CT_{index} = \frac{t}{62} \times \frac{l_{75}}{D} \times \frac{G_f}{|m_{75}|} \tag{7-1}$$

where:

t = specimen thickness (mm).

D = specimen diameter (mm).

G_f = fracture energy (Joules/m^2), $G_f = \frac{W_f}{D \times t} \times 10^6$, where W_f is the fracture work (Joules).

l_{75} = displacement at 75% of the peak load (mm).

$|m_{75}|$ = absolute value of the post-peak slope at 75% of the peak load (kN/mm)

Each parameter in the equation above has a specific physical meaning. m_{75} is a modulus parameter that represents the overall stiffness of a cracked asphalt mixture sample. The stiffer the mix, the faster the cracking growing rate, thus the faster load reduction, which results in a higher $|m_{75}|$ value. l_{75}/D is a strain tolerance parameter; a higher l_{75}/D suggests that the sample can withstand more deformation under loading, indicating greater flexibility to deform and then resist crack propagation. Previous research has shown that a large portion of fracture energy is consumed due to plastic deformation before cracking

initiation [157]. Therefore, instead of using the failure work during the whole test period, another modified CT_{index} can be computed using the post-peak failure work, W_{f_post} (see Figure 7.1), which is denoted as CT_{index_post} in this paper. So, this modified index only focuses on the crack propagation stage after reaching the peak load.

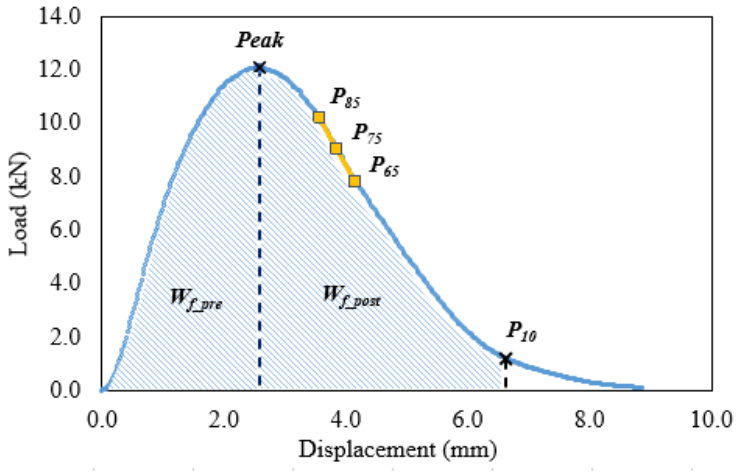

Figure 7.1 Illustration of parameters in the load-displacement curve

Apart from CT_{index} and CT_{index_post}, two other cracking performance indicators were also computed for comparison, the cracking resistance index (CRI) and the rate dependent cracking index (RDCI). Kaseer et al. developed CRI as an alternative cracking index for SCB-IFIT [158]. Since for an extremely brittle mixture, the test sample can fracture once the peak load is reached; therefore, no post-peak displacement data is available to calculate $|m_{75}|$ and l_{75}. Equation (7-2) shows that CRI is determined by normalizing the fracture energy with the peak load. Nemati et al. proposed the new cracking performance index, RDCI, to take into account the rate dependency of the fracture process [159]. As shown in Equation (7-3), this index is calculated using the cumulative fracture work (W_c), as a function of time, and the instantaneous power at peak load (P_{tpeak}). Figure 7.2 shows the curve of cumulative fracture work against time, the time step was constant because of the fixed loading rate. P_{tpeak} is the slope of the cumulative work versus the time curve at the peak load point, which can be also calculated as the scalar product of force and velocity at any time (see Figure 7.2). Therefore, RDCI captures the fracture energy and the cracking velocity in a rate-dependent manner. The ligament area is the specimen thickness times the ligament length.

$$CRI = \frac{G_f}{P_{max}} \tag{7-2}$$

where:

G_f = fracture energy (Joules/m^2).

P_{max} = peak load (kN).

$$RDCI = \frac{\int_{t_{peak}}^{t_{0.1peak}} W_c dt}{P_{tpeak} \times ligament\ area} \times C \tag{7-3}$$

where:

$\int_{t_{peak}}^{t_{0.1peak}} W_c dt$ = the post-peak area under the cumulative work versus time curve (s^2/m^2).

P_{tpeak} = the instantaneous power at peak load (N·m/s).

C = the unit correction factor set to 0.01.

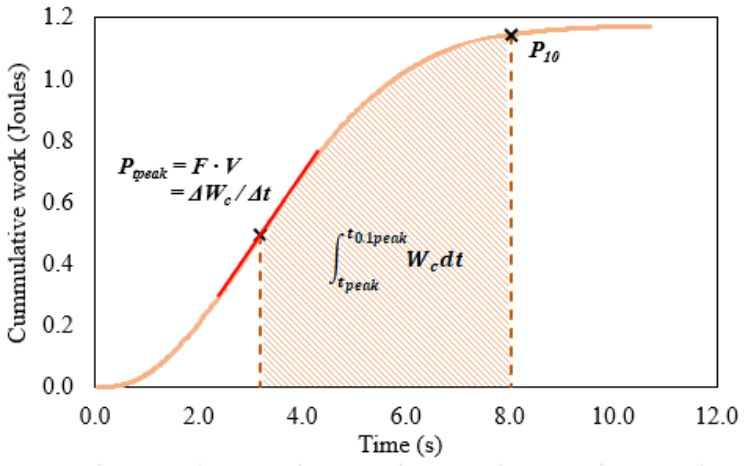

Figure 7.2 Illustration of parameters in the W_c-time curve

There are four cracking resistance indicators, CT_{index}, CT_{index_post}, CRI, and RDCI, computed with at least three replicates tested for each mix type. Statistical analysis, including the t-test, One-way ANOVA with Tukey's LSD or Bonferroni corrected Fisher's LSD, were used for determining the significance of the rejuvenator type and conditioning time on the cracking performance of asphalt mixes.

7.4.3 HWT procedure and rutting resistance indicators

The Hamburg-Wheel Tracking (HWT) test, as per AASHTO T324-17 [106], was applied in this study to evaluate both the rutting and moisture resistance of the high RAP mixes at a high in-service pavement temperature range. Four SGC samples with a diameter of 150mm and a thickness of 63mm were fabricated for testing, with two pairs of the samples moulded on each wheel track side and submerged in a heated water bath during the cyclic wheel loading. The load on each side of the wheel is 705 ± 4.5N. The test is programmed to finish when the number of wheel passes reaches 20000 or the rut depth reaches the maximum allowable value, usually 20mm. The rut depth data versus the number of wheel passes will be recorded during the test.

The AASHTO standard does not specify the water bath temperature for the HWT test, state or provincial DOTs usually will have their own recommended HWT test temperature and failure criteria [126,134]. In Ontario, the HWT test temperature is based on the high PG of the binder used in the mix sample. In this study, the test temperature of 50℃ was selected because the previous binder testing results showed that both the control and rejuvenated high RAP mixes had the equivalent binder high PG of 64℃, which indicated that all the mixes could also pass the HWT criteria at 50℃ for a PG 64-XX binder grade. In addition, using a higher test temperature should be more capable of discriminating between different types of mixes than the test conducted at a lower temperature, in which all the mixes might pass the threshold. The test was started by pre-condoning the samples for 45 minutes in the water bath, then the rut depth results against the number of wheel passes were recorded from the time starting the cyclic wheel loading to the samples reaching 20mm rut depth or surviving 20000 wheel passes.

Table 7.2 Recommended HWT test temperature in Ontario

Test temperature (°C)	Binder high PG (°C)	Rut depth threshold (mm)	Minimum wheel passes
44	52 and 58	12.5	20000
50	64	12.5	20000
50	70	6.0	20000

The number of passes when the rut depth reaches 12.5mm is used for evaluating the overall performance of the samples in the submerged HWT test. The rutting resistance index (RRI) [140] and creep slope (CS) [138,160] developed from previous studies were reported to be well correlated to the field rutting data,

which can be used as rutting performance indicators rather than solely rely on the rut depth and wheel passing number results. In addition, the novel parameter visco-plastic ratio (VR) developed by Lv and Bahia was also computed as an alternative rutting parameter, because it was separated from the effect of post-compaction and stripping stages and showed relatively lower variation (see Chapter 6) [136,137].

7.5 Results and discussion

7.5.1 Correlation between cracking indices

Table 7.3 shows the pairwise correlation coefficients between different cracking indices obtained from all the test replicates using the Pearson correlation method. The highest correlation coefficient value was observed between CT_{index} and CT_{index_post}, implying that calculating cracking performance indicators using post-peak fracture work will not result in significantly different conclusions for the same IDEAL-CT data. The histogram presented in Figure 7.3 explained the high correlation between these two indices and the post-peak fracture work measured from each sample was approximately 60% of the total fracture work. CRI had a moderately strong correlation with both the CT_{index} and the RDCI. The main difference between CT_{index} and CRI is that the equations use different denominators, post-peak slope and peak load, in the equations, and these two parameters had a strong positive correlation as well (r = 0.943). For samples with a higher peak load reached in the test, a sharper decrease was usually expected in the post-peak stage, which delivered a larger $|m_{75}|$ value. This is consistent with previous research, which found that the CRI and FI values determined from different lab and field samples are well correlated [158]. Nevertheless, for each pair of indices, they exhibited a reasonably good positive correlation, indicating that using different indices will result in consistent ranking in terms of the sample's cracking performance.

Table 7.3 Correlation coefficient between cracking indices

Parameters	CT_{index}	CRI	RDCI
CRI	0.936	-	-
RDCI	0.849	0.932	-
CT_{index_post}	0.988	0.925	0.867

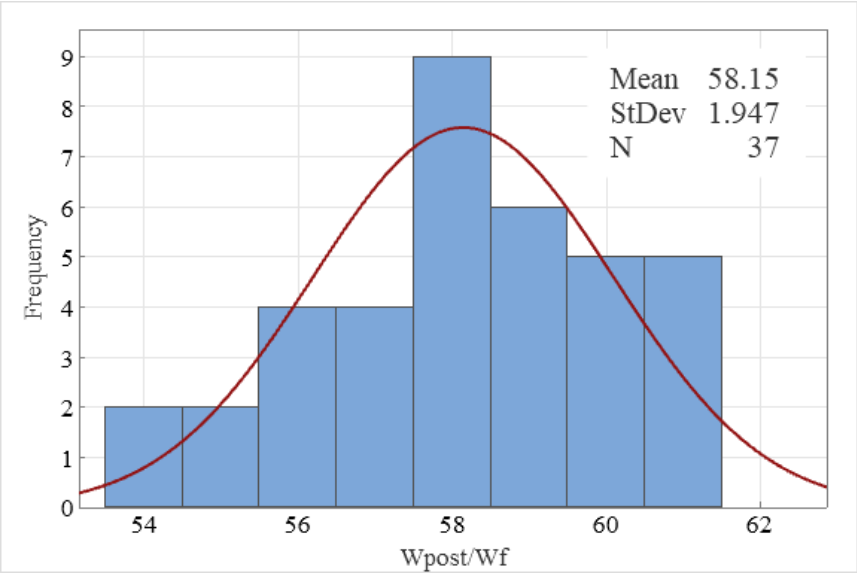

Figure 7.3 Histogram of the ratio (%) between W_{f_post} and W_f

7.5.2 Variations of cracking indices

Table 7.4 displays the coefficient of variation (CV) of the test replicates for each cracking index associated with every mix type. For all the mixes, CRI showed the lowest variation among these indices, ranging from 2.5% to 10.6%. The higher variation of CT_{index} and RDCI compared to CRI was also noticed in the previous study [161], the possible reason can be attributed to the presence of the slope component in their equations. Meanwhile, using the post-peak area for the calculation of CT_{index} did not reduce the variability. Concerning the mix type, increasing the RAP content from 20% to 50% significantly increased the variation regardless of the cracking indices. Extending the conditioning time was anticipated to continue to homogenize the mix, especially with the addition of rejuvenators or soft binders. From the results of mixes with rejuvenator B in Table 7.4, increasing the conditioning time to 10 hours or reducing the rejuvenator content led to lower variation, a similar trend was observed in the R50-SB mix. However, the high RAP mix with F experienced the reversed trend in which R50-F with 10 hours of conditioning exhibited much higher variation than its counterpart conditioned for 4 hours. Since CT_{index_post} did not show any inconsistency or reduced variation compared to CT_{index}, there is no need to include CT_{index_post} in the next sections.

Table 7.4 Coefficient of variation (CV%) of different cracking indices

Sample ID	CT_{index}	CT_{index_post}	CRI	RDCI
R20	3.9	4.5	2.6	4.5
R50	10.1	13.6	4.2	14.5
R50-B-4h	29.3	31.1	9.9	29.5
R50-B*-4h	7.1	9.2	3.0	13.6
R50-B-10h	6.4	4.6	2.7	10.6
R50-F-4h	7.1	4.3	2.5	8.5
R50-F-10h	24.5	25.2	10.6	21.5
R50-SB-4h	19.5	20.0	6.3	16.1
R50-SB-10h	5.7	14.3	2.5	7.0

7.5.3 Cracking indices

Figure 7.4 (a)-(c) displays the average values of three cracking indices for different mix types. For mixes conditioned with the 4-hour conventional oven aging, the 50% RAP mix showed the lowest average values for all three indices. With the addition of a rejuvenator or soft binder, the cracking indices increased to be slightly higher than the control mix (R20). Reducing the rejuvenator content (i.e., R50-B* mix) led to smaller cracking index results compared to the R50-B mix. However, the larger variation of the R50-B mix was observed in the graph, and the error bars (standard deviation) overlapped with those of the R50-B* mix for all three indices. One-way ANOVA was applied to determine whether different types of mixes showed statistically different cracking performances. The letters labelled in the bar charts are the grouping information obtained by pairwise comparison using the Tukey method or Bonferroni corrected Fishier method. These two multiple comparison methods provided the same grouping information for both the 4-hour and 10-hour conditioned mixes. According to the ANOVA results, there is no significant difference between the three rejuvenated high RAP mixes after 10 hours of conditioning as the p-values were higher than 0.46. Therefore, no grouping information is presented in the bar charts for 10h mixes. However, what stands out in the figure is that the average values of the cracking indices showed clear decreases after extended conditioning time, especially CT_{index}. Regarding the 4h mixes, the grouping information from RDCI results showed that all mixes shared the same letter, indicating no significant difference between them (p-value = 0.175). But the ANOVA results of CT_{index} (p-value = 0.022) and CRI (p-value = 0.031)

suggested that not all mix types had a similar cracking performance. The grouping information identified in Figure 7.4 (a) and (b) was the same, with only R50-SB yielding statistically higher CT_{index} and CRI values than those of R50. The control mix and the other rejuvenated high RAP mixes connected with the compact letters AB, indicating they were not significantly different from each other or either R50-SB and R50.

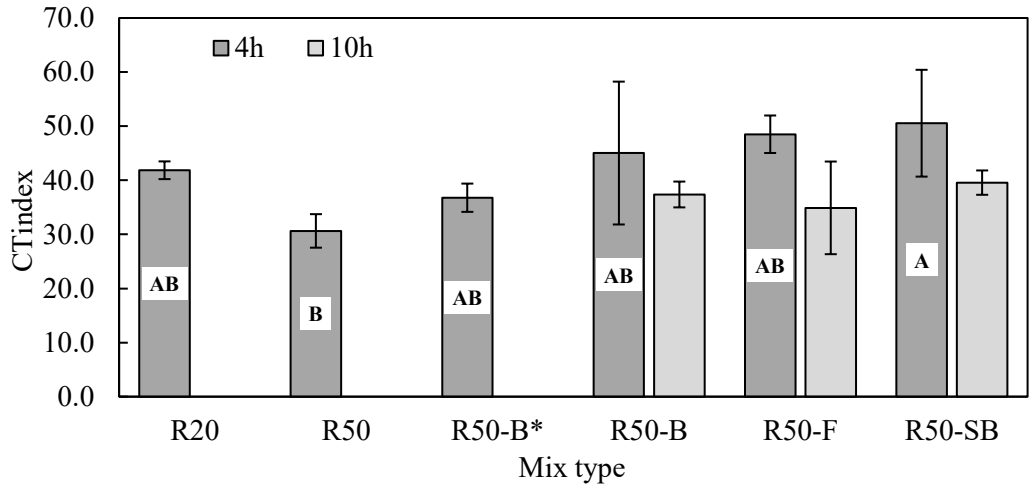

(a)

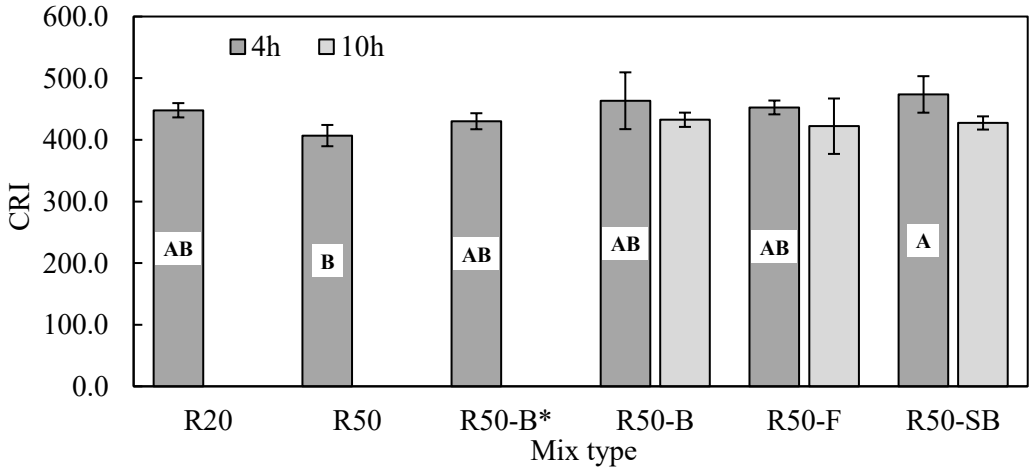

(b)

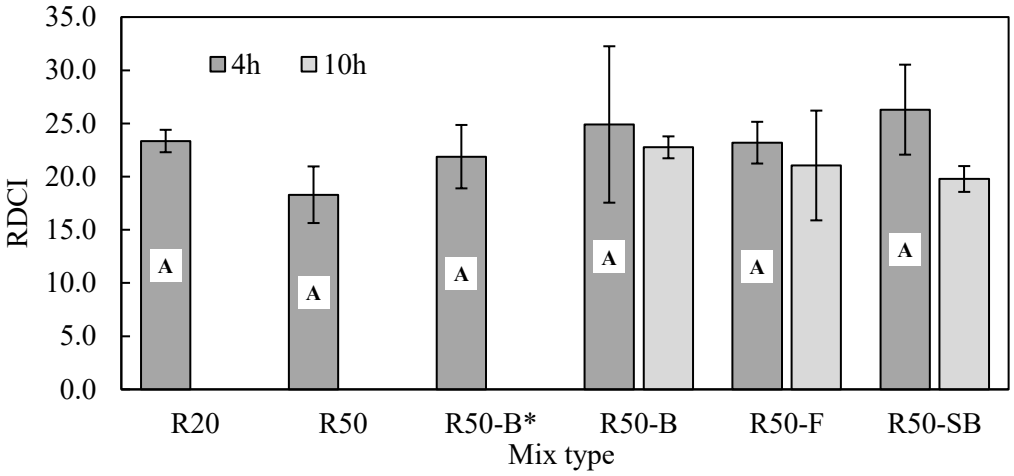

(c)

Figure 7.4 Cracking indices of different mixes: (a) CT_{index}, (b) CRI, (c) RDCI

Table 7.5 provides the p-value results from the two-sample t-tests conducted for each cracking index to determine the significance of extended conditioning time. As can be seen from the table, R50-B showed no significant changes after extending the condoning time to 10 hours as relatively larger p-values were obtained for all three cracking indices. In contrast, the 50% RAP mix with soft binder experienced significant reductions in all three indices after 10 hours of conditioning, with p-values less than 0.05 provided in Table 7.5. For mix with rejuvenator F, the significant difference was only observed in CT_{index}. From the bar charts, we can also notice that the average values of the cracking indices showed the least prominent decrease in mix R50-B, compared to R50-SB and R50-F. Even though the data of R50-B and R50-SB under 4 hours of conditioning had larger variabilities, it could still conclude that R50-SB was more affected by the extended oven conditioning compared to R50-B regarding the changes of cracking indices obtained at different conditioning times.

Table 7.5 p-values from two-sample t-test

Mix type	CT_{index}	CRI	RDCI
R50-B	0.253	0.204	0.569
R50-F	0.020	0.199	0.390
R50-SB	0.041	0.011	0.011

It was claimed that 8-hour conditioning at 135℃ could result in the equivalent standard binder PAV aging for 20 hours [162]. Therefore, the decrease in cracking indices can be attributed to the possible binder aging that happened during the conditioning. Since the extended conditioning also promoted the diffusion between the RAP binder and virgin binder with rejuvenators at the same time, the cracking performance was affected by a combined effect of aging and rejuvenation. The witnessed decrease in cracking indices for rejuvenated high RAP mix offered the information that the aging rate of soft binder was probably faster than the diffusion rate with the aged binder. However, we should not neglect that if diffusion dominated the conditioning process, the effective binder blend would contain more aged binder content, thus resulting in increased overall stiffness.

Together these results provide important insight into the cracking performance of rejuvenated high RAP mixes under different conditioning periods. Although the variation of the cracking indices was not surprisingly higher than that was reported in other studies [150,159,161], the unavoidable discrepancy still caused difficulties in statistically discriminating the mixes in this study. CT_{index} and CRI were more sensitive to the changes in mix composition compared to RDCI. Regardless of the cracking indices, the extended conditioning only led to a significant decrease in the cracking performance of R50-SB.

7.5.4 Effect of conditioning time on rutting resistance

Figure 7.5 and Figure 7.6 present results of the number of passes at 12.5 mm rut depth and parameter RRI, which both reflect the overall performance of asphalt mixes using the HWT test. The number of passes to reach 12.5mm was commonly used as an HWT failure criterion in DOT specifications. The calculation of RRI considers both the final rut depth and the number of passes when the test is completed. A higher RRI value indicates the sample survives more wheel passes and has a smaller final rut depth. Since the HWT results of R50-F after 4 hours of conditioning already failed the Ontario criteria at the test temperature of 44℃, this mix was not included in the 50℃ HWT test. Also, the author needs to clarify that the final rut depth results of R50-B-10h and R50-F-10h showed a noticeable difference (>10mm) between the two track sides even after the second trial of these two mixes. Therefore, the results of R50-B-10h and R50-F-10h in Figure 7.5 and Figure 7.6 were adopted from the trackside where the HWT data that reached 20mm (i.e. failure side) to show the possible worst case occurred in the test.

As can be seen from the figures, R50-B exhibited better overall performance compared to the R50-SB mix, with more passes required to reach 12.5 mm rut depth and a larger RRI value was achieved. As the conditioning time increased to 10 hours, R50-SB outperformed both R50-B and R50-F, showing the

greatest increase in the number of passes and RRI. It is consistent with the cracking test results, as the most significant drop in cracking performance indices was disclosed in R50-SB, which was attributed to the possible aging and increased binder blend stiffness.

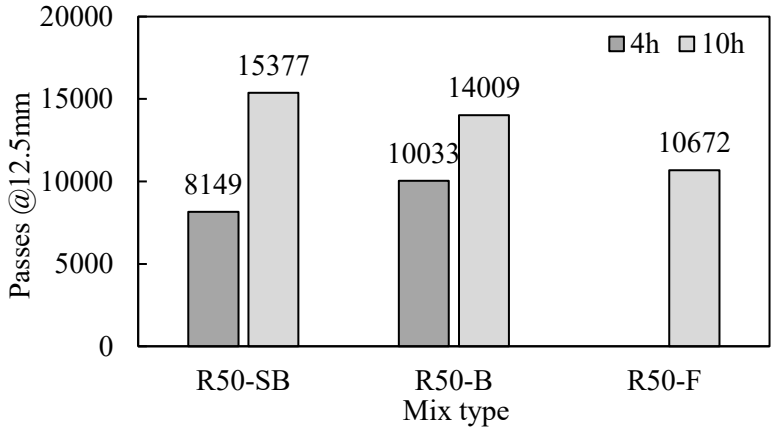

Figure 7.5 Number of passes to reach 12.5 mm rut depth (50°C) of rejuvenated high RAP mixes

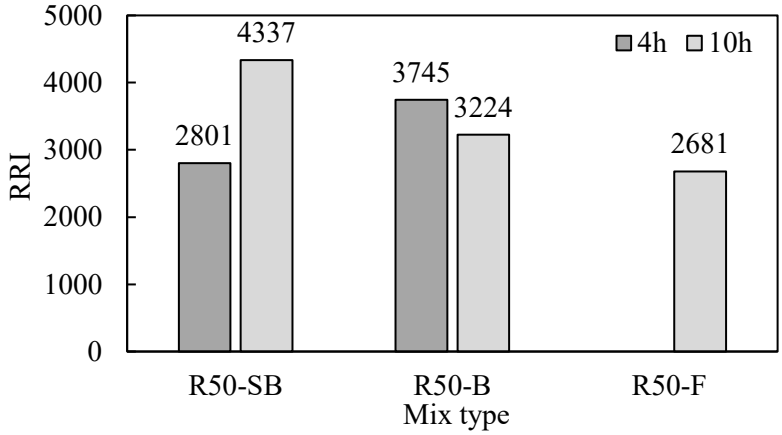

Figure 7.6 RRI (50°C) of rejuvenated high RAP mixes

The variability data of Figure 7.5 and Figure 7.6 are not presented, since the two trials of the R50-B-10h and R50-F-10h mixes have shown very different results. As mentioned above, the HWT results are invalid if the difference in the final rut depths measured from the two sides is larger than 6mm [106]. The final depression in the HWT samples was caused by the combined effect of the confounding effect of post-compaction, plastic deformation, and moisture damage. Figure 7.7 shows the rut depth data versus the number of passes obtained from the second trial of R50-B-10h. The final rut depth difference of the left and right tracks was around 8mm; however, the two recorded rut depth results were almost identical until

stripping happened (before 8000 passes). Likewise, the two HWT results displayed in Figure 7.8 showed a similar trend before the rut depth started to rapidly increase, even though the right-side rut depth recorded at the first 1000 passes was higher than the other trackside. Hence, the advantage of creep slope (CS) and visco-plastic ratio (VR) is they can capture the rutting resistance by considering the characteristics of the rut depth curve at the creep stage. Parameters generated before the stripping and final failure occur can still be meaningful if the final rut depth difference is larger than the threshold (6mm). Table 7.6 presents the CS and VR results of the rejuvenated high RAP mixes with different conditioning times and the associated coefficient of variations (CV). The CS results show a much higher variation compared to VR results; the possible reason might be that CS is determined from the sixth-order polynomial function which is used for fitting the whole rut depth data, but VR was computed from the fitting function only using the data after 1000 passes and before stripping starts (i.e., the normalized creep stage), which was less affected by the post-compaction and moisture damage. The mean values of the rutting parameters were averaged from the two trials conducted for R50-B-10h and R50-F-10h, respectively. R50-SB with 4h conditioning showed the highest CS and VR values, indicating the worst resistance to visco-plastic deformation. For the 10h mixes, the p-values obtained from One-way ANOVA (rutting parameter versus mix type) for CS and VR were 0.454 and 0.080, respectively. Therefore, there is no significant difference in the rutting resistance among these three mixes after 10 hours of conditioning. Comparing the mixes conditioned after 4 hours and 10 hours, both R50-SB and R50-B experienced an obvious reduction in the two rutting parameters after the extended conditioning, especially R50-SB. It was also noticed that R50-SB after 10 hours of conditioning endured more wheel passes and showed a larger RRI value than those of R50-B. However, the R50-B mix achieved slightly lower average CS and VR values compared to R50-SB, which suggested a similar rutting resistance between R50-B and R50-SB. The worse overall performance of R50-B could be attributed to a possible earlier stripping phase.

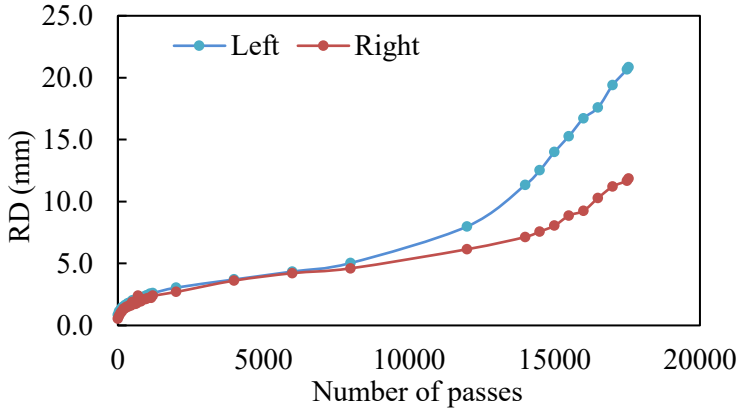

Figure 7.7 Second HWT trial of R50-B-10h mix

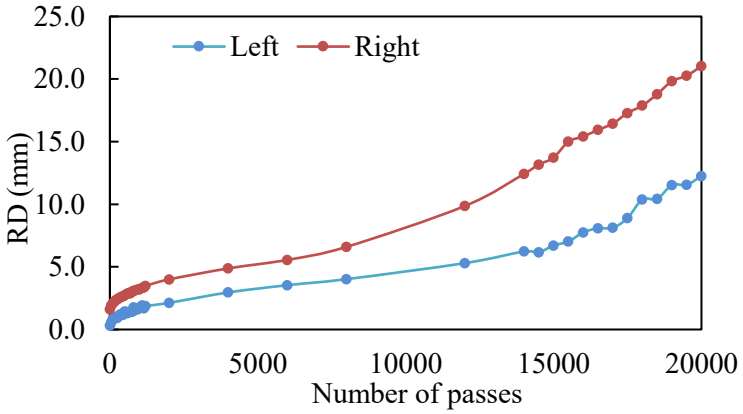

Figure 7.8 Second HWT trial of R50-F-10h mix

Table 7.6 Creep slope (CS) and visco-plastic ratio (VR) of rejuvenated high RAP mixes

Sample ID	CS (10^{-4})				VR			
	Left	Right	Mean	CV (%)	Left	Right	Mean	CV (%)
R50-SB-4h	6.55	9.39	7.97	25.2	0.88	0.90	0.89	2.1
R50-B-4h	5.41	5.97	5.69	7.0	0.87	0.85	0.86	1.1
R50-SB-10h	2.12	3.42	2.77	33.3	0.78	0.82	0.80	3.2
R50-B-10h	2.49	2.50	2.46	35.3	0.79	0.78	0.77	5.8
	3.48	1.36			0.80	0.70		
R50-F-10h	7.99	3.25	4.12	63.2	0.89	0.90	0.85	5.8
	2.80	2.44			0.83	0.80		

Overall, the results of the rutting parameters were somehow consistent with the cracking index results. The rejuvenated high RAP mixes can hardly be distinguished using either the cracking indices or the rutting parameters with robust statistical analysis. Except for the fact that they performed similarly in terms of cracking and rutting resistance, the inevitable variations in the mix testing caused a wide range of data distribution. The most important finding was that the extended oven conditioning led to a significant impact on the mix performances.

7.6 Conclusions

This study aims to evaluate the effects of extended oven conditioning on the cracking and rutting performances of highly recycled asphalt mixes containing bio-based rejuvenators or soft binders. performance-based tests, including IDEAL-CT and HWT, were implemented in this study for developing several cracking and rutting performance indicators to differentiate different types of mixes. These two tests were recommended by many agencies and contractors due to their sensitivities to the mix properties, good correlations with field data, and potential for BMD tests and quick QC and QA routines. Meanwhile, the oven conditioning was extended to 10 hours to simulate the silo-storage to facilitate the blending between aged binder and virgin binder plus the rejuvenators if applied. Overall, the rejuvenated high RAP mixes with different types of rejuvenators or soft binder replacement did not show any statistically significant dissimilarities to each other, but they were able to resemble similar cracking performance to that of the control mix with less RAP content (20%). Although prolonging the oven conditioning time resulted in decreased cracking indices and increased rutting parameters for the rejuvenated high RAP mixes, peculiarly the 50% RAP mix was prepared with the soft virgin binder (PG 46-34). Based on the major findings in the test results, the following conclusion can be made:

- The three cracking indices, CT_{index}, CRI, and RDCI, showed a good correlation with each other. The indices calculated using the post-peak data, such as CT_{index_post} and RDCI, still provided similar results compared to CT_{index}. Moreover, the coefficient of variation computed from the replicates in this study proved moderate variabilities in IDEAL-CT measurements, with up to 30% observed in CT_{index} and RDCI and 10% in CRI.
- Though the cracking performance of high RAP mixes was inferred to be improved since the cracking indices increased with the addition of rejuvenators and soft virgin binder. The statistical

analysis, however, only demonstrated the mix with the soft binder (R50-SB) exhibited significantly greater indices compared to the R50 mix. The rest rejuvenated high RAP mixes (R50-B and R50-F) showed the same grouping results as the control mix (R20) based on the pairwise comparison, but they were associated with the R50 mix. In addition, CT_{index} and CRI could better discriminate the mixes than RDCI.

- The extended aging showed a prominent impact on the cracking performance of the mixes with rejuvenators or soft virgin binders. R50-B expected the smallest decrease in the average values of the three cracking indices compared to R50-F and R50-SB, and the t-test results confirmed the significant difference between the indices obtained from 4 hours and 10 hours conditioned R50-SB mixes.
- The original HWT results could be interpreted by the rutting parameters that are exclusively determined from the creep stage. Creep slope (CS) and visco-plastic ratio (VR) could be still computed even if the failure rut depths of the two sides exhibited large discrepancies. For the 10-hour conditioned mixes, R50-SB showed the best overall performance in terms of more passes required reaching 12.5mm rut depth and higher RRI value. However, based on the CS and VR results, R50-B would have slightly better rutting resistance than R50-SB; but similar to the cracking indices, there was no solid statistical information to prove that. What is consistent between the rutting and cracking test results is that the R50-SB mix experienced the most significant hardening after extending the conditioning time from 4 hours to 10 hours.
- There were two assumed mechanisms for the effect of extended conditioning on the rejuvenated high RAP mixes. The high-temperature atmosphere enhanced the mobilization of the RAP binder and diffusion between the RAP binder and the virgin binder or the rejuvenated binder blend, which increases the overall stiffness of the effective binder film. The second assumption is that the aging of the virgin biner and the rejuvenator dominated the conditioning process, and the increase in overall brittleness and stiffness was attributed to the aging of the blend containing the virgin binder, rejuvenator (if applied), and activated RAP binder. The two scenarios could both result in similar changes in the mix performance and occur at the same time as a combined effect.

As mentioned in previous sections, the major limitation of this study is the unavoidable oxidation aging during oven conditioning. The possibility of aging could not be quantified because diffusion and rejuvenation continue at high temperatures. It is possible to obtain the extracted and recovered binder from

the unconditioned and conditioned rejuvenated mixes and characterize and quantify the aging effect using chemical analysis methods. Nonetheless, the findings of this study provided useful information about the effect of extended oven conditioning on recycled asphalt mixes prepared with rejuvenators and soft binders. Furthermore, due to their high variability and inability to differentiate mixes, not all IDEAL-CT cracking indices and HWT parameters are suitable performance indicators. It is recommended to use plant-produced mixes, if practical, to reduce operation errors when using lab-mixed and compacted samples.

Chapter 8

Rheological characterization of rejuvenated high RAP mixes under dynamic loading and long-term oven aging

This chapter is based on a paper manuscript entitled "Rheological characterization of rejuvenated high RAP mixes under dynamic loading and long-term oven aging". It focuses on the rheological properties of the rejuvenated high RAP mixes compared to the control mix with allowable RAP content. The linear viscoelastic behavior of asphalt mixes was captured using the non-destructive dynamic modulus test which applies the cyclic sinusoidal loading to monitor the strain responses of the mixes. In the meantime, the long-term performance of the rejuvenated high RAP mixes was considered via an accelerated lab long-term oven aging (LTOA) protocol.

8.1 Introduction

Reclaimed asphalt pavement (RAP) is one of the most reusable materials in North America. It is usually returned to the pavement structure in the form of being incorporated into paving materials through hot or cold recycling or used as an aggregate base or subbase construction. The use of RAP in pavement construction and rehabilitation has been favored over the use of virgin materials because it preserves non-renewable petrochemical materials (e.g., asphalt), saves the cost of using virgin materials, and reduces the environmental impact of discarded materials [2,23]. According to the published survey, 87 million tons of RAP were used in new asphalt pavement construction across the US in 2020; unfortunately, the average RAP rate was only 21.3% [9]. The major concern is that the excessive RAP content may reduce the cracking resistance at low temperatures and fatigue resistance under traffic loading. Recently, researchers have shown great interest in using asphalt binder rejuvenators to increase the percentage of RAP in asphalt mixtures to overcome the [20,77]. Rejuvenators are promising in restoring the performance of the aged binder contained in RAP. From a chemical point of view, they refill the soft medium (i.e., aromatics and/or resins) that are volatilized during field aging and break the clusters of asphaltenes; thus, reducing the viscosity and stiffness, increasing the ductility of the aged binder [163,164]. Therefore, the aged binder will possess the resembled rheological behavior to that of the fresh asphalt binder.

The time and temperature dependency of the asphalt binder endow the viscoelastic nature of asphalt mixtures [165,166]. When under cyclic sinusoidal loading, the strain response is not simultaneous with the applied stress, in which the resulting strain exhibits a phase lag to the applied stress. The stress-strain

relationship is usually defined by a complex number, which is the ratio between the applied sinusoidal stress and the responded sinusoidal strain. The real part of this complex number is defined as the storage modulus, which represents the elastic stiffness of the material; while the imaginary part is called the loss modulus, representing the viscous damping. The magnitude of this complex number is defined as the dynamic modulus (or complex dynamic modulus) of the asphalt mix, also computed as the ratio between the stress amplitude and the strain amplitude. Therefore, the storage modulus and the loss modulus can be calculated using the measured dynamic modulus ($|E^*|$) and the phase angle (φ): $E' = |E^*| \cos\varphi$, $E^{"} = |E^*| \sin\varphi$. The physical meaning of the phase angle is a quantification of the strain lags the stress and an indication of the viscoelastic property of the material. For pure elastic and pure viscous material, φ is 0° and 90°, respectively.

$$E^*(i\omega) = \frac{\sigma}{\varepsilon} = \frac{\sigma_0 e^{i\omega t}}{\varepsilon_0 e^{i(\omega t-\varphi)}} \tag{8-1}$$

$$E^*(i\omega) = E' + iE^{"} \tag{8-2}$$

$$|E^*| = \frac{\sigma_0}{\varepsilon_0} = \sqrt{E'^2 + E^{"2}} \tag{8-3}$$

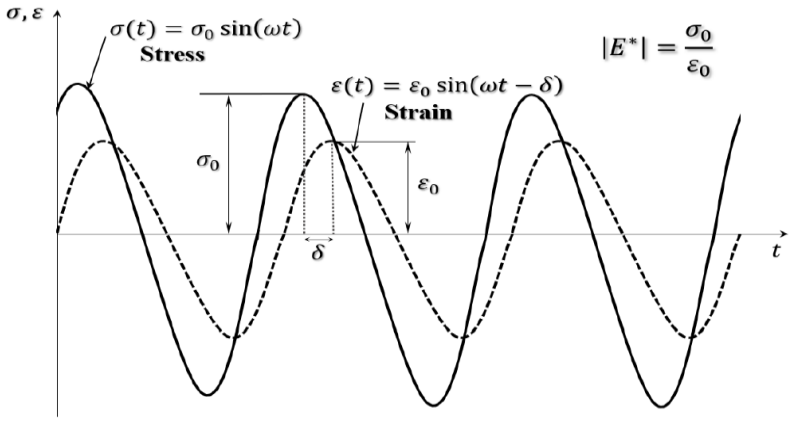

Figure 8.1 Cyclic loading and the strain response curve for asphalt mixes [167]

Due to the viscoelastic nature, asphalt materials follow the time-temperature superposition principle (TTSP), which means the behavior of asphalt binders or mixes is substitutable at different temperatures and loading speeds [168]. Therefore, the performance of asphalt mixes can be assessed by constructing a master curve of asphalt mixes, which enables the comparison between samples when the test is conducted under different loading frequencies and test temperatures. It also allows capturing the viscoelastic behavior in a wider frequency (or temperature) range at a reference temperature (frequency). Dynamic modulus is measured when the sample is tested in a small range of strains, which ensures the sample is in the linear viscoelastic (LVE) range [169,170]. It is a fundamental design parameter of flexible pavements which can be used to determine the response of asphalt mix under traffic loading and thermal conditions. A proper understanding of the dynamic response of asphalt mixes prepared with high RAP content and rejuvenators is essential for assuring the effectiveness of the rejuvenator. Meanwhile, limited studies have been conducted thus far to investigate the effect of long-term aging on the performance of rejuvenated high RAO mixes. Investigating the long-term aging effect on rheological characteristics would be of great help in building a long-lasting flexible pavement with satisfied field performance.

8.2 Research objectives

This study is set to characterize the rheological behavior of asphalt mixes with high RAP content and rejuvenators. The high RAP mixes prepared with two rejuvenation methods (a softer binder and a bio-based rejuvenator) and conditioned with both short-term and long-term aging methods were used for comparison with the control mix that has been validated as qualified hot mix asphalt (HMA) used in field construction. The dynamic modulus test was conducted under different temperature and landing frequency combinations to fulfill the purpose of this study. The following specific objectives are defined in this study:

- To evaluate the effectiveness of the use of soft binder and bio-based rejuvenator in restoring the stiffness and flexibility of recycled asphalt mixes to compensate for the consequence of increased RAP content.
- To apply different master curve models and shift factor equations and generate different rheological parameters to evaluate the performance of rejuvenated high RAP mixes.
- To investigate the influence of long-term aging on the rheological behavior of asphalt mixes containing boosted RAP content and rejuvenators.

8.3 Materials and methodology

8.3.1 Asphalt mixture sample information and conditioning protocol

The materials description and mix design details were the same as the information described in Chapter 3. In this chapter, three representative mixes were selected to fabricate the dynamic modulus specimens with different aging conditions, which were the control mix with 20% RAP (R20), the 50% RAP mix incorporated with the softer binder (R50-SB), and the 50% RAP mix prepared with the virgin binder containing 4.01% rejuvenator B (R50-B). For the control mix with 20% RAP, the mixing and compaction temperatures remained the same (146℃ and 135℃ for the base binder, PG 58-28) and the RAP did not require preheating before mixing. However, it is challenging to maintain the mixing temperature using an open mixing drum without a heating source due to the limitations of the laboratory mixing equipment. The mixing procedure of the 50% RAP mix should be adjusted to compensate for the increased RAP content and heat loss during the mixing. To achieve this, the preheating temperatures of the blended binders were increased to 160°C and the RAP was preheated to 110°C for less than two hours before mixing. The sample preparation was completed by following steps:

(1) Preheat aggregates to 10℃ above the mixing temperature overnight (more than 16 hours).

(2) Preheat RAP to 110℃ (if RAP content is more than 20%) and maintain the temperature for less than 2 hours before mixing.

(3) Preheat the base binder to the mixing temperature and add the rejuvenator at its optimized dosage described in Table 6.2 into the base binder to achieve a homogenous binder blend using the regular binder blender. Then put back the blended binder in the oven at the mixing temperature for less than 1 hour before mixing.

(4) Premix the virgin aggregates with RAP for 45 seconds (30 seconds if %RAP is no more than 20%), and then add the binder to mix for another 90 seconds (60 seconds if %RAP is no more than 20%).

(5) The loose mix will then be conditioned following the short-term oven aging (STOA) protocol and the long-term oven aging (LTOA) protocol:

   a. The STOA is conducted by conditioning the loose mix at 135℃ for four hours to simulate the aging that occurred in asphalt plant production and transportation as per AASHTO R30 [139]. An extended conditioning time was also applied on the R50-B mix.

b. The LTOA is conducted on the loose mixes that have already been short-term aged for five days at 95°C.

The LTOA protocol used in this study is different from that recommended in the AASHTO standard [139], which is five days at 85°C on compacted mixes. However, it has been proved that the standard LTOA method underestimates the field aging that occurs in as little as five years in many climates [171]. And using the compacted mixes will result in gradient aging from the sample surface to the inside. Moreover, there is a possibility of sample distortion during aging, especially for mixes with softer binder grades. Therefore, it is recommended to use the loose mixes at a higher temperature (95°C) for the accelerated lab LOTA protocol; and the aging duration will be selected based on the climate region and pavement depth [171]. The LTOA protocol used in this study is designed to simulate the field aging that occurs at 6mm below the pavement surface after five years. After the conditioning, the loose mix was compacted at the compaction temperature using the Superpave Gyratory Compactor (SGC). The cylindrical samples were then cored and saw cut to produce specimens with 100mm diameter and 150mm height.

8.3.2 Dynamic modulus test

Dynamic modulus tests were performed as per AASHTO T342 [108] by applying sinusoidal axial compression loads at six frequencies (25 Hz, 10 Hz, 5 Hz, 1 Hz, 0.5 Hz, and 0.1 Hz) and five temperatures (-10°C, 4°C, 21°C, 37°C, and 54°C (and/or 44°C)). The applied stress was adjusted for each mix to achieve a recommended strain range (50με to 150με) according to the standard. The strain response and phase lag were computed based on the readings from three extensometers (120° against each other) attached to the magnetics mounted on the specimen surface. The test was running from the lowest temperature to the highest test temperature in a frequency sweep mode starting from 25Hz and gradually reduced to 0.1Hz. A dummy specimen of the same dimensions was made, and a thermocouple was installed into the center of it. Readings from the thermocouple were used as the actual test temperature for data measured dynamic modulus and phase angle data.

8.3.3 Mater curve construction

Master curve models

The standard sigmoidal model, as shown in Equation (8-4), is currently used in Mechanistic-Empirical Pavement Design Guide (MEPDG) [172,173]. It is an analytical model, in which expressions of dynamic

modulus or other rheological measurements are employed to fit the experimental data using a mathematical function.

$$log|E^*| = \delta + \frac{\alpha}{1 + e^{\beta+\gamma\, log\, \omega_r}} \tag{8-4}$$

where:

$|E^*|$ = absolute value of the complex dynamic modulus (MPa).

δ = the lower asymptote of the curve.

α = the difference between the values of upper and lower asymptote.

ω_r = reduced frequency.

β, γ = shape parameters, which define the shape between asymptotes and the location of the inflection point.

Parameter β determines the horizontal turning point of the curve and parameter γ affects the steepness of the function, the changing rate between the maximum and minimum. The upper part of the curve approaches an asymptote which is the maximum stiffness of the sample at cold temperatures. At the lower part, associated with the low frequency (high temperature) region, the aggregate structure becomes more dominant than the viscous binder and the stiffness of the mix will toward an equilibrium value which is dependent on the aggregate gradation. However, there are certain drawbacks to the standard sigmoidal model. First, is only applicable when the measured modulus data is symmetrical to the inflection point of the master curve, which does not apply to many types of asphalt mixes with binder modifiers and recycled additives [174]. Also, the phase angle master curve is ignored since the storage modulus E' and especially the loss modulus E'' do not follow the sigmodal format [165]. Rowe et al. [174] developed the generalized logistic sigmoidal model known as a Richards curve by introducing a parameter λ. Based on the Kramers-Kronig (K–K) relationship, the semi-log generalized sigmoidal model can be derived from Equation (8-5) for the phase angle (see Equation (8-6)) [175].

$$log|E^*| = \delta + \frac{\alpha}{(1 + \lambda e^{(\beta+\gamma\, log\, \omega_r)})^{\frac{1}{\lambda}}} \tag{8-5}$$

$$\varphi = -\frac{\pi}{2} \cdot \frac{\alpha\gamma e^{(\beta+\gamma\, log\, \omega_r)}}{(1 + \lambda e^{(\beta+\gamma\, log\, \omega_r)})^{(\frac{1}{\lambda}+1)}} \tag{8-6}$$

Figure 8.2 shows the effect of different λ values on the shape of the asphalt binder master curve (δ = 0, β =1, and γ = -1). The generalized relationship of a sigmoid follows the same S-shape format of the standard sigmodal model, but the position of the inflection point varies with different λ values, which allows the curve to take a non-symmetric shape. When λ equals one, the curve represents the standard sigmoidal model, in which the inflection point is at the mid-point between the upper and lower asymptotes. The inflection point moves upward when λ is increasing and downward when λ is approaching to zero, which results in a skewed curve form. The generalized model format works well to describe the shape of a master curve and it is non-symmetrical about the inflection point. The analysis of the binder master curve with various modifiers, including polymer, crumbled rubber, and fibres, demonstrated that a non-symmetric sigmoid format is required for more accurate master curve modelling [174,176]

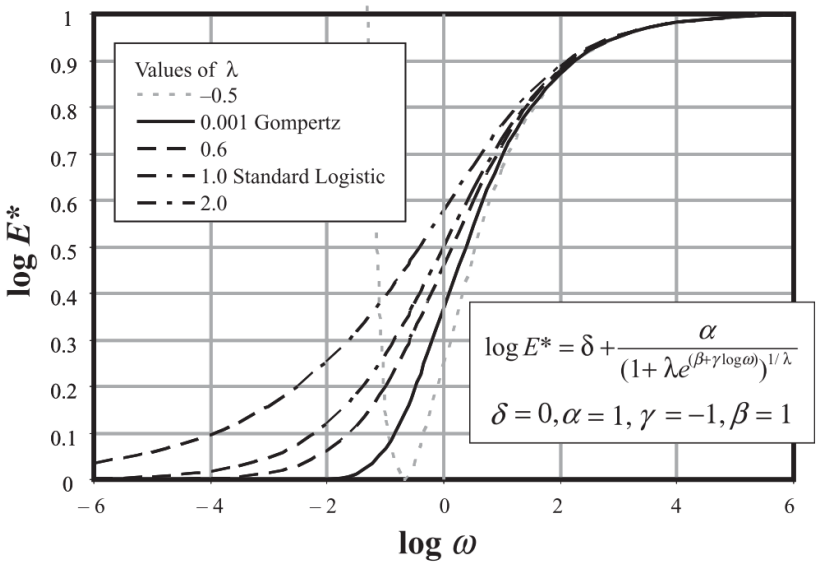

Figure 8.2 Generalized sigmoidal master curve with different λ values [174]

Another category of the master curve model is the analogical model, in which the linear viscoelastic response is described with a combination of physical elements (spring, dashpot and parabolic element). As shown in Figure 8.3, the 2S2P1D model (see Equation (8-7)) developed by Olard and Di Benedetto is a generalization of the Huet-Sayegh model by adding a linear dashpot in series with the two parabolic elements and the spring of rigidity ($E_\infty - E_0$) [177]. 2SPID model is one of the most representative and widely used analogical models for both asphalt binders and asphalt mixes [169,178,179]. For asphalt mix, the static modulus (when ω tends to 0) is the stiffness of the aggregate skeleton, the glassy modulus (when ω tends to infinity) relates to the stiffness of the material at very cold temperatures (high frequencies), also known as the instantaneous modulus. For binders, the experimental static modulus is very close to zero, the model is equivalent to a linear dashpot at a very low frequency.

$$E^*(i\omega\tau) = E_0 + \frac{E_\infty - E_0}{1 + \delta(i\omega\tau)^{-k} + (i\omega\tau)^{-h} + (i\omega\beta\tau)^{-1}} \tag{8-7}$$

where:

E_0 = the static modulus when $\omega\tau \to 0$.

E_∞ = the glassy modulus when $\omega\tau \to \infty$.

h, k = parabolic creep parameters ($0 < k < h < 1$).

τ = characteristic time (temperature dependent).

δ, β = dimensionless parameters.

$\eta = (E_\infty - E_0)\beta\tau$, which represents the Newtonian viscosity

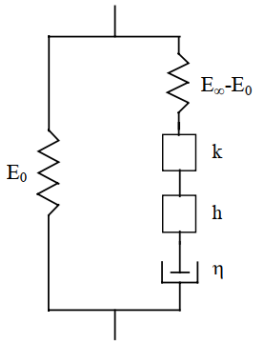

Figure 8.3 Analogical representation of the 2S2P1D model [177]

Shift factor functions

The reduced frequency in the master curve model is obtained by shifting the dynamic modulus and phase angle measured at the testing frequencies to form a single master curve. The shifting is completed by multiplying the testing frequency with a shift factor ($a(T)$) at a given temperature.

In the master curve construction, the time-temperature superposition can be done in two different ways.

1. Shifting the measured data without assuming any equations for the time-temperature superposition relationship, is called experimental shifting. The shift factors and model parameters are optimized simultaneously.
2. Shifting the measured data based on certain time-temperature superposition equations. The shifting equation coefficients and model parameters were optimized at the same time.

The first method is done by solving the shift factors for each test temperature (or frequency) and the master curve model parameters at the same time. As for the second method, the shifting equation coefficients and the model parameters are optimized together. The experimental shifting was claimed to have the better fit compared to using shifting equations since it has the most degree freedom; however, it showed a good correlation with several shifting equations, such as the Arrhenius shifting equation and the William-Landel-Ferry (WLF) equation [165].

The WLF equation is an empirical function associated with the time-temperature superposition principle, which was found to fit well the shift factors for a wide range of asphalt binders that were tested between -20℃ (close to the glass transition temperature (T_g) of the binder) and 60℃. The WLF method has been proven to suit the rheological data measured between T_g and T_g + 100℃ [165,180].

$$log\ a(T) = \frac{-C_1(T - T_r)}{C_2 + T - T_r} \tag{8-8}$$

where:

C_1, C_2 = empirical constants.

T = test temperature, ℃.

T_r = reference temperature, ℃.

The Arrhenius equation is used to describe the time-temperature superposition principle in amorphous polymers below T_g. The activation energy ΔE_a represents the barrier that the molecules must cross for reaction. For the shift factor, the Arrhenius equation depicts the temperature dependency of reaction rates.

$$log\ a(T) = -\frac{\Delta E_a}{2.303R}(\frac{1}{T} - \frac{1}{T_r}) \tag{8-9}$$

where:

ΔE_a = apparent activation energy, J/mol.

R = universal gas constant, 8.314 J/K·mol.

T = test temperature in Kelvin.

T_r = reference temperature in Kelvin.

As mentioned above, the WLF equation and Arrhenius equation are typically used for temperatures above and below T_g . However, both equations have a hyperbolic form, with the values at lower temperatures tending to have high values of shift factors as the temperature decreases [172,174]. Therefore, an alternate shifting equation, the Kaelble-modified WLF equation (Equation (8-10)), was developed by changing the denominator of the WLF equation with a magnitude value $|T - T_d|$. Thus, the Kaelble method shows a sigmoid type of behaviour which does not result in excessively high shift factors as the temperature drops. The new parameter T_d is called the defining temperature, similar to the concept of T_g, which controls the inflection point of the sigmoidal format of the shift factors. Equation (8-10) can be rewrote as (8-11) so it can be applied on data shifting to a reference temperature [176].

$$log\ a(T) = \frac{-C_1(T - T_d)}{C_2 + |T - T_d|} \tag{8-10}$$

$$log\ a_T = -C_1(\frac{T - T_d}{C_2 + |T - T_d|} - \frac{T_r - T_d}{C_2 + |T_r - T_d|}) \tag{8-11}$$

where:

C_1, C_2 = empirical constants.

T = test temperature, ℃.

T_d = defining temperature, ℃.

T_r = reference temperature, ℃.

In summary, there were two master curve models, the generalized sigmoidal model and the 2S2P1D model, and three shifting equations known as the WLF equation, Arrhenius equation, and Kaelble modified WLF equation used in this study. The construction of the sigmoid format master curve was completed by optimizing the fitting of dynamic modulus and phase angle at the same time, with the shift factors constrained by the WLF equation. While the "free shifting" method was applied when constructing the 2S2P1D master curves, and the shift factors were then fitted to the three shifting equations to obtain different equation constants. The master curve modelling was accomplished by minimizing the root mean square error (RMSE) between the measured dynamic modulus (phase angle) and the predicted dynamic modulus (phase angle) at a reference temperature of 21℃.

8.4 Results and discussion

8.4.1 Dynamic modulus test results

As mentioned above, the dynamic modulus and phase angle data were obtained by averaging the measured values from two replicate samples for each mix. As shown in Equation (8-12), the percent difference is calculated as the absolute difference between the measured dynamic modulus (or phase angle) of two samples divided by the average dynamic modulus (or phase angle). This index represents the relative difference of the measured dynamic modulus or phase angle between two replicates.

$$Percent\ difference\ (\%) = \frac{||E^*|_1 - |E^*|_2|}{|\overline{E^*}|} \times 100 \quad (8\text{-}12)$$

Figure 8.4 and Figure 8.5 show the box plots of the calculated percent difference values of R20, R50-SB, and R50-B mixes under different test temperatures and frequencies. Each set of box plot data was derived from the percent difference at the six testing frequencies (i.e., 25Hz, 10Hz, 5Hz, 1Hz, 0.5Hz, and 0.1Hz) and the six test temperatures (i.e., -10℃, 4℃, 21℃, 37℃, 44℃, and 54℃). In general, the short-term aged mixes showed a higher average percent difference and smaller spread of the data distribution compared to the long-term aged mixes. For dynamic modulus, the long-term aged R50-B mix had the smallest percent difference (less than 5%), with no outliers observed in the plot, indicating the measured dynamic modulus was consistent between the two replicates. Although the long-term aged R50-SB showed a similar result with R50-B, there were prominent outliers identified in this data group. The four observed outliers were obtained from the dynamic modulus measured under 1Hz, 0.5Hz, and 0.1Hz at 54℃ and 0.1Hz at 44℃. R50-SB and R50-B with 4 hours of oven aging had a similar average percent difference of around 25%; however, the spread of the R50-SB plot suggested a much higher variation in the data and the maximum percent difference approached approximately 40%. In terms of the phase angle, all the plots showed comparatively smaller average values against the dynamic modulus data, except R20-4H, which showed an outlier obtained at the test condition combination of 0.1Hz and 44℃. With four hours of conditioning, the three mixes shared a similar average (or median) value of the percent difference, but the R50-B mix data group is more distributed, with a maximum value of over 30%. In contrast to the dynamic modulus result, R50-SB showed more steady phase angle measurements compared to the R50-B mix. After long-term oven aging, all mixes experienced an obvious reduction in the percent difference, with R50-B displaying the smallest average value and data distribution. In addition, each mix showed outliers in their data groups and R50-SB exhibited obvious upward skewed data distribution. The most far away percent difference outlier was witnessed in R50-SB, which was measured at 0.5Hz and 54℃.

Overall, the percent difference results provide insight into the reliability of the measured dynamic modulus and phase angle results. Most of the two replicate results showed a relative difference of less than 15%, especially the phase angle, with higher consistency observed in long-term aged mixes containing rejuvenators and higher RAP content. Moreover, it should be noted that the outliers in a specific mix were mostly derived from higher testing temperatures and lower loading frequencies, which indicates that the

mixes were less stable in these situations. Since the mixes become more viscous at a high temperature (or low loading frequency), the behavior of asphalt mixes is more complicated compared to its elastic state.

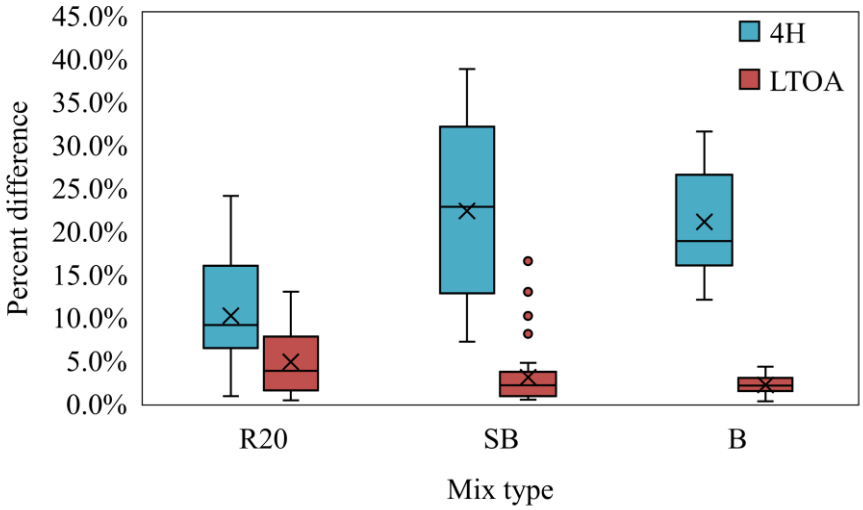

Figure 8.4 Box plots of percent difference in dynamic modulus

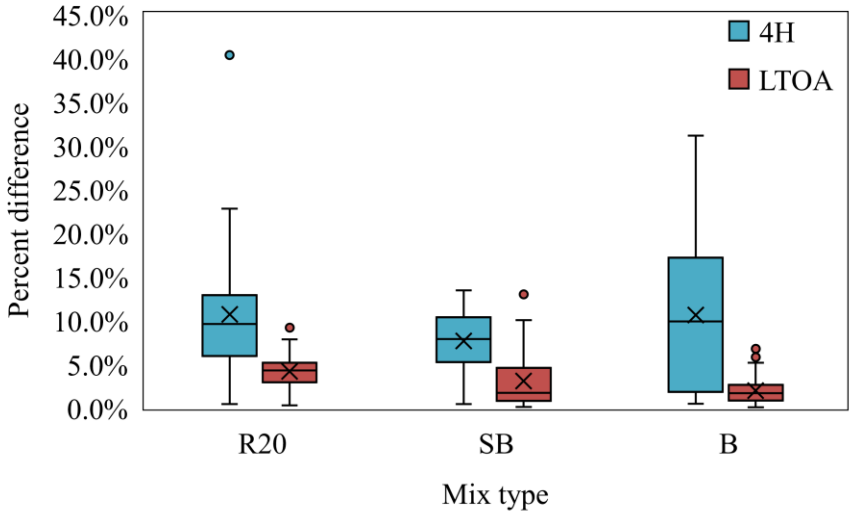

Figure 8.5 Box plots of percent difference in phase angle

Figure 8.6 displays the measured dynamic modulus values of R20, R50-SB, and R50-B. Regardless of the test temperature, the measured dynamic modulus showed a reducing trend as the loading frequency decreased, which was expected since the asphalt binder was less elastic under lower loading frequencies. It is also apparent from the figure that the three mixes showed relatively similar dynamic modulus values

before and after long-term aging when the test temperatures were -10℃ and 4℃. As the test temperature increased to 21℃ and 37℃, the short-term aged R20 mix exhibited slightly higher modulus than the rejuvenated high RAP mixes. However, with the testing temperature above 37℃, the modulus of the R50-B mix was constantly larger than those of R20 and R50-SB after long-term aging. Meanwhile, the difference between short-term aged and long-term aged mixes was more significant at intermediate and high testing temperatures.

Baaj et al. [181] applied three main criteria from the dynamic test results to compare the stiffness of asphalt mixes modified with high contents of RAS and RAP to facilitate different pavement service temperatures. Similarly, the stiffness at the lowest test temperature (-10℃) and high loading frequencies (10Hz and 25Hz) provides the material's properties under low pavement temperature and high-speed traffic cases. From the data in Figure 8.6 (a), the increased RAP content and addition of the soft binder or a rejuvenator did not show a significant impact on the stiffness of the mixes, which is a benefit of maintaining acceptable thermal cracking resistance as the control mix. The values at higher test temperatures (44℃ and 54℃) and frequencies lower than 1Hz can be used as indicators of rutting resistance. Apparently, the difference between these mixes was marginal, with the long-term aged R50-B showing higher stiffness compared to R20 and R50-SB. The stiffness at intermediate temperature (e.g., 21℃) was used as an input (resilient modulus) in the empirical pavement design method for the past few decades [182]. While with the development of mechanistic-empirical pavement design methods, the dynamic modulus becomes a primary input in the MEPDG to define the loading rate–temperature dependency of the asphalt mixture. The correlation between the resilient modulus and the dynamic modulus was established based on the conversion of an estimated field loading pulse (0.03 second) and the cyclic frequency of the dynamic modulus test [183,184]. It is found that the resilient modulus is equivalent to the dynamic modulus at the same temperature and a 5 Hz continuous loading frequency. As can be seen from Figure 8.6 (c), the highest modulus of the short-termed aged mixes was observed in R20, followed by R50-SB and R50-B at 5Hz loading frequency, indicating that mixes were softened by the addition of the rejuvenator and the soft binder despite increased RAP content. However, the long-term aged mixes showed insignificant stiffness difference, with R50-B achieving a slightly higher dynamic modulus.

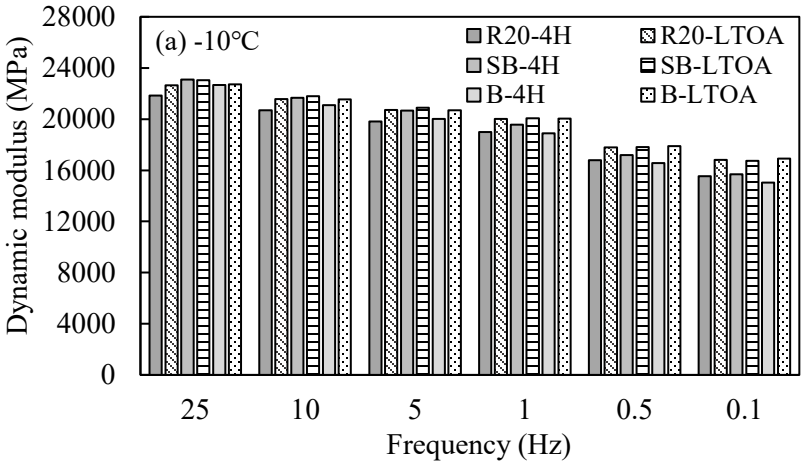
(a) -10℃
R20-4H
R20-LTOA
SB-4H
SB-LTOA
B-4H
B-LTOA
Dynamic modulus (MPa)
28000
24000
20000
16000
12000
8000
4000
0
25
10
5
1
0.5
0.1
Frequency (Hz)

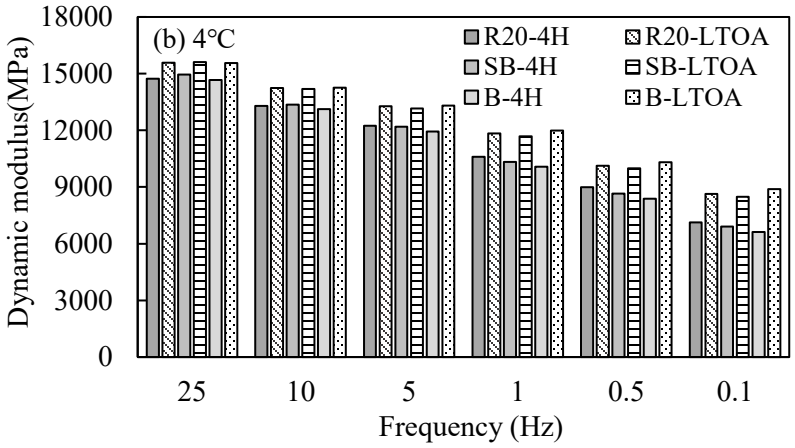
(b) 4℃
R20-4H
R20-LTOA
SB-4H
SB-LTOA
B-4H
B-LTOA
Dynamic modulus(MPa)
18000
15000
12000
9000
6000
3000
0
25
10
5
1
0.5
0.1
Frequency (Hz)

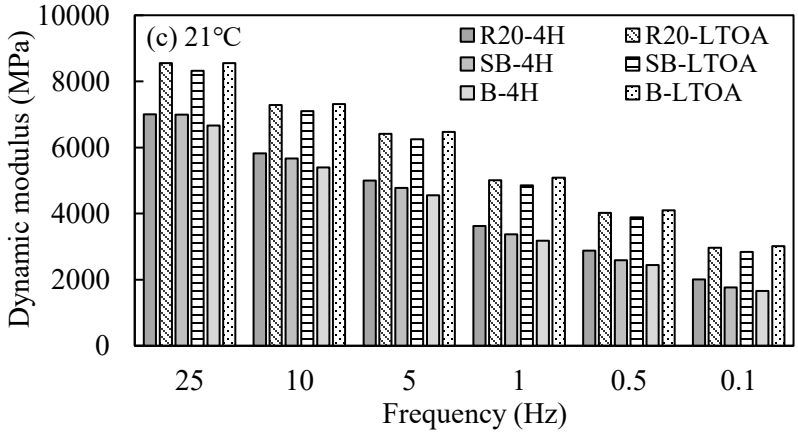
(c) 21℃
R20-4H
R20-LTOA
SB-4H
SB-LTOA
B-4H
B-LTOA
Dynamic modulus (MPa)
10000
8000
6000
4000
2000
0
25
10
5
1
0.5
0.1
Frequency (Hz)

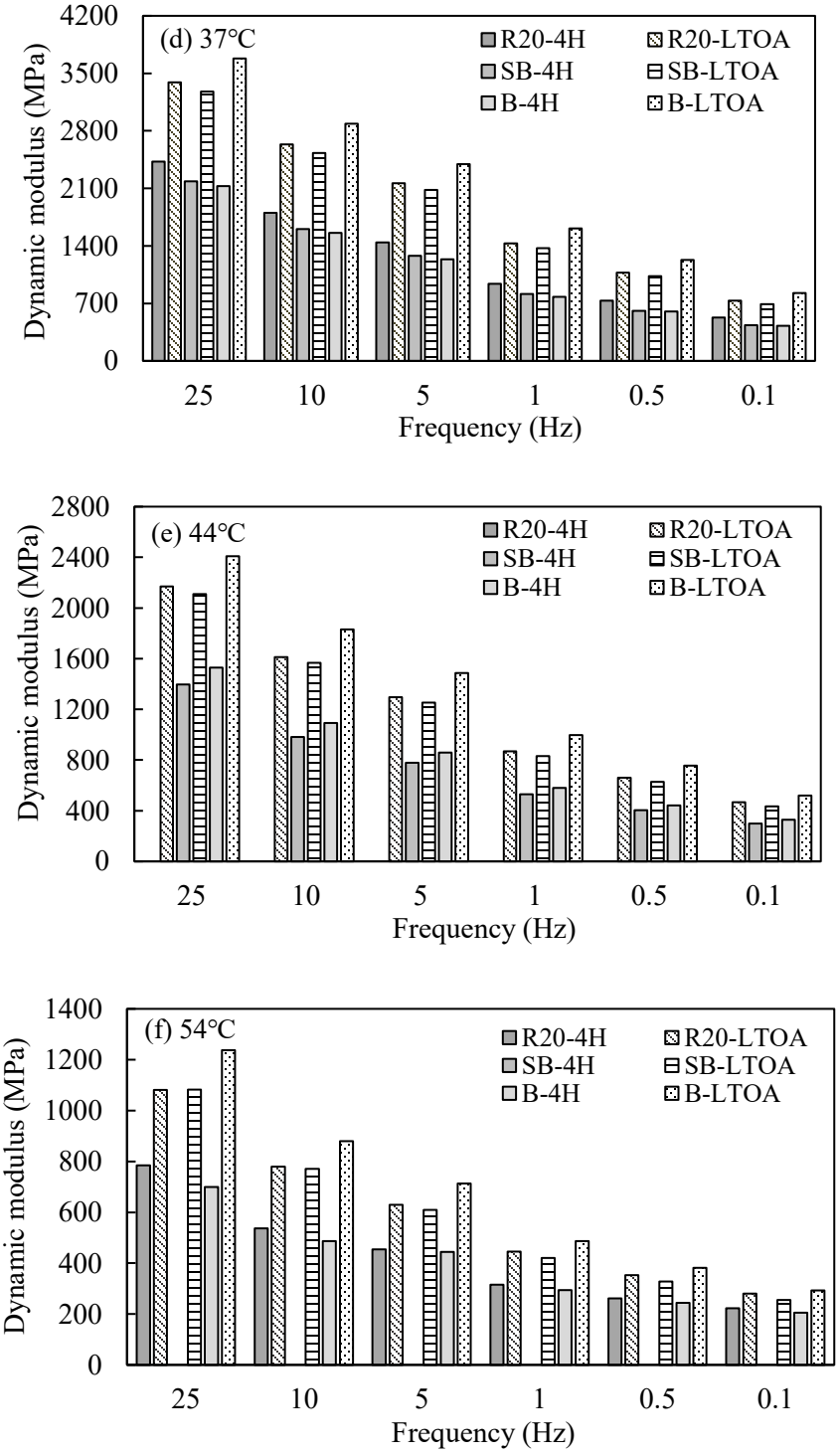

Figure 8.6 Dynamic modulus values obtained at different temperatures and frequencies

8.4.2 Master curve constructed by Generalized sigmoidal model and 2S2P1D model

The master curves of dynamic modulus and phase angle were built to a reference temperature of 21℃ using both the generalized sigmoidal model and the 2S2P1D model. Figure 8.7 to Figure 8.9 display the dynamic modulus and phase master curves of the three mixes with different aging conditions. The shifting of isotherms was completed using the "free shifting" concept when fitting the measured data to the 2S2P1D model. However, the fitted sigmodal master curve seemed highly agreed with the curve fitted by the 2S2P1D model, except for the phase angle at the very low frequency range (less than 10^{-4} Hz). What stands out in the dynamic modulus master curves is the obvious gap between the two fitted curves before and after the long-term oven aging. While the gap only started to emerge when the frequency was lower than 10^{4} Hz, which is compatible with the abovementioned observations in the measured dynamic modulus values at -10℃ and 25Hz, in which the dynamic modulus showed a marginal difference in a testing combination of high frequency and low temperature.

As for the phase angle, the fitted master curves shifted to a lower frequency range while maintaining a similar shape. The hump-shaped phase angle master was caused by the fact that the measured phase angle showed an increasing trend with the loading frequency when the test temperature was lower than 37℃. But at the same time, the phase angle decreased with the increasing frequency at a higher test temperature (54℃). The reason for this phenomenon is the asphalt mix behaves more elastic at lower temperatures and has no significant phase lag between the stress and strain under loading. However, as the temperature increases, the asphalt binder becomes softer, resulting in a larger phase angle (above 25°). Meanwhile, the phase angle of the asphalt mix is more affected by the aggregate skeleton at higher temperatures and lower loading frequencies; therefore, the phase angle decreases with the decreasing loading frequency due to the elasticity of aggregates [175]. The phase angle data obtained at 37℃ (or 44℃) first increased and then started to decrease as the frequency continued decreasing, which implied a "transition point" at which the loading speed was slow enough to cause the asphalt mix to be more viscous, similar to the idea of the crossover temperature (or frequency) of the asphalt binder. Hence, the shift of the curve hump represented the "transition point" that occurred at a lower frequency (or higher temperature) circumstance because of the increased elasticity of the asphalt mix after aging.

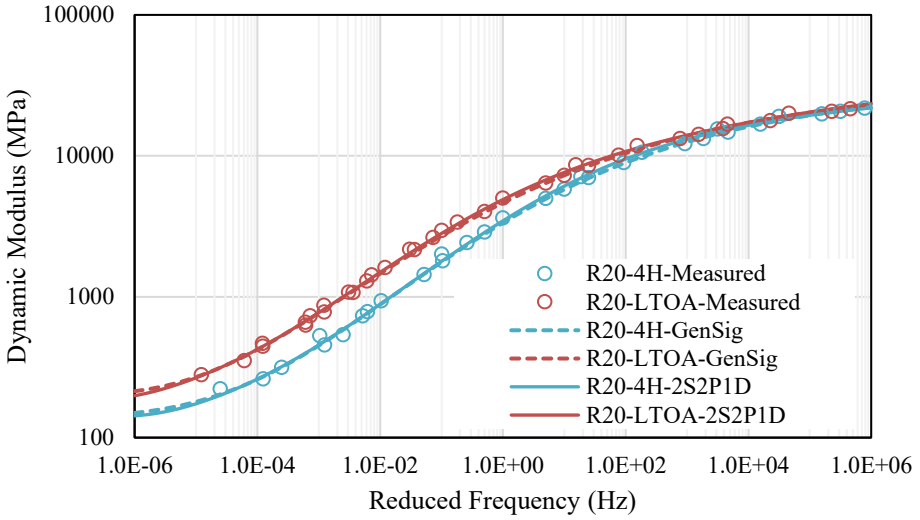

(a) Dynamic modulus

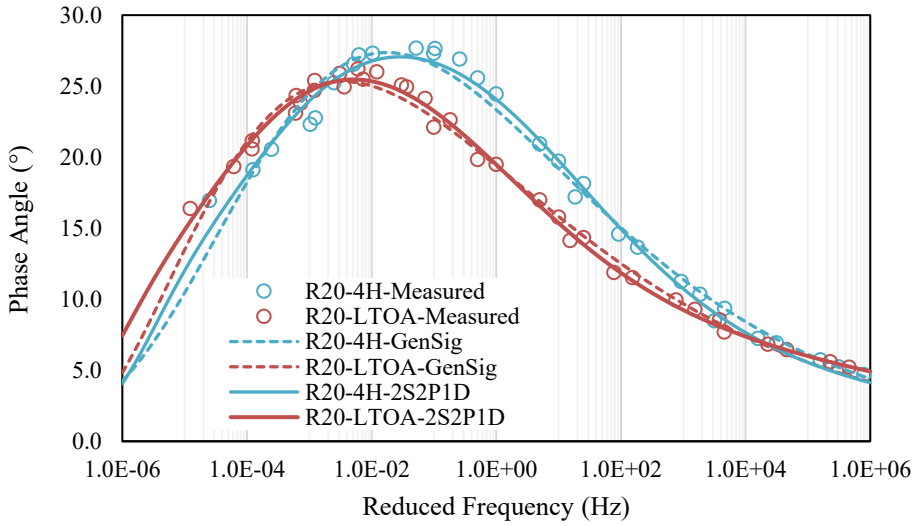

(b) Phase angle

Figure 8.7 Master curves of R20 mixes: (a) dynamic modulus, (b) phase angle

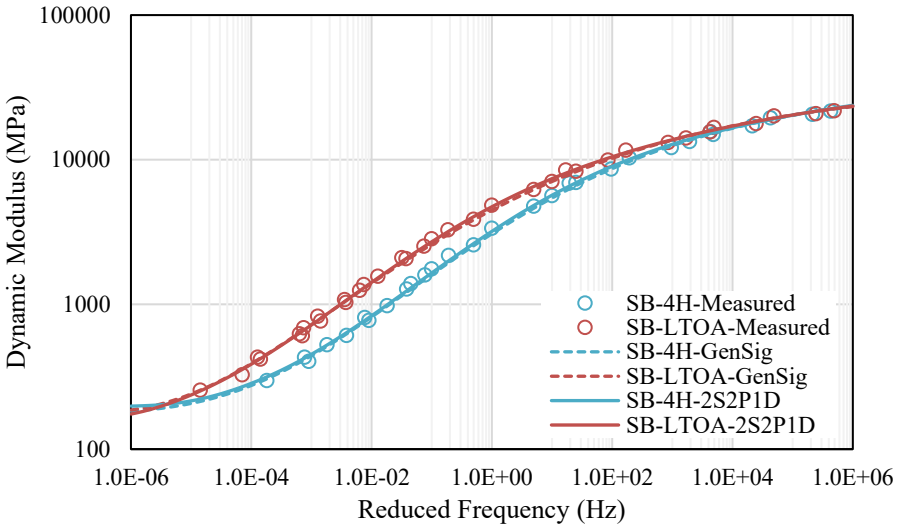

(a) Dynamic modulus

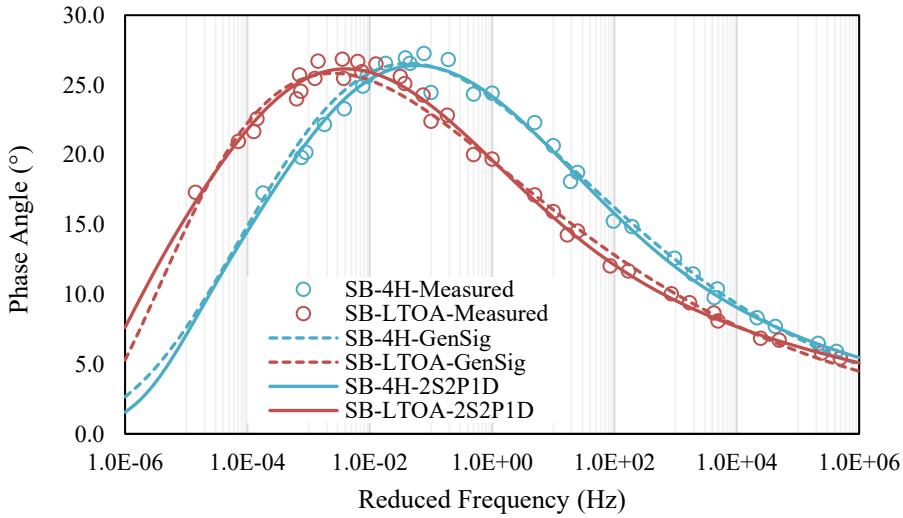

(b) Phase angle

Figure 8.8 Master curves of R50-SB mixes: (a) dynamic modulus, (b) phase angle

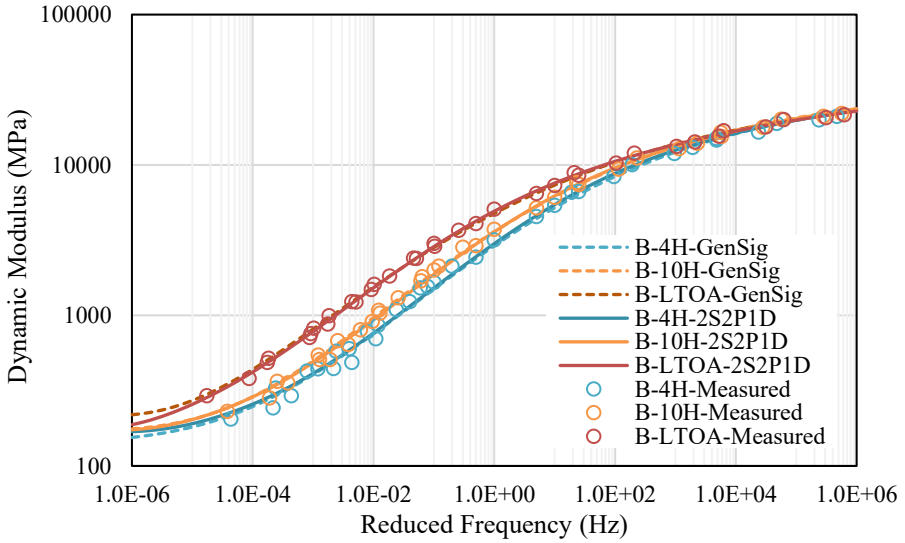

(a) Dynamic modulus

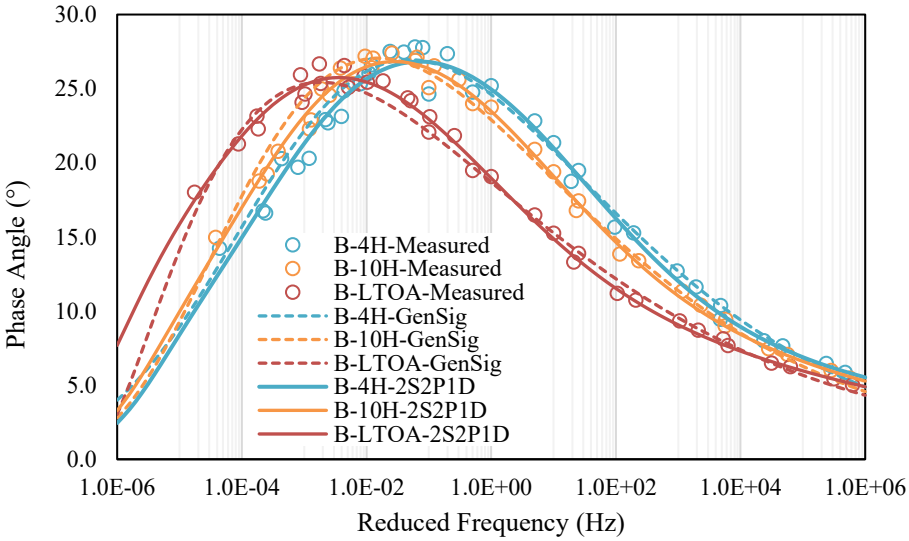

(b) Phase angle

Figure 8.9 Master curves of R50-B mixes: (a) dynamic modulus, (b) phase angle

Table 8.1 and Table 8.2 summarize the parameters of the generalized sigmoidal model and 2S2P1D model. As discussed in section 8.3.3, α and δ denote the upper and lower asymptotes of the modulus master curve, the mix modulus will be approaching to 10^{δ} and $10^{\alpha+\delta}$ at the lowest and highest frequency regimes, respectively. From Table 8.1, we can see that δ experienced a noticeable increase from the short-aging to

long-term aging, except for the R50-SB mix, whereas the difference between different mix types was insignificant. Also, it is expected that the $\alpha + \delta$ value of each sample was close regardless of the aging time and mix type, as the generalized sigmoidal master curves were almost overlapped when the reduced frequency was over 10^4 Hz. β controls the horizontal shifting of the curve turning point, a more negative β value means the curve is more shifted on the left side, indicating the higher modulus at the same reduced frequency. The LTOA mixes showed a larger magnitude of β compared to their counterparts with 4 hours conditioning. Moreover, a larger magnitude of γ will lead to a steeper master curve, in which isotherms will need less horizontal shifting compared to those with less negative γ values. The long-term aged mixes showed constantly less negative γ values compared to their corresponding short-term aged mixes. It is obvious that the LTOA mixes showed larger magnitude of β compared to their counterparts with 4 hours conditioning. Moreover, a larger magnitude of γ will lead to a steeper master curve, in which isotherms will need less horizontal shifting compared to those with less negative γ values. From the results in Table 8.1, the long-term aged mixes constantly showed less negative γ values compared to their corresponding short-term aged mixes, it can be inferred that the aged mixes were more susceptible to temperature changes since the measured date needed to shift more to build a master curve. The findings in the trend of model parameters with aging can be potential indices to evaluate the long-term performance of asphalt mixes. Likewise, some parameters provided in Table 8.2 also exhibited a particular trend with aging, such as δ and τ. The computed parameter, $\eta = (E_\infty - E_0)\beta\tau$ which is known as the dashpot viscosity, was proved to be well correlated with the chemical compositions (e.g., asphaltene content) of asphalt binder, which can be a good aging index candidate for both asphalt binder and mixes [185,186]. More details about the aging effect will be discussed in the next section.

Table 8.1 Generalized sigmoidal model and WLF equation parameters

Sample ID	C_1	C_2	α	β	δ	$\alpha+\delta$	γ	λ
R20-4H	38.2	293.2	2.344	-0.630	2.142	4.486	-0.358	0.032
R20-LTOA	64.0	471.7	2.208	-0.772	2.306	4.514	-0.312	-0.198
R50-SB-4H	53.9	402.9	2.289	-0.487	2.244	4.533	-0.355	0.030
R50-SB-LTOA	56.5	418.8	2.293	-0.773	2.247	4.54	-0.297	-0.249
R50-B-4H	32.4	254.8	2.364	-0.486	2.150	4.514	-0.369	0.148
R50-B-10H	34.1	266.8	2.295	-0.621	2.232	4.527	-0.343	-0.076
R50-B-LTOA	45.4	340.4	2.196	-0.792	2.334	4.53	-0.290	-0.331

Table 8.2 2S2P1D model parameters

Sample ID	E_0	E_∞	δ	τ	k	h	β
R20-4H	138.45	32129.33	1.402	0.008	0.126	0.383	59060.78
R20-LTOA	180.80	40634.92	2.612	0.032	0.123	0.389	47154.68
R50-SB-4H	197.00	40566.85	2.167	0.005	0.134	0.399	33900.19
R50-SB-LTOA	159.20	39957.99	2.824	0.040	0.132	0.400	34540.47
R50-B-4H	166.14	48145.87	2.250	0.002	0.104	0.386	133140.25
R50-B-10H	169.61	41599.30	2.278	0.007	0.125	0.398	54719.08
R50-B-LTOA	171.95	38890.82	2.744	0.048	0.126	0.396	29867.40

8.4.3 Effect of long-term aging on rheological properties

The area difference under the dynamic modulus curve has been used for quantifying the effect of mix conditioning, like moisture and oven aging [187,188]. Tarbox et al. [187] applied the area under the master curve and calculated the percent of change in the area using the unaged master curve as a baseline to evaluate the aging effect on asphalt mixes with different RAP rates. The results showed that the area difference increased with the aging duration from two days to eight days. From Figure 8.7 to Figure 8.9, we have noticed that the modulus master curve gap was only significant at the frequency range under 10^4 Hz. Therefore, the area under the dynamic modulus master curve (from 10^{-4} to 10^4 Hz) was used as an index for calculating the area difference (%) for different mixes.

As can be seen in Figure 8.10, the LTOA protocol in this study resulted in an average increase, approximately 16.4% to 25.8%, in the dynamic modulus, depending on the mix type and master curve model. The generalized sigmoidal model showed a slightly higher area difference compared to the 2S2P1D model. However, both two models achieved a similar trend in the area difference of the three mixes, with the R50-B mix showing a more significant stiffness increase compared to R20 and R50-SB. In addition, the 10 hours conditioned R50-B mix showed 12.2% and 8.7% curve area differences when using the generalized sigmoidal model and 2S2P1D model, respectively. Previous studies have shown that asphalt mixes with higher RAP content aged slower than mixes with less RAP content [189,190]. Whereas from the results illustrated in Figure 8.10, the addition of a rejuvenator resulted in higher aging susceptibility although the RAP content was increased to 50%.

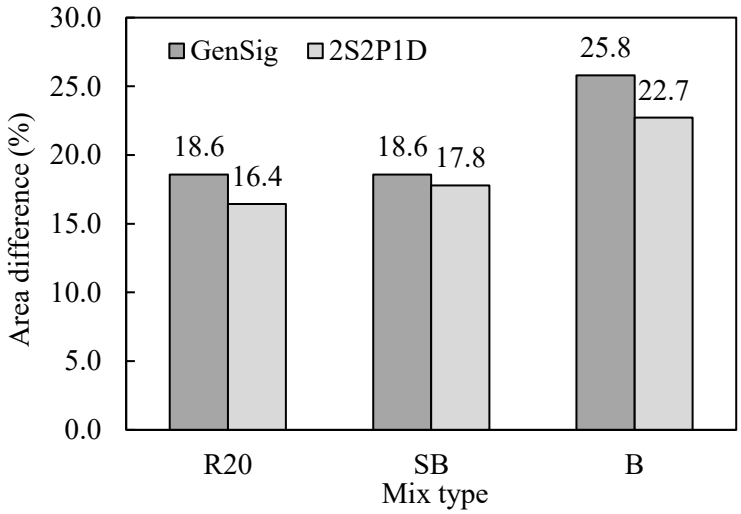

Figure 8.10 AR (%) using the area under dynamic modulus master curve

The model parameter selected here is the dashpot viscosity from the 2S2P1D model since it considers both the elasticity and viscosity portions. Table 8.3 displays the calculated dashpot viscosity of three mixes with different aging conditions. R50-SB exhibited the smallest value at 4 hours of conditioning but increased to a comparable level of the R50-B mix after long-term aging. It is expected that R50-SB and R50-B had lower values compared to the control mix since the effective binder blends were much less viscous due to the replacement of a softer binder and the addition of a rejuvenator. As the conditioning continues, R50-B achieved a similar value to that of the R20 mix after 10 hours of conditioning. After the mixes were subjected to the LTOA protocol, this parameter increased by four to eight times regarding different mix types, with the least growth in the dashpot viscosity revealed in R20-mix which indicates a better aging resistance regarding maintaining the viscoelasticity. Nevertheless, the long-term aged R50-SB and R50-B mixes had lower values compared to the control mixes despite that they suffered more loss of flexibility.

Table 8.3 Dashpot viscosity (10^7 MPa·s) computed from the 2S2P1D model

Mix type	4H	10H	LTOA	Ratio (10H/4H)	Ratio (LTOA/4H)
R20	1.56	-	6.12	-	3.9
R50-SB	0.69	-	5.55	-	8.1
R50-B	1.05	1.63	5.59	1.5	5.3

As for the coefficients of shifting factors, C_2 from the WLF equation and activation energy from the Arrhenius equation were used as indicators for evaluating the aging effect. As C_2 parameter is linked to the thermal dependency of the asphalt binders with an increase in C_2 value with aging [180]. In addition, the aging condition will potentially alter the ΔE_a values, as the temperature sensitivity of the viscoelastic material is sensitive to age hardening [168]. Figure 8.11 and Figure 8.12 illustrate the constant C_2 generated in the WLF equation when constructing the master curve using the generalized sigmoidal model and THE 2S2P1D model. Figure 8.13 shows the obtained ΔE_a values when fitting the shift factors with the Arrhenius equation. From the values denoted in the figures below, the C_2 values showed the same tendency with aging regardless of the master curve model, with the R20 mix showing the most significant increase after long-term aging. And both Figure 8.11 and Figure 8.12 demonstrated that R50-SB was the most sensitive to thermal changes at the beginning (4 hours conditioning time) but experienced the least increment in the C_2 constant. Although R50-B exhibited more increase in C_2, it remained the lowest C_2 values in both STOA and LTOA conditions compared to R20 and R50-SB. As for ΔE_a, the difference between mixes before and after LTOA was marginal, while it still provided the same results in terms of the parameter changes with aging for all three mixes. Additionally, unlike the stiffness and dashpot viscosity, R50-B with 10 hours of conditioning showed an insignificant change in both C_2 and ΔE_a values. Parameter C_2 is a dimensionless constant which is only relative to the thermal dependency of the material, whereas ΔE_a has a specific physical meaning which is the minimum energy required for asphalt materials to become flowable. However, based on the results in this section, ΔE_a seemed to be a less preferable parameter to capture the aging effect, since it was less capable of differentiating the samples conditioned with STOA and LTOA protocols.

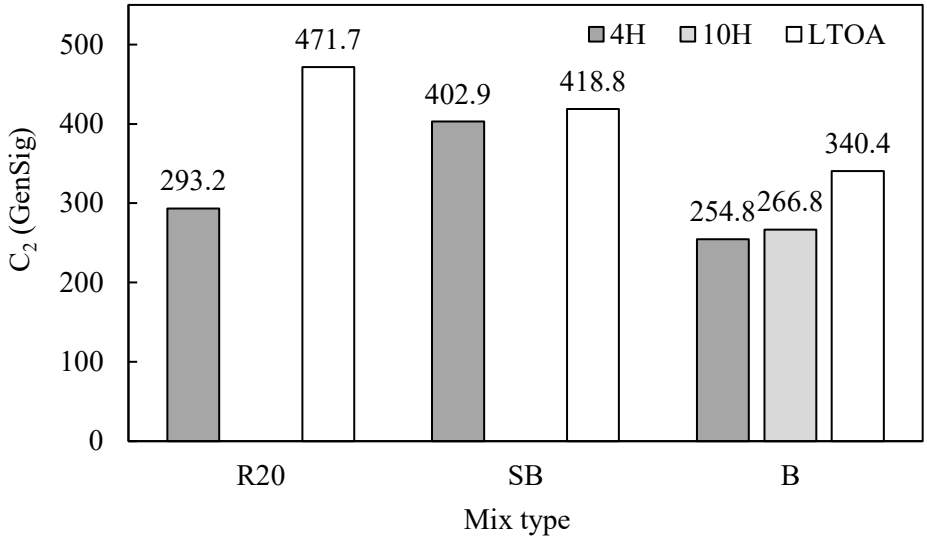

Figure 8.11 Parameter C_2 from WLF equation (generalized sigmoidal model)

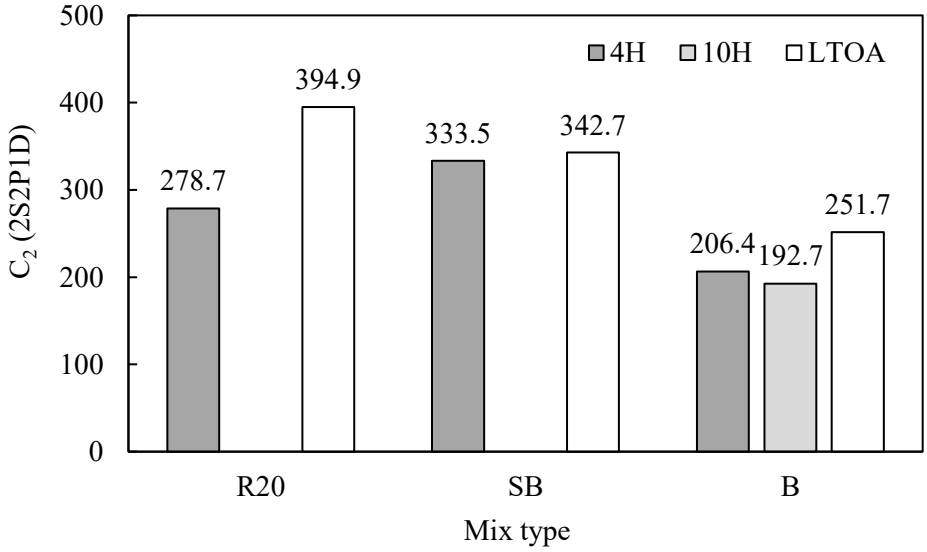

Figure 8.12 Parameter C_2 from WLF equation (2S2P1D model)

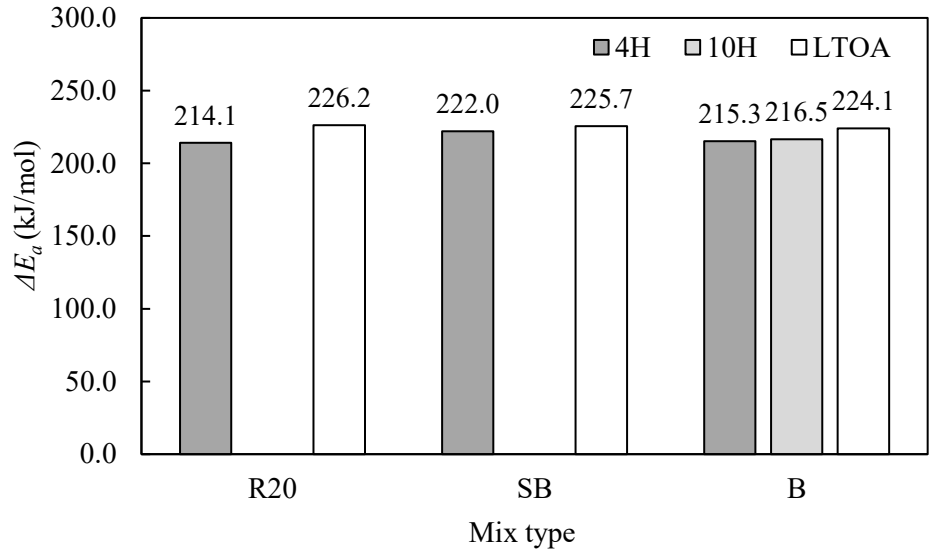

Figure 8.13 Activation energy (ΔE_a) from Arrhenius equation (2S2P1D model)

Overall, from the results displayed in this section, the influence of aging on asphalt mixes could be reflected via parameters obtained from master curve models and shift factor equations. The findings discovered on stiffness increment after aging did not align with the results of the dashpot viscosity in the 2S2P1D model and the thermal dependent indices in the WLF equation and Arrhenius equation. Nonetheless, the larger stiffness increment observed in the R50-B mix is beneficial to the rutting resistance and potentially the fatigue resistance. Although the rejuvenated high RAP mixes experienced a more increase in dashpot viscosity, they were still less sensitive to thermal changes.

8.5 Conclusions

This paper is initiated to characterize the rheological behavior of asphalt mixes with high RAP content (i.e., 50%) and the addition of a soft binder or a rejuvenator. The soft binder is two grades lower than the commonly used virgin binder (PG 58-28) in southern Ontario, while the rejuvenator is blended with the base binder (PG 58-28) via an optimized dosage determined from the binder testing results. To fulfill this purpose, the dynamic modulus test was conducted on the rejuvenated high RAP mix specimens along with a control mix with an allowable RAP content of 20%. Two master curve models namely the generalized sigmoidal model and 2S2P1D and different shifting methods were used to construct the dynamic modulus master curve and the phase angle master curve. In addition, the LTOA protocol on loose mixes was

implemented to examine the effect of long-term aging on the mix behaviors. Based on the findings in this paper, the following conclusion can be made:

- The measured dynamic modulus and phase angle values were less repeatable in higher temperatures and lower loading frequencies. Since the mixes became softer at a high temperature (or low loading frequency), the behavior of asphalt mixes is more dependent on the gradation as well. It reflected the potential issue of the inhomogeneity of the mix gradation.
- The rejuvenated high RAP mixes showed relatively similar dynamic modulus values before and after long-term aging when the test temperatures were -10℃ and 4℃. As the test temperature increased to 21℃ and 37℃, the short-term aged R20 mix exhibited slightly higher modulus than the rejuvenated high RAP mixes. Moreover, the comparison between LTOA and STOA mixes demonstrated that the effect of aging was more prominent at intermediate and high temperatures (medium and low frequencies). And R50-B mix was constantly larger than those of R20 and R50-SB after long-term aging when the test temperature was higher than 37℃, which is desirable for rutting resistance.
- The fitted sigmodal master curve seemed highly agreed with the curve fitted by the 2S2P1D model. Both models exhibited an obvious gap between the two curves before and after the long-term oven aging. While the gap only started to emerge when the frequency was lower than 10^4 Hz. The hump-shaped phase angle master curve was achieved for all the mixes, with similar maximum phase angle values (around 27°) shared within the mixes. The long-term aging resulted in the phase angle master curve shifting to a lower frequency range while keeping the identical shape.
- The model parameters derived from the generalized sigmoidal model and 2S2P1D model supported the previous findings in the dynamic modulus data and fitted master curves. The changes in some parameters showed a perceptible trend of the aging effect on the rheological properties of mixes.
- The effect of aging on asphalt mixes could be reflected via the area difference under the dynamic modulus curve, the dashpot viscosity, and thermal-dependent indices from the shift factor equations. The R50-B mix showed the most stiffness increase after long-term aging; however, preserved relatively better flexibility and temperature sensitivity compared to the other two mixes. In addition, the extended short-term conditioning (10 hours at 135℃) seemed only increased the overall stiffness of the rejuvenated high RAP mix, with insignificant influence observed on the mix rheology and temperature sensitivity.

Notwithstanding the relatively limited sample, this work offers valuable insights into on long-term performance of rejuvenated high RAP mixes by investigating the viscoelastic behavior concerning the time and temperature dependency. The applied model parameters were reasonably sensitive to the changes in mix components and oxidative aging. Further research in this field would be of great help in using plant mixes to improve the mixing homogeneity and increase the blending between rejuvenators (or soft binders) and aged binders. Also, the major contribution to the rheological changes in asphalt mixes is the oxidation of the asphalt binder at the molecular level, chemical characterization tools could be essential in quantifying the aging effect on rejuvenated binder blends in mixes and establishing correlations between chemical characteristics and rheological parameters derived from mix testing.

Chapter 9
Summary, conclusions, and recommendations

9.1 Overall summary

The present research aims to explore the use of commercial rejuvenators as a practical solution in producing recycled hot mix asphalt (HMA) with the maximum RAP content depending on the local asphalt plant capacity. This research started with an in-depth literature review study related to the research topic. Then online research was conducted to summarize a commercial rejuvenator product list from the asphalt industry market to select candidate materials to begin the experimental work. Finally, for lab testing, seven commercial rejuvenators, including one petroleum-based rejuvenator, six bio-based rejuvenators, and a soft virgin binder were selected, as well as RAP, aggregates, and base binder supplied by industry partners. The rejuvenating effects of the seven rejuvenators and the soft binder were first inspected using rheological testing and thermal testing methods. Different rheological parameters were obtained from the rejuvenated binder blends to compare with those of the target virgin binder (PG 58-28). Four bio-based rejuvenators were selected from the binder testing screening process due to their outperformed restoring ability in lowering the viscosity and stiffness and recovering the relaxation capacity of the aged asphalt binder. Hence, the selected rejuvenators were continued for dosage optimization using the blending chart and response surface modelling methods. The optimized dosages resulted in promising PG results of the binder blends with 43% RAP binder replacement which was associated with 50% RAP in asphalt mixtures.

Because the four rejuvenators demonstrated comparable and satisfying rejuvenating efficacy, preliminary mix testing was required to evaluate the performance of their corresponding high RAP mixes. The HWT and IDEAL-CT tests were used to investigate rutting, moisture, and cracking resistances using various testing conditions, mixing conditioning durations, data analysis methods, and performance indicators. The HWT test at higher test temperatures appeared to be promising for differentiating asphalt mixes with different rejuvenator types, rejuvenator contents, RAP fractions, and conditioning periods. While the aforementioned factors had less of an impact on the cracking performance of rejuvenated high RAP mixes. Ultimately, two rejuvenators (one bio-based rejuvenator and the soft binder) were chosen to continue the next task, which focused on the rheological properties of the rejuvenated high RAP mixes compared to the control mix with allowable RAP content. The non-destructive dynamic modulus test, which employs cyclic sinusoidal loading to monitor the strain responses of the mixes, was used to capture the linear viscoelastic behaviour of asphalt mixes. Meanwhile, the long-term performance of the rejuvenated high RAP mixes was

investigated using an accelerated lab long-term oven aging (LTOA) protocol. The use of analytical and analogical models, as well as the time-temperature supposition principle, for constructing the master curves, yielded valuable results in revealing the effect of rejuvenators and oxidative aging.

9.2 Conclusions

This study investigated the use of rejuvenators to optimize the performance of lab-mixed and lab-compacted (LMLC) asphalt mixes containing high RAP content. Several laboratory tests and analyzing tools were used during this research, which was described comprehensively in previous chapters. The following shows the general conclusions of this research.

- The ability in restoring continuous temperatures varies by rejuvenator types, dosages, and the selected criteria. Comparing the crossover temperature with the intermediate PG is critical to rule out the "fake" rejuvenation situation in which the rejuvenator only reduces the stiffness but failed to restore the viscoelastic property of the binder. And a more positive ΔT_c did not necessarily imply a better restoring effectiveness when looking at the continuous low PG. Most of the bio-based rejuvenators used in this study outperformed the petroleum-based product and the soft binder.
- The blending chart method is a reliable method for determining the optimum rejuvenator dosage at the binder testing phase because most of the rheological indices are expected to have a linear relationship with the rejuvenator dosage and RAP binder ratio, which have been confirmed by the results of a factorial DOE method.
- Some rheological indices, such as the low continuous temperature based on creep stiffness (PGL_S) and the intermediate continuous temperature (PGI), may only account for the required rejuvenator dosage solely based on its ability to reduce the binder stiffness, rather than restoring the binder flexibility. The rejuvenator dosage using optimized using the recommended criteria, PGL_m and T_{cross}, has the potential to ensure that the rejuvenated binder blends have adequate cacking resistance without compromising the resistance to permeant deformation at high temperatures.
- Increasing the RAP content to 50% significantly improved the rutting resistance of the asphalt mix and the moisture susceptibility was not adversely affected by the increased RAP content. Adding bio-based rejuvenators or replacing the virgin binder with a softer binder in high RAP mixes resulted in a prominent reduction in rutting and moisture resistance. However, the rejuvenated high RAP mixes showed better performance compared to the control mix at the higher test temperature.

- The confounding effects of loading and moisture could result in deceptive interpretations based on the HWT criteria. Rejuvenator D and F led to asphalt failing the rut depth (or the number of passes) criteria at the end of the test, but it turned out the high RAP mix with rejuvenator F exhibited close performance in terms of resisting plastic deformation compared with other mixes which met the failure criteria. Therefore, the major concern of R50-F mix is the adhesion loss between binders and aggregates after stripping occurred, which might be due to the slightly higher rejuvenator dosage (0.5% by the binder content). Potential solutions, such as adding anti-stripping agents or improving diffusion between rejuvenator and aged binder assisted by manufacturing processes.
- In contrast to the conventional HWT data analysis methods, the novel methods applied in this paper isolated the moisture-induced deformation from the total permanent deformation. The novel rutting resistance parameters determined from the normalized rut depth data showed less variation compared to other parameters that did consider the post-compaction stage in model fitting.
- Overall, the HWT results showed that the rutting resistance of rejuvenated high RAP mixes varied depending on the rejuvenator type and rejuvenator dosage. Reducing the rejuvenator content significantly improved the rutting resistance and moisture damage resistance. Although it delayed the emergence of stripping, the moisture-induced deformation was still the major concern that contributed to more than half of the rut depth failure as the test temperature increased.
- High RAP mixes were inferred to have a better cracking resistance with the addition of rejuvenators and soft virgin binders since the average values of cracking indices were higher than the control mix and the high RAP mix without rejuvenators. The statistical analysis, however, only demonstrated the mix with the soft binder (R50-SB) exhibited significantly greater indices compared to the R50 mix. All rejuvenated mixes shared the same grouping information as the control mix (R20) based on the pairwise comparison.
- The extended short-term aging showed a prominent impact on the cracking performance of the mixes with rejuvenators or soft virgin binders. High RAP mix with rejuvenator B exhibited the least decrease in cracking indices but only the asphalt mix prepared with soft binder showed a statistically significant reduction in cracking index values. It was consistent with the rutting parameter (e.g., creep slope and visco-plastic ratio) results that the R50-SB mix experienced the most significant hardening after extending the conditioning time from 4 hours to 10 hours. In general, the HWT results were more affected by the extended conditioning time and the mix

composition, such as RAP content, virgin binder grade, and addition of rejuvenators, compared to the IDEAL-CT results, which enabled the HWT test a good candidate for discriminating the rejuvenated high RAP mixes.

- The effect of aging was more prominent at intermediate and high temperatures (medium and low frequencies) via the comparison between the measured dynamic modulus of LTOA and STOA mixes. The R50-B mix showed higher stiffness than those of R20 and R50-SB after long-term aging when the test temperature was higher than 37°C, which is desirable for rutting resistance. However, it might be assumed that this mix was more prone to oxidative aging.
- The long-term aging impact was able to be witnessed in the dynamic modulus and phase angle master curves. Hence, the model parameters derived from the generalized sigmoidal model and 2S2P1D model could be used as indicators for evaluating the aging resistance of the asphalt mixes, such as the area difference under the dynamic modulus curve, the dashpot viscosity, and thermal-dependent indices from the shift factor equations. The changes in some parameters showed a perceptible trend of the aging effect on the rheological properties of mixes. The high RAP asphalt mixes with the addition of a rejuvenator (R50-B) showed the most stiffness increase after long-term aging; however, preserved relatively better flexibility and temperature sensitivity compared to the other mixes.
- Despite the long-term aging protocol, the extended short-term condition (10 hours at 135°C) revealed meaningful discoveries in the rejuvenated high RAP mixes, with the noticeable increase of stiffness observed based on dynamic modulus test results and HWT test results. Also, this approach showed insignificant influence on the cracking tolerance, mix rheology, and temperature sensitivity. This could be attributed to the continued mobilization of the RAP binder and diffusion between the RAP binder and the virgin binder or the rejuvenated binder blend, which increases the overall stiffness of the effective binder film. However, the possible oxidative aging of asphalt binders and rejuvenators will need further investigation.

9.3 Recommendations and future research directions

Based on the conclusions from the previous section, we should be able to answer the questions listed in Chapter 1 (Section 1.2) and the following recommendations can be summarized for future studies:

- Do all rejuvenators improve the performance of the asphalt binder or mix?

The binder testing rejuvenators demonstrated conclusively that commercial rejuvenators must be screened before being used in actual productions with local paving materials. Because of their better rejuvenating efficiencies, bio-based rejuvenators are preferred over petroleum-based rejuvenators. It is important to validate other parameters, such as the crossover temperature, rather than relying solely on the PG results. It is also critical to select the appropriate optimization criteria for determining rejuvenator dosages. This study recommended two rheological parameters, T_{cross} and PGL_m, which are interchangeable because they resulted in similar dosages of four bio-based rejuvenators It is worth noting, however, that rejuvenator dosage optimization at the binder testing stage assumes a full blending scenario, which rarely occurs in the actual plant production of high RAP mixes. Therefore, it is crucial and recommended to verify the optimum rejuvenator dosage using mix performance testing.

- Does the selected rejuvenator (with optimized dosage) lead to any insufficient rutting, moisture, or cracking resistance compared to the traditional asphalt mixes?

  Based on the preliminary mix testing results, the high RAP asphalt mixes with optimized rejuvenator contents did perform distinctively despite that their associated rejuvenated binder blends possessed similar rheological properties. The HWT test is useful to screen out the rejuvenated mixes which failed the criteria recommended by the Ontario specifications. However, it is also helpful to use novel HWT parameters to separate the visco-plastic deformation and the moisture-induced damages to better understand the mix performance during the submerged HWT test. This study also suggests that testing the mixes at a higher water bath temperature allows us to better distinguish the asphalt mixes, especially when they have similarly graded binders. Nevertheless, some rejuvenated high RAP mixes achieved a better rutting resistance and similar cracking resistance to the control asphalt mix. It is recommended to use the HWT test as a primary performance test for mix design and optimization purposes and use the cracking test as a supplementary test for quality control or assurance due to its simplicity and practicability. In addition, the extended conditioning period is promising to attain better mix performance whereas the possible oxidative aging is a potential concern.

- Will the selected rejuvenator retain its efficiency after the long-term lab aging protocol?

  According to the results of the dynamic modulus tests, the proposed LTOA protocol had a significant impact on the mix stiffness and flexibility. Although the rejuvenated high RAP mix had

a higher stiffness than the control mix, it was more flexible and had less thermal dependency. Therefore, the addition of a rejuvenator appears to have the potential to maintain its effectiveness when compared to the control mix used in this study, which was previously used in pavement construction. In addition, some parameters derived from master curve models and shit factor equations can be used to evaluate the long-term performance of asphalt mixes.

The findings of this study would provide a fruitful ground for future research. However, the scope of this study was limited by the use of LMLC mixes rather than plant trial mixes. The variation in the test results also suggested that the samples were not homogeneous. Furthermore, additional uncontrolled factors, such as the actual degree of blending (DOB) in the LMLC mixes and the quantification of the aging effect at the micro-scale level, were not thoroughly investigated in this study. More research in this area would be beneficial in determining the DOB levels in the rejuvenated high RAP mixes. The precise mechanisms that were assumed but not limited to RAP binder activation, binder-rejuvenator diffusion, and oxidative aging during the extended conditioning period remain unknown. Last but not least, it will be of great benefit in conducting the life-cycle cost analysis (LCCA) of the use of rejuvenators in high RAP mixes to address the economic benefits and environmental impacts of reusing higher RAP content against the cost of rejuvenators, the possible effort for upgrading the current plant mixing facilities, the sustainability of bio-based oils, and the re-recycling of rejuvenated asphalt.

References

[1] M. Zaumanis, R.B. Mallick, R. Frank, 100% recycled hot mix asphalt: A review and analysis, Resour. Conserv. Recycl. 92 (2014) 230–245. https://doi.org/10.1016/J.RESCONREC.2014.07.007.

[2] T. Baghaee Moghaddam, H. Baaj, The use of rejuvenating agents in production of recycled hot mix asphalt: A systematic review, Constr. Build. Mater. 114 (2016) 805–816. https://doi.org/10.1016/J.CONBUILDMAT.2016.04.015.

[3] D.C. Ambaiowei, X. Sanchez, S. Tighe, V. Aurilio, Rutting Behaviour of Typical Ontario RAP-HMA Mixtures (Poster), in: Transp. 2014 Past, Present. Futur. Conf. Exhib. Transp. Assoc. Canada//Transport 2014 Du Passé Vers l'avenir-2014 Congrès Expo. de'Association Des Transp. Du Canada, 2014.

[4] D.C. Ambaiowei, X. Sanchez, S.L. Tighe, S. Tabib, Rutting Characterization of Typical Ontario Rubberized-RAP Hot Mix Asphalt Mixtures, in: Proc. Fifty-Ninth Annu. Conf. Can. Tech. Asph. Assoc. Winnipeg, Manitoba, 2014.

[5] X. Sanchez, D.C. Ambaiowei, S.L. Tighe, Low Temperature Performance of Superpave Recycled Hot Mixtures in Ontario, in: Airf. Highw. Pavements 2015, 2015: pp. 143–154.

[6] S. Varamini, D. Ambaiowei, X. Sanchez, S.L. Tighe, Evaluation of Asphalt Binder Characteristics of Typical Ontario Superpave CRM and RAP-HMA Mixtures, in: Transp. 2014 Past, Present. Futur. Conf. Exhib. Transp. Assoc. Canada//Transport 2014 Du Passé Vers l'avenir-2014 Congrès Expo. de'Association Des Transp. Du Canada, 2014.

[7] H. Kadhim, Improving Durability of Asphalt Mixes Produced With Reclaimed Asphalt Pavement (Rap) by Enhancing Binder Blending, University of Waterloo, 2019.

[8] A. Copeland, Reclaimed Asphalt Pavement in Asphalt Mixtures: State of the Practice, McLean, VA: Turner-Fairbank Highway Research Center, Federal Highway Administration, Report Number FHWA-HRT-11-021, 2011.

[9] B.A. Williams, J.R. Willis, J. Shacat, T.C. Ross, Asphalt Pavement Industry Survey on Recycled Materials and Warm-Mix Asphalt Usage: 2020, 2021. https://www.asphaltpavement.org/uploads/documents/IS138/IS138-2018_RAP-RAS-

WMA_Survey_Final.pdf.

[10] Ministry of Transportation Ontario, Material Specification for Hot Mix Asphalt (OPSS.MUNI 1150), (2018) 1–20.

[11] R. McDaniel, R. Michael Anderson, Recommended Use of Reclaimed Asphalt Pavement in the Superpave Mix Design Method: Technician's Manual, Washington D.C.: Transportation Research Board National Research Council, 2001.

[12] R. West, J.R. Willis, M. Marasteanu, Improved Mix Design, Evaluation, and Materials Management Practices for Hot Mix Asphalt with High Reclaimed Asphalt Pavement Content, Washington D.C.: Transportation Research Board, NCHRP Report 752, 2013. https://doi.org/10.17226/22554.

[13] Ontario Asphalt Pavement Council, The ABCs of RAP, Ontario, Canada, 2017.

[14] Ontario Asphalt Pavement Council, The ABCs of PGAC, Ontario, Canada, 1999.

[15] W. Rogers, Influence Of Warm Mix Additives Upon High RAP Asphalt Mixes, Clemson University, 2011.

[16] B. Yu, X. Gu, M. Wu, F. Ni, Application of a high percentage of reclaimed asphalt pavement in an asphalt mixture: blending process and performance investigation, Road Mater. Pavement Des. 18 (2017) 753–765. https://doi.org/10.1080/14680629.2016.1182941.

[17] A. Behnood, Application of rejuvenators to improve the rheological and mechanical properties of asphalt binders and mixtures: A review, J. Clean. Prod. 231 (2019) 171–182. https://doi.org/10.1016/j.jclepro.2019.05.209.

[18] D. Lesueur, The colloidal structure of bitumen: Consequences on the rheology and on the mechanisms of bitumen modification, Adv. Colloid Interface Sci. 145 (2009) 42–82. https://doi.org/10.1016/j.cis.2008.08.011.

[19] A. Behnood, M. Modiri Gharehveran, Morphology, rheology, and physical properties of polymer-modified asphalt binders, Eur. Polym. J. 112 (2019) 766–791. https://doi.org/10.1016/j.eurpolymj.2018.10.049.

[20] Z.H. Al-Saffar, H. Yaacob, M.K.I.M. Satar, M.K. Saleem, J.C. Lai, R. Putra Jaya, A review on rejuvenating materials used with reclaimed hot mix asphalt, Can. J. Civ. Eng. 48 (2021) 233–

249. https://doi.org/10.1139/cjce-2019-0635.

[21] S. Weigel, D. Stephan, Relationships between the chemistry and the physical properties of bitumen, Road Mater. Pavement Des. 19 (2018) 1636–1650. https://doi.org/10.1080/14680629.2017.1338189.

[22] Y. Azimi Alamdary, S. Singh, H. Baaj, Laboratory simulation of the impact of solar radiation and moisture on long-term age conditioning of asphalt mixes, Road Mater. Pavement Des. 20 (2019) S521–S532. https://doi.org/10.1080/14680629.2019.1587496.

[23] F. Kaseer, A. Epps, E. Arámbula-mercado, Use of recycling agents in asphalt mixtures with high recycled materials contents in the United States: A literature review, Constr. Build. Mater. 211 (2019) 974–987. https://doi.org/10.1016/j.conbuildmat.2019.03.286.

[24] A. Ongel, M. Hugener, Impact of rejuvenators on aging properties of bitumen, Constr. Build. Mater. 94 (2015) 467–474. https://doi.org/10.1016/j.conbuildmat.2015.07.030.

[25] M. Chen, B. Leng, S. Wu, Y. Sang, Physical, chemical and rheological properties of waste edible vegetable oil rejuvenated asphalt binders, Constr. Build. Mater. 66 (2014) 286–298. https://doi.org/10.1016/j.conbuildmat.2014.05.033.

[26] M.C. Cavalli, M. Zaumanis, Microstructural Investigation of Reclaimed Asphalt Binder with Bio-Based Rejuvenators, RILEM Bookseries. 2 (2019) 39–43. https://doi.org/10.1007/978-3-030-00476-7.

[27] X. Yu, M. Zaumanis, L.D. Poulikakos, Rheological, microscopic, and chemical characterization of the rejuvenating effect on asphalt binders, Fuel. 135 (2014) 162–171. https://doi.org/10.1016/j.fuel.2014.06.038.

[28] I. Menapace, L. Garcia, F. Kaseer, E. Arámbula-mercado, A. Epps, E. Masad, G. King, Effect of recycling agents in recycled asphalt binders observed with microstructural and rheological tests, Constr. Build. Mater. 158 (2018) 61–74. https://doi.org/10.1016/j.conbuildmat.2017.10.017.

[29] M. Zaumanis, R.B. Mallick, Review of very high-content reclaimed asphalt use in plant-produced pavements: state of the art, Int. J. Pavement Eng. 16 (2015) 39–55. https://doi.org/10.1080/10298436.2014.893331.

[30] A.I. Rajib, A. Samieadel, A. Zalghout, K.E. Kaloush, B.K. Sharma, E.H. Fini, Do all rejuvenators improve asphalt performance?, Road Mater. Pavement Des. 0 (2020) 1–19. https://doi.org/10.1080/14680629.2020.1826348.

[31] R.B. Ahmed, K. Hossain, Waste cooking oil as an asphalt rejuvenator: A state-of-the-art review, Constr. Build. Mater. 230 (2020) 116985. https://doi.org/10.1016/j.conbuildmat.2019.116985.

[32] Z. Cao, M. Chen, Z. Liu, B. He, J. Yu, L. Xue, Effect of different rejuvenators on the rheological properties of aged SBS modified bitumen in long term aging, Constr. Build. Mater. 215 (2019) 709–717. https://doi.org/10.1016/j.conbuildmat.2019.04.257.

[33] H.A. Tabatabaee, T.L. Kurth, Analytical investigation of the impact of a novel bio-based recycling agent on the colloidal stability of aged bitumen, Road Mater. Pavement Des. 18 (2017) 131–140. https://doi.org/10.1080/14680629.2017.1304257.

[34] J.R.W. Samuel H. Carpenter, Modifier influence in the characterization of hot-mix recycled material, Transp. Res. Rec. (1980) 15–22.

[35] M. Zaumanis, R.B. Mallick, Finite element modeling of rejuvenator diffusion in RAP binder film–simulation of plant mixing process, in: N. Kringos, B. Birgisson, D. Frost, L. Wang (Eds.), Multi-Scale Model. Charact. Infrastruct. Mater., Springer Netherlands, Dordrecht, 2013: pp. 407–419.

[36] G. Xu, H. Wang, W. Sun, Molecular dynamics study of rejuvenator effect on RAP binder: Diffusion behavior and molecular structure, Constr. Build. Mater. 158 (2018) 1046–1054. https://doi.org/10.1016/j.conbuildmat.2017.09.192.

[37] R. Karlsson, U. Isacsson, J. Ekblad, Rheological characterisation of bitumen diffusion, J. Mater. Sci. 42 (2007) 101–108. https://doi.org/10.1007/s10853-006-1047-y.

[38] P. Kriz, D.L. Grant, B.A. Veloza, M.J. Gale, A.G. Blahey, J.H. Brownie, R.D. Shirts, S. Maccarrone, P. Kriz, D.L. Grant, B.A. Veloza, M.J. Gale, A.G. Blahey, J.H. Brownie, R.D. Shirts, S.M. Blending, Blending and diffusion of reclaimed asphalt pavement and virgin asphalt binders, Road Mater. Pavement Des. 15 (2014) 78–112. https://doi.org/10.1080/14680629.2014.927411.

[39] J. Wu, Q. Liu, Y. Wang, J. Chen, D. Wang, L. Xie, C. Ago, Effect of mixing time and temperature on the homogeneity of asphalt mixtures containing reclaimed asphalt pavement

material, Transp. Res. Rec. 2672 (2018) 167–177. https://doi.org/10.1177/0361198118796967.

[40] D. Lo Presti, K. Vasconcelos, M. Orešković, G.M. Pires, S. Bressi, On the degree of binder activity of reclaimed asphalt and degree of blending with recycling agents, Road Mater. Pavement Des. 21 (2020) 2071–2090. https://doi.org/10.1080/14680629.2019.1607537.

[41] M. Orešković, G. Menegusso Pires, S. Bressi, K. Vasconcelos, D. Lo Presti, Quantitative assessment of the parameters linked to the blending between reclaimed asphalt binder and recycling agent: A literature review, Constr. Build. Mater. 234 (2020). https://doi.org/10.1016/j.conbuildmat.2019.117323.

[42] G. Menegusso Pires, D. Lo Presti, G.D. Airey, A practical approach to estimate the degree of binder activity of reclaimed asphalt materials, Road Mater. Pavement Des. 22 (2021) 1093–1116. https://doi.org/10.1080/14680629.2019.1663244.

[43] B. Huang, G. Li, D. Vukosavljevic, X. Shu, B.K. Egan, Laboratory investigation of mixing hot-mix asphalt with reclaimed asphalt pavement, Transp. Res. Rec. (2005) 37–45. https://doi.org/10.3141/1929-05.

[44] S. Zhao, B. Huang, X. Shu, Investigation on binder homogeneity of RAP/RAS mixtures through staged extraction, Constr. Build. Mater. 82 (2015) 184–191. https://doi.org/10.1016/j.conbuildmat.2015.02.013.

[45] S. Yu, S. Shen, X. Zhou, X. Li, Effect of partial blending on high content reclaimed asphalt pavement (RAP) mix design and mixture properties, Transp. Res. Rec. 2672 (2018) 79–87. https://doi.org/10.1177/0361198118780703.

[46] D.M. Abd, H. Al-Khalid, R. Akhtar, Novel Methodology to Investigate and Obtain a Complete Blend between RAP and Virgin Materials, J. Mater. Civ. Eng. 30 (2018) 04018060. https://doi.org/10.1061/(asce)mt.1943-5533.0002230.

[47] S. Yu, S. Shen, C. Zhang, W. Zhang, X. Jia, Evaluation of the Blending Effectiveness of Reclaimed Asphalt Pavement Binder, J. Mater. Civ. Eng. 29 (2017) 04017230. https://doi.org/10.1061/(asce)mt.1943-5533.0002095.

[48] F. Kaseer, E. Arámbula-Mercado, A.E. Martin, A Method to Quantify Reclaimed Asphalt Pavement Binder Availability (Effective RAP Binder) in Recycled Asphalt Mixes, Transp. Res. Rec. 2673 (2019) 205–216. https://doi.org/10.1177/0361198118821366.

[49] S. Zhao, B. Huang, X. Shu, M.E. Woods, Quantitative characterization of binder blending: how much recycled binder is mobilized during mixing?, Transp. Res. Rec. 2506 (2015) 72–80. https://doi.org/10.3141/2506-08.

[50] A. Abed, N. Thom, D. Lo Presti, Design considerations of high RAP-content asphalt produced at reduced temperatures, Mater. Struct. Constr. 51 (2018) 1–16. https://doi.org/10.1617/s11527-018-1220-1.

[51] S. Zhao, B. Bowers, B. Huang, X. Shu, Characterizing Rheological Properties of Binder and Blending Efficiency of Asphalt Paving Mixtures Containing RAS through GPC, J. Mater. Civ. Eng. 26 (2014) 941–946. https://doi.org/10.1061/(asce)mt.1943-5533.0000896.

[52] B.F. Bowers, B. Huang, X. Shu, B.C. Miller, Investigation of Reclaimed Asphalt Pavement blending efficiency through GPC and FTIR, Constr. Build. Mater. 50 (2014) 517–523. https://doi.org/10.1016/j.conbuildmat.2013.10.003.

[53] B.F. Bowers, J. Moore, B. Huang, X. Shu, Blending efficiency of reclaimed asphalt pavement: An approach utilizing rheological properties and molecular weight distributions, Fuel. 135 (2014) 63–68. https://doi.org/10.1016/j.fuel.2014.05.059.

[54] S. Zhao, B. Huang, X. Shu, M.E. Woods, Quantitative evaluation of blending and diffusion in high RAP and RAS mixtures, Mater. Des. 89 (2016) 1161–1170. https://doi.org/10.1016/j.matdes.2015.10.086.

[55] W.S. Mogawer, E.H. Fini, A.J. Austerman, A. Booshehrian, B. Zada, Performance characteristics of high reclaimed asphalt pavement containing bio-modifier, Road Mater. Pavement Des. 17 (2016) 753–767. https://doi.org/10.1080/14680629.2015.1096820.

[56] W.S. Mogawer, A. Booshehrian, S. Vahidi, A.J. Austerman, Evaluating the effect of rejuvenators on the degree of blending and performance of high RAP, RAS, and RAP/RAS mixtures, Road Mater. Pavement Des. 14 (2013) 193–213. https://doi.org/10.1080/14680629.2013.812836.

[57] D.W. Christensen Jr, T. Pellinen, R.F. Bonaquist, Hirsch model for estimating the modulus of asphalt concrete, J. Assoc. Asph. Paving Technol. 72 (2003) 97–121.

[58] S.N. Nahar, M. Mohajeri, A.J.M. Schmets, A. Scarpas, M.F.C. Van De Ven, G. Schitter, First Observation of Blending-Zone Morphology at Interface of Reclaimed Asphalt Binder and

Virgin Bitumen, Transp. Res. Rec. 2370 (2013) 1–9. https://doi.org/10.3141/2370-01.

[59] M. Zaumanis, R. Mallick, R. Frank, Evaluation of rejuvenator's effectiveness with conventional mix testing for 100% reclaimed Asphalt pavement mixtures, Transp. Res. Rec. (2013) 17–25. https://doi.org/10.3141/2370-03.

[60] M. Zaumanis, R.B. Mallick, L. Poulikakos, R. Frank, Influence of six rejuvenators on the performance properties of Reclaimed Asphalt Pavement (RAP) binder and 100% recycled asphalt mixtures, Constr. Build. Mater. 71 (2014) 538–550. https://doi.org/10.1016/j.conbuildmat.2014.08.073.

[61] W.S. Mogawer, A. Austerman, R. Roque, Ageing and rejuvenators: evaluating their impact on high RAP mixtures fatigue cracking characteristics using advanced mechanistic models and testing methods, Road Mater. Pavement Des. 16 (2015) 1–28. https://doi.org/10.1080/14680629.2015.1076996.

[62] M. Baqersad, H. Ali, Rheological and chemical characteristics of asphalt binders recycled using different recycling agents, Constr. Build. Mater. 228 (2019) 116738. https://doi.org/10.1016/j.conbuildmat.2019.116738.

[63] S. Matolia, G. Guduru, B. Gottumukkala, K.K. Kuna, An investigation into the influence of aging and rejuvenation on surface free energy components and chemical composition of bitumen, Constr. Build. Mater. 245 (2020) 118378. https://doi.org/10.1016/j.conbuildmat.2020.118378.

[64] M. Chen, F. Xiao, B. Putman, B. Leng, S. Wu, High temperature properties of rejuvenating recovered binder with rejuvenator, waste cooking and cotton seed oils, Constr. Build. Mater. 59 (2014) 10–16. https://doi.org/10.1016/j.conbuildmat.2014.02.032.

[65] M.C. Cavalli, M. Zaumanis, E. Mazza, M.N. Partl, L.D. Poulikakos, Aging effect on rheology and cracking behaviour of reclaimed binder with bio-based rejuvenators, J. Clean. Prod. 189 (2018) 88–97. https://doi.org/10.1016/j.jclepro.2018.03.305.

[66] M. Elkashef, J. Podolsky, R.C. Williams, W. Eric, E.W. Cochran, Introducing a soybean oil-derived material as a potential rejuvenator of asphalt through rheology , mix characterisation and Fourier Transform Infrared analysis, Road Mater. Pavement Des. 0629 (2018) 1750–1770. https://doi.org/10.1080/14680629.2017.1345781.

[67] Z. Xie, H. Rizvi, C. Purdy, A. Ali, Y. Mehta, Effect of rejuvenator types and mixing procedures on volumetric properties of asphalt mixtures with 50% RAP, Constr. Build. Mater. 218 (2019) 457–464. https://doi.org/10.1016/j.conbuildmat.2019.05.093.

[68] A. Foroutan, S. Amid, I. Hoff, S. Dessouky, C. Ho, Performance evaluation of asphalt mixtures containing high-RAP binder content and bio-oil rejuvenator, Constr. Build. Mater. 227 (2019) 116465. https://doi.org/10.1016/j.conbuildmat.2019.07.191.

[69] M. Zeng, J. Li, W. Zhu, Y. Xia, Laboratory evaluation on residue in castor oil production as rejuvenator for aged paving asphalt binder, Constr. Build. Mater. 193 (2018) 276–285. https://doi.org/10.1016/j.conbuildmat.2018.10.204.

[70] P. Nayak, U.C. Sahoo, A rheological study on aged binder rejuvenated with Pongamia oil and Composite castor oil, Int. J. Pavement Eng. 18 (2017) 595–607. https://doi.org/10.1080/10298436.2015.1103851.

[71] S.K. Pradhan, U.C. Sahoo, Effectiveness of Polanga Oil as Rejuvenator for Asphalt with High RAP Content, in: Airf. Highw. Pavements 2019, 2019: pp. 115–126.

[72] M. Zaumanis, R.B. Mallick, R. Frank, Evaluation of different recycling agents for restoring aged asphalt binder and performance of 100% recycled asphalt, Mater. Struct. 48 (2015) 2475–2488. https://doi.org/10.1617/s11527-014-0332-5.

[73] P. Apostolidis, X. Liu, C. Kasbergen, A.T. Scarpas, Synthesis of asphalt binder aging and the state of the art of antiaging technologies, Transp. Res. Rec. 2633 (2017) 147–153. https://doi.org/10.3141/2633-17.

[74] A. Bajaj, A. Epps Martin, G. King, C. Glover, F. Kaseer, E. Arámbula-Mercado, Evaluation and classification of recycling agents for asphalt binders, Constr. Build. Mater. 260 (2020) 119864. https://doi.org/10.1016/j.conbuildmat.2020.119864.

[75] Standard Classification for Hot-Mix Recycling Agents, ASTM D4552/D4552M−20, West Conshohocken, PA: ASTM International, 2020. https://doi.org/10.1520/D4552.

[76] NCAT, NCAT Researchers Explore Multiple Uses of Rejuvenators, Asph. Technol. News. 26 (2014) 7–16. http://www.ncat.us/info-pubs/newsletters/spring-2014/rejuvenators.html.

[77] J.E. Sias, E. V. Dave, R. Zhang, Use of Recycling Agents in Asphalt Concrete Mixtures,

Washington, DC: The National Academies Press, 2022. https://doi.org/10.17226/26601.

[78] L. De Bock, N. Piérard, S. Vansteenkiste, A. Vanelstraete, Categorisation and analysis of rejuvenators for asphalt recycling, 2020.

[79] M. Elkashef, M.D. Elwardany, Y. Liang, D. Jones, J. Harvey, N.D. Bolton, J.P. Planche, Effect of Using Rejuvenators on the Chemical, Thermal, and Rheological Properties of Asphalt Binders, Energy and Fuels. 34 (2020) 2152–2159. https://doi.org/10.1021/acs.energyfuels.9b03689.

[80] E. Arámbula-Mercado, F. Kaseer, A. Epps Martin, F. Yin, L. Garcia Cucalon, Evaluation of recycling agent dosage selection and incorporation methods for asphalt mixtures with high RAP and RAS contents, Constr. Build. Mater. 158 (2018) 432–442. https://doi.org/10.1016/j.conbuildmat.2017.10.024.

[81] S. Im, P. Karki, F. Zhou, Development of new mix design method for asphalt mixtures containing RAP and rejuvenators, Constr. Build. Mater. 115 (2016) 727–734. https://doi.org/10.1016/j.conbuildmat.2016.04.081.

[82] A.E. Martin, F. Kaseer, E. Arambula-Mercado, A. Bajaj, L.G. Cucalon, F. Yin, A. Chowdhury, J. Epps, C. Glover, E.Y. Hajj, N. Morian, J.S. Daniel, M. Oshone, R. Rahbar-Rastegar, C. Ogbo, G. King, Evaluating the Effects of Recycling Agents on Asphalt Mixtures with High RAS and RAP Binder Ratios, Transportation Research Board, Washington D.C.: Transportation Research Board National Research Council, 2020. https://doi.org/10.17226/25749.

[83] M. Mohammadafzali, H. Ali, G.A. Sholar, W.A. Rilko, M. Baqersad, Effects of Rejuvenation and Aging on Binder Homogeneity of Recycled Asphalt Mixtures, J. Transp. Eng. Part B Pavements. 145 (2019) 1–9. https://doi.org/10.1061/JPEODX.0000089.

[84] M. Zaumanis, R.B. Mallick, R. Frank, Determining optimum rejuvenator dose for asphalt recycling based on Superpave performance grade specifications, Constr. Build. Mater. 69 (2014) 159–166. https://doi.org/10.1016/j.conbuildmat.2014.07.035.

[85] M.D. Nazzal, W. Mogawer, A. Austerman, L. Abu, S. Kaya, Multi-scale evaluation of the effect of rejuvenators on the performance of high RAP content mixtures, Constr. Build. Mater. 101 (2015) 50–56. https://doi.org/10.1016/j.conbuildmat.2015.10.029.

[86] M. Elkashef, R.C. Williams, E. Cochran, Investigation of fatigue and thermal cracking behavior

of rejuvenated reclaimed asphalt pavement binders and mixtures, Int. J. Fatigue. 108 (2018) 90–95. https://doi.org/10.1016/j.ijfatigue.2017.11.013.

[87] M. Elkashef, R.C. Williams, Improving fatigue and low temperature performance of 100% RAP mixtures using a soybean-derived rejuvenator, Constr. Build. Mater. 151 (2017) 345–352. https://doi.org/10.1016/j.conbuildmat.2017.06.099.

[88] M.C. Cavalli, M. Zaumanis, E. Mazza, M.N. Partl, L.D. Poulikakos, Effect of ageing on the mechanical and chemical properties of binder from RAP treated with bio-based rejuvenators, Compos. Part B Eng. 141 (2018) 174–181. https://doi.org/10.1016/J.COMPOSITESB.2017.12.060.

[89] J. Zhang, H. Sun, H. Jiang, X. Xu, M. Liang, Y. Hou, Z. Yao, Experimental assessment of reclaimed bitumen and RAP asphalt mixtures incorporating a developed rejuvenator, Constr. Build. Mater. 215 (2019) 660–669. https://doi.org/10.1016/j.conbuildmat.2019.04.202.

[90] H. Jiang, J. Zhang, C. Sun, S. Liu, M. Liang, Z. Yao, Experimental assessment on engineering properties of aged bitumen incorporating a developed rejuvenator, Constr. Build. Mater. 179 (2018) 1–10. https://doi.org/10.1016/j.conbuildmat.2018.05.211.

[91] M.C. Cavalli, L.D. Poulikakos, Micromechanical Surface Investigation of Bio-modified RAP Binder, in: M. Pasetto, M.N. Partl, G. Tebaldi (Eds.), Proc. 5th Int. Symp. Asph. Pavements Environ., Springer International Publishing, Cham, 2020: pp. 14–22.

[92] P. Cong, H. Hao, Y. Zhang, W. Luo, D. Yao, Investigation of diffusion of rejuvenator in aged asphalt, Int. J. Pavement Res. Technol. 9 (2016) 280–288. https://doi.org/10.1016/j.ijprt.2016.08.001.

[93] F. Kaseer, E. Arámbula-Mercado, L.G. Cucalon, A.E. Martin, Performance of asphalt mixtures with high recycled materials content and recycling agents, Int. J. Pavement Eng. (2018) 1–15. https://doi.org/10.1080/10298436.2018.1511990.

[94] M. Rathore, M. Zaumanis, Impact of laboratory mixing procedure on the properties of reclaimed asphalt pavement mixtures, Constr. Build. Mater. 264 (2020) 120709. https://doi.org/10.1016/j.conbuildmat.2020.120709.

[95] M. Zaumanis, L. Boesiger, B. Kunz, M.C. Cavalli, L. Poulikakos, Determining optimum rejuvenator addition location in asphalt production plant, Constr. Build. Mater. 198 (2019) 368–

378. https://doi.org/10.1016/j.conbuildmat.2018.11.239.

[96] M. Zaumanis, M.C. Cavalli, L.D. Poulikakos, Effect of rejuvenator addition location in plant on mechanical and chemical properties of RAP binder, Int. J. Pavement Eng. 21 (2020) 507–515. https://doi.org/10.1080/10298436.2018.1492133.

[97] H. Shao, L. Sun, L. Liu, Z. You, X. Yang, A novel double-drum mixing technique for plant hot mix asphalt recycling with high reclaimed asphalt pavement content and rejuvenator, Constr. Build. Mater. 134 (2017) 236–244. https://doi.org/10.1016/j.conbuildmat.2016.12.077.

[98] Standard Specification for Performance-Graded Asphalt Binder, AASHTO M320-17, Washington D.C.: American Association of State Highway and Transportation Officials, 2017.

[99] Ministry of Transportation Ontario, Method of Test for Quantitative Extraction of Asphalt Cement and Analysis of Extracted Aggregate, LS-282 - Rev. No.33, 2017.

[100] Ministry of Transportation Ontario, Method of Test for Recovery of Asphalt From Solution By Rotary Evaporator, LS-284 - Rev. No.34, 2020.

[101] Standard Specification for Superpave Volumetric Mix Design, AASHTO M 323-17, Washington D.C.: American Association of State Highway and Transportation Officials, 2017.

[102] Ministry of Transportation Ontario, Design Procedure for Recycled Hot Mix Asphalt, LS-307 - Rev. No.33, 2019.

[103] Standard Test Method for Effect of Heat and Air on a Moving Film of Asphalt (Rolling Thin-Film Oven Test), ASTM D2872-12, West Conshohocken, PA: ASTM International, 2012. https://doi.org/10.1520/D2872.

[104] Standard Practice for Accelerated Aging of Asphalt Binder Using a Pressurized Aging Vessel (PAV), ASTM D6521-18, West Conshohocken, PA: ASTM International, 2016. https://doi.org/10.1520/D6521-18.1.5.

[105] Ministry of Transportation Ontario, Method of Test for Determining the Corssover Temperature of Asphalt Cement, LS-319 - Rev. No.33, 2019.

[106] Standard Method of Test for Hamburg Wheel-Track Testing of Compacted Asphalt Mixtures, AASHTO T324-17, Washington D.C.: American Association of State Highway and Transportation Officials, 2017.

[107] Standard Test Method for Determination of Cracking Tolerance Index of Asphalt Mixture Using the Indirect Tensile Cracking Test at, ASTM D8225-19, West Conshohocken, PA: ASTM International, 2019. https://doi.org/10.1520/D8225-19.Copyright.

[108] Standard Method of Test for Determining Dynamic Modulus of Hot Mix Asphalt (HMA), AASTHO T342-11, Washington D.C.: American Association of State Highway and Transportation Officials, 2015.

[109] P. Pirzadeh, H. Kadhim, D.L. Grant, J.D. Webb, H. Baaj, P. Kriz, Impact of hot mix asphalt plant silo storage conditions on blending and diffusion between virgin and RAP binders, Road Mater. Pavement Des. 22 (2021) 1231–1253. https://doi.org/10.1080/14680629.2019.1684346.

[110] Standard Method of Test for Determining the Rheological Properties of Asphalt Binder Using a Dynamic Shear Rheometer (DSR), AASHTO T315-19, Washington D.C.: American Association of State Highway and Transportation Officials, 2019.

[111] Standard Method of Test for Determining the Flexural Creep Stiffness of Asphalt Binder Using the Bending Beam Rheometer (BBR), AASHTO T313-19, Washington D.C.: American Association of State Highway and Transportation Officials, 2019.

[112] Standard Method of Test for Multiple Stress Creep Recovery (MSCR) Test of Asphalt Binder Using a Dynamic Shear Rheometer (DSR), AASHTO T 350-19, Washington D.C.: American Association of State Highway and Transportation Officials, 2019.

[113] M. Elkashef, D. Jones, L. Jiao, R.C. Williams, J. Harvey, Using Thermal Analytical Techniques to Study Rejuvenators and Rejuvenated Reclaimed Asphalt Pavement Binders, Energy and Fuels. 33 (2019) 2651–2658. https://doi.org/10.1021/acs.energyfuels.8b03427.

[114] N. Nciri, T. Shin, N. Kim, A. Caron, H. Ben Ismail, N. Cho, Towards the use of waste pig fat as a novel potential bio-based rejuvenator for recycled asphalt pavement, Materials (Basel). 13 (2020). https://doi.org/10.3390/ma13041002.

[115] P. Nayak, U.C. Sahoo, Rheological, chemical and thermal investigations on an aged binder rejuvenated with two non-edible oils, Road Mater. Pavement Des. 18 (2017) 612–629. https://doi.org/10.1080/14680629.2016.1182058.

[116] R.K. Veeraragavan, R.B. Mallick, M. Tao, M. Zaumanis, R. Frank, R.L. Bradbury, Laboratory comparison of rejuvenated 50% reclaimed asphalt pavement hot-mix asphalt with conventional

20% RAP mix, Transp. Res. Rec. 2633 (2017) 69–79. https://doi.org/10.3141/2633-09.

[117] W.S. Mogawer, A.J. Austerman, R. Kluttz, S. Puchalski, Using polymer modification and rejuvenators to improve the performance of high reclaimed asphalt pavement mixtures, Transp. Res. Rec. 2575 (2016) 10–18. https://doi.org/10.3141/2575-02.

[118] Standard Method of Test for Viscosity Determination of Asphalt Binder Using Rotational Viscometer, AASTHO T 316-13, Washington D.C.: American Association of State Highway and Transportation Officials, 2017.

[119] L. Garcia Cucalon, F. Kaseer, E. Arámbula-Mercado, A. Epps Martin, N. Morian, S. Pournoman, E. Hajj, The crossover temperature: significance and application towards engineering balanced recycled binder blends, Road Mater. Pavement Des. 20 (2019) 1391–1412. https://doi.org/10.1080/14680629.2018.1447504.

[120] F. Zhou, S. Im, D. Morton, R. Lee, S. Hu, T. Scullion, Rejuvenator characterization, blend characteristics, and proposed mix design method, J. Assoc. Asph. Paving Technol. 84 (2015) 675–704.

[121] Z. Zhou, X. Gu, J. Jiang, F. Ni, Y. Jiang, Nonrecoverable behavior of polymer modified and reclaimed asphalt pavement modified binder under different multiple stress creep recovery tests, Transp. Res. Rec. 2672 (2018) 324–336. https://doi.org/10.1177/0361198118782029.

[122] F. Kaseer, L.G. Cucalon, E. Arámbula-Mercado, A.E. Martin, J. Epps, Practical tools for optimizing recycled materials content and recycling agent dosage for improved short- and long-term performance of rejuvenated binder blends and mixtures, Asph. Paving Technol. Assoc. Asph. Paving Technol. Tech. Sess. 87 (2018) 513–555. https://doi.org/10.12783/aapt2018/33816.

[123] H. Kadhim, H. Baaj, Evaluating the performance of the asphalt mixes containing reclaimed asphalt pavement by considering the effect of silo storage time, J. Test. Eval. 48 (2020). https://doi.org/10.1520/JTE20180957.

[124] L.N. Mohammad, M. Elseifi, W. Cao, A. Raghavendra, M. Ye, Evaluation of the Hamburg Wheel-Tracking Test Device and AASHTO T 324 Specification for Rutting Testing of Asphalt Mixes, Asph. Paving Technol. Assoc. Asph. Paving Technol. Tech. Sess. 86 (2017) 165–185. https://doi.org/10.1080/14680629.2017.1389092.

[125] Q. Lv, W. Huang, H. Sadek, F. Xiao, C. Yan, Investigation of the rutting performance of various modified asphalt mixtures using the Hamburg Wheel-Tracking Device test and Multiple Stress Creep Recovery test, Constr. Build. Mater. 206 (2019) 62–70. https://doi.org/10.1016/j.conbuildmat.2019.02.015.

[126] R. West, C. Rodezno, F. Leiva, F. Yin, Development of a framework for balanced mix design, NCHRP Project 20-07/Task 406, National Center for Asphalt Technology at Auburn University, Auburn, AL, 2018.

[127] B.K. Bairgi, R.A. Tarefder, M.U. Ahmed, Long-term rutting and stripping characteristics of foamed warm-mix asphalt (WMA) through laboratory and field investigation, Constr. Build. Mater. 170 (2018) 790–800. https://doi.org/10.1016/j.conbuildmat.2018.03.055.

[128] R. Ghabchi, D. Singh, M. Zaman, Evaluation of moisture susceptibility of asphalt mixes containing RAP and different types of aggregates and asphalt binders using the surface free energy method, Constr. Build. Mater. 73 (2014) 479–489. https://doi.org/10.1016/j.conbuildmat.2014.09.042.

[129] S. Zhao, B. Huang, X. Shu, M. Woods, Comparative evaluation of warm mix asphalt containing high percentages of reclaimed asphalt pavement, Constr. Build. Mater. 44 (2013) 92–100. https://doi.org/10.1016/j.conbuildmat.2013.03.010.

[130] G. Guduru, C. Kumara, B. Gottumukkala, K.K. Kuna, Effectiveness of Different Categories of Rejuvenators in Recycled Asphalt Mixtures, J. Transp. Eng. Part B Pavements. 147 (2021) 04021006. https://doi.org/10.1061/jpeodx.0000255.

[131] J. Zhang, C.C. Guo, T. Chen, W. Zhang, K. Yao, C. Fan, M. Liang, C.C. Guo, Z. Yao, Evaluation on the mechanical performance of recycled asphalt mixtures incorporated with high percentage of RAP and self-developed rejuvenators, Constr. Build. Mater. 269 (2021) 121337. https://doi.org/10.1016/j.conbuildmat.2020.121337.

[132] Y. He, Z. Alavi, J. Harvey, D. Jones, Evaluating diffusion and aging mechanisms in blending of new and age-hardened binders during mixing and paving, Transp. Res. Rec. 2574 (2016) 64–73. https://doi.org/10.3141/2574-07.

[133] B.W. Tsai, E. Coleri, J.T. Harvey, C.L. Monismith, Evaluation of AASHTO T 324 Hamburg-Wheel Track Device test, Constr. Build. Mater. 114 (2016) 248–260.

https://doi.org/10.1016/j.conbuildmat.2016.03.171.

[134] F. Yin, C. Chen, R. West, A.E. Martin, E. Arambula-Mercado, Determining the Relationship Among Hamburg Wheel-Tracking Test Parameters and Correlation to Field Performance of Asphalt Pavements, Transp. Res. Rec. 2674 (2020) 281–291. https://doi.org/10.1177/0361198120912430.

[135] F. Yin, E. Arambula, R. Lytton, A.E. Martin, L.G. Cucalon, Novel method for moisture susceptibility and rutting evaluation using Hamburg wheel tracking test, Transp. Res. Rec. 2446 (2014) 1–7. https://doi.org/10.3141/2446-01.

[136] Q. Lv, H.U. Bahia, Separating effects of loading from moisture in wet Hamburg wheel-track test, J. Assoc. Asph. Paving Technol. 88 (2019) 751–781.

[137] P. Chaturabong, H.U. Bahia, The evaluation of relative effect of moisture in Hamburg wheel tracking test, Constr. Build. Mater. 153 (2017) 337–345. https://doi.org/10.1016/j.conbuildmat.2017.07.133.

[138] Iowa Department of Transportation, IM 319 Moisture Sensitivity Testing of Asphalt Mixtures, (2013). https://iowadot.gov/erl/current/im/content/319.htm.

[139] Standard Practice for Mixture Conditioning of Hot Mix Asphalt (HMA), AASTHO R30-02, Washington D.C.: American Association of State Highway and Transportation Officials, 2002.

[140] H. Wen, S. Wu, L.N. Mohammad, W. Zhang, S. Shen, A. Faheem, Long-term field rutting and moisture susceptibility performance of warm-mix asphalt pavement, Transp. Res. Rec. 2575 (2016) 103–112. https://doi.org/10.3141/2575-11.

[141] Y. Zhang, H.U. Bahia, Effects of recycling agents (RAs) on rutting resistance and moisture susceptibility of mixtures with high RAP/RAS content, Constr. Build. Mater. 270 (2021) 121369. https://doi.org/10.1016/j.conbuildmat.2020.121369.

[142] B.A. Williams, J.R. Willis, J. Shacat, Asphalt Pavement Industry Survey on Recycled Materials and Warm-Mix Asphalt Usage 2020, 2020.

[143] P. Cong, Y. Zhang, N. Liu, Investigation of the properties of asphalt mixtures incorporating reclaimed SBS modified asphalt pavement, Constr. Build. Mater. 113 (2016) 334–340. https://doi.org/10.1016/j.conbuildmat.2016.03.059.

[144] F. Zhou, S. Im, L. Sun, T. Scullion, Development of an IDEAL cracking test for asphalt mix design and QC/QA, Asph. Paving Technol. Assoc. Asph. Paving Technol. Tech. Sess. 86 (2017) 549–577. https://doi.org/10.1080/14680629.2017.1389082.

[145] T.S. F. Zhou, S. Im, L. Sun, Development of an IDEAL Cracking Test for Asphalt Mix Design, Quality Control and Quality Assurance, Road Mater. Pavement Des. 18 (2017) 405–427. https://doi.org/10.1080/14680629.2017.1389082.

[146] H. Chen, Y. Zhang, H.U. Bahia, The role of binders in mixture cracking resistance measured by ideal-CT test, Int. J. Fatigue. 142 (2021) 105947. https://doi.org/10.1016/j.ijfatigue.2020.105947.

[147] P. Saha Chowdhury, S.L.A. Noojilla, M.A. Reddy, Evaluation of fatigue characteristics of asphalt mixtures using Cracking Tolerance index (CTIndex), Constr. Build. Mater. 342 (2022) 128030. https://doi.org/10.1016/j.conbuildmat.2022.128030.

[148] R. West, F. Yin, C. Rodezno, A. Taylor, Balanced Mixture Design Implementation Support, (2021).

[149] W. Zhang, J. Tang, Z. Dong, T. Ma, M.A. Akber, X. Huang, J. Zhu, Y. Luan, Performance Characterization of Recycled-Asphalt Pavement with Stabilized Rubber–Modified Asphalt Using Balanced Mix Design Method, J. Mater. Civ. Eng. 32 (2020) 04020387. https://doi.org/10.1061/(asce)mt.1943-5533.0003486.

[150] C. Yan, Y. Zhang, H.U. Bahia, Comparison between SCB-IFIT, un-notched SCB-IFIT and IDEAL-CT for measuring cracking resistance of asphalt mixtures, Constr. Build. Mater. 252 (2020) 119060. https://doi.org/10.1016/j.conbuildmat.2020.119060.

[151] P. Tavassoti, A. Wakefield, X. Sanchez, S. Varamini, Performance Evaluation of In-situ and Laboratory Prepared Asphalt Materials: Practical Considerations for Sample Preparation and Testing Methodology, in: 2022 TAC Conf. Exhib., Edmonton, AB, 2022. https://www.who.int/news-room/fact-sheets/detail/autism-spectrum-disorders.

[152] A. Seitllari, I. Boz, J. Habbouche, S.D. Diefenderfer, Assessment of cracking performance indices of asphalt mixtures at intermediate temperatures, Int. J. Pavement Eng. 23 (2022) 70–79. https://doi.org/10.1080/10298436.2020.1730838.

[153] H. Kadhim, H. Baaj, Evaluation of the Impact of Silo Storage on Thermal Cracking of the Hot

Mix, in: TAC 2018 Innov. Technol. Evol. Transp. Conf. Exhib. Transp. Assoc. Canada., 2018.

[154] M. Elkashef, J. Harvey, D. Jones, L. Jiao, The impact of silo storage on the fatigue and cracking resistance of asphalt mixes, Constr. Build. Mater. 326 (2022) 126880. https://doi.org/10.1016/j.conbuildmat.2022.126880.

[155] Y. Ma, P. Polaczyk, R. Xiao, X. Jiang, M. Zhang, Y. Liu, B. Huang, Influence of mobilized RAP content on the effective binder quality and performance of 100% hot in-place recycled asphalt mixtures, Constr. Build. Mater. 342 (2022) 127941. https://doi.org/10.1016/j.conbuildmat.2022.127941.

[156] A.F. Espinoza-Luque, I.L. Al-Qadi, H. Ozer, Optimizing rejuvenator content in asphalt concrete to enhance its durability, Constr. Build. Mater. 179 (2018) 642–648. https://doi.org/10.1016/j.conbuildmat.2018.05.256.

[157] I.L. Al-Qadi, I.M. Said, U.M. Ali, J.R. Kaddo, Cracking prediction of asphalt concrete using fracture and strength tests, Int. J. Pavement Eng. 23 (2022) 3333–3345. https://doi.org/10.1080/10298436.2021.1892108.

[158] F. Kaseer, F. Yin, E. Arámbula-Mercado, A. Epps Martin, J.S. Daniel, S. Salari, Development of an index to evaluate the cracking potential of asphalt mixtures using the semi-circular bending test, Constr. Build. Mater. 167 (2018) 286–298. https://doi.org/10.1016/j.conbuildmat.2018.02.014.

[159] R. Nemati, K. Haslett, E. V. Dave, J.E. Sias, Development of a rate-dependent cumulative work and instantaneous power-based asphalt cracking performance index, Road Mater. Pavement Des. 20 (2019) S315–S331. https://doi.org/10.1080/14680629.2019.1586753.

[160] Iowa Department of Transportation, Section 2303. Flexible Pavement, (n.d.). https://www.iowadot.gov/erl/current/GS/content/2303.htm#Section230302E.

[161] B.P. Das, A.K. Siddagangaiah, Identification of parameter to assess cracking resistance of asphalt mixtures subjected to aging and moisture conditioning, J. Traffic Transp. Eng. (English Ed. 9 (2022) 293–304. https://doi.org/10.1016/j.jtte.2021.02.004.

[162] H. Chen, M. Sc, The role of binders in cracking resistance of mixtures measured with the IFIT procedure, in: 64th Annu. Meet. Can. Tech. Asph. Assoc., Montreal, Canada., 2019.

[163] R. Bin Ahmed, K. Hossain, R.M. Hajj, Chemical, Morphological, and Fundamental Properties of Rejuvenated Asphalt Binders, J. Mater. Civ. Eng. 33 (2021) 04020461. https://doi.org/10.1061/(asce)mt.1943-5533.0003564.

[164] E. Fini, A.I. Rajib, D. Oldham, A. Samieadel, S. Hosseinnezhad, Role of Chemical Composition of Recycling Agents in Their Interactions with Oxidized Asphaltene Molecules, J. Mater. Civ. Eng. 32 (2020) 04020268. https://doi.org/10.1061/(asce)mt.1943-5533.0003352.

[165] T.K. Pellinen, M.W. Witczak, R.F. Bonaquist, Asphalt Mix Master Curve Construction Using Sigmoidal Fitting Function with Non-Linear Least Squares Optimization, in: Recent Adv. Mater. Charact. Model. Pavement Syst., 2003: pp. 83–101. https://doi.org/10.1061/40709(257)6.

[166] A.J. del Barco Carrión, D. Lo Presti, S. Pouget, G. Airey, E. Chailleux, Linear viscoelastic properties of high reclaimed asphalt content mixes with biobinders, Road Mater. Pavement Des. 18 (2017) 241–251. https://doi.org/10.1080/14680629.2017.1304253.

[167] Y.A. Alamdary, Investigation of Different Factors Affecting Asphalt Cement Ageing and Durability, University of Waterloo, 2019.

[168] Y.A. Alamdary, H. Baaj, Time-temperature superposition of asphalt materials and temperature sensitivity of rheological parameters (TSRP), Can. J. Civ. Eng. 48 (2021) 1354–1363. https://doi.org/10.1139/cjce-2020-0490.

[169] T.B. Moghaddam, H. Baaj, Rheological characterization of high-modulus asphalt mix with modified asphalt binders, Constr. Build. Mater. 193 (2018) 142–152. https://doi.org/10.1016/j.conbuildmat.2018.10.194.

[170] S. Raschia, T.B. Moghaddam, D. Perraton, H. Baaj, A. Carter, A. Graziani, Effect of RAP Source on Compactability and Behavior of Cold-Recycled Mixtures in the Small Strain Domain, J. Mater. Civ. Eng. 33 (2021) 1–11. https://doi.org/10.1061/(asce)mt.1943-5533.0003614.

[171] Y.R. Kim, C. Castorena, M. Elwardany, F.Y. Rad, S. Underwood, A. Gundha, P. Gudipudi, M.J. Farrar, R.R. Glaser, Long-Term Aging of Asphalt Mixtures for Performance Testing and Prediction, Washington D.C.: Transportation Research Board, NCHRP Report 871, 2017. https://doi.org/10.17226/24959.

[172] H. Chen, D.M. Barbieri, X. Zhang, I. Hoff, Reliability of Calculation of Dynamic Modulus for

Asphalt Mixtures Using Different Master Curve Models and Shift Factor Equations, Materials (Basel). 15 (2022). https://doi.org/10.3390/ma15124325.

[173] M. Nobakht, M.S. Sakhaeifar, Dynamic modulus and phase angle prediction of laboratory aged asphalt mixtures, Constr. Build. Mater. 190 (2018) 740–751. https://doi.org/10.1016/j.conbuildmat.2018.09.160.

[174] G. Rowe, G. Baumgardner, M. Sharrock, Functional forms for master curve analysis of bituminous materials, Adv. Test. Charact. Bitum. Mater. (2009) 81–92. https://doi.org/10.1201/9780203092989.ch9.

[175] G. Tan, W. Wang, Y. Cheng, Y. Wang, Z. Zhu, Establishment of complex modulus master curves based on generalized sigmoidal model for freeze-thaw resistance evaluation of basalt fiber-modified asphalt mixtures, Polymers (Basel). 12 (2020). https://doi.org/10.3390/POLYM12081698.

[176] G.M. Rowe, M.J. Sharrock, Alternate shift factor relationship for describing temperature dependency of viscoelastic behavior of asphalt materials, Transp. Res. Rec. (2011) 125–135. https://doi.org/10.3141/2207-16.

[177] F. Olard, H. Di Benedetto, General “2S2P1D” Model and Relation Between the Linear Viscoelastic Behaviours of Bituminous Binders and Mixes, Road Mater. Pavement Des. 4 (2003) 185–224. https://doi.org/10.1080/14680629.2003.9689946.

[178] N. Tapsoba, C. Sauzéat, H. Di Benedetto, H. Baaj, M. Ech, Behaviour of asphalt mixtures containing reclaimed asphalt pavement and asphalt shingle, Road Mater. Pavement Des. 15 (2014) 330–347. https://doi.org/10.1080/14680629.2013.871091.

[179] N.I.M. Yusoff, D. Mounier, G. Marc-Stéphane, M. Rosli Hainin, G.D. Airey, H. Di Benedetto, Modelling the rheological properties of bituminous binders using the 2S2P1D Model, Constr. Build. Mater. 38 (2013) 395–406. https://doi.org/10.1016/j.conbuildmat.2012.08.038.

[180] N.I.M. Yusoff, E. Chailleux, G.D. Airey, A comparative study of the influence of shift factor equations on master curve construction, Int. J. Pavement Res. Technol. 4 (2011) 324–336. https://doi.org/10.6135/ijprt.org.tw/2011.4(6).324.

[181] H. Baaj, M. Ech, N. Tapsoba, C. Sauzeat, H. Di Benedetto, Thermomechanical characterization of asphalt mixtures modified with high contents of asphalt shingle modifier (ASM®) and

reclaimed asphalt pavement (RAP), Mater. Struct. Constr. 46 (2013) 1747–1763. https://doi.org/10.1617/s11527-013-0015-7.

[182] AASHTO Guide for Design of Pavement Structures, 1993.

[183] I.L. Al-Qadi, W. Xie, M.A. Elseifi, Frequency determination from vehicular loading time pulse to predict appropriate complex modulus in MEPDG, Asph. Paving Technol. Assoc. Asph. Paving Technol. Tech. Sess. 77 (2008) 739–771.

[184] I.L. Al-Qadi, M.A. Elseifi, P.J. Yoo, S.H. Dessouky, N. Gibson, T. Harman, J. D'Angelo, K. Petros, Accuracy of current complex modulus selection procedure from vehicular load pulse: NCHRP project 1-37a mechanistic-empirical pavement design guide, Transp. Res. Rec. (2008) 81–90. https://doi.org/10.3141/2087-09.

[185] S. Mangiafico, H. Di Benedetto, C. Sauzéat, F. Olard, S. Pouget, L. Planque, Effect of colloidal structure of bituminous binder blends on linear viscoelastic behaviour of mixtures containing Reclaimed Asphalt Pavement, Mater. Des. 111 (2016) 126–139. https://doi.org/10.1016/j.matdes.2016.07.124.

[186] X. Cai, J. Zhang, G. Xu, M. Gong, X. Chen, J. Yang, Internal aging indexes to characterize the aging behavior of two bio-rejuvenated asphalts, J. Clean. Prod. 220 (2019) 1231–1238. https://doi.org/10.1016/j.jclepro.2019.02.203.

[187] S. Tarbox, J. Daniel, Effects of long-term oven aging on reclaimed asphalt pavement mixtures, Transp. Res. Rec. (2012) 1–15. https://doi.org/10.3141/2294-01.

[188] C. Brondani, P. Menezes Vestena, C. Faccin, S. Lisboa Schuster, L. Pivoto Specht, D. da Silva Pereira, Moisture susceptibility of asphalt mixtures: 2S2P1D rheological model approach and new index based on dynamic modulus master curve changes, Constr. Build. Mater. 331 (2022) 17–21. https://doi.org/10.1016/j.conbuildmat.2022.127316.

[189] D. Singh, M. Zaman, S. Commuri, A laboratory investigation into the effect of long-term oven aging on RAP mixes using dynamic modulus test, Int. J. Pavement Res. Technol. 5 (2012) 142–152.

[190] E.D. Anderson, J.S. Daniel, Long-Term Performance of Pavement with High Recycled Asphalt Content Case Studies, Transp. Res. Rec. 2371 (2013) 1–12. https://doi.org/10.3141/2371-01.

Appendix A: Statistical analysis of binder testing results

RTFO mass loss (single factor ANOVA):

(1) Rejuvenator dosage:

Groups	Count	Sum	Average	Variance
5%	14	0.1086	0.0078	6.83E-06
10%	14	0.1310	0.0094	3.90E-06

Source of Variation	SS	df	MS	F	P-value	F crit
Between Groups	1.8E-05	1	1.8E-05	3.3473	0.0788	4.2252
Within Groups	0.00014	26	5.36E-06			
Total	0.00016	27				

(2) Rejuvenator type:

Groups	Count	Sum	Average	Variance
A	4	0.0474	0.0118	2.72E-07
B	4	0.0426	0.0106	1.31E-06
C	4	0.0376	0.0094	3.81E-06
D	4	0.0343	0.0086	4.58E-06
E	4	0.0244	0.0061	1.82E-06
F	4	0.0287	0.0072	8.68E-07
G	4	0.0249	0.0062	6.92E-07

Source of Variation	SS	df	MS	F	P-value	F crit
Between Groups	1.174E-04	6	1.96E-05	10.2566	2.43E-05	2.5727
Within Groups	4.005E-05	21	1.91E-06			
Total	0.00016	27				

Rotational viscosity at 135°C (single factor ANOVA):

(1) Rejuvenator dosage:

Groups	Count	Sum	Average	Variance
5%	14	5.605	0.4004	0.0023
10%	14	4.0947	0.2925	0.0032

Source of Variation	SS	df	MS	F	P-value	F crit
Between Groups	0.0815	1	0.0815	29.7004	1.03E-05	4.2252
Within Groups	0.0713	26	0.0027			
Total	0.1528	27				

(2) Rejuvenator type:

Groups	Count	Sum	Average	Variance
A	4	1.1333	0.2833	0.0036
B	4	1.2043	0.3011	0.0034
C	4	1.4547	0.3637	0.0026
D	4	1.2320	0.3080	0.0068
E	4	1.4983	0.3746	0.0047
F	4	1.4260	0.3565	0.0050
G	4	1.7510	0.4378	0.0022

Source of Variation	SS	df	MS	F	P-value	F crit
Between Groups	0.0682	6	0.0114	2.8204	0.0357	2.5727
Within Groups	0.0846	21	0.0040			
Total	0.1528	27				

Rotational viscosity at 135°C (two factor ANOVA with replication):

Source	SS	df	MS	F	P-value	F crit
Rej type	0.0682	6	0.0114	386.285	1.00E-14	2.848
Dosage	0.0815	1	0.0815	2769.452	1.71E-17	4.600
Interaction	0.0027	6	0.0005	15.448	1.89E-05	2.848
Treatment	0.1524	13	0.0117	398.450	1.20E-15	
Error	0.0004	14	0.0000			
Total	0.1528	27				

	Mean diff.	DF	Std.	t observed	t crit	Fisher's LSD
dosage						
5% vs 10%	0.1079	1	0.0005	196.9069	2.0555	0.0011
rejuvenator type						
A vs B	0.0178	1	0.0019	9.2565	3.3659	0.0065
A vs C	0.0803	1		41.8933		
A vs D	0.0247	1		12.8635		
B vs C	0.0626	1		32.6367		
B vs D	0.0069	1		3.6070		
C vs D	0.0557	1		29.0298		
A vs E	0.0913	1		47.5862		
B vs E	0.0735	1		38.3297		
C vs E	0.0109	1		5.6930		
D vs E	0.0666	1		34.7227		
A vs F	0.0732	1		38.1559		
A vs G	0.1544	1		80.5272		
B vs F	0.0554	1		28.8994		
B vs G	0.1367	1		71.2707		
C vs F	0.0072	1		3.7374		
C vs G	0.0741	1		38.6339		
D vs F	0.0485	1		25.2924		
D vs G	0.1298	1		67.6637		
E vs F	0.0181	1		9.4303		
E vs G	0.0632	1		32.9409		
F vs G	0.0813	1		42.3713		

Rotational viscosity at 165°C (single factor ANOVA):

(1) Rejuvenator dosage:

Groups	Count	Sum	Average	Variance
5%	14	1.5838	0.1131	8.26E-05
10%	14	1.2425	0.0888	0.0002

Source of Variation	SS	df	MS	F	P-value	F crit
Between Groups	0.0042	1	0.0042	32.7816	5.01E-06	4.2252
Within Groups	0.0033	26	0.0001			
Total	0.0075	27				

(2) Rejuvenator type:

Groups	Count	Sum	Average	Variance
A	4	0.3570	0.0893	0.0002
B	4	0.3735	0.0934	0.0002
C	4	0.4103	0.1026	0.0001
D	4	0.3697	0.0924	0.0004
E	4	0.4177	0.1044	0.0003
F	4	0.4080	0.1020	0.0002
G	4	0.4902	0.1225	0.0001

Source of Variation	SS	df	MS	F	P-value	F crit
Between Groups	0.0030	6	0.0005	2.3488	0.0681	2.5727
Within Groups	0.0045	21	0.0002			
Total	0.0075	27				

Rotational viscosity at 165°C (two factor ANOVA with replication):

Source	SS	df	MS	F	P-value	F crit
Rej	0.0030	6	0.0005	159.500	4.546E-12	2.848
Dosage	0.0042	1	0.0042	1328.999	2.815E-15	4.600
Interaction	0.0003	6	0.0000	13.845	3.570E-05	2.848
Treatment	0.0074	13	0.0006	182.236	2.768E-13	
Error	0.0000	14	0.0000			
Total	0.0075	27				

	Mean diff.	DF	Std.	t observed	t crit	Fisher's LSD
dosage						
5% vs 10%	0.0290	1	0.00018	162.2459	2.0555	0.0004
rejuvenator type						
A vs B	0.0041	1	0.00063	6.5937	3.3659	0.0021
A vs C	0.0133	1		21.3131		
A vs D	0.0032	1		5.0619		
B vs C	0.0092	1		14.7194		
B vs D	0.0010	1		1.5318		
C vs D	0.0102	1		16.2512		
A vs E	0.0152	1		24.2436		
B vs E	0.0110	1		17.6499		
C vs E	0.0018	1		2.9306		
D vs E	0.0120	1		19.1818		
A vs F	0.0128	1		20.3806		
A vs G	0.0333	1		53.2161		
B vs F	0.0086	1		13.7869		
B vs G	0.0292	1		46.6224		
C vs F	0.0006	1		0.9324		
C vs G	0.0200	1		31.9030		
D vs F	0.0096	1		15.3188		
D vs G	0.0301	1		48.1543		
E vs F	0.0024	1		3.8630		
E vs G	0.0181	1		28.9725		
F vs G	0.0205	1		32.8355		

Continuous high temperature PG (RTFO):

(1) Sigle factor (rejuvenator dosage):

Groups	Count	Sum	Average	Variance
5%	14	934.1	66.7214	3.06181
10%	14	827.6	59.1143	10.0259

Source of Variation	SS	df	MS	F	P-value	F crit
Between Groups	405.0804	1	405.0804	61.90229	2.41E-08	4.22529
Within Groups	170.1407	26	6.5439			
Total	575.2211	27				

(2) Sigle factor (rejuvenator type):

Groups	Count	Sum	Average	Variance
A	4	243.8	60.95	24.08333
B	4	244.4	61.1	22.41333
C	4	253.4	63.35	21.87
D	4	242.1	60.525	25.54917
E	4	267	66.75	8.676667
F	4	246.9	61.725	26.7025
G	4	264.1	66.025	10.6425

Source of Variation	SS	df	MS	F	P-value	F crit
Between Groups	155.4086	6	25.9014	1.2956	0.30195	2.5727
Within Groups	419.8125	21	19.9911			
Total	575.2211	27				

(3) Two factor ANOVA with replication:

Source	SS	df	MS	F	P-value	F crit
Rej	155.409	6	25.901	3153.217	4.346E-21	2.848
Dosage	405.080	1	405.080	49314.130	3.108E-26	4.600
Interaction	14.617	6	2.436	296.580	6.272E-14	2.848
Treatment	575.106	13	44.239	5385.609	1.504E-23	
Error	0.115	14	0.008			
Total	575.221	27				

	Mean diff.	DF	Std.	t observed	t crit	Fisher's LSD
dosage						
5% vs 10%	7.6071	1	0.009	830.902	2.056	0.0188
rejuvenator type						
A vs B	0.15	1	0.032	4.681	3.366	0.1079
A vs C	2.4	1		74.898		
A vs D	0.425	1		13.263		
B vs C	2.25	1		70.217		
B vs D	0.575	1		17.944		
C vs D	2.825	1		88.161		
A vs E	5.8	1		181.004		
B vs E	5.65	1		176.323		
C vs E	3.4	1		106.106		
D vs E	6.225	1		194.267		
A vs F	0.775	1		24.186		
A vs G	5.075	1		158.378		
B vs F	0.625	1		19.505		
B vs G	4.925	1		153.697		
C vs F	1.625	1		50.712		
C vs G	2.675	1		83.480		
D vs F	1.2	1		37.449		
D vs G	5.5	1		171.642		
E vs F	5.025	1		156.818		
E vs G	0.725	1		22.625		
F vs G	4.3	1		134.193		

Continuous intermediate temperature PG:

(1) Sigle factor (rejuvenator dosage):

Groups	Count	Sum	Average	Variance
5%	14	248.8	17.7714	2.5837
10%	14	148	10.5714	7.2330

Source of Variation	SS	df	MS	F	P-value	F crit
Between Groups	362.88	1	362.88	73.9311	4.46E-09	4.2252
Within Groups	127.6171	26	4.9084			
Total	490.4971	27				

(2) Single factor (rejuvenator type):

Groups	Count	Sum	Average	Variance
A	4	51.4	12.85	20.3367
B	4	52	13	18.7667
C	4	70	17.5	12.0267
D	4	47.6	11.9	24.0867
E	4	64.4	16.1	10.4533
F	4	48.5	12.125	24.3825
G	4	62.9	15.725	13.8758

Source of Variation	SS	df	MS	F	P-value	F crit
Between Groups	118.7121	6	19.7854	1.1176	0.3857	2.5727
Within Groups	371.785	21	17.7040			
Total	490.4971	27				

(3) Two factor ANOVA with replication:

Source	SS	df	MS	F	P-value	F crit
Rej	118.712	6	19.785	728.934	1.206E-16	2.848
Dosage	362.88	1	362.880	13369.263	2.873E-22	4.600
Interaction	8.525	6	1.421	52.346	8.596E-09	2.848
Treatment	490.117	13	37.701	1388.996	1.967E-19	
Error	0.38	14	0.027			
Total	490.497	27				

	Mean diff.	DF	Std.	t observed	t crit	Fisher's LSD
dosage						
5% vs 10%	7.2	1	0.017	432.631	2.056	0.0342
rejuvenator type						
A vs B	0.15	1	0.058	2.575	3.366	0.1961
A vs C	4.65	1		79.831		
A vs D	0.95	1		16.310		
B vs C	4.5	1		77.256		
B vs D	1.1	1		18.885		
C vs D	5.6	1		96.140		
A vs E	3.25	1		55.796		
B vs E	3.1	1		53.220		
C vs E	1.4	1		24.035		
D vs E	4.2	1		72.105		
A vs F	0.725	1		12.447		
A vs G	2.875	1		49.358		
B vs F	0.875	1		15.022		
B vs G	2.725	1		46.783		
C vs F	5.375	1		92.277		
C vs G	1.775	1		30.473		
D vs F	0.225	1		3.863		
D vs G	3.825	1		65.667		
E vs F	3.975	1		68.242		
E vs G	0.375	1		6.438		
F vs G	3.6	1		61.804		

Crossover temperature:

(1) Sigle factor (rejuvenator dosage):

Groups	Count	Sum	Average	Variance
0.05	14	260.86	18.6329	6.8683
0.1	14	165.25	11.8036	41.4641

Source of Variation	SS	df	MS	F	P-value	F crit
Between Groups	326.4740	1	326.4740	13.5095	0.0011	4.2252
Within Groups	628.3218	26	24.1662			
Total	954.7958	27				

(2) Single factor (rejuvenator type):

Groups	Count	Sum	Average	Variance
A	4	53.64	13.41	20.8537
B	4	50.84	12.71	25.7231
C	4	57.42	14.355	21.2844
D	4	51.25	12.8125	27.2102
E	4	102.88	25.72	1.7421
F	4	51.61	12.9025	23.8411
G	4	58.47	14.6175	21.4718

Source of Variation	SS	df	MS	F	P-value	F crit
Between Groups	528.4171	6	88.0695	4.3376	0.0053	2.5727
Within Groups	426.3787	21	20.3037			
Total	954.7958	27				

(3) Two factor ANOVA with replication:

Source	SS	df	MS	F	P-value	F crit
Rej	528.4171	6	88.070	531.397	1.090E-15	2.848
Dosage	326.4740	1	326.474	1969.889	1.831E-16	4.600
Interaction	97.5845	6	16.264	98.135	1.259E-10	2.848
Treatment	952.4756	13	73.267	442.083	5.831E-16	
Error	2.3202	14	0.166			
Total	954.7958	27				

	Mean diff.	DF	Std.	t observed	t crit	Fisher's LSD
dosage						
5% vs 10%	6.83	1	0.041	166.068	2.056	0.0845
rejuvenator type						
A vs B	0.7	1	0.144	4.863	3.366	0.4844
A vs C	0.945	1		6.566		
A vs D	0.5975	1		4.151		
B vs C	1.645	1		11.429		
B vs D	0.1025	1		0.712		
C vs D	1.5425	1		10.717		
A vs E	12.31	1		85.526		
B vs E	13.01	1		90.390		
C vs E	11.365	1		78.961		
D vs E	12.9075	1		89.678		
A vs F	0.5075	1		3.526		
A vs G	1.2075	1		8.389		
B vs F	0.1925	1		1.337		
B vs G	1.9075	1		13.253		
C vs F	1.4525	1		10.092		
C vs G	0.2625	1		1.824		
D vs F	0.09	1		0.625		
D vs G	1.805	1		12.541		
E vs F	12.8175	1		89.052		
E vs G	11.1025	1		77.137		
F vs G	1.715	1		11.915		

Continuous low temperature PG (creep stiffness):

Two factor ANOVA without replication:

SUMMARY	Count	Sum	Average	Variance
A	2	-74.1	-37.05	21.125
B	2	-72.2	-36.1	21.78
C	2	-62.5	-31.25	12.005
D	2	-74.7	-37.35	21.125
E	2	-70.3	-35.15	16.245
F	2	-72.9	-36.45	19.845
G	2	-64.7	-32.35	7.605
0.05	7	-225.5	-32.2143	3.7581
0.1	7	-265.9	-37.9857	8.1248

Source of Variation	SS	df	MS	F	P-value	F crit
Rows	68.15	6	11.3583	21.6546	0.0008	4.2839
Columns	116.5829	1	116.5829	222.2642	0.0000	5.9874
Error	3.1471	6	0.5245			
Total	187.88	13				

Continuous low temperature PG (m-value):

Two factor ANOVA without replication:

SUMMARY	Count	Sum	Average	Variance
A	2	-74.2	-37.1	24.5
B	2	-74.7	-37.35	22.445
C	2	-64.2	-32.1	23.12
D	2	-75	-37.5	24.5
E	2	-56.6	-28.3	0.32
F	2	-73.7	-36.85	31.205
G	2	-65	-32.5	12.5
0.05	7	-221.1	-31.5857	6.9781
0.1	7	-262.3	-37.4714	21.7790

Source of Variation	SS	df	MS	F	P-value	F crit
Rows	155.1986	6	25.8664	8.9481	0.0087	4.2839
Columns	121.2457	1	121.2457	41.9432	0.0006	5.9874
Error	17.3443	6	2.8907			
Total	293.7886	13				

Appendix B: Blending chart example

Continuous low temperature based on m-value:

(1) Determine the slop rate of rejuvenator A and B:

According to the linear regression equations of rejuvenator A and B, the slope rates of A and B are -1.61 and -1.62, respectively.

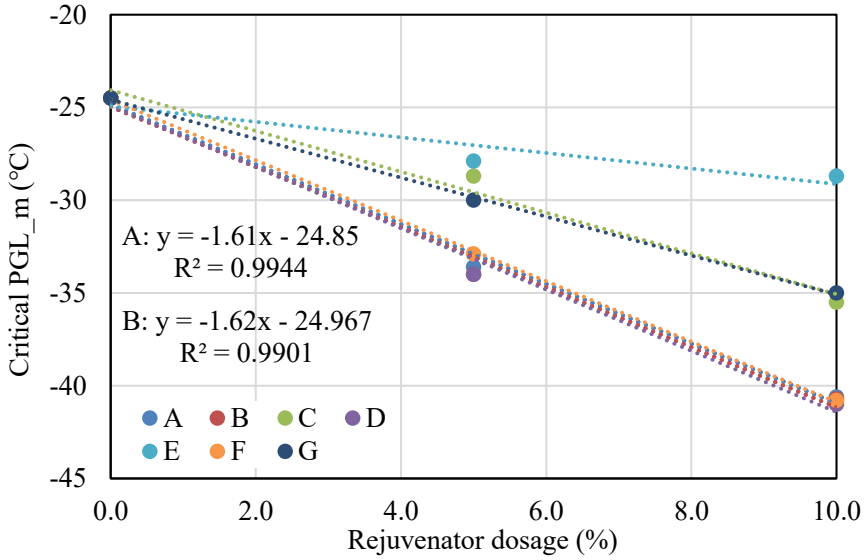

(2) Determine the continuous low temperature of blended binder using the following equation:

$$T_{blend} = (1 - 0.43) \times (-31.9) + 0.43 \times (-16.8) = -25.407$$

(3) Determine the rejuvenator dosage using the following equations:

$$\%A = \frac{-25.407 - (-31.9)}{-1.61} = 4.03\%$$

$$\%B = \frac{-25.407 - (-31.9)}{-1.62} = 4.01\%$$

Appendix C: RSM example

Rejuvenator D:

The response in this example is the continuous high temperature of RTFO residue.

(1) Factor level combinations and response yields

X1	X2	X1X2	Replicate 1	Replicate 2
-1	-1	1	67.4	67.3
1	-1	-1	50.0	49.9
-1	1	-1	80.7	80.6
1	1	1	63.4	63.3
0	0	0	65.1	
0	0	0	64.7	

(2) ANOVA table:

Source	*SS*	*DF*	*MS*	*F*	*F crit*	*Effect*	*β0 and βi*
Model	958.495	3	319.498	4927.995			β0: 65.240
x1	602.045	1	602.045	9286.041	5.987	-17.35	β1: -8.675
x2	356.445	1	356.445	5497.866		13.35	β2: 6.675
x1x2	0.005	1	0.005	0.077		0.05	β12: 0.025
PE	0.080	1	0.080				
LOF	0.309	5	0.062	0.773	230.162		
Error	0.389	6	0.065				
Total	958.884	9					

Interaction check: *F observed (0.077) < F critical (5.987)*, remove the interaction term into the error term.

(3) ANOVA table without interaction term.

Source	*SS*	*DF*	*MS*	*F*	*F crit*
Model	958.490	2	479.245	7391.954	
x1	602.045	1	602.045	9286.041	5.987
x2	356.445	1	356.445	5497.866	
PE	0.080	1	0.080		
LOF	0.314	6	0.0523	0.654	233.986
Error	0.394	7	0.0563		
Total	958.884	9			

Curvature check: (1) F observed (0.654) < F critical (233.986); (2) $\hat{y}_f - \hat{y}_c$= 65.325 – 64.9 = 0.425. No significant lack of fit (LOF) is observed and the difference between the mean of factorial points and the mean of center points is relatively small, indicating no curvature in the model.

(4) Final model with uncoded parameters:

The first-degree coded model will be: $\hat{y} = 65.24 - 8.675x1 + 6.675x2$, and it needs to be transformed into a model uncoded parameters.

$$\hat{y} = 65.24 - 8.675 * \frac{x1' - 5}{(10-0)/2} + 6.675 \frac{x2' - 50}{(75-25)/2}$$

The final model to determine a target rejuvenator dosage is:

$$\hat{y} = 60.565 - 1.735x1' + 0.267x2'$$

Appendix D: FTIR results of optimized binder blends

FTIR data processing:

- Baseline correction.
- Normalization (absorbance at 2923cm^{-1} = 1).
- Select interested absorbance peak groups in the spectrum.
- Compute the indices using Spectragryph software: area under the spectrum (integration in individual baseline on the selected spectral range), maximum value, peak position.

FTIR spectrum of recycled binder blend (no rejuvenator):

- Three groups denoted for asphalt binders with different aging conditions: (1) Carbonyl group: 1666cm^{-1} - 1746cm^{-1} (peak around 1699cm^{-1}); (2) Sulfoxide group: 924cm^{-1} - 1066cm^{-1} (peak around 1030cm^{-1}); (3) Reference group: 1319cm^{-1} - 1520cm^{-1} (peak around 1456cm^{-1}).

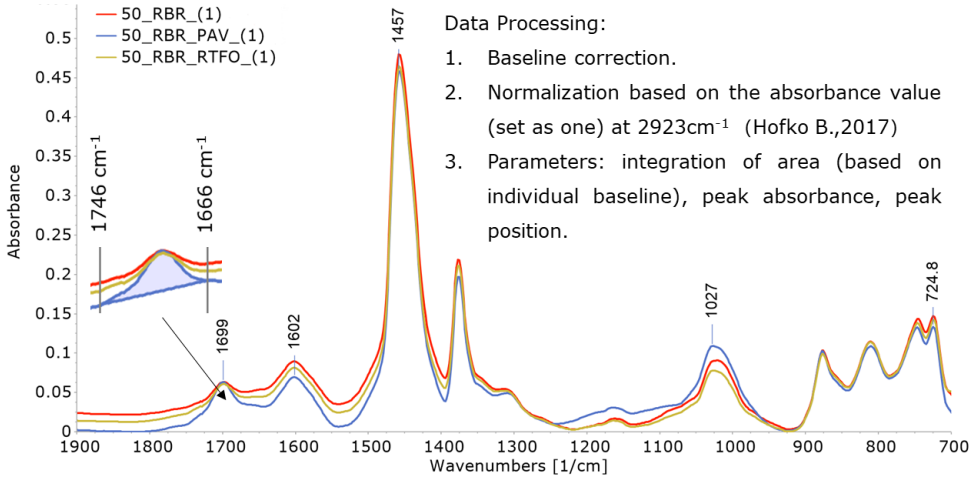

Carbonyl		Sulfoxide		Reference	
Range	Peak	Range	Peak	Range	Peak
1666-1746	1699	924-1066	1030	1319-1520	1456
1666-1725	1699				

FTIR spectrum of recycled binder blend (no rejuvenator):

- Four groups denoted for rejuvenated binder (or rejuvenator): (1) Peak #1: 1725cm^{-1} -1765cm^{-1} (peak around 1744cm^{-1}), so the carbonyl range needs to be adjusted to 1666cm^{-1} -1725cm^{-1} to avoid the influence of rejuvenator peak #1 on the carbonyl group; (2) Peak #2: at 1462cm^{-1}, but it overlaps the reference group in the rejuvenated binder blends; (3) Peak #3: 1128cm^{-1} - 1200cm^{-1} (peak around 1160cm^{-1}), but it may be interfered by the small peak show in the spectrum of the asphalt binder, especially after aging; (4) Peak #4 (723cm^{-1}): it appears in the binder as well, but it will mix up with other multiple peaks in the binder below 900cm^{-1}.
- Conclusion: peak #1 will be used for detecting the effect of rejuvenators.

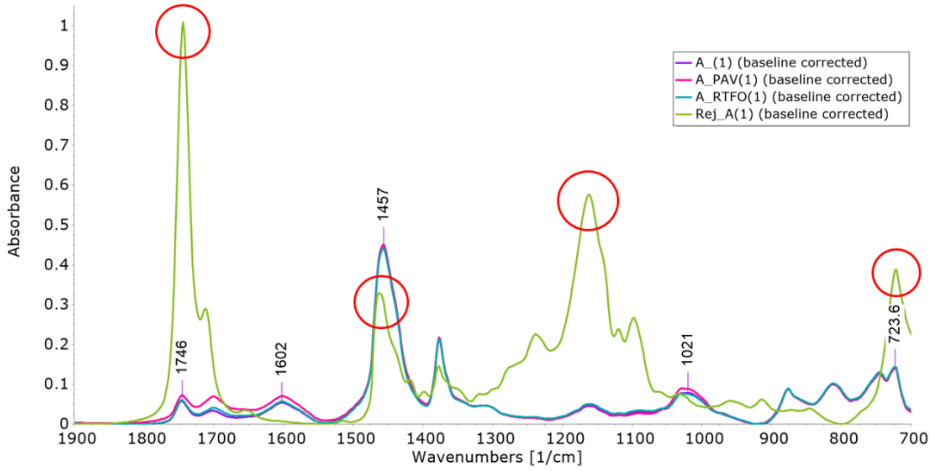

#1		#2	#3		#4
Range	Peak	Peak	Range	Peak	Peak
1725-1765	1744	1462	1128-1200	1160	723

Results of virgin binder and recovered RAP binder (carbonyl index):

$$Peak\ ratio_{C=O} = \frac{Peak\ (1699\ cm^{-1})}{Peak\ (1456\ cm^{-1})}$$

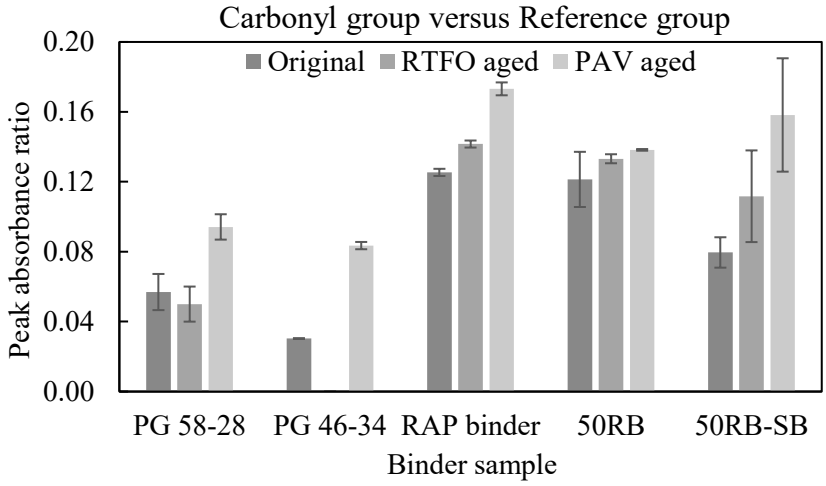

$$Area\ ratio_{C=O} = \frac{Area\ (1666\ cm^{-1} - 1746\ cm^{-1})}{Area\ (1319\ cm^{-1} - 1520\ cm^{-1})}$$

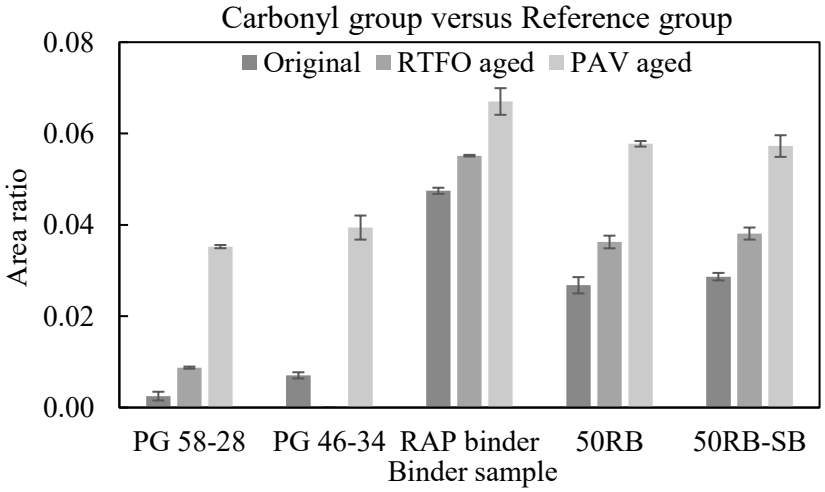

Results of virgin and recovered RAP binder (sulfoxide index):

$$Peak\ ratio_{S=O} = \frac{Peak\ (1030\ cm^{-1})}{Peak\ (1456\ cm^{-1})}$$

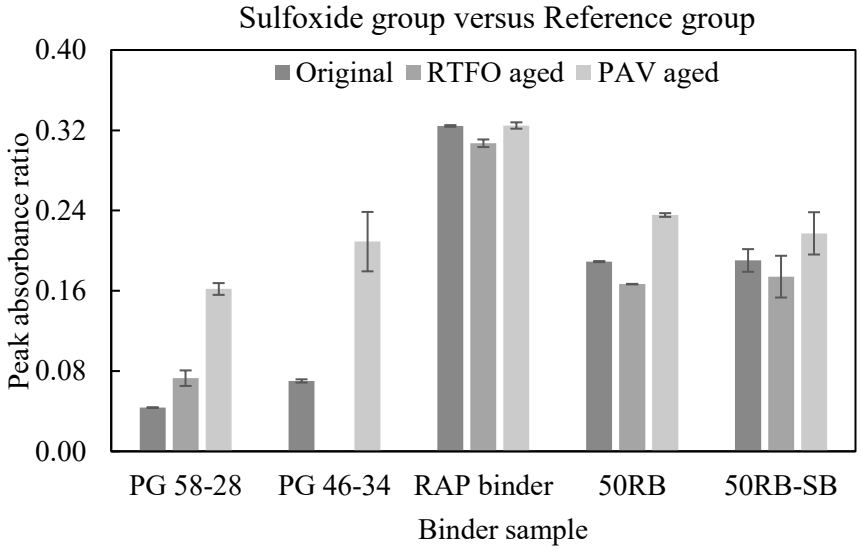

$$Area\ ratio_{S=O} = \frac{Area\ (924\ cm^{-1} - 1066\ cm^{-1})}{Area\ (1319\ cm^{-1} - 1520\ cm^{-1})}$$

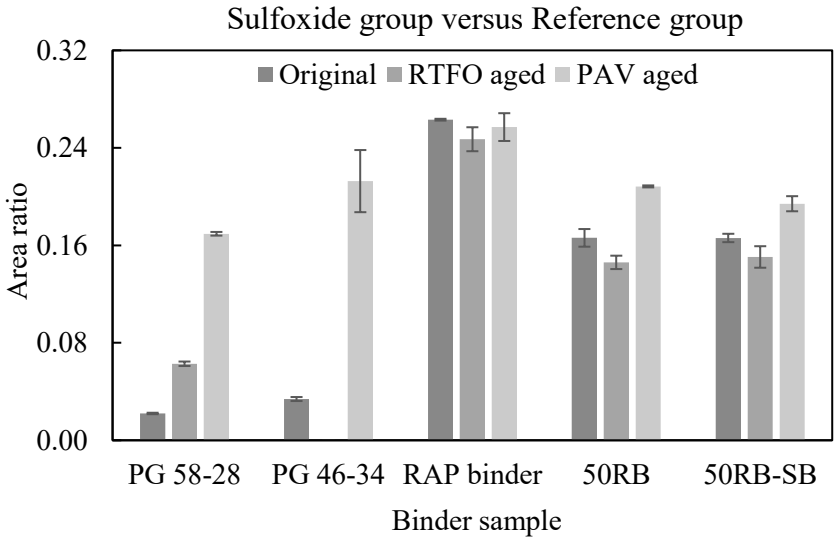

Results of virgin and RAP binder after RTFO and PAV aging:

$$Aging\ index = \frac{Carbonyl_{RTFO}/Carbonyl_{PAV}}{Carbonyl_{Original}}$$

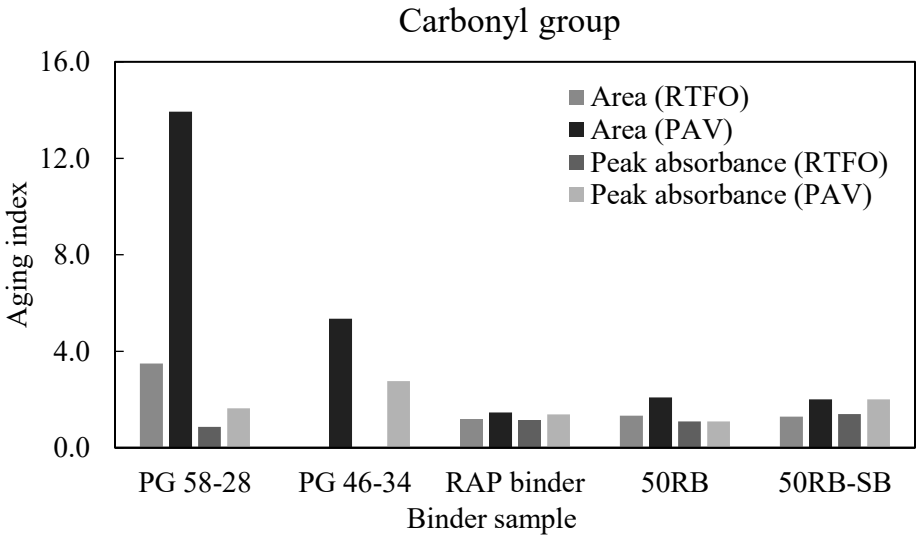

$$Aging\ index = \frac{Sulfoxide_{RTFO}/Sulfoxide_{PAV}}{Sulfoxide_{Original}}$$

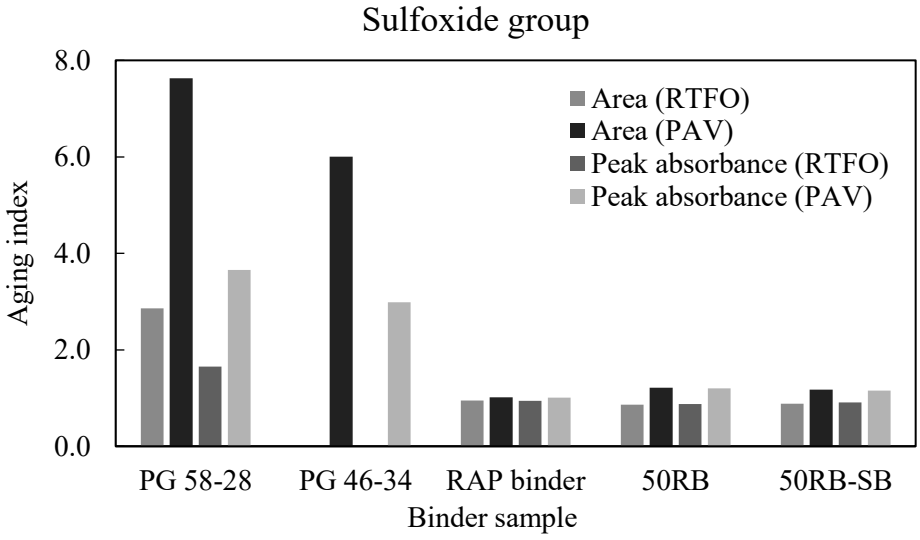

Results of rejuvenated binder blends (carbonyl index):

$$Peak\ ratio_{C=O} = \frac{Peak\ (1699\ cm^{-1})}{Peak\ (1456\ cm^{-1})}$$

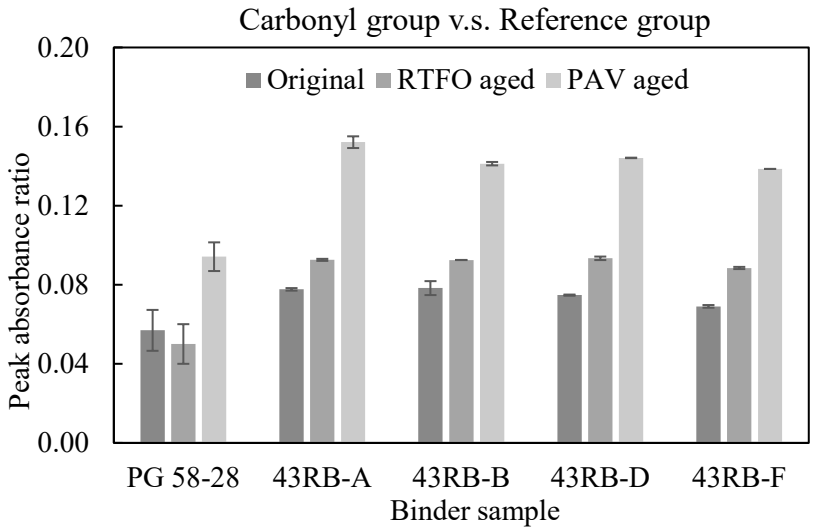

$$Area\ ratio_{C=O} = \frac{Area\ (1666\ cm^{-1} - 1725\ cm^{-1})}{Area\ (1319\ cm^{-1} - 1520\ cm^{-1})}$$

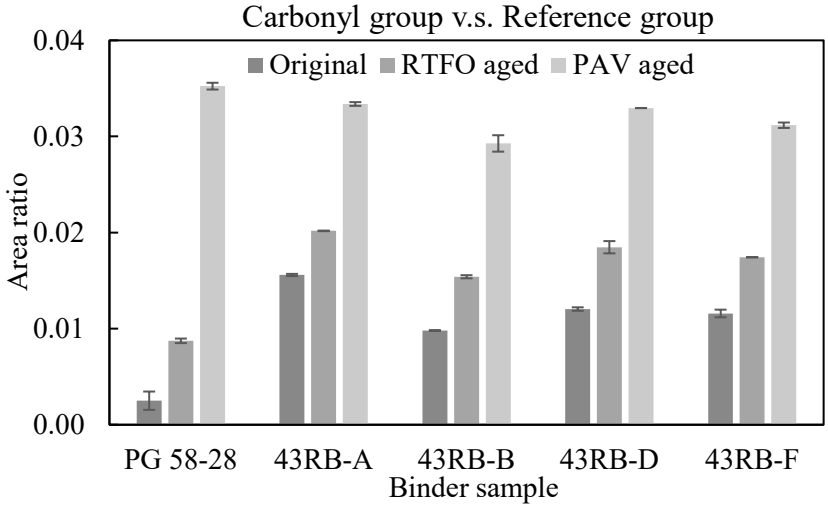

Results of rejuvenated binder blends (sulfoxide index):

$$Peak\ ratio_{S=O} = \frac{Peak\ (1030\ cm^{-1})}{Peak\ (1456\ cm^{-1})}$$

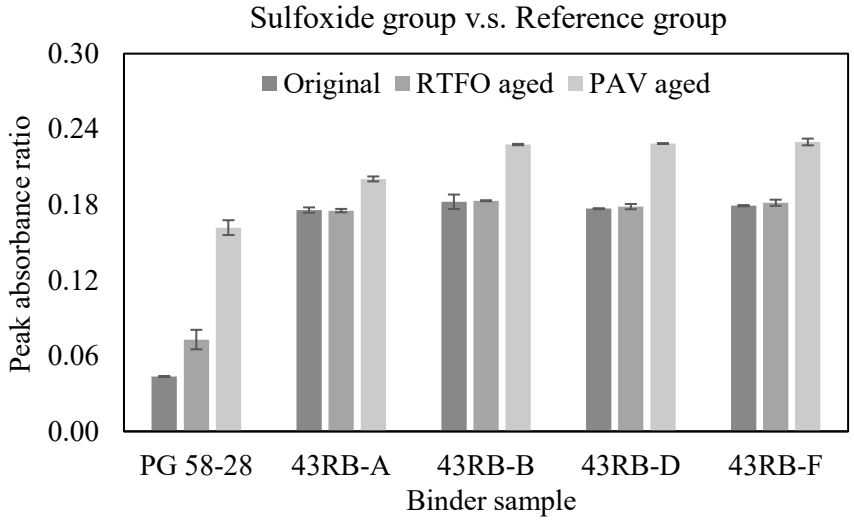

$$Area\ ratio_{S=O} = \frac{Area\ (924\ cm^{-1} - 1066\ cm^{-1})}{Area\ (1319\ cm^{-1} - 1520\ cm^{-1})}$$

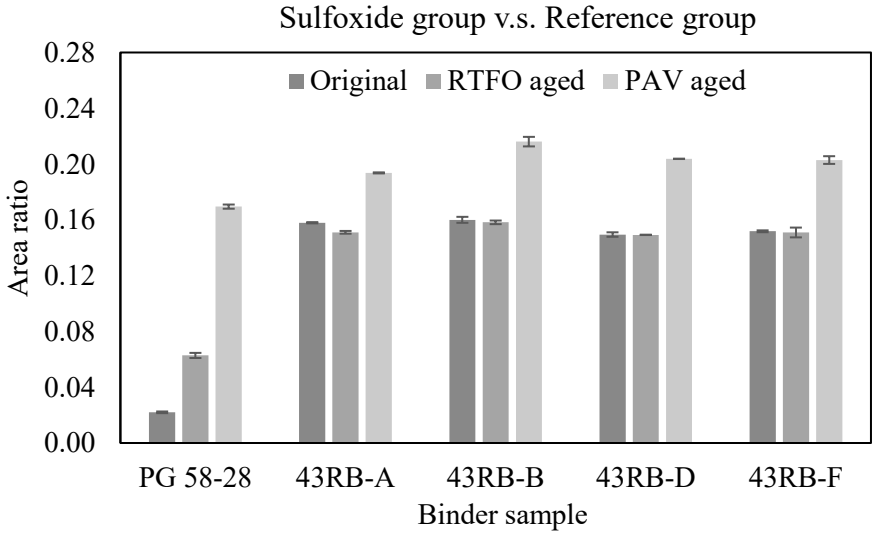

Loss of rejuvenator effectiveness after aging:

$$Rejuvenator\ loss = \frac{Rej\ peak_{RTFO}/Rej\ peak_{PAV}}{Rej\ peak_{original}}$$

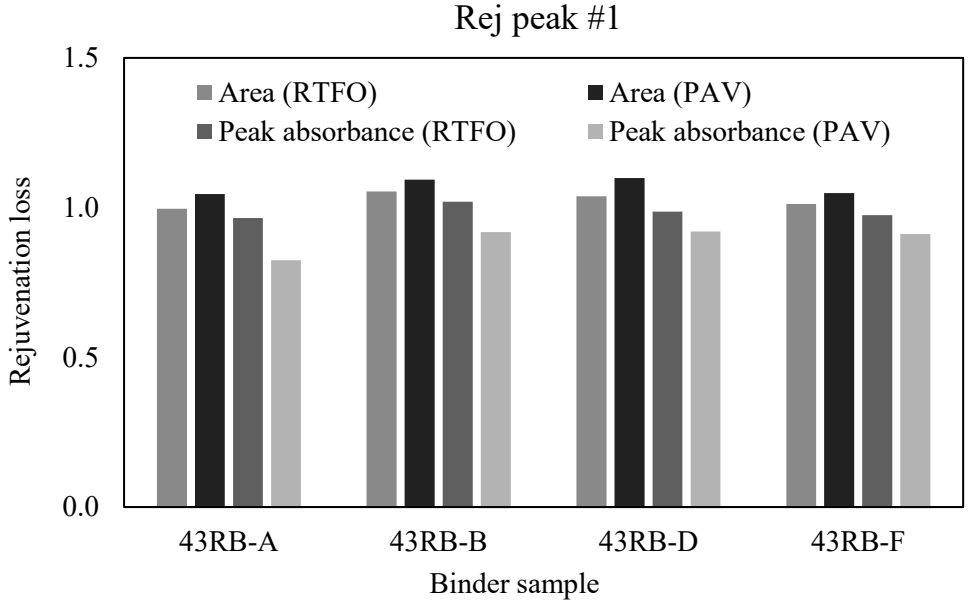

Appendix E: SARA results of optimized binder blends

Analysis of asphalt composition using SAR-AD™

1. Base binder (PG 58-28)

Sample ID	PG 58-28	RTFO PG 58-28	PAV PG 58-28
Saturates %	16.272	16.245	16.202
Aromatics I %	10.223	10.200	10.220
Aromatics II %	14.879	14.418	12.967
Aromatics III %	32.684	30.409	26.496
Resins %	11.646	11.836	12.429
Asphaltenes I %	3.231	3.472	3.225
Asphaltenes II %	10.562	12.869	17.580
Asphaltenes III %	0.503	0.551	0.881
CII	0.440	0.496	0.610

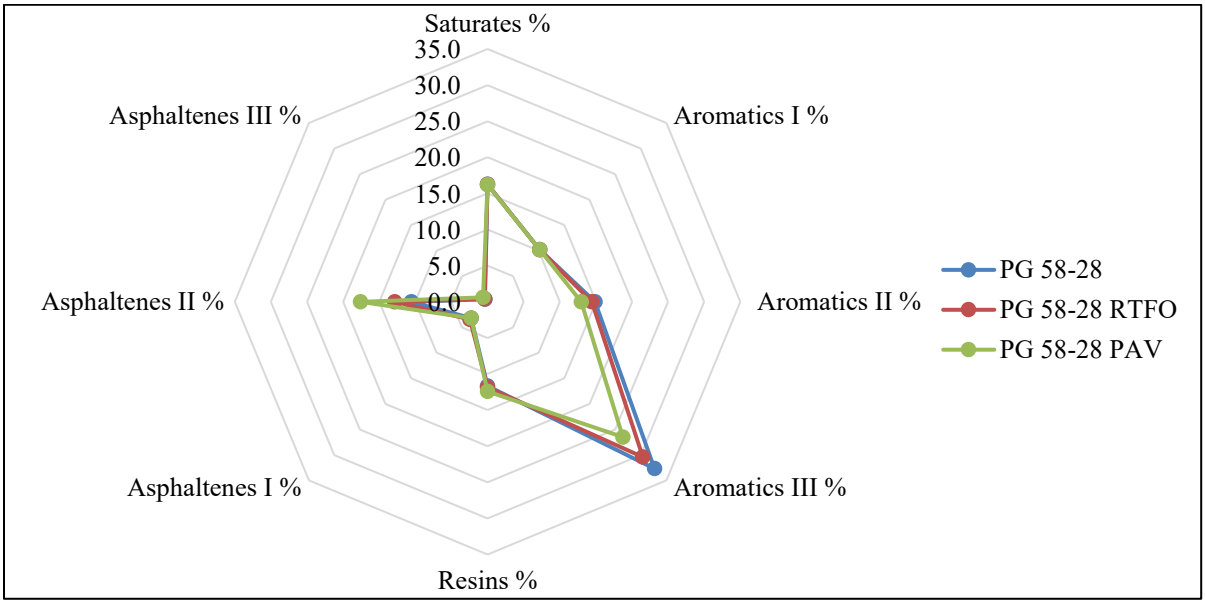

2. 43RB-A (4.03% rejuvenator A):

Sample ID	43RB_A	43RB_A RTFO	43RB_A PAV
Saturates %	14.422	14.466	14.642
Aromatics I %	8.888	8.993	9.051
Aromatics II %	12.211	11.987	11.605
Aromatics III %	31.570	30.570	27.476
Resins %	14.809	14.266	14.505
Asphaltenes I %	3.093	3.615	3.514
Asphaltenes II %	14.142	15.275	18.151
Asphaltenes III %	0.866	0.829	1.057
CII	0.482	0.519	0.597

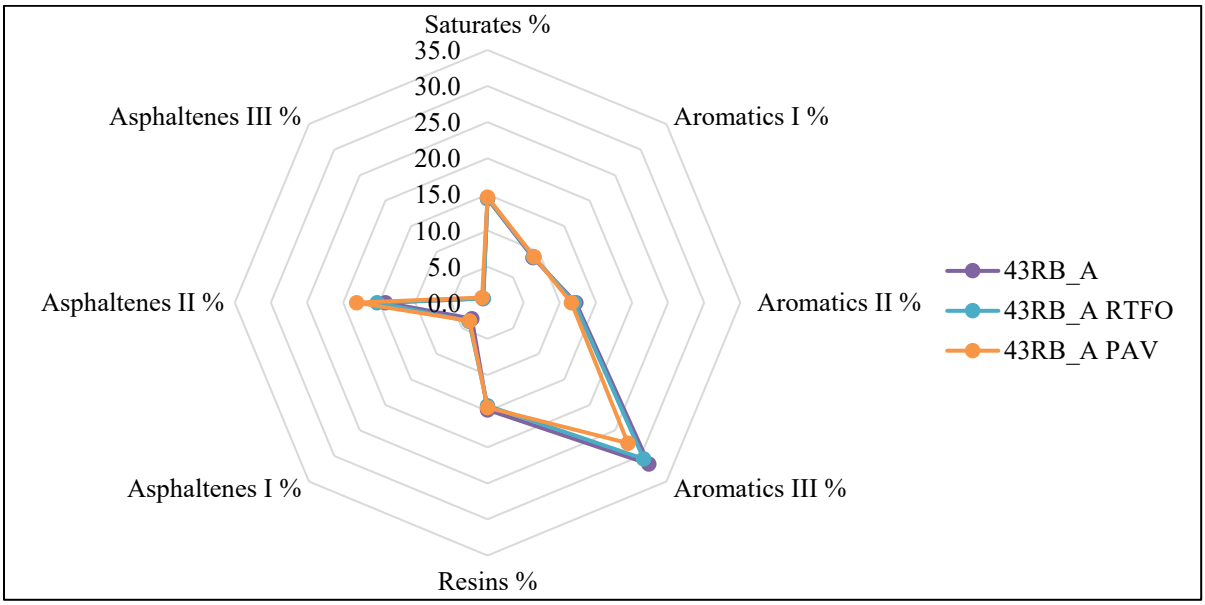

3. 43RB_B (4.01% rejuvenator B):

Sample ID	43RB_B	43RB_B RTFO	43RB_B PAV
Saturates %	14.242	14.346	14.495
Aromatics I %	8.965	8.965	8.902
Aromatics II %	12.107	12.074	11.318
Aromatics III %	32.451	31.005	27.471
Resins %	14.836	14.345	14.627
Asphaltenes I %	3.080	3.544	3.669
Asphaltenes II %	13.497	15.032	18.468
Asphaltenes III %	0.822	0.689	1.051
CII	0.463	0.506	0.605

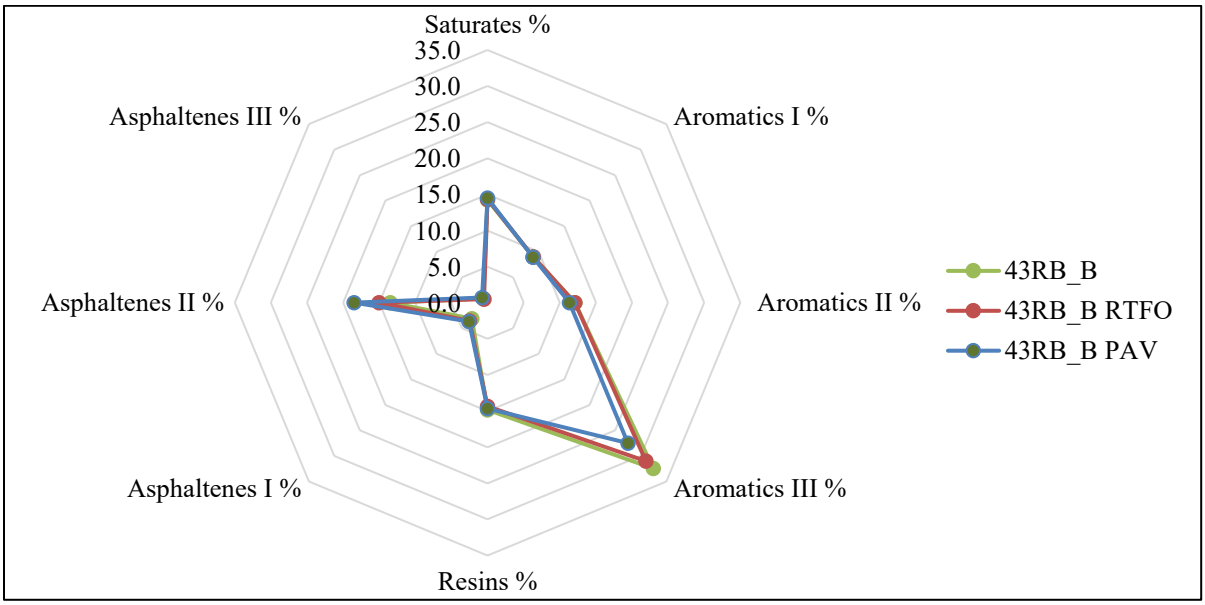

4. 43RB_D (4.27% rejuvenator D):

Sample ID	43RB_D	43RB_D RTFO	43RB_D PAV
Saturates %	14.086	14.243	14.367
Aromatics I %	9.021	8.886	8.802
Aromatics II %	12.455	12.266	11.602
Aromatics III %	32.512	31.104	27.748
Resins %	14.374	13.997	14.243
Asphaltenes I %	3.067	3.707	3.638
Asphaltenes II %	13.664	15.040	18.603
Asphaltenes III %	0.821	0.759	0.998
CII	0.463	0.509	0.603

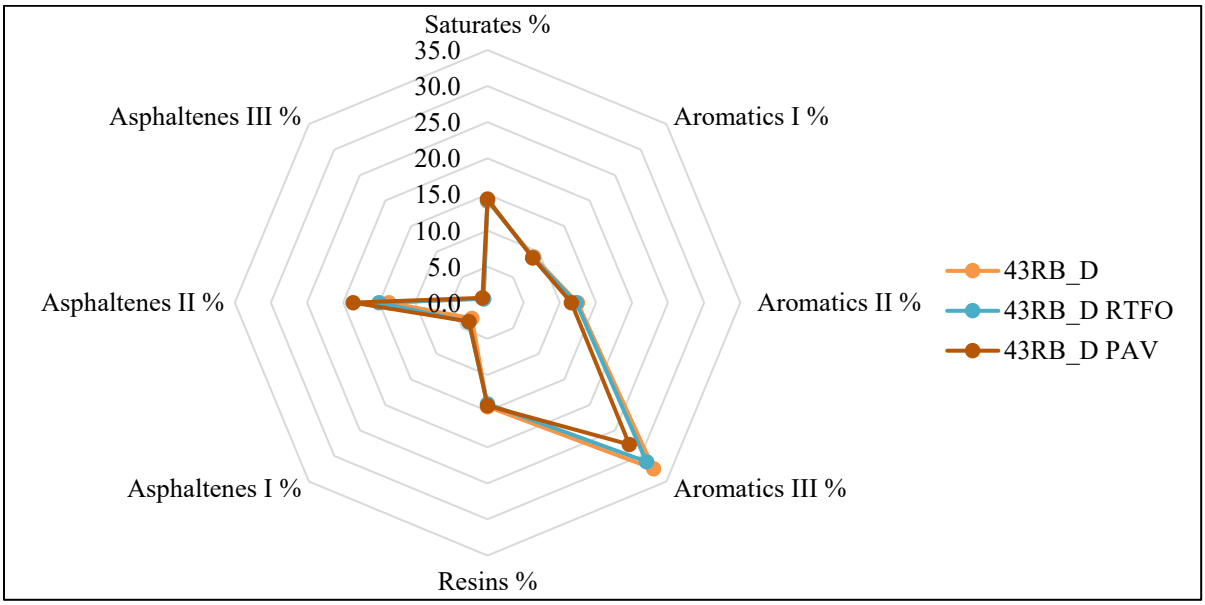

Appendix F: HWT rut depth versus number of passes

1. Test temperature: 44°C

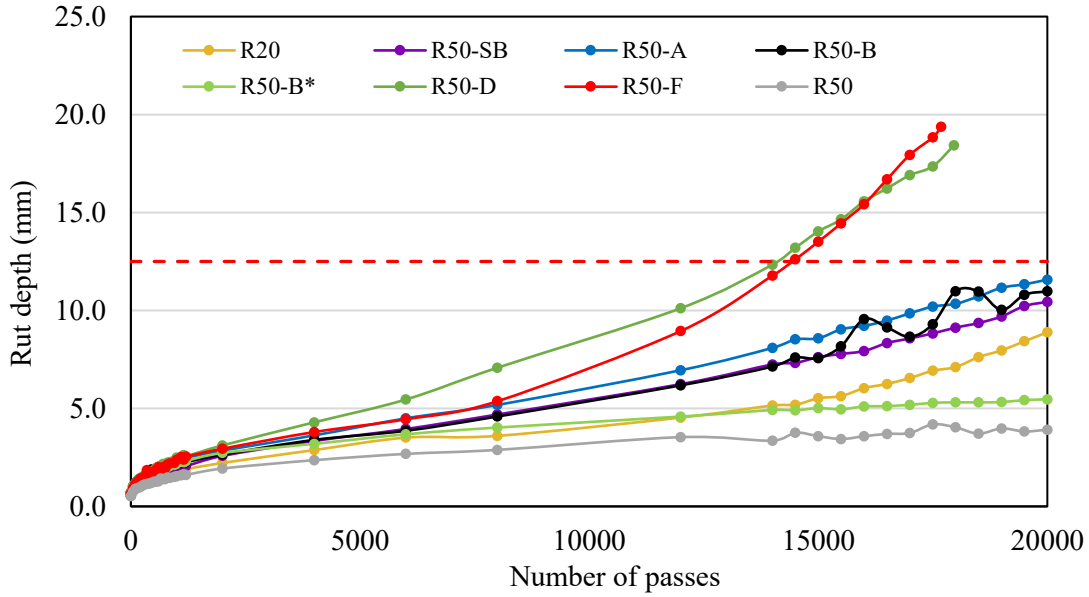

2. Test temperature: 50°C

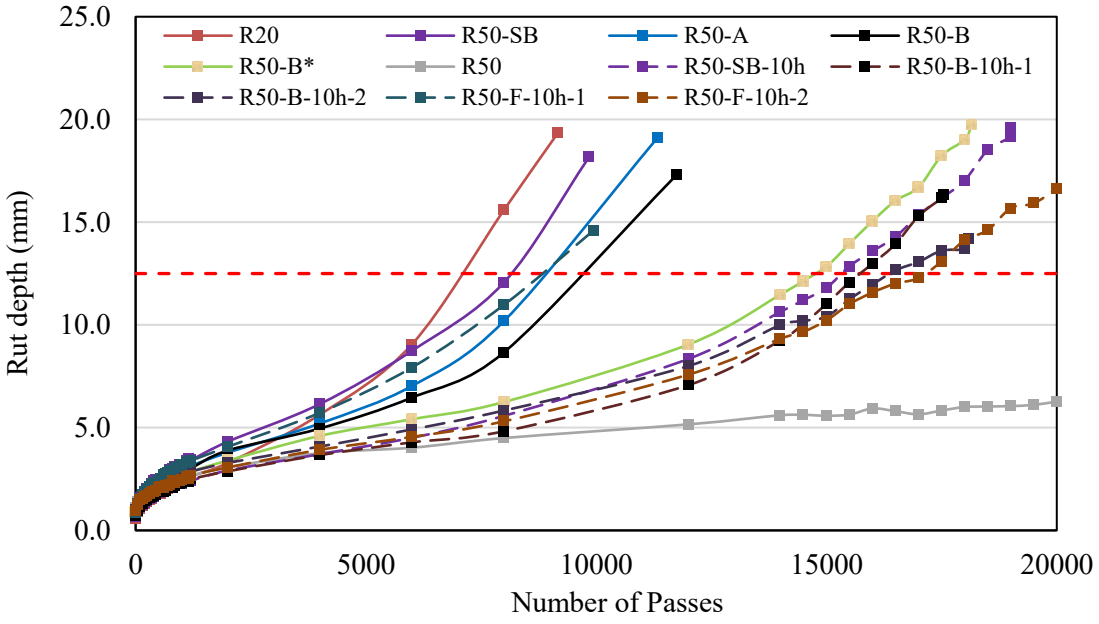

Appendix G: Statistical analysis of mix test results

One-way ANOVA

1. CT_{index} versus 4h mixes (R20, R50, R50-B, R50-B*, R50-F, R50-SB)

Source	DF	Adj SS	Adj MS	F-Value	P-Value
Mix type	5	1127	225.33	3.49	0.022
Error	18	1162	64.53		
Total	23	2288			

2. CRI versus 4h mixes (R20, R50, R50-B, R50-B*, R50-F, R50-SB)

Source	DF	Adj SS	Adj MS	F-Value	P-Value
Mix type	5	12262	2452.4	3.18	0.031
Error	18	13887	771.5		
Total	23	26149			

3. RDCI versus 4h mixes (R20, R50, R50-B, R50-B*, R50-F, R50-SB)

Source	DF	Adj SS	Adj MS	F-Value	P-Value
Mix type	5	163.8	32.76	1.75	0.175
Error	18	337.8	18.77		
Total	23	501.7			

4. CT_{index} versus 10h mixes (R50-B, R50-F, R50-SB)

Source	DF	Adj SS	Adj MS	F-Value	P-Value
Mix type	2	54.47	27.24	0.84	0.461
Error	10	324.99	32.50		
Total	12	379.46			

5. CRI versus 10h mixes (R50-B, R50-F, R50-SB)

Source	DF	Adj SS	Adj MS	F-Value	P-Value
Mix type	2	209.9	104.9	0.12	0.889
Error	10	8809.2	880.9		
Total	12	9019.1			

6. RDCI versus 10h mixes (R50-B, R50-F, R50-SB)

Source	DF	Adj SS	Adj MS	F-Value	P-Value
Mix type	2	16.67	8.337	0.83	0.465
Error	10	100.83	10.083		
Total	12	117.50			

7. CS versus 10h mixes (R50-B, R50-F, R50-SB)

Source	DF	Adj SS	Adj MS	F-Value	P-Value
Mix type	2	5.930	2.965	0.89	0.454
Error	7	23.410	3.344		
Total	9	29.340			

8. VR versus 10h mixes (R50-B, R50-F, R50-SB)

Source	DF	Adj SS	Adj MS	F-Value	P-Value
Mix type	2	0.01485	0.007425	3.69	0.080
Error	7	0.01408	0.002011		
Total	9	0.02893			

Two sample t-test

1. R20 versus R50

CT_{index}	R20	R50
Mean	41.85	30.64
Variance	2.67	9.60
Observations	4	4
H_0	$\mu_{4h} = \mu_{10h}$	
DF	6	
t stat	6.40	
t critical	2.45	
P(T<=t) two-tail	0.0007	

CRI	R20	R50
Mean	447.95	406.85
Variance	134.34	297.49
Observations	4	4
H_0	$\mu_{4h} = \mu_{10h}$	
DF	6	
t stat	3.96	
t critical	2.45	
P(T<=t) two-tail	0.0075	

RDCI	R20	R50
Mean	23.35	18.30
Variance	1.11	7.08
Observations	4	4
H_0	$\mu_{4h} = \mu_{10h}$	
DF	6	
t stat	2.13	
t critical	2.45	
P(T<=t) two-tail	0.0124	

2. R50-B:

CT_{index}	4h	10h
Mean	45.04	37.38
Variance	174.34	5.70
Observations	5	3
H_0	$\mu_{4h} = \mu_{10h}$	
DF	6	
t stat	1.26	
t critical	2.45	
P(T<=t) two-tail	0.2535	

CRI	4h	10h
Mean	463.42	432.52
Variance	2123.34	133.89
Observations	5	3
H_0	$\mu_{4h} = \mu_{10h}$	
DF	6	
t stat	1.43	
t critical	2.45	
P(T<=t) two-tail	0.2036	

RDCI	4h	10h
Mean	24.90	22.75
Variance	54.06	5.80
Observations	5	3
H_0	$\mu_{4h} = \mu_{10h}$	
DF	6	
t stat	0.60	
t critical	2.45	
P(T<=t) two-tail	0.5693	

3. R50-F:

CT_{index}	4h	10h
Mean	48.51	34.90
Variance	12.01	73.33
Observations	3	5
H_0	$\mu_{4h} = \mu_{10h}$	
DF	6	
t stat	3.15	
t critical	2.45	
P(T<=t) two-tail	0.0198	

CRI	4h	10h
Mean	452.53	422.08
Variance	126.01	2020.54
Observations	3	5
H_0	$\mu_{4h} = \mu_{10h}$	
DF	6	
t stat	1.44	
t critical	2.45	
P(T<=t) two-tail	0.1994	

RDCI	4h	10h
Mean	23.19	21.05
Variance	3.85	20.40
Observations	3	5
H_0	$\mu_{4h} = \mu_{10h}$	
DF	6	
t stat	0.93	
t critical	2.45	
P(T<=t) two-tail	0.3901	

4. R50-SB

CT_{index}	4h	10h
Mean	50.55	39.57
Variance	97.43	5.07
Observations	5	5
H_0	$\mu_{4h} = \mu_{10h}$	
DF	8	
t stat	2.43	
t critical	2.31	
P(T<=t) two-tail	0.0415	

CRI	4h	10h
Mean	473.63	427.33
Variance	876.84	114.81
Observations	5	5
H_0	$\mu_{4h} = \mu_{10h}$	
DF	8	
t stat	3.29	
t critical	2.31	
P(T<=t) two-tail	0.0111	

RDCI	4h	10h
Mean	26.29	19.78
Variance	17.89	1.90
Observations	5	5
H_0	$\mu_{4h} = \mu_{10h}$	
DF	8	
t stat	3.28	
t critical	2.45	
P(T<=t) two-tail	0.0113	

Appendix H: Black space diagram, Cole-Cole plane, *E'* and *E"*

1. R20 mixes:

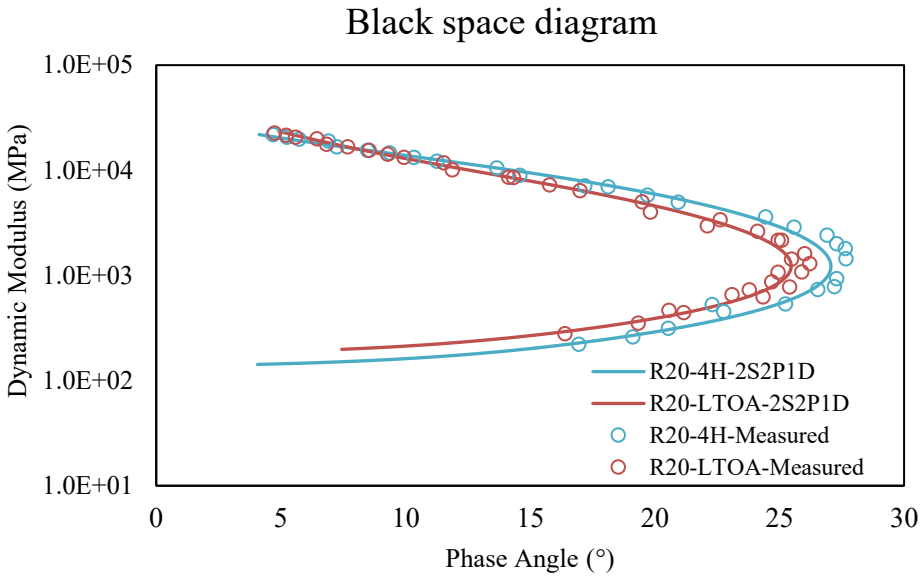

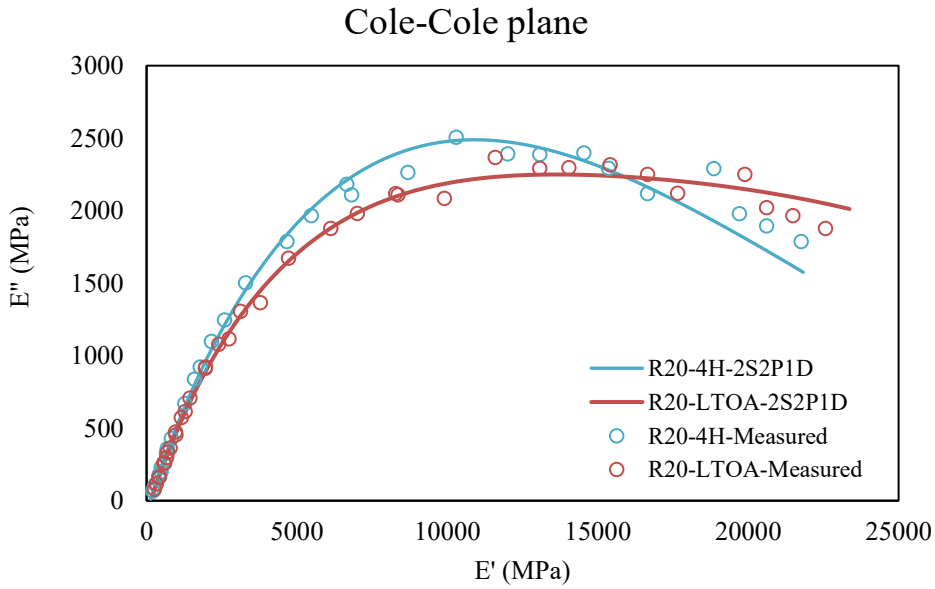

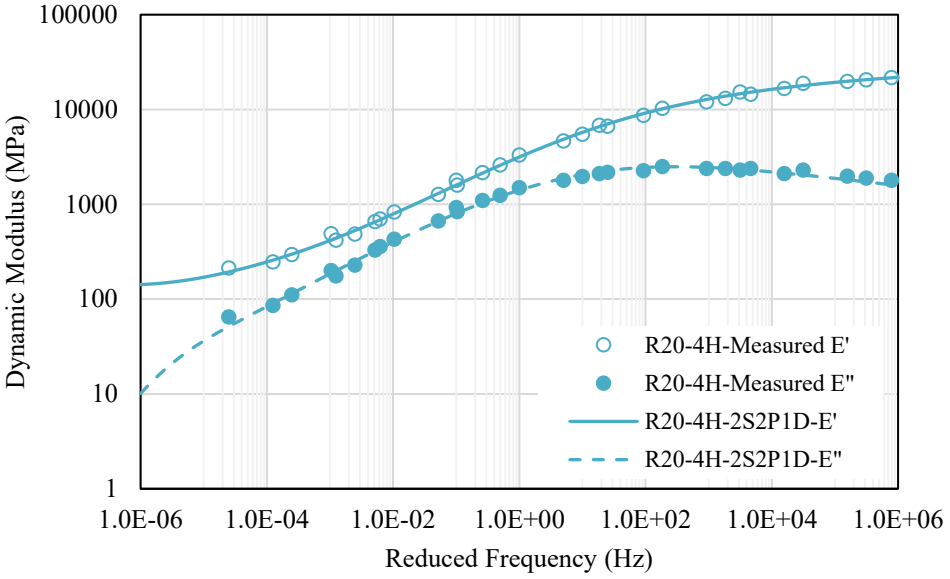
100000
10000
1000
100
10
1
Dynamic Modulus (MPa)
1.0E-06
1.0E-04
1.0E-02
1.0E+00
1.0E+02
1.0E+04
1.0E+06
Reduced Frequency (Hz)
R20-4H-Measured E'
R20-4H-Measured E"
R20-4H-2S2P1D-E'
R20-4H-2S2P1D-E"

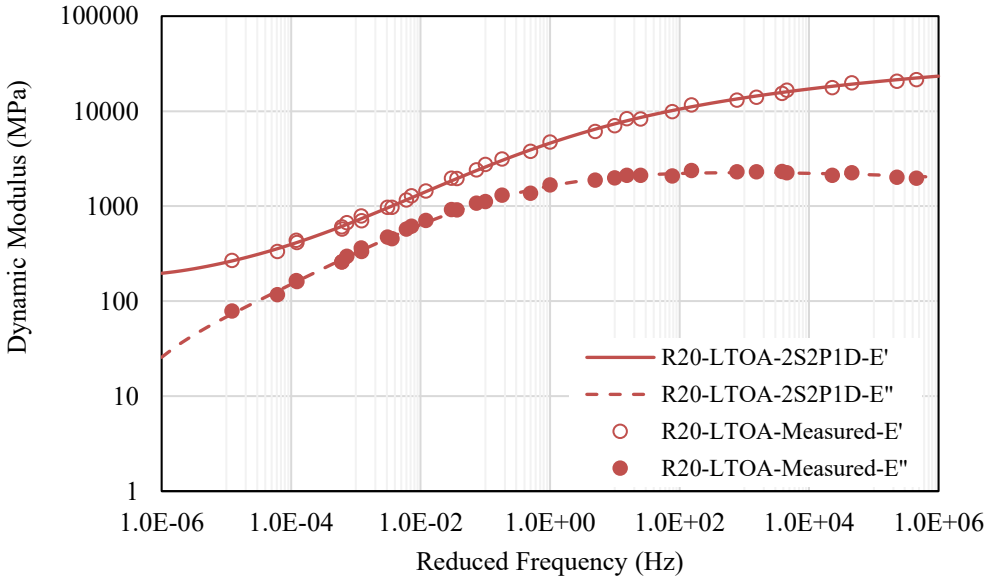
100000
10000
1000
100
10
1
Dynamic Modulus (MPa)
1.0E-06
1.0E-04
1.0E-02
1.0E+00
1.0E+02
1.0E+04
1.0E+06
Reduced Frequency (Hz)
R20-LTOA-2S2P1D-E'
R20-LTOA-2S2P1D-E"
R20-LTOA-Measured-E'
R20-LTOA-Measured-E"

2. R50-SB mixes:

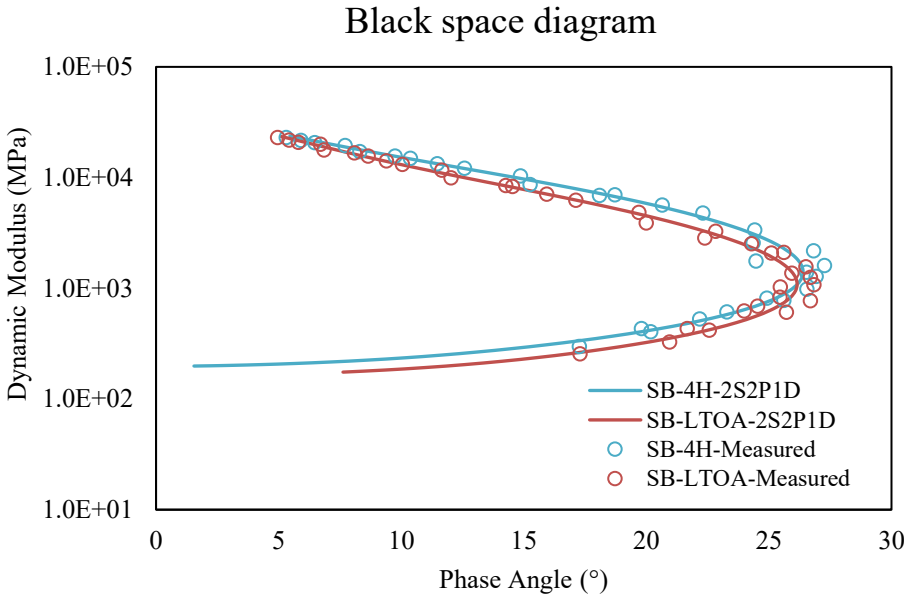

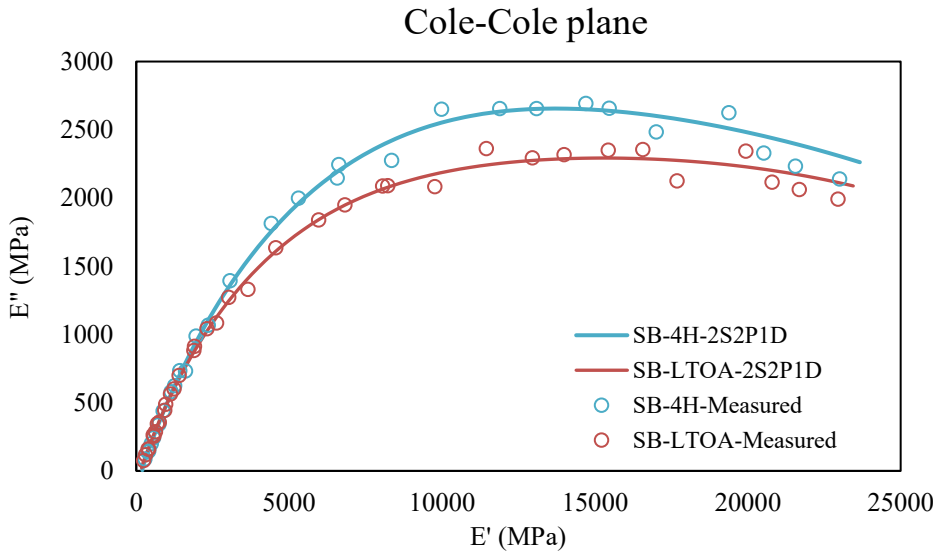

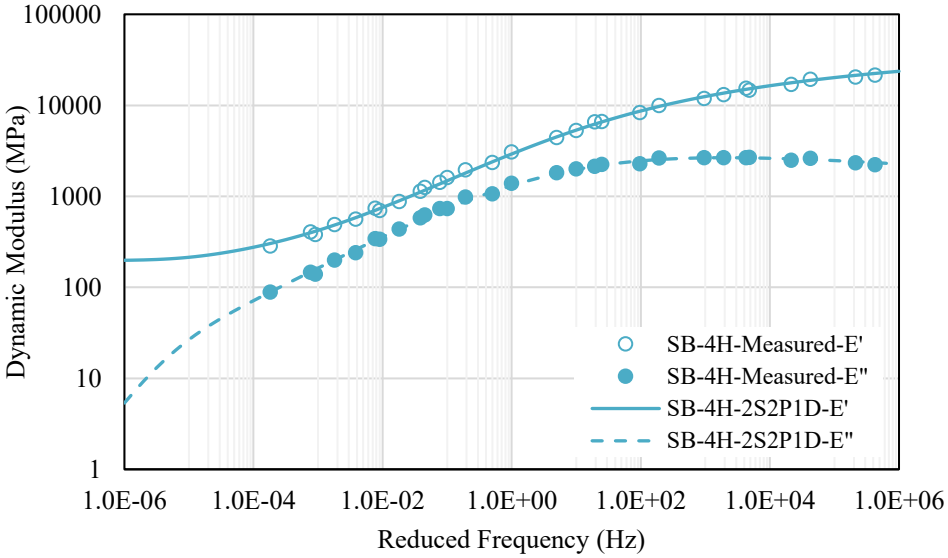
100000
10000
1000
100
10
1
Dynamic Modulus (MPa)
1.0E-06
1.0E-04
1.0E-02
1.0E+00
1.0E+02
1.0E+04
1.0E+06
Reduced Frequency (Hz)
SB-4H-Measured-E'
SB-4H-Measured-E"
SB-4H-2S2P1D-E'
SB-4H-2S2P1D-E"

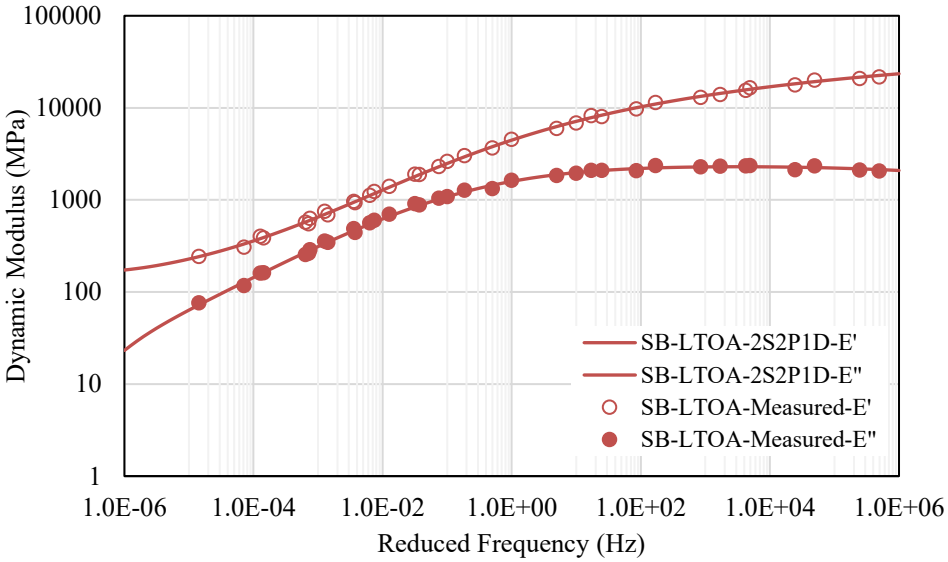
100000
10000
1000
100
10
1
Dynamic Modulus (MPa)
1.0E-06
1.0E-04
1.0E-02
1.0E+00
1.0E+02
1.0E+04
1.0E+06
Reduced Frequency (Hz)
SB-LTOA-2S2P1D-E'
SB-LTOA-2S2P1D-E"
SB-LTOA-Measured-E'
SB-LTOA-Measured-E"

3. R50-B mixes:

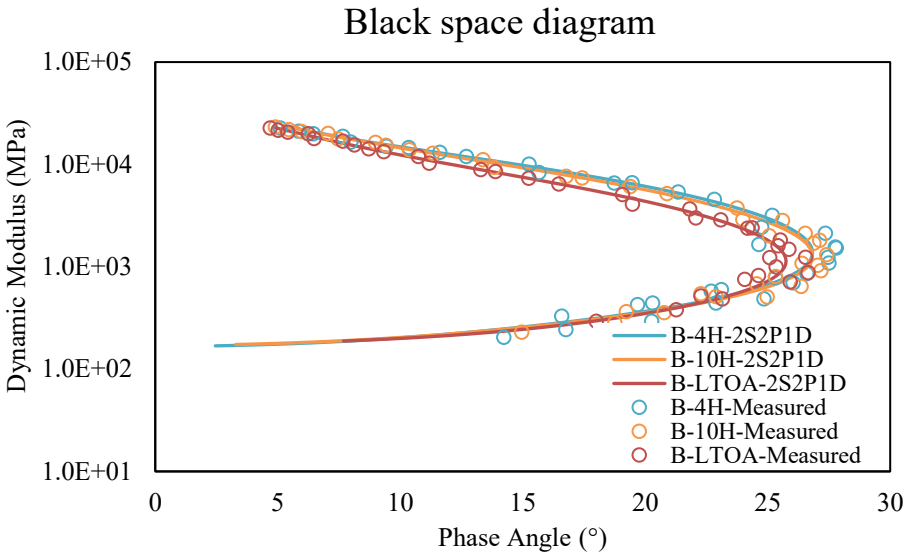
Black space diagram
Dynamic Modulus (MPa)
1.0E+05
1.0E+04
1.0E+03
1.0E+02
1.0E+01
0
5
10
15
20
25
30
Phase Angle (°)
B-4H-2S2P1D
B-10H-2S2P1D
B-LTOA-2S2P1D
B-4H-Measured
B-10H-Measured
B-LTOA-Measured

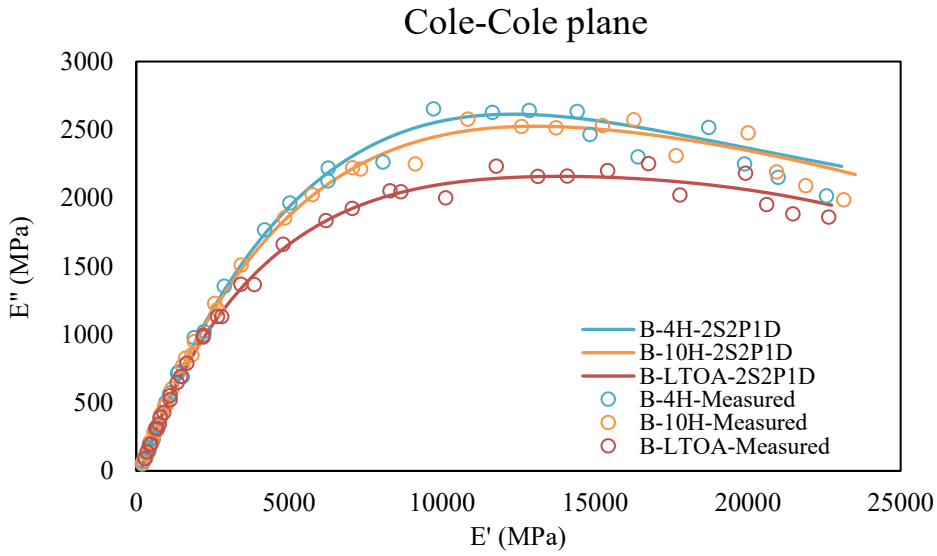
Cole-Cole plane
E'' (MPa)
3000
2500
2000
1500
1000
500
0
0
5000
10000
15000
20000
25000
E' (MPa)
B-4H-2S2P1D
B-10H-2S2P1D
B-LTOA-2S2P1D
B-4H-Measured
B-10H-Measured
B-LTOA-Measured

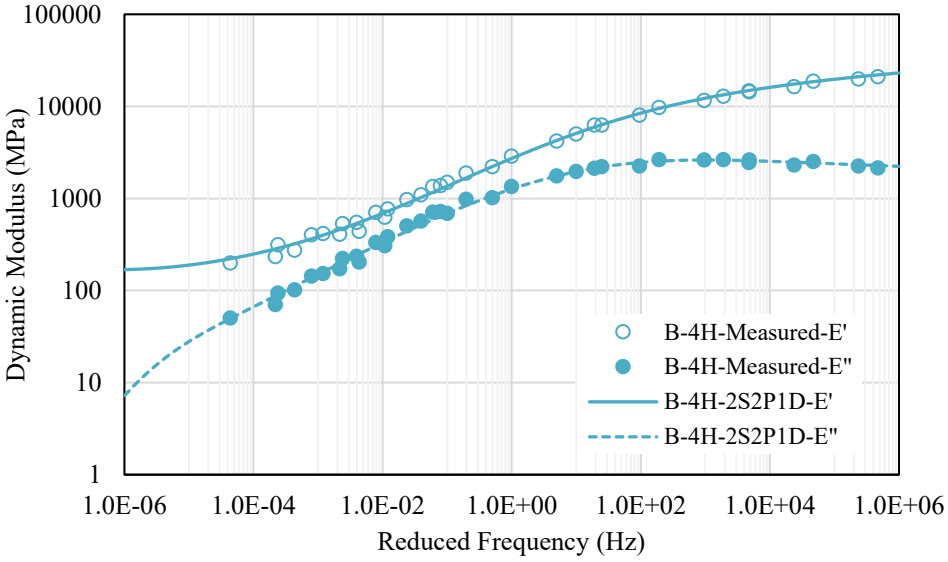
100000
10000
1000
100
10
1
Dynamic Modulus (MPa)
1.0E-06
1.0E-04
1.0E-02
1.0E+00
1.0E+02
1.0E+04
1.0E+06
Reduced Frequency (Hz)
B-4H-Measured-E'
B-4H-Measured-E"
B-4H-2S2P1D-E'
B-4H-2S2P1D-E"

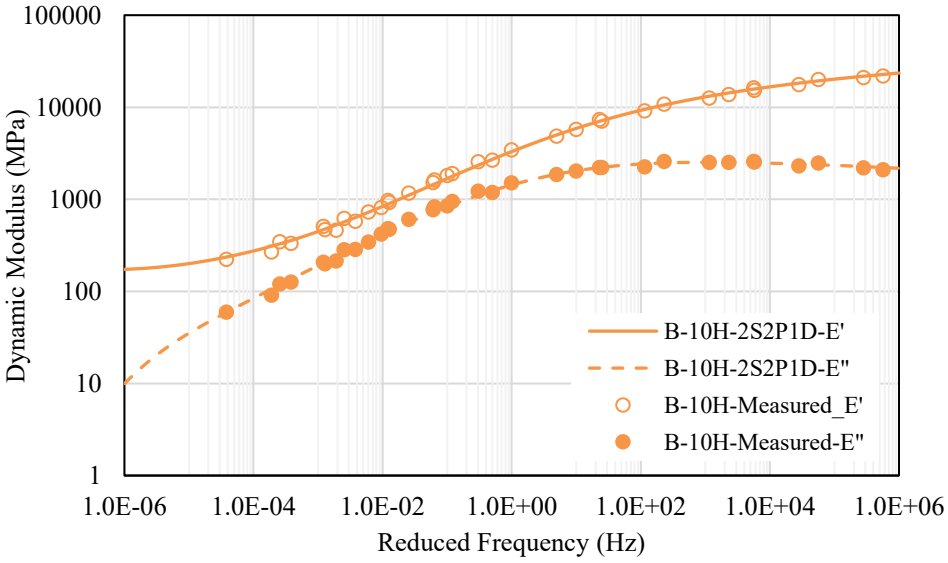
100000
10000
1000
100
10
1
Dynamic Modulus (MPa)
1.0E-06
1.0E-04
1.0E-02
1.0E+00
1.0E+02
1.0E+04
1.0E+06
Reduced Frequency (Hz)
B-10H-2S2P1D-E'
B-10H-2S2P1D-E"
B-10H-Measured_E'
B-10H-Measured-E"

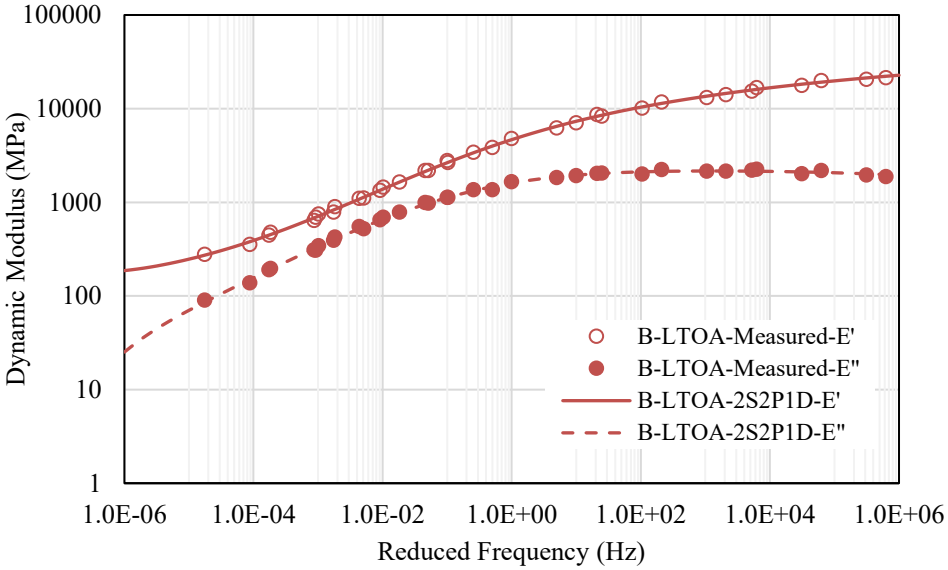
100000
10000
1000
100
10
1
Dynamic Modulus (MPa)
1.0E-06
1.0E-04
1.0E-02
1.0E+00
1.0E+02
1.0E+04
1.0E+06
Reduced Frequency (Hz)
B-LTOA-Measured-E'
B-LTOA-Measured-E"
B-LTOA-2S2P1D-E'
B-LTOA-2S2P1D-E"

Appendix I: Shift factors

WLF equation and the generalized sigmoidal model:

Test temperature (℃)	R20-4H	R20-LTOA	SB-4H	SB-LTOA	R50-4H	B-10H	B-LTOA
-10	4.502	4.480	4.473	4.499	4.473	4.463	4.532
4	2.357	2.394	2.377	2.395	2.322	2.324	2.391
21	0	0	0	0	0	0	0
37	-1.931	-2.047	-2.008	-2.029	-1.871	-1.883	-1.990
44	N/A	-2.846	-2.786	-2.817	-2.574	-2.594	-2.753
54	-3.681	-3.971	N/A	-3.922	-3.542	-3.573	-3.817

Free shifting and the 2S2P1D model:

Test temperature (℃)	R20-4H	R20-LTOA	SB-4H	SB-LTOA	R50-4H	B-10H	B-LTOA
-10	4.498	4.659	4.631	4.692	4.675	4.752	4.796
4	2.268	2.187	2.285	2.231	2.282	2.363	2.321
21	0	0	0	0	0	0	0
37	-1.983	-2.139	-2.114	-2.126	-2.101	-1.916	-1.990
44	N/A	-2.918	-2.742	-2.895	-2.621	-2.593	-2.737
54	-3.603	-3.911	N/A	-3.846	-3.362	-3.420	-3.757